Generation and characterisation of an in vitro TREM2-deficient microglia model

Lim, Yau Mun

Awarding institution:
King's College London

Generation and characterisation of an *in vitro* TREM2-deficient microglia model

Yau Mun LIM

Submitted to King's College London University in fulfilment of the requirements for the degree of Doctor of Philosophy

2018

Abstract

Rare variants of TREM2 have been associated with increased risk of developing several neurodegenerative diseases. In particular, the heterozygous p.R47H variant (rs75932628) has been associated with approximately three times increased risk to develop Alzheimer's disease (AD). Other homozygous TREM2 variants have been associated with developing Nasu-Hakola disease and frontotemporal-like dementia. This PhD project aimed to develop an *in vitro* TREM2 model endogeneously expressing the disease-associated variants with intact downstream signalling pathways. This cell model would be suitable in screening assays including for use to identify disease-modifying therapeutic compounds.

CRISPR/Cas9 genome editing was used to knock in the disease-associated variants into BV2 immortalised mouse microglia cell line. Various steps in the CRISPR/Cas9 workflow were optimised for use with BV2 cells. Despite four iterative improvements in experimental design, knock-in of the variants were unsuccessful. This has been attributed to very low efficiency of homogeneous editing in individual cells with chromosomal instability and hyperploidy that frequently occur in immortalised cell lines. Nevertheless, four clonal lines with homogeneous editing resulting in indels in *Trem2* were generated and predicted to result in loss of functional TREM2 expression.

Post-mortem hippocampal brain tissue from AD cases with and without a disease-associated TREM2 variant were immunostained for functional microglial activation markers: CD68, HLA-DP, -DQ, -DR and Iba-1 to investigate the effects of these variants on microglia. AD cases with disease-associated TREM2 variants, particularly p.R47H, have decreased CD68 expression and fewer HLA-DP, -DQ, -DR-expressing cells compared to those without variants in hippocampal CA4 despite no differences in the density of Iba-1-expressing cells.

DNA indels generated in the *Trem2*-edited cell lines were stable and the correct clonal lines were selected and expanded from cryopreservation in 96-well culture plates. Protein-coding *Trem2* transcripts were disrupted in these cells and functional TREM2 protein was not expressed as predicted from changes in *Trem2* DNA sequence. Functional characterisation of these cell lines using a TREM2-activating antibody revealed potential co-regulation of shared immunoreceptor tyrosine-based activation motif (ITAM)-mediated signalling pathways downstream of TREM2 and FcγR. Furthermore, TREM2 deficiency did not affect protein levels of CD68 and Iba-1 after stimulation with the TREM2-activating antibody, unlike in AD cases with a disease-associated TREM2 variant. Low or tonic ligand-binding

avidity from monoclonal antibody stimulation or amino acid variants of these receptors that decrease ligand-binding may result in inhibitory ITAM signals that can suppress innate immune responses. This suggests a disease-causing mechanism conveyed by TREM2 variants that impair ligand binding, such as the p.R47H, p.R62H and p.D87N variants.

Acknowledgements

First and foremost, I would like to thank my parents for their continuous encouragement throughout my journey in higher education. Without their neverending support, I would not have been able to pursue the opportunities that got me to where I am today.

Next, I would like to thank my PhD supervisors Dr Angela Hodges and Dr Richard Killick for the opportunity to undertake this PhD project and for the experiences that has allowed the exponential growth of my personal and professional skills.

I would like to give special thanks to Dr Christina Elliot who has been a great mentor and friend. If not for her advice and and constant support, this journey would have been a lot more challenging.

Further, I would also like to extend my gratitude to other colleagues in the Department of Old Age Psychiatry, especially Hannah Rutter, Dr Abdul Hye and Dr Nicholas Ashton for their company as well as technical support and advice.

Last but not least, I am grateful for my friends who have been supportive throughout this journey and have put up with my numerous rants and complaints.

This PhD Studentship was funded by the Alzheimer's Society.

Contents

List of Tables

List of Figures

Abbreviations

Aβ	Amyloid-beta
ABC	Avidin-biotin complex
AD	Alzheimer's disease
AF	Alexa Fluor
AICD	APP intracellular cytoplasmic domain
AIF1	Allograft inflammatory factor 1
AmpR	Ampicillin resistance gene
ANCOVA	Analysis of covariance
APC	Antigen-presenting cell
ApoE	Apolipoprotein E
ApoJ	Apolipoprotein J/clusterin
ATP	Adenosine 5'-triphosphate
BCA	Bicinchoninic acid
BDNF	Brain-derived neurotrophic factor
bGH polyA	bovine growth hormone polyadenylation terminator signal
BMDM	Bone marrow-derived macrophages
Cas9	CRISPR-associated protein 9
Cas9n	Cas9 nickase
CBh	Hybrid CMV enhancer/chicken β-actin promoter
CBS	Citrate-buffered saline
CD	Cluster of differentiation
cDNA	Complementary DNA
CIITA	Class II, major histocompatibility complex, transactivator
CMV	Cytomegalovirus
CNS	Central nervous system
CR3	Complement receptor 3
CRISPR	Clustered regularly interspaced palindromic repeats
CSF	Cerebrospinal fluid
CTF	Carboxy-terminal fragment
CX3CR1	C-X3-C chemokine receptor 1/fractalkine receptor
DAB	3,3'-diaminobenzidine tetrahydrochloride

DAMP	Damage-associated molecular pattern
DAP12	DNAX-Activation Protein 12
ddH_2O	Double-distilled 18.2 megaohm-cm water
DEPC	Diethyl pyrocarbonate
dH_2O	Distilled water
DMEM	Dulbecco's Modified Eagle Medium
DMSO	Dimethyl sulfoxide
DNA	Deoxyribonucleic acid
dNTP	Deoxynucleotide
DPBS	Dulbecco's phosphate-buffered saline
DTT	Dithiothreitol
EDTA	Ethylenediaminetetraacetic acid
Erk	Extracellular signal-regulated kinase
Fab	Antigen-binding fragment
FACS	Fluorescence-activated cell sorting
FBS	Foetal bovine serum
Fc	Fragment crystallisable
FcγR	Fc-gamma receptor
FcRγ	Fc receptor gamma-chain
FFPE	Formalin-fixed paraffin-embedded
FSC	Forward scatter
FTD	Frontotemporal dementia
GAPDH	Glyceraldehyde 3-phosphate dehydrogenase
GFAP	Glial fibrillary acidic protein
GFP	Green fluorescent protein
GWAS	Genome-wide association studies
H_2O_2	Hydrogen peroxide
HCl	Hydrochloric acid
HDL	High-density lipoprotein
HDR	Homology-directed repair
HDLS	Hereditary diffuse leukoencephalopathy with axonal spheroids
Hexb	Hexosaminidase B
HIER	Heat-induced epitope retrieval
HLA	Human leucocyte antigen

HRP	Horseradish peroxidase
Hsp60	Heat-shock protein 60
hSpCsn1	Human-codon optimised *Streptococcus pyogenes*-derived Cas9
Iba-1	Ionised calcium-binding adaptor molecule 1
IDE	Insulin-degrading enzyme
IFN-γ	Interferon-gamma
Ig	Immunoglobulin
IL	Interleukin
IMS	Industrial methylated spirit
iNOS	Inducible nitric oxide synthase
iPSC	Induced pluripotent stem cell
ITAM	Immunoreceptor tyrosine-based activation motif
KASP	Competitive allele specific PCR
KO	Knockout
LDL	Low-density lipoprotein
LDS	Lithium dodecyl sulfate
LOAD	Late onset Alzheimer's disease
LTP	Long-term potentiation
MAF	Minor allele frequency
MAPK	Mitogen-activated protein kinase
MHC	Major histocompatibility complex
MOG	Myelin oligodendrocyte glycoprotein
MOPS	3-(N-morpholino)propanesulfonic acid
MRI	Magnetic resonance imaging
N2A	Neuro-2A
NaCl	Sodium chloride
NBF	Neutral buffered formalin
NFT	Neurofibrillary tangles
NGS	Normal goat serum
NHD	Nasu-Hakola disease
NHEJ	Non-homologous end-joining
NINCDS/ADRDA	National Institute on Neurological and Communicative Disorders and Stroke and the Alzheimer's Disease and Related Disorders Association
NLS	Nuclear localisation sequence

NMS	Normal mouse serum
NO	Nitric oxide
NPT	Neuropil threads
NSS	Normal swine serum
nt	Nucleotide
p-tau	Phosphorylated tau
P2RY12	Purinergic receptor P2Y12
PAM	Protospacer adjacent motif
PAMP	Pattern-associated molecular pattern
PBMC	Peripheral blood mononuclear cells
PCI	Phenol/chloroform/isoamyl alcohol
PCR	Polymerase chain reaction
PET	Positron emission tomography
PI3K	Phosphatidylinositol 3-kinase
PiB	Pittsburgh Compound B
PNK	Polynucleotide kinase
POLD	Pigmentary orthochromatic leukodystrophy
PS	Penicillin-streptomycin
pUC ori	pUC origin of replication
PuroR	Puromycin resistance gene
px	Pixel(s)
Pyk2	Proline-rich tyrosine kinase 2
Rbfox3	RNA binding protein fox-1 homolog 3/NeuN
R-ITR	R-inverted terminal repeat
RNA	Ribonucleic acid
ROI	Region of interest
ROS	Reactive oxygen species
RPMI	Roswell Park Memorial Institute
RT	Room temperature
RT-PCR	Reverse transcription polymerase chain reaction
RXR	Retinoid X receptor
SBA	Sodium boric acid
SDS	Sodium dodecyl sulfate
sgRNA	Short-guide RNA

SH2	Src homology 2
SNP	Single-nucleotide polymorphism
SR-A	Class A scavenger receptor
SSC	Side scatter
ssDNA	Single-stranded DNA
sTREM2	Soluble TREM2
Syk	Spleen tyrosine kinase
T2A	*Thoseaasigna* virus 2A self-cleaving peptide
TAE	Tris-acetate-EDTA
TALEN	Transcription activator-like effector-based nuclease
TBI	Traumatic brain injury
TBS	Tris-buffered saline
TBS-T 0.1%	TBS with 0.1% Tween 20
TBS-Tx 0.1%	TBS with 0.1% Triton X-100
TBS-Tx 0.25%	TBS with 0.25% Triton X-100
TBE	Tris-borate-EDTA
TF	Transcription factors
TFS	Thermo Fisher Scientific
TLR	Toll-like receptor
TNF	Tumour necrosis factor
TREM2	Triggering receptor expressed on myeloid cells 2
v/v	Volume to volume
w/v	Weight (mass) to volume
WT	Wild-type
ZAP70	Zeta-chain-associated protein kinase 70
ZFN	Zinc finger nuclease

Chapter 1

Introduction

1.1 History of Alzheimer's disease

Alzheimer's disease (AD) is first described by psychiatrist and neuropathologist Alois Alzheimer in 1906 on his patient Auguste Deter. Before her death, Auguste Deter had untreatable paranoia and rapid progression of several neurological disorders including sleep disorders, disturbances of memory, aggressiveness, crying and confusion[1]. After her death in 1906, Alzheimer found these symptoms were associated with extensive cerebral atrophy and two distinctive pathologies, senile plaques and neurofibrillary tangles (NFT)[2].

About 80 years later, the main components of senile plaques and NFT that Alzheimer described were found to be amyloid beta (Aβ)[3] and hyperphosphorylated microtubule-associated protein tau[4], respectively. In 1991, genetic studies identified the first causative gene for familial AD, *APP* which encodes for the amyloid precursor protein[5], and shortly followed by *PSEN1*[6] and *PSEN2*[7]. Since then, the number of studies on AD rapidly increased, with the first major AD risk gene, *APOE* encoding apolipoprotein E (ApoE), was described in 1993 where the ε4 variant allele was associated with an increased risk of developing AD[8]. In 1996, the acetylecholinesterase inhibitor Donepezil was approved as the first symptomatic treatment for AD[9]. In 2004, the discovery of the Pittsburgh Compound B (PiB) allowed clinicians to monitor the progression of amyloid deposition in living patients by positron emission tomography (PET) scan[10]. In 2010, studies found the development of AD pathology can precede the onset of clinical symptoms by decades[11], which resulted in a new revision of criteria and guidelines to diagnose AD[12]. Despite the progression in our understanding of AD, there still are no disease-modifying treatments for AD up until today.

This is a worrying prospect because the risk of developing AD increases with age and the average lifespan of the global population is steadily increasing. It has been estimated that the risk of developing sporadic AD is 2% at 65 years old and this further increases up to 40% over the age of 80[13]. The incidence of AD over the age of 65 is 40–58%[14,15] and its prevalence will continue to increase. In 1976, AD was declared the most common cause of dementia, accounting for 60–80% of all cases with an estimated prevalence of about 1 million people in the USA in 1970[16]. At present, 850,000 people in the UK and more than 40 million people globally are diagnosed with dementia. This is predicted to

double every 20 years to about 2 million in the UK and 115 million people globally by the year 2050[17,18] as developing countries are set to contribute proportionally more than Western Europe and the USA due to improved healthcare and lower mortality rates[19]. This puts a tremendous economic burden on international healthcare as dementia care worldwide has been estimated to cost USD604 billion in 2010[20] and is predicted to increase by approximately 85% within the next 20 years because of the increasing prevalence.

1.2 Amyloid cascade hypothesis

The amyloid cascade hypothesis is a landmark proposal that kickstarted the amyloidocentric research of AD and became the basis for therapeutic interventions[21]. It is proposed by Selkoe (1991)[22] and coined by Hardy and Higgins (1992)[23] after the discovery that mutations in *APP* result in AD[5]. The hypothesis proposed Aβ as the causative agent of AD pathology, preceding and causing abnormal tau hyperphosphorylation, neuronal death, vascular damage and dementia (Figure 1.1). The hypothesis is later refined[24] after the discovery of additional AD-causing mutations in *PSEN1*[6] and *PSEN2*[7] genes encoding for presenilin 1 and 2, respectively, which are part of the γ-secretase complex involved in APP processing. *APP* mutations cluster at or very close to α-, β- or γ-secretase cleavage sites in the APP protein, which affect its processing[24].

APP can be cleaved by one of two pathways to generate extracellular fragments that are non-amyloidogenic (mediated by α-secretase, ADAM10 in neurons[26]) or amyloidogenic (mediated by β-secretase, BACE1 in neurons[27]). The remaining membrane-bound peptides after α- or β-secretase cleavage are then cleaved by γ-secretase to produce the P3 or Aβ peptide, respectively, and APP intracellular cytoplasmic domain (AICD)[28,29] (Figure 1.2). γ-secretase cleaves at multiple sites within the transmembrane region of APP, resulting in Aβ peptides varying in length between 38—43 amino acids[30]. Regardless, cleavage products from α- and γ-secretase processing of APP are non-amyloidogenic and are potentially neurotrophic and neuroprotective[31,32]. On the other hand, β- and γ-secretase cleavage yields the amyloidogenic Aβ peptide.

Mutations in the familial AD genes promote amyloidogenic processing of APP through β- and γ-secretase cleavage to produce Aβ[33–36]. Moreover, mutations within the Aβ sequence

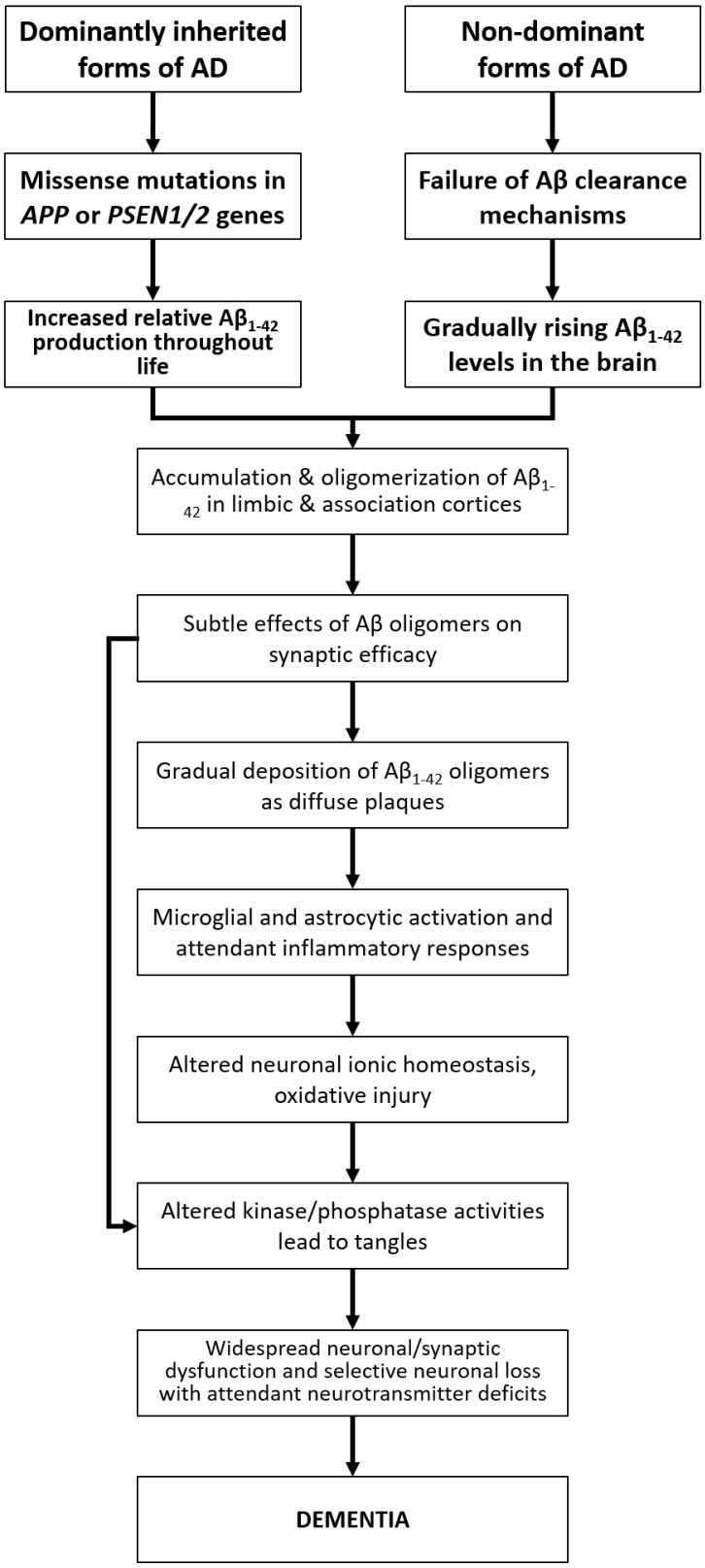

Figure 1.1. The amyloid cascade hypothesis proposed that Aβ is the primary cause of Alzheimer's disease and leads to several pathogenic events and the onset of dementia.
Aβ oligomers can directly affect phosphorylation of tau as well.
Figure adapted from Selkoe and Hardy (2016)[25].

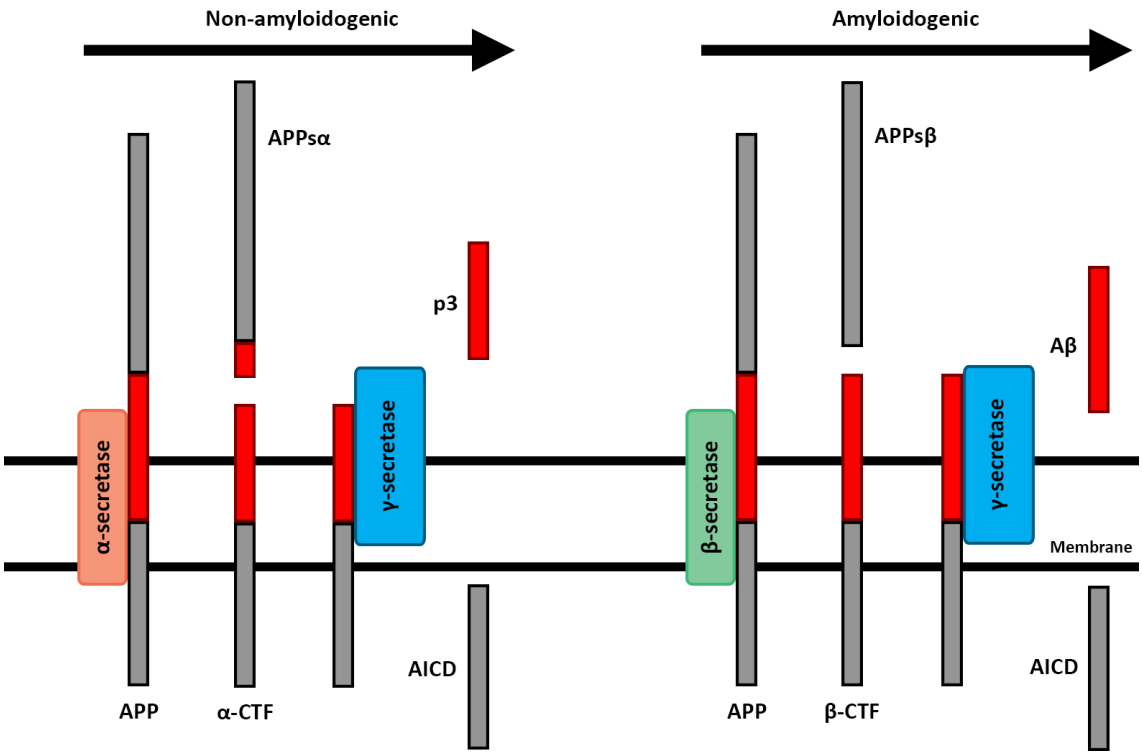

Figure 1.2. Non-amyloidogenic or amyloidogenic processing of APP is mediated by α-secretase or β-secretase, respectively, followed by γ-secretase cleavage.

Various peptides are produced from the sequential cleavage of the secretases, including the amyloidogenic Aβ peptide.

Figure adapted from O'Brien and Wong (2011)[29].

of *APP* increase the propensity for self-aggregation of Aβ into amyloid fibrils[37]. The presenilin genes encode for the active site on γ-secretase[38,39]. Mutations in *PSEN1* and *PSEN2* tend to promote the cleavage of APP to produce the 42-amino acid rather than the 40-amino acid Aβ peptide, increasing the $A\beta_{1–42}$:$A\beta_{1–40}$ ratio[30].

Since the proposal of the amyloid cascade hypothesis, various pieces of evidence have been found to support it. Individuals with Down's syndrome, a disease associated with the trisomy of chromosome 21 where the *APP* gene is located, have been found to also develop AD pathology. This has been attributed to increased *APP* gene copy number[40] and not the other genes located within chromosome 21[41]. This suggested that lifelong overexpression of APP even without familial AD mutations can cause AD[25]. Additionally, mutations in the *MAPT* gene encoding the microtubule-associated protein tau cause severe tau aggregation in the brain but are not associated with amyloid deposition. Therefore, it has been posited that the NFT observed in AD is likely to occur after changes in Aβ metabolism[42]. In animal studies, mutant human APP and tau transgenic mice have increased tau pathology but there is no additional amyloid pathology compared to tau transgenic-only mice[43]. This has been thought to indicate that altered APP processing occurs before tau dysfunction[24].

1.3 Progression of Alzheimer's disease

1.3.1 Clinical

A definitive diagnosis of AD can only be made in post-mortem with pathological confirmation of the presence of amyloid plaques and NFT pathology. While the patient is alive, only a "probable" diagnosis of AD can be made from the manifestation of multiple cognitive deficits and memory decline. These symptoms are often assessed by detailed history reported by patients or their carers to determine their impact on social or occupational functioning[44]. The National Institute on Neurological and Communicative Disorders and Stroke and the Alzheimer's Disease and Related Disorders Association (NINCDS/ADRDA) proposed the first criteria for the diagnosis of AD in 1984[45]. Subsequent revisions of the diagnostic criteria have incorporated new findings in clinical, imaging and fluids assessments to improve sensitivity and specificity for diagnosing as early as possibly[11,12,46,47]. It was in the 2011 iteration of the NINCDS/ADRDA criteria that suggested the clinical diagnosis of

AD is only "probable" while the patient is still alive and a "definite" AD diagnosis can only be made after post-mortem neuropathological assessments. This criteria also was the first time that the assessment of AD pathology in vivo using PiB-PET was considered. These guidelines generally have good sensitivity and specificity of more than 80% to distinguish AD patients from non-demented individuals but were inconsistent in distinguishing between dementia subtypes[48]. A more recent criteria proposed by the International Working Group for New Research Criteria for the Diagnosis of Alzheimer's Disease included *in vivo* biomarker evidence of pathophysiology indicative of AD[47]. Some of the biomarkers include the detection of Aβ[49] and tau[50] pathology and neuroinflammation (TSPO)[51] PET imaging, brain volume by magnetic resonance imaging (MRI)[52–54], and cerebrospinal fluid (CSF) A$\beta_{1–42}$, total tau and phosphorylated tau (p-tau)[55–57].

There is a long preclinical, asymptomatic phase of AD pathology preceding the early presentation of cognitive impairment[58]. In early AD, patients tend to be clinically normal with only slight impediment of daily living. Signs of cognitive decline are variable but often manifest slowly in the early symptomatic phase. Common complaints at this stage include significant decline in short term memory, aphasia and spatial disorientation[59]. Patients are often affected by problems with executive function and decreased verbal fluency. Less common symptoms include subtle mood changes in about 20–30% of patients and personality changes in 25–50% of patients[60]. As the disease progresses, patients often show signs of agitation, psychosis and anxiety[61]. In moderate to severe AD, patients start to develop functional impairment and dependency on others marked by extreme difficulty in retaining new information, prosopagnosia (difficulty in recognising familiar people) and significant deterioration of executive function. Behavioural symptoms such as hallucinations, delusions, aggression and anxiety are not always apparent but are more common in the advanced stages of AD. In severe AD, dysphagia (impairment of basic motor functions) can manifest alongside an almost complete loss of cognitive function and patients are usually completely dependent on comprehensive care.

1.3.2 Pathology

AD is characterised by the pathological hallmarks of extracellular deposits of amyloid plaques and intracellular aggregates of NFT. Amyloid plaques consist of aggregated Aβ

peptides, particularly $A\beta_{1-42}$[3], while NFTs consist of aggregated hyperphosphorylated tau protein[62,63]. NFT pathology have been found to correlate better than Aβ deposition to neurodegeneration, synaptic loss and cognitive symptoms[64]. The *MAPT* gene encodes for six tau isoforms which are generated by alternative splicing of exon 10[65,66]. This leads to a protein with three or four microtubule-binding domain repeats (3R or 4R) in the C-terminal region. This structure is involved in microtubule polymerisation and stabilisation[67] and normally regulates cytoskeletal organisation. In disease, hyperphosphorylation of tau impairs its binding to microtubules. This leads to destabilisation of axons and disruption of axonal transport. Eventually, this causes axonal degeneration and neuronal death[68]. In AD, all isoforms of tau can become hyperphosphorylated and form insoluble aggregates known as paired helical filaments[69] which are the main component of NFTs[70]. Tau from AD brains are four times more phosphorylated than in non-AD brains[71]. Despite the characteristic amyloid plaques and NFT, synaptic loss is still the best pathological correlate to cognitive impairment in AD[72–74].

AD pathogenesis is known to begin many years before clinical symptoms manifest[75]. Although the amyloid cascade hypothesis has suggested that amyloid pathology precedes tau pathology, these pathologies develop spatially and temporally independent of each other within the AD brain. Amyloid and hyperphosphorylated tau have characteristic patterns of deposition as disease progresses. The Braak tau staging was developed to characterise the spatial and temporal progression of tau pathology [NFT and neuropil threads (NPT)] burden in the brain on a 6-point scale[76,77]. In AD, tau pathology begins in the transentorhinal region and spread into the entorhinal cortex and hippocampus, as well as into the limbic regions including the amygdala, thalamus, putamen and nucleus accumbens. Tau pathology eventually reaches the neocortical regions including the temporal, occipital and frontal cortices. Separately, the Thal amyloid staging[78] assesses the spatial and temporal progression of amyloid pathology which tends to begin in the neocortical region including the frontal, parietal, temporal and occipital cortices. It then spreads to the entorhinal region and hippocampus before progressing into the subcortical regions including the caudate nucleus, putamen, claustrum, basal forebrain nuclei, substatia innominata, thalamus, hypothalamus, lateral habenular nucleus and white matter tracts. Towards end stage AD, amyloid pathology develops deeper into the midbrain, brainstem and finally the cerebellum.

Alongside the abnormal protein aggregation, degeneration of cholinergic neurons in the nucleus basalis of Meynert, which is the primary nucleus of cholinergic neurons that project to the neocortex[79], is also characteristic in early AD[80]. As AD progresses, increasing neurodegeneration can be found in the cerebral cortex, mainly the lateral temporal and medial parietal cortex followed by atrophy of the lateral parietal and frontal lobes[81]. By the time clinical symptoms develop, the temporal, parietal and frontal cortices would have undergone extensive atrophy but with relative preservation of the occipital and primary sensory-motor cortex[80,82].

1.4 Risk factors of Alzheimer's disease

1.4.1 Genetic

Mutations in the *APP*[5], *PSEN1*[6] and *PSEN2*[7] genes have been identified to cause familial AD, which accounts for ∼4% of people with AD[83,84]. Additional rare variants in *APP*, *PSEN1*, *PSEN2* and *ADAM10* also modulate sporadic AD risk[85–90]. Other than the familial AD genes, risk genes for sporadic AD were also discovered. *APOE* is the first AD risk gene to be described[8]. Its association with AD has been consistently replicated in many independent studies and remains the top-ranking gene with variants conferring risk for AD. Three haplotypes (ε2, ε3 and ε4) based on two variants in the coding region of the *APOE* gene have different association with AD[8]. The ε3 allele is the most common variant with about 77% of the total population carrying it. The ε4 allele is found to convey an increased risk of developing AD with homozygous ε4 alleles associated with a 12-fold increased AD risk and heterozygous ε3/ε4 alleles associated with a 3-fold increased AD risk[8,91–93]. The ε4 allele variant is also associated with the decreased age of onset[8,94] and the increased rate of cognitive decline[95,96]. It has been reported that 15% of the total population carries the ε4 allele[97] and in the AD population, about 60% of people can be expected to carry the allele[98]. Meanwhile, the ε2 allele can be found in 8% of the total population[97] and appears to be protective. It conveys a decreased risk of developing AD and is associated with a later age of onset[8,91,99–101]. ApoE has a central role in cholesterol metabolism[102] and is important in mediating several functions in the central nervous system (CNS) including cholesterol transport, neuroplasticity and inflammation[103]. ApoE also binds Aβ to mediate

the clearance of soluble and aggregated Aβ[103,104]. Moreover, ApoE indirectly regulates Aβ metabolism through the interaction with receptors such as LRP1[105] and more recently has been shown to bind to TREM2[106–108]. The *APOE* ε4 allele produces a protein variant that is less efficient at mediating the clearance of Aβ[104].

Recently, next-generation whole-genome and whole-exome sequencing have identified rare variants in genes like *TREM2*, *ABI3*, *PLD3* and *PLCG2* that convey a substantial increase in the risk of developing AD[109–112]. Furthermore, genome-wide association studies (GWAS) have identified many other AD risk genes including *ABCA7*, *BIN1*, *CASS4*, *CD33*, *CELF1*, *CLU*, *CR1*, *CD2AP*, *DSG2*, *EPHA1*, *FERMT2*, *HLA-DRB5–DRB1*, *INPP5D*, *MEF2C*, *MS4A6A–MS4A4E*, *NME8*, *PICALM*, *PTK2B*, *SLC24A4*, *SORL1* and *ZCWPW1*[113–117] (Figure 1.3). In addition to APP metabolism, these genes highlight the involvement of cholesterol metabolism, inflammation, endocytosis, cytoskeleton/axon development and epigenetics in the pathogenesis of AD (Figure 1.3). Variants in these genes have varying population frequency and convey different risk values to develop sporadic AD (Figure 1.3).

1.4.2 Epigenetic

The study of epigenetics and its role in AD is relatively recent. Epigenetic regulation is associated with changes in gene regulation through modifications to DNA packaging proteins or small chemical groups that are attached to DNA without changes to the actual DNA sequence[118,119]. Epigenetics has been found to be a major component of aging[120,121]. Similar changes in epigenetics have also been observed in AD brains[122–124]. Another study found that epigenetic regulation is involved in the loss of phenotypic plasticity associated with aging[125]. As aging is the biggest risk factor for AD, it is not surprising that aging-associated epigenetic modulation is involved in the pathogenesis of AD[126,127]. There are two main forms of epigenetic modifications: methylation of DNA mediated by DNA methyltransferases[128] and the binding of epigenetic factors, such as acetylation, methylation and phosphorylation, to histones that package DNA[129,130]. The latter is mediated by enzymes including histone acetyltransferases and deacetylases, histone methyltransferases and demethylases, and kinase and phosphatases, which attach and remove the small chemical groups from histones[131].

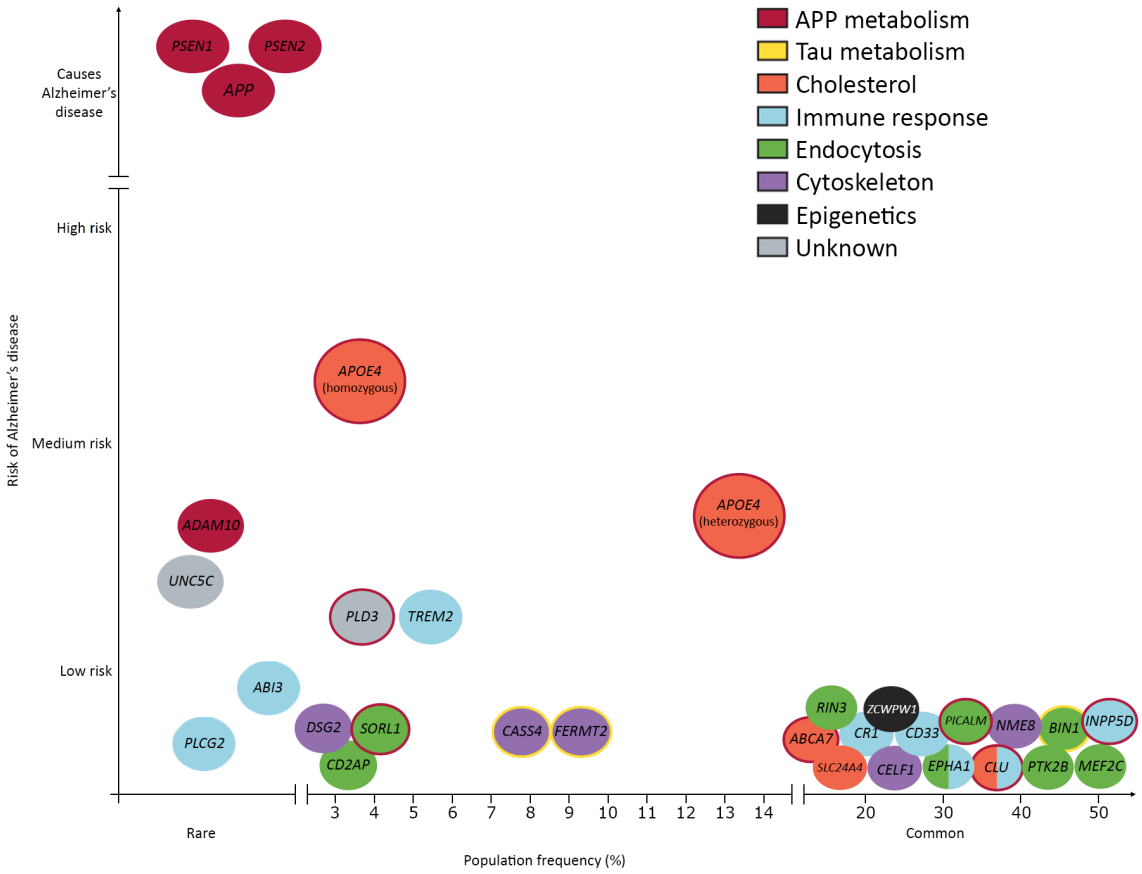

Figure 1.3. Recent whole-genome sequencing and genome-wide association studies have identified novel AD-associated risk genes.
These genes convey varying risks and have different population frequencies. They highlight various functional pathways involved in the pathogenesis of AD.
Figure adapted from Scheltens *et al.* (2016)[19].

Several studies observed genome-wide changes in DNA methylation in AD compared to non-AD patients[132–134]. Epigenome-wide association studies also found hypermethylation in genes such as *SORBS3* and *ANK1*, associated with cytoskeletal function, in AD vulnerable brain regions[131,135,136]. There have been mixed findings on histone modifications in AD post-mortem studies with some finding increased[137] and decreased[138] modifications. The role of epigenetics in the pathogenesis of AD is an interesting avenue for therapeutics as epigenetic changes in AD patients can potentially be pharmacologically targeted and may provide benefits. For example, folic acid and vitamin B12 have been shown to modulate DNA methylation through a mechanism mediated by 1-carbon metabolism[139]. Additionally, histone deacetylase modifiers like 2-valproate can modulate the removal of histone acetylation[140].

1.4.3 Lifestyle

Many studies have found that physical activity and exercise[141–143], midlife obesity[144], alcohol consumption[145], nutrition[146], education[147] and smoking[148,149] affect the risk of developing AD.

Physical exercise, even at low intensities, is beneficial and delays the onset of AD[142,143]. It has been shown to induce hippocampal neurogenesis[150] and improve learning in rodents[151]. Interestingly, the protective effect of exercise is more pronounced in individuals with the *APOE* ε4 risk allele[152]. Increased BMI at midlife is also a risk factor for not only AD but also many dementias[144,153]. Obesity is associated with cognitive decline and directly associated with AD[154,155]. Besides that, alcohol consumption is a well-known risk for dementia. Middle-aged heavy drinkers have a 3-fold higher risk to develop AD[156] while light and moderate drinkers have significantly lower risk relative to heavy drinkers[157,158]. Regardless, any level of alcohol consumption is associated with increased brain atrophy[159]. Additionally, a large-scale study has found that increased cognitive reserve from mental activity, occupation and especially education level conveyed a significant protective effect and delay the onset of dementia[160]. The protective effect of cognitive reserve can be beneficial even in older adults who performed mental exercises and cognitive stimulation[160,161]. Furthermore, several studies on smoking have suggested that current smokers have 1.5-fold increased risk of developing AD[149].

Many of the lifestyle risk factors for AD are also associated with poor cardiovascular health. Stroke[162,163], atherosclerosis[164,165], type-2 diabetes[166–170], hypertension[165,171,172] and hypercholesterolaemia[173–175] increase the risk of developing AD. Findings from a large population study suggested that if cardiovascular risks could be managed or prevented, the incidence of dementia would decrease by about 30%[172]. Compromised cardiovascular health is likely related to dysregulated cholesterol and energy metabolism, both of which are implicated in AD[176,177]. Moreover, hypertension is linked to increased brain atrophy and NFT deposition[178]. However, clinical trials that managed hypertension reported that there are minimal benefits in lowering the risk of developing dementia[179]. Evidence for dietary factors contributing to AD risk is mixed. While the Mediterranean diet appears to have a positive effect on cognition[180,181], dietary supplements and vitamins have failed to show any effects on the risk of developing AD[182–184].

1.5 Neuroinflammation in Alzheimer's disease

A link between inflammation and AD has been suggested as early as in the original amyloid hypothesis[22]. Recent genetic evidence indicates inflammation may even have a causal role in the pathogenesis of AD, contributing as much as plaques and tangles[185]. Furthermore, its role in AD is highlighted by the discovery of immune-related AD risk genes like *TREM2*[109,110] and *CD33*[186,187]. In the CNS, neuroinflammation is predominantly mediated by microglia and astrocytes.

1.5.1 Microglia

Microglia are the resident phagocytes of the CNS. They originate from yolk sac-derived erythromyeloid progenitors[188–190] and are distributed throughout the brain. In adulthood, they are considered very long-lived cells and can proliferate when required[191]. They have highly motile processes that survey the microenvironment for pathogens or cellular debris and simultaneously provide factors to support tissue maintenance and homeostasis[192]. Recent evidence suggests microglia may also contribute to the remodelling and protection of synapses[193]. These functions are mediated by trophic factors such as brain-derived neurotrophic factor (BDNF), which is a key factor involved in memory formation[194]. Microglia

also recognise dying neurons or protein aggregates which cause them to extend processes and migrate to the lesion site as part of the innate immune response[195]. Pathological stimuli are detected by damage- or pathogen-associated molecular pattern (DAMP/PAMP) recognition receptors[195] which cause them to switch from surveillance to a reactive phenotype, whereby they become more amoeboid in shape[196] and express specific activation markers depending on the stimulus[197,198].

In AD, microglia can bind and recognise soluble and fibrillar Aβ through receptors including SCARA1, CD36, CD14, α6β1 integrin, CD47, Toll-like receptors TLR2, TLR4, TLR6 and TLR9[199–202] resulting in activation of microglia to produce proinflammatory cytokines and chemokines[201–205]. CD36, TLR4 and TLR6 deficiency *in vitro* result in decreased Aβ-induced cytokine production[201,205,206]. Absence of these receptors also prevent early intracellular Aβ accumulation and the activation of inflammasomes[206]. On ligand binding, microglia phagocytose Aβ fibrils which enter the endolysosomal pathway[195]. Meanwhile, soluble oligomeric Aβ can be degraded by various extracellular proteases such as neprilysin and insulin-degrading enzyme (IDE)[207]. In sporadic AD, inefficient Aβ clearance is recognised to be a major contributor of pathogenesis[208]. This is associated with increased cytokine production and downregulation of Aβ-binding receptors which leads to insufficient microglial phagocytosis of Aβ[209]. Interestingly while microglia can still phagocytose fibrillar Aβ, they are ineffective at doing so and microglia-deficiency in AD mice do not appear to affect amyloid load in the brain[210–212].

Microglial activation can result in a spectrum of phenotypes reflecting their high degree of plasticity and their ability to respond to a wide range of stimuli. In peripheral macrophages, inflammatory activation can lead to the classic proinflammatory phenotype, coined M1, associated with the expression of genes involved in cytotoxic function[213] or the non-inflammatory M2 phenotype associated with the expression of *ARG1*, *FIZZ1*, *YM1* and *IGF1* genes implicated in tissue repair and resolution of inflammation[214,215]. The M1 activation state is characterised by an increased expression of proinflammatory cytokines such as TNF-α, IL-1, IL-6, IL-12, IL-18 and reduced phagocytosis[216]. Alternatively, the M2 activation state is characterised by the expression of anti-inflammatory cytokines like IL-4, IL-10, IL-13, TGF-β and increased phagocytosis without nitric oxide (NO) release[217–219]. The M1 and M2 states represent the extreme ends of an activation spectrum which does not

fully capture the many phenotypes that microglia can exhibit depending on the stimulus. As such, the M2 classification has been expanded into subgroups M2a (response to Th2 activation), M2b (Th2-activating) and M2c (immunoregulation) to account for additional activation phenotypes[220].

Microglial activation in AD has been described as both beneficial and detrimental to the pathogenesis of AD. Microglia can have varying functions and roles depending on the stimuli, disease stage or brain region affected. Typically after exposure to pathology or cellular debris, microglia respond immediately to remove the offending stimuli. In AD, this inflammatory response is sterile where it involves similar receptors but do not have living pathogens associated. This short term or acute response usually resolves pathology with immediate benefit to the microenvironment. However the continuous formation of Aβ in AD causes positive feedback loops between Aβ production and inflammatory responses, characterised by production of inflammatory mediators IL-1, IL-6, IL-12, IL-23, GM-CSF and TNF[221–224] and damaging oxidative radicals[195,225,226], which prevent its resolution.

Thus, chronic exposure to Aβ, cytokines, chemokines and other inflammatory mediators lead to dysfunctional microglia which can be found next to amyloid plaques[227,228]. Supporting this, IL-10-deficient AD mice exhibit lower amyloid burden and increased microglia-mediated phagocytosis of Aβ[229]. Conversely when IL-10 is overexpressed, amyloid burden is increased and phagocytosis of Aβ is impaired[230]. CD33, another microglial-enriched receptor also inhibit phagocytosis of Aβ[187]. The protective gene variant of *CD33* reduces its protein expression due to reduced expression of an RNA isoform with the extracellular immunoglobulin domain[186,187]. CD33-deficient AD mice produce less amyloid than mice with normal CD33 expression[187]. Besides that, decreased expression of microglial autophagy-associated protein Beclin-1 in AD interferes with efficient phagocytosis and lead to dysfunctional receptor recycling of CD36 and TREM2[231]. Beclin-1 is involved in the retromer-mediated sorting of proteins including receptors like TREM2, APP, BACE1 and CD36 in the endolysosomal pathway for degradation[231].

The resolution of inflammation in microglia is just as critical as their activation. Prolonged activation can lead to by-stander damage due to the release of neurotoxic mediators like IL-1β, TNF-α and NO[195]. The resolution has been associated with the conversion from the proinflammatory M1-like state to the alternative M2-like state associated with tissue

repair, phagocytosis of debris and release of anti-inflammatory factors[195]. This conversion was suggested to be linked with the modulation of proinflammatory signalling pathways such as the NLRP3 inflammasome[195].

The role of microglia in neurodegenerative diseases is highlighted by studies on CSF1R signalling. Mutations in the *CSF1R* gene result in white matter disease including hereditary diffuse leukoencephalopathy with axonal spheroids (HDLS)[232–234] and pigmentary orthochromatic leukodystrophy (POLD)[235]. These diseases are associated with white matter degeneration with axonal spheroids and pigmented glia[236]. CSF1R signalling plays a crucial role in microglial activation and proliferation. Microglia in neurodegenerative diseases including prion disease and AD have increased proliferation that is associated with upregulation of CSF1R-mediated mitogenic signalling pathways[237,238]. Pharmacological inhibition of CSF1R signalling in the APP/PS1 mouse model of AD prevented microglial proliferation and resulted in the skewing towards an anti-inflammatory microglial phenotype[238]. This translated into improved cognition and prevented synaptic loss in the mice[238], which demonstrates a beneficial effect of dampening the chronic and neurotoxic microglial activation in neurodegenerative diseases.

In addition to microglia, there is some evidence that infiltrating peripheral macrophages may be involved in inflammatory responses during AD pathogenesis. Some studies have observed plaque-associated myeloid cells that express high levels of CD45 and low P2RY12 that is characteristic of peripheral macrophages[239]. However, the expression levels of CD45 and P2RY12 in microglia can vary depending on stimuli and activation state[240], which could explain the observation of plaque-associated $CD45^{hi}$-$P2RY12^{lo}$ cells. Parabiosis experiments using CD45.2-expressing AD mice and CD45.1 B6 congenic mice do not show any significant infiltration of peripheral macrophages into the brain nor their association with amyloid plaques[241]. However, peripheral macrophage recruitment into the brain has been observed in microglia-deficient AD mice but were ineffective at responding towards amyloid plaques[210,212]. Together, these evidences suggest that microglia are likely to be the dominant plaque-associated immune cell population in AD.

1.5.2 Astrocytes

Besides microglia, astrocytes can also undergo activation or astrogliosis in response to pathology. Astrogliosis usually involves complex, multistage and pathology-specific reactions to provide neuroprotection and recovery of injured CNS tissue[242,243]. In normal physiological conditions, astrocytes are important for the maintenance of synaptic transmission. Dysfunctional astrocytes can lead to cognitive deficits[244–248]. In disease, astrocytes can often be found clustered next to microglia at lesion sites such as amyloid plaques in AD[244,249]. Some studies have suggested that glial activation including microglia and astrocytes may even precede Aβ deposition in AD[250].

Activated or reactive astrocytes are characterised by increased expression of GFAP and signs of dysfunction[245]. *In vivo* studies using AD animal models have detected an early response to disease associated with the loss of astrocytes[244]. The loss of astrocytes appears to follow a spatial and temporal progression that first start in the entorhinal cortex and later progressing to even affecting astrocytes far from amyloid plaques[195]. Like microglia, astrocytes can also release cytokines, NO and other cytotoxic mediators in response to Aβ. This is supported by *in vivo* studies that inhibited a key astrocytic signalling pathway, the calcineurin/NFAT signalling, which decrease astrocytic activation and result in improved cognition and low Aβ load[251]. Besides that, astrocytes *in vivo* can endocytose and degrade Aβ[252] through an APOE-mediated mechanism[253]. Furthermore, lipidation of APOE by astrocytes increases microglial clearance of Aβ[254,255], highlighting a concerted role of microglia and astrocytes in AD. Plaque-associated astrocytes upregulate the expression of extracellular Aβ-degrading enzymes including neprilysin, IDE, endothelin-converting enzyme 2 and angiotensin I-converting enzyme[256], suggesting that the loss of astrocytes in AD may contribute to decreased proteolytic clearance of oligomeric Aβ. Additionally, astrocytes have been implicated in paravenous drainage of soluble Aβ from the brain, a process that is dependent on the astrocytic water channel aquaporin 4[257]. A recent study has described that astrocytes are also capable of activation into a neurotoxic A1 state or neuroprotective A2 state akin to macrophage activation states[258]. The study found that A1 astrocytes are induced by activated microglia and these astrocytes have decreased phagocytic capabilities, are synaptotoxic and highly neurotoxic. Moreover, in microglia-deficient *Csf1r*$^{-/-}$ mice, A1 astrocytes could not be induced[258]. Also, *in vitro* experiments

revealed that IL-1α, TNF-α and C1q could induce these neurotoxic A1 astrocytes[258].

1.5.3 Cytokines

In neurodegenerative diseases like AD, microglia and astrocytes are major sources of cytokines which contribute to inflammatory responses including pro- and anti-inflammation, cytotoxicity and chemotaxis. In aging mouse models of AD, increased amyloid deposition is associated with increased proinflammatory cytokines such as TNF-α, IL-1α, IL-6 and GM-CSF[222]. *In vitro* treatment of microglia with fibrillar $A\beta_{1–42}$ result in increased production of similar proinflammatory cytokines including IL-1β, IL-6, TNF-α, MIP-1α and M-CSF[259]. Besides that, caspase 1 activity, which is crucial to convert inactive IL-1β into its active form, is higher in MCI and AD brains[260]. This leads to the detection of increased IL-1β production by plaque-associated microglia and in CSF[260]. IL-1β signalling may be involved in AD pathogenesis by increasing Aβ deposition by affecting APP expression and its processing[261].

Proinflammatory cytokines produced in AD can be cytotoxic and neurotoxic. In patients, increased TNF-α and decreased TGF-β levels in CSF have been associated with an increased risk of converting from MCI to AD[262]. Supporting this, rheumatoid arthritis patients on anti-TNF-α therapy have a decreased risk of developing AD later in life[263]. The proinflammatory cytokines IL-1β and TNF-α impair neuronal function early by suppressing long-term potentiation (LTP) of synaptic transmission[195]. In *in vitro* studies, treatment of neuron-microglia co-cultures with Aβ and interferon-γ (IFN-γ) or CD40L resulted in the release of TNF-α and reactive oxygen species (ROS)[264–266]. Similarly, stimulation of the TLR4 receptor elevated TNF-α and MIP-1α levels in AD mouse models[267].

Interestingly, some of the same proinflammatory responses have been shown to be beneficial, at least in AD mouse models. Decreased amyloid plaque burden have been observed from transgenic TNF-α AD mice, which has been associated with increased microglial activation[268]. Besides that, increased expression of IFN-γ, IL-6 or TNF-α enhance clearance of amyloid exhibited by decreased soluble Aβ and amyloid plaque burden, which are associated with increased microglia and astrocyte activation[269–271]. Additionally, transgenic expression of IL-1β also induce inflammatory responses and decrease amyloid plaque

deposition[272,273].

1.5.4 Chemokines

Chemokines function to recruit microglia to sites of neuroinflammation in response to AD pathology in the CNS[274]. In the AD brain, increased expression of CCL2, CCR3 and CCR5 in microglia[275,276] and CCL4 in plaque-associated astrocytes[275] have been observed. CCR2 and CCR5 modulate AD progression through its role in inducing chemotaxis in microglia[277–280]. Besides that, experimental *in vitro* treatment of Aβ cause production of CXCL8, CCL2 and CCL3 in microglia and astrocytes[281,282]. Additionally, CX3CL1/CX3CR1 (fractalkine and its receptor) signalling between neurons and microglia mediate neuronal survival[283] and protect against cognitive deficits[284] in AD mouse models. Interestingly, CX3CR1 deficiency reduces amyloid plaque burden and is associated with enhanced microglial Aβ phagocytosis[285]. This could be due to elevated expression of IL-6 and TNF-α observed in CX3CR1- or CX3CL1-deficient animals[286] resulting in activation of microglia to mediate clearance of Aβ.

1.5.5 Nitric oxide and reactive oxygen species

Proinflammatory cytokines can stimulate the expression of inducible nitric oxide synthase (iNOS) in microglia and astrocytes to produce the cytotoxic NO[195]. iNOS is upregulated in the AD brain[287]. In contrast, iNOS deficiency in AD mice appears to be neuroprotective, reducing premature mortality, amyloid burden, protein tyrosine nitration, and activation of astrocytes and microglia[288]. However, there are differences in the production of NO in human macrophages compared to rodent macrophages[289–293], which can affect the interpretation of NO-related findings in rodent AD models. The synthesis of NO in mice from L-arginine requires arginase and the synthesis of the co-factor tetrahydrobiopterin. These systems are not functional in human macrophages and thus, they do not produce NO[294,295]. Even so, NO production in humans do occur but in other cell types such as hepatocytes and smooth muscle cells[296,297].

Another source of cytotoxic molecules in inflammation is from NADPH oxidase which produces ROS. NADPH oxidase expression is enriched in microglia and is upregulated in

AD and after Aβ treatment *in vitro*. This leads to the production of hydrogen peroxide (H_2O_2) which itself can activate microglia[225,226]. H_2O_2 can also react with NO to form peroxynitrite, a strong oxidising and nitrating agent that can damage DNA and proteins[298]. Oxidative stress can induce the nitration of Aβ peptides at the tyrosine 10 residue and this increases its propensity to aggregate[299,300]. Nitrated Aβ is found in the core of amyloid plaques and has been shown to induce plaque formation in AD mice[300]. Moreover, nitrated Aβ can suppress hippocampal LTP more effectively than unmodified Aβ[300].

1.5.6 Caspases

Caspases are cysteine-aspartic proteases commonly associated with apoptosis and inflammation. While ubiquitously expressed in most cells, in microglia, caspase-1 is not only involved in apoptosis but also the autocatalysis and the subsequent conversion of inactive IL-1β and IL-17 into their active forms[301,302]. Caspase-1 involvement in microglial apoptosis is established by the prevention of chromogranin A-induced apoptosis with IL-1β-converting enzyme-like caspase inhibitor YVAD-CHO or caspase-1 inhibitor z-Tryp-Glu(OMe)-His-Asp(OMe)-fluoromethyl ketone[303,304]. The role of caspase-1 in mediating microglial apoptosis is unaffected by changes in active IL-1β production as the blocking of IL-1β activity with antibodies did not prevent apoptosis[304]. Caspase-1 activity is regulated by signal-dependent autoactivation within inflammasomes[301,302]. One form of inflammasome, NLRP3, is found to be activated by Aβ fibrils by lysosomal damage in microglia[305]. AD mice deficient in NLRP3 or caspase-1 are protected from cognitive deficits associated with AD[260]. The lack of NLRP3 or caspase-1 appear to shift microglial activation from the proinflammatory M1-like state to the alternative anti-inflammatory M2-like phenotype[260]. Other caspases involved in neuroinflammation include caspase-8 and caspase-3/7, which are found activated in microglia responding to various proinflammatory factors *in vitro* and in microglia within AD brains[195,306]. Activated caspase-3 has been shown to modulate NFκB activation through PKCδ that results in the production of proinflammatory and cytotoxic factors such as IL-1β, TNF-α and NO[307–309]. Inhibition of these caspases suppresses microglial activation and neurotoxicity, and thus has neuroprotective effects[307–309].

1.5.7 Complement system

The complement system is a major component of the innate immune system involved in the response against pathogens. Activation of the complement cascade by specific immune responses lead to the opsonisation and lysis of invading microorganisms through the action of the membrane attack complex[310]. Although components of the complement system are primarily synthesised by hepatocytes, microglia and astrocytes in the CNS can express most of the proteins involved in the complement system in response to injury[311,312]. Multiple elements of the classical complement cascade (C1q, C3d, C4d, C5b–C9) have been detected in AD brain tissue[313] and complement receptors such as CR3 have been found around amyloid plaques[314]. In addition, *in vitro* studies found that Aβ can activate the complement system[314], suggesting that Aβ may act as a mimic for pathogenic microorganisms.

Complement and microglia appear to mediate synaptic pruning during brain development[315,316] and synaptic loss in early AD[317]. Super-resolution microscopy revealed increased C1q and C3 colocalisation with PSD95, a post-synaptic marker, in the hippocampus of J20 mouse model of AD overexpressing human APP carrying two familial AD mutations compared to WT mice[317]. This suggests that there are more synapses targeted with components of the complement system for removal by microglia. When *C1qa* and *C3* are knocked out from J20 or APP/PS1 mice, the characteristic synaptic loss was ameliorated[317], further suggesting that the complement pathway is involved in the microglia-mediated elimination of synapses in AD. Indeed, all CR3-expressing cells also express P2RY12, indicating that they are resident microglia[317]. Furthermore, CR3 KO mice rescued synaptic loss compared to WT mice when treated with synaptotoxic soluble Aβ oligomers[317].

Recently, gene variants of *CLU* encoding clusterin/apolipoprotein J (ApoJ) and *CR1* encoding complement receptor 1 have been associated with AD[113,114]. Both clusterin and complement receptor 1 are inhibitors of the complement system. Clusterin can bind directly to and inactivate C7, C8β and the b domain of C9[318]. On the other hand, complement receptor 1 acts as a competitive inhibitor to several complement convertases and promotes the clearance of opsonised immune complexes[319].

1.5.8 Systemic inflammation

Systemic inflammation appears to play a role in the pathogenesis of neurodegenerative diseases including AD. For example, upper respiratory tract infections are associated with approximately 33% of relapses in multiple sclerosis patients[320,321]. Besides that, delirium caused by infection is associated with developing cognitive impairment and increased risk of dementia[322]. AD patients with delirium is also associated with an increased rate of cognitive decline[323,324]. Similarly, acute systemic inflammation in AD patients associated with elevated serum TNF-α result in an increased rate of cognitive decline[325]. This is in contrast with AD patients with lower serum levels of TNF-α that remained cognitively stable during the study[325]. In animal models of AD, such as human APP transgenic mice, systemic LPS injection results in increased production of IL-1, amyloid deposition and cognitive impairment compared to control mice[326].

Systemic inflammation could impact neurodegenerative diseases through microglial priming, in which microglia exhibit an exaggerated inflammatory response after exposure to an initial stimuli[327]. Neuronal and glial injury in early chronic neurodegeneration has been suggested to induce microglial activation and priming[327]. When this is combined with systemic inflammation, the cytokines produced could result in excessive activation and inflammatory response of microglia associated with increased production of IL-1, TNF and IL-6[328–330].

1.6 Triggering receptor expressed on myeloid cells 2

Rare homozygous mutations in the triggering receptor expressed on myeloid cells 2 (TREM2) receptor have been found in people with polycystic lipomembraneous osteodysplasia with sclerosing leucoencephalopathy otherwise known as Nasu-Hakola disease (NHD). NHD is characterised by dementia, changes in the brain white matter and bone cysts associated with bone fractures[331]. The onset of clinical symptoms in NHD can begin as early as the second decade of life[332]. Some of these homozygous mutations can also cause a frontotemporal dementia (FTD)-like syndrome but without bone involvement[333]. Recently, it is found that additional rare heterozygous variants in the *TREM2* gene increase the risk of developing AD by 2.65–4.35 fold[109,110,334–337] (Table 1.1). The most common and established AD risk variant of TREM2 in Caucasian populations is the rs75932628, which results in the p.R47H amino acid substitution. It has a minor allele frequency (MAF) of 0.0012–0.0063 in healthy populations[110] and 0.009–0.02 amongst AD cases[109]. Other TREM2 variants have since been associated with AD and other neurodegenerative diseases including Parkinson's disease, FTD and amyotrophic lateral sclerosis, with varying MAFs in different populations (Table 1.1).

Amino acid change	Gene variant	SNP ID	Associated disease(s)	Population(s)	MAF (%)	OR (95% CI)	References
p.Q33X	c.97C>T	rs104894002	AD	Caucasian	0.15	7.21 (1.28–40.78)*	[338]
			FTD/FTLD	Italian	0.9	N/A	[339]
			PD	Han Chinese	0	N/A	[340]
			NHD	‡	–	–	[341–343]
p.Y38C	c.113A>G	rs797044603	AD	Caucasian	0.27	ns	[109]
			FTD/FTLD	‡	–	–	[333,344]
			NHD	‡	–	–	[342]
			PD	Han Chinese	0	N/A	[340]
p.W44X	c.132G>A	rs104894001	NHD	‡	–	–	[331]
p.R47H	c.140G>A	rs75932628	AD	Caucasian	0.12–2	3.40 (2.65–4.35)*	[109,110,334–338]
				African American	0.11	ns	[345]
				East Asian	0.02	ns*	[340,346–354]
			ALS	Caucasian	0.45	2.40 (1.29–4.15)	[355]
				Han Chinese	0	N/A	[350]
			FTD/FTLD	Caucasian	2.1	5.06 (1.9–13.51)	[356]
			MSA	Han Chinese	0.12	ns	[347]
			PD	Caucasian	0.3–1.32	2.67 (1.13–6.33)	[335,356]
				Spanish	0.45	N/A	[335]
				Han Chinese	0–0.2	ns	[340,347–349]
			PSP	Caucasian	0.6	ns	[356]
			Stroke	Caucasian	0.7	ns	[356]
p.R62H	c.185G>A	rs143332484	AD	Caucasian	1.53	1.65 (1.24–2.21)*	[338,357]
				African American	0.17	ns	[345]
			PD	Han Chinese	0	N/A	[340]
p.T66M	c.197C>T	rs201258663	AD	Caucasian	0.09	ns	[109]
			FTD/FTLD	‡	–	–	[333,344,358]
			PD	Han Chinese	0	N/A	[340]
			NHD	‡	–	–	[342]

Amino acid change	Gene variant	SNP ID	Associated disease(s)	Population(s)	MAF (%)	OR (95% CI)	References
p.W78X	c.233G>A	rs104893998	NHD	‡	–	–	[331]
p.D86V	c.257A>T	novel	FTD/FTLD	‡	–	–	[344]
p.D87N	c.259G>A	rs142232675	AD	Caucasian	0.55	N/A	[109,359]
				African American	0.06	ns	[345]
			PD	Han Chinese	0	N/A	[340]
p.T96K†	c.287C>A	rs2234253	AD	Caucasian	0.37	ns	[109]
			FTD/FTLD	Caucasian	0.5	N/A	[360]
			PD	Han Chinese	0	N/A	[348]
p.A105V	c.314C>T	rs145080901	AD	African American	0.2	ns	[345]
p.V126G	c.377T>G	rs121908402	NHD	‡	–	–	[342]
p.D134G	c.401A>G	rs28939079	NHD	‡	–	–	[331]
p.E151K	c.451G>A	rs79011726	AD	African American	0.35	ns	[345]
p.H157Y	c.469C>T	rs2234255	AD	Han Chinese	0.4	11.01 (1.38–88.05)	[361]
				Caucasian	0.36	ns	[109]
p.K186N	c.558G>A	rs28937876	NHD	‡	–	–	[331]
p.W191X	c.572G>A	rs2234258	AD	African American	3.96	ns	[345]
p.W198X	c.594G>A	novel	FTD/FTLD	‡	–	–	[334]
p.L211P†	c.632T>C	rs2234256	AD	African American	12.67	1.27 (1.05–1.54)	[345]
				Caucasian	0	N/A	[109]
			FTD/FTLD	Caucasian	0.5	N/A	[360]

Table 1.1. Disease-associated TREM2 variants.
Population-specific minor allele frequencies (MAFs) shown if available. Odds ratio (OR) shown for variants significantly associated with disease.
*: meta-analysis, †: in linkage disequilibrium, ‡: family/individual studies, ns: no statistical significance.
AD: Alzheimer's disease, ALS: amyotrophic lateral sclerosis, FTD: frontotemporal dementia, FTLD: frontotemporal-like dementia, NHD: Nasu-Hakola disease, PD: Parkinson's disease, PSP: progressive supranuclear palsy.

1.6.1 *TREM2* gene expression

The *TREM2* gene is located on chromosome 6q21.1 clustered with other TREM family genes, including *TREM1*, *TREM4*, *TREM5*, *TREML1* and *TREML2*[362]. Three alternatively spliced transcripts are expressed from the human *TREM2* gene[357]. The longest transcript produces isoform 1, a transmembrane protein with 230 amino acids residues which is the most highly expressed isoform in human brain[363]. The other splice variants produce 219- and 222-amino acid isoforms that lack the transmembrane domain and the resulting proteins are predicted to be secreted. The 219-amino acid isoform has a lower expression in the hippocampus of AD brains compared to isoform 1[364] whereas the expression pattern of the 222-amino acid isoform is still unknown[362].

The expression of *TREM2* is regulated by various factors including transcription factors, epigenetics and post-transcriptional processing. Binding sites for transcriptional factors such as PU.1, the master regulator of myeloid cell fate[365], and retinoid X receptor (RXR)[366] are found in the promotor sequences of *TREM2* or upstream of the *TREM* gene cluster. Increased binding of RXR at this locus is observed only in AD mice but not WT mice when treated with a RXR agonist[367], suggesting that expression of *TREM* genes may be modulated in a disease-specific context. Furthermore, it has been suggested that the transcription factor NFκB may negatively regulate *TREM2* expression through a microRNA34a-mediated mechanism[368–373].

Besides that, evidence of epigenetic modulation of *TREM2* expression have been found. A marker of active demethylation, 5-hydroxymethylcytosine (5hmc), on the transcriptional start site of *TREM2* positively correlate with *TREM2* mRNA levels in the hippocampus of human brains[363]. Other forms of epigenetic changes in AD include increased methylation upstream of the *TREM2* transcription start site that positively correlate with TREM2 protein expression[134]. Conversely, decreased methylation of CpG sites in Intron 1 of *TREM2* in leucocytes of AD patients correlate with lower *TREM2* mRNA[374]. Moreover, histone-associated epigenetic markers of active gene transcription H3Kme2 and H3Kme3 are increased at the *TREM2* locus in differentiating dendritic cells and macrophages[375] as well as in *db/db* mice (model for diabetic dyslipidaemia)[376]. Both cases have elevated *TREM2* mRNA levels, indicating that histone modifications can modulate *TREM2* expression.

Activation of TLR signalling significantly decrease the half-life of *TREM2* mRNA in human-derived peripheral blood mononuclear cells (PBMC)[377], suggesting that there may be post-transcriptional downregulation of TREM2 by pro-inflammatory TLR signalling occurring in AD.

1.6.2 TREM2 protein

The TREM2 protein is a single-pass transmembrane receptor with an extracellular V-type immunoglobulin (Ig) domain[378] containing N-linked glycosylation sites[379–382]. TREM2 has a short cytoplasmic tail with no known function[383] and therefore must associate with the intracellular signalling adaptor protein DNAX-activation protein 12 (DAP12), encoded by *TYROBP*, to mediate downstream signalling[380,384–386]. Binding between TREM2 and DAP12 occurs at the lysine residue 186 on TREM2 and aspartic acid residue 50 on DAP12 on their respective transmembrane domains[387–389] (Figure 1.4).

On TREM2 activation, tyrosine residues within the immunoreceptor tyrosine-based activation motif (ITAM) on DAP12 become phosphorylated by PKC at residues 79–81 and by Src-family kinases at residues 85–88[390]. Src-family kinases consist of eight proteins with a similar domain arrangement that can be grouped into two subfamilies: Src-related (Src, Fgr, Fyn, Yes) and Lyn-related (Lyn, Blk, Hck, Lck)[391]. The expression of Src-family kinases can vary between cell types[392] and it is not fully established which of these mediate the phosphorylation of DAP12 ITAMs after TREM2 activation. The phosphorylated tyrosine residues on DAP12 ITAMs then become binding sites for Syk (Figure 1.4). Syk further activates downstream signalling cascades including phosphatidylinositol 3-kinase (PI3K)–Akt, mitogen-activated protein kinases (MAPKs), Rac, Vav and intracellular Ca^{2+} mobilisation through IP3-gated Ca^{2+} stores[380,384,393–400]. Activation of TREM2 and subsequent signalling cascades result in immune-related responses such as phagocytosis, cell migration, proliferation, survival and production of cytokines and chemokines[401].

TREM2 is predominantly expressed in myeloid cells including mononuclear phagocytes such as dendritic cells[375,380,402–405], granulocytes[406], bone marrow- and monocyte-derived macrophages[375,403,405,407,408], and tissue macrophages such as microglia[384,402,409–417], osteoclasts[385,418,419], Kupffer cells[420], alveolar macrophages[421,422] and splenocytes[384]. There

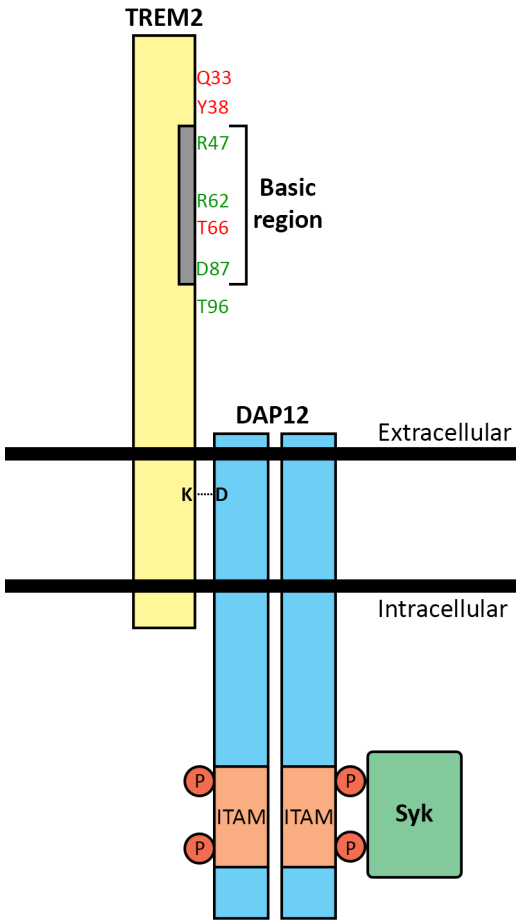

Figure 1.4. TREM2 associates with DAP12 to mediate downstream signalling. Binding between these proteins occurs at lysine (K) residue 186 on TREM2 and aspartic acid (D) 50 on DAP12. The extracellular basic region on TREM2 is associated with anionic ligand binding which results in phosphorylation of tyrosine residues in the ITAM of DAP12 and recruitment of intermediate signalling proteins. TREM2 variants associated with NHD (red) and AD (green) affect protein function.
Figure adapted from Ulrich *et al.* (2017)[362].

are some contradicting evidence for TREM2 expression in monocytes with some studies reporting a lack of TREM2 expression in circulating monocytes[241,375,402,405,423] and others that did detect TREM2 expression in whole blood[374,424–426]. Meanwhile, microglial expression of TREM2 is well established, although several *in vivo* studies have observed that only a subset of microglia appear to express TREM2[394,427–430]. In the brain, TREM2 is highly expressed but not limited to cells in the white matter[402,431], hippocampus[402,416,431] and spinal cord[331,416]. This expression pattern is likely to reflect the high density of microglia in these regions[402].

TREM2 is normally located intracellularly[432] on membranes associated with the trans-Golgi network[416,433,434] and in exocytic vesicles[434]. The translocation of TREM2 to the cell surface membrane appears to be mediated by an increase in intracellular Ca^{2+} levels[434] that occurs on immune activation. Membrane-bound TREM2 also appears to be recycled in clathrin-coated vesicles mediated by Beclin-1[231] and Vps35[231,435]. When TREM2 recycling is inhibited, the receptor associates with lysosomes and is proteolytically degraded[435].

1.6.3 TREM2 ligands

It is not entirely clear what the *in vivo* ligands of TREM2 are, nor which are the most relevant to AD. Several *in vitro* experiments and binding assays have identified lipid components of the cell membrane, lipoproteins, nucleotides and other anionic molecules as candidate ligands[378,423,429,436–439]. ApoE, which is the major apolipoprotein in the CNS and is strongly associated with AD risk, was found to bind to TREM2[106–108,440]. The lipidated form of ApoE binds to TREM2 at a much higher affinity than its non-lipidated form[108]. However, TREM2 appears to bind all ApoE isoforms equally, so this interaction does not appear to connect these two risk genes to AD vulnerability[108,440]. ApoE can also bind to apoptotic cells[106] and Aβ[103,104,441], suggesting that TREM2 may indirectly bind to these and mediate phagocytosis through ApoE[383]. Additional apolipoproteins such as ApoA1, ApoB and ApoJ/clusterin, particularly when lipidated, can also bind to TREM2[108]. High-density lipoprotein (HDL) and low-density lipoprotein (LDL) also activate TREM2 signalling, potentially through their lipid moieties[108,423]. In addition, TREM2 can bind heparin sulfate proteoglycans and other negatively charged carbohydrates[378] as well as high molecular weight nucleic acids[429] and heat-shock protein 60 (Hsp60)[442].

Some studies have suggested that TREM2 can modulate myeloid cell activity in response to bacterial components[443]. TREM2 binds to some bacteria including *S. aureus*, *E. coli* and *F. tularensis*[444,445] but not *S. cerevisiae*[439,446], *Salmonella* or *Typinmurin*[447]. Furthermore, toxins from pertusis[448] and cholera[449] have been observed to bind to TREM2.

There have been reports of several unidentified TREM2 ligands found on the surface of macrophages[450], astrocytoma[439], dendritic cells[451], neuroblastoma[378,412], monocytes[378] and apoptotic cells[429]. TREM2 deficiency leads to the impairment of microglial responses against apoptotic cells[108,412,429] and it has been suggested that TREM2 binding to apoptotic cells can occur through externalised phosphatidylserine[412] or myelin debris from neuronal death[437].

1.6.4 Effects of disease-associated variants on TREM2 protein

NHD-associated TREM2 variants like the p.Q33X, p.Y38C and p.T66M result in the functional loss of TREM2. The p.Q33X results in premature truncation of the protein whereas p.Y38C and p.T66M impair trafficking of TREM2 to the cell surface[378,379,432,452,453]. The latter variants cause the protein to accumulate in the endoplasmic reticulum[379,452] and lead to an increase in proteosomal degradation of TREM2[393]. Structural studies reveal that these residues are located within the Ig fold and these amino acid changes disrupt disulfide bonds and protein folding of TREM2, which result in decreased protein stability[333,378]. The p.T66M variant may also affect gene expression as decreased *TREM2* mRNA is found in carriers of the variant[454]. Despite this, the p.T66M variant appears to enhance TREM2-DAP12 binding when expressed[432]. The NHD-associated variants suggest that other disease-associated TREM2 variants are likely to increase disease risk through loss of normal TREM2 function.

The most frequent AD-associated p.R47H variant does not appear to impact protein folding, trafficking, stability or the levels of mRNA or protein[364,378,423,438,452,455]. However, there have been mixed findings on the effect of p.R47H on the maturation of TREM2. An *in vitro* study found decreased glycosylation of TREM2 with p.R47H[452] whereas human studies have reported no difference in glycosylation levels[364] but instead saw changes in glycosylation patterns[379,382]. Another study reported that the TREM2 p.R47H variant

appears to increase lysosomal degradation, which is mediated by decreased association with Vps35[435].

Variants located on the extracellular domain is found to impact ligand binding rather than alter protein structure. The p.R47H, p.R62H and p.D87N variants have been reported to decrease ApoE binding to TREM2[106,108,378]. In addition, p.R47H and p.R62H also decrease proteoglycan binding to TREM2[378]. Conversely, p.T96K appears to have an opposite effect by increasing TREM2 binding affinity to proteoglycans[378]. Electrostatic mapping and structural analyses reveal that the p.R47 and p.R62 residues are located within a large basic region associated with binding of anionic ligands[378] (Figure 1.4). On the other hand, the p.T96 residue is located adjacent to this basic region and the p.T96K variant is predicted to extend the basic ligand binding region and enhance affinity for anionic ligands[378] (Figure 1.4).

In contrast, variants within the stalk region of TREM2 including p.R136W, p.E151K and p.H157Y or the intracellular domain such as p.L211P are not expected to affect ligand binding[383]. Recently, it has been suggested that the p.H157Y variant may enhance TREM2 cleavage by ADAM10 and ADAM17 to produce soluble TREM2 (sTREM2)[456].

1.6.5 TREM2 and Alzheimer's disease

1.6.5.1 TREM2 effects in AD

A weighted gene co-expression network analysis in several AD mouse models has highlighted *Trem2* as a central gene in an immune-enriched gene module which also contains other AD risk genes such as *Cd33*, *Inpp5d* and *Ms4a6d*[457]. A Bayesian network analysis of gene expression in late onset AD patients found that *TYROBP* (DAP12) is highly upregulated and appears to be a key regulatory gene within a complement-enriched gene module[185,457]. Additionally, TREM2 protein expression is increased in AD brains[363,364,409,458–462] and AD mice[239,417,433,457,463–465], which correlated with amyloid burden[417,466,467] especially in plaque-associated microglia[461,462,468–470]. AD tau mouse models also exhibit increased TREM2 expression[457,471]. The increase in TREM2 expression levels after NFT pathology is well established in these mice[457] and consistent with increased TREM2 levels in the

later stages of human AD[461]. Together, these findings highlight the role of innate immune responses mediated by TREM2 in microglia during AD progression.

1.6.5.2 TREM2 and plaque-associated microglia

Studies using AD mouse models have consistently shown that TREM2 mediates microglial clustering around amyloid plaques. AD mice haploinsufficient or deficient for TREM2 have fewer plaque-associated microglia[239,241,438,468,470,472], especially in younger mice at the very early stages of pathology[241,468]. Two of these studies have also observed decreased total microglial population[241,468]. Similarly, there are fewer plaque-associated microglia in DAP12-deficient AD mice[470]. In humans, AD patients with the TREM2 p.R47H variant also have fewer plaque-associated microglia compared to AD patients without TREM2 variants[470,473]. These similar observations between TREM2-deficient mice and AD patients with the p.R47H variant support the view that the variant conveys a loss-of-function of TREM2.

1.6.5.3 Role of TREM2 in microglia

High-resolution microscopy of plaque-associated microglia in AD mouse models revealed microglial processes in contact with amyloid fibrils are highly enriched with TREM2, DAP12 and phosphorylated tyrosine residues that indicate increased activation of the TREM2–DAP12 signalling pathway[470]. In haploinsufficient or TREM2-deficient and DAP12-deficient AD mice, amyloid plaques appear less compact[241,470]. Amyloid plaque filaments are longer in TREM2-deficient mice which suggest that TREM2 function is crucial for microglia-mediated capping of amyloid filament growth and plaque compaction[470]. AD patients with TREM2 p.R47H variant also exhibit a relative increase in the number of filamentous, uncompacted plaques similar to amyloid plaque morphology in TREM2-deficient mice[470].

These findings suggest that microglial processes surrounding amyloid plaques may function to limit exposure of neurotoxic protofibrillar Aβ to adjacent neurons[474]. Supporting this, regions of amyloid plaques with the highest $A\beta_{1–42}$ incorporation also have increased microglial presence and tend to have increased numbers of dystrophic axons[474]. Consistent with this, TREM2- and DAP12-deficient AD mice and AD patients with TREM2 p.R47H

variant exhibit a greater level of plaque-associated dystrophic axons[241,470]. Thus, loss of TREM2 function may result in neuronal damage from increased exposure to neurotoxic Aβ due to failure of microglia to form a protective barrier around amyloid plaques.

A study has suggested that peripherally-derived macrophages contribute to the TREM2-expressing cell population in the CNS[239]. TREM2 is found expressed on $CD45^{hi}$–$Ly6C^{+}$–$P2RY12^{-}$ cells, which are associated with peripheral monocytes, in the brain[239]. It has been recently reported that TREM2 expression in post-mortem human brains is exclusive to intravascular and invading monocytes[475]. In that study, Iba-1-expressing microglia and perivascular macrophages were found to be TREM2-negative[475], suggesting that disease-causing mechanisms due to TREM2 variants may not originate in CNS microglia.

1.6.5.4 TREM2 and amyloid pathology burden

Despite consistent observations on the effects of dysfunctional TREM2 on plaque-associated microglia, the role of TREM2 on amyloid plaque burden is still unclear. While TREM2 haploinsufficiency in APP/PS1 mice did not affect cortical amyloid burden compared to normal TREM2[472], complete deficiency of TREM2 in APP/PS1 mice appear to have age-dependent effects on amyloid deposition. In these TREM2-deficient APP/PS1 mice, at 2 m old they have decreased cortical amyloid burden, at 4 m old mice they have similar cortical amyloid burden and at 8m old they have increased cortical amyloid burden compared to control APP/PS1 mice[239,468]. In the 5XFAD mouse model, cortical and hippocampal insoluble $A\beta_{1–42}$ and $A\beta_{1–40}$ load is not affected by TREM2 deficiency at 4 m[241] whereas at 8.5 m, insoluble $A\beta_{1–42}$ and $A\beta_{1–40}$ load is increased in the hippocampus but not in the cortex of TREM2-deficient 5XFAD mice[438]. The differences observed may be due to differences in the AD mouse models used that affected the rate of amyloid accumulation.

AD cases with the TREM2 p.R47H variant have more rapid disease progression than normal[473], but their degree of amyloid plaque deposition compared to other people with AD is less clear. Some studies do not see a difference[476] while others find increased amyloid plaque deposition[455] in AD cases with the TREM2 p.R47H compared to AD cases without TREM2 variants. Mechanisms in which TREM2 modulate amyloid burden is still not completely understood but evidence so far indicate that dysfunctional TREM2

impairs phagocytosis and clearance of amyloid by microglia. Alternatively, findings from a genome-wide siRNA screen indicate that TREM2 signalling could alter APP processing and therefore the production of Aβ[477].

1.6.5.5 TREM2 and neuritic dystrophy

TREM2-deficient AD mice[241,470] and AD cases with the TREM2 p.R47H variant[455] exhibit increased neuritic dystrophy around amyloid plaques. In contrast, overexpressing TREM2 increases the levels of synaptophysin, a synaptic marker, in 7-m but not 18-m old AD mice, hinting that increased TREM2 signalling may be protective against Aβ-mediated synaptotoxicity[417,478]. It has been suggested that larger, diffuse amyloid plaques associated with the later stages in TREM2 deficiency[468] have higher levels of soluble Aβ[470] which are synaptotoxic and neurotoxic. Indeed, soluble Aβ oligomers can block LTP[479] and induce tau hyperphosphorylation, resulting in its aggregation[480,481]. Therefore, dysfunctional TREM2 may alter microglial cytoskeletal responses to negatively impact microglial clustering and barrier formation around amyloid plaques, which are necessary to restrict neuritic dystrophy[383] as well as being required for effective phagocytosis. In addition, TREM2 may also mediate phagocytosis and clearance of dystrophic neurites[467].

1.6.5.6 TREM2 and tau pathology

Like amyloid pathology, the contribution of TREM2 to tau pathology originating in dystrophic neurites remain uncertain. Studies have observed both increased[241] and decreased[239] tau hyperphosphorylation adjacent to amyloid plaques in TREM2-deficient AD amyloid mouse models. In a recent study using a TREM2-deficient tau mouse model of FTD[482], these mice exhibited decreased brain atrophy with preserved entorhinal and piriform cortex volume and less synapse loss compared to mice expressing TREM2. Thus, an absence of TREM2 which leads to fewer activated microglia and astrocytes may be protective in the context of tauopathies[482]. However, the degree of tau pathology appears to be unaffected by TREM2 deficiency in these mice[482]. In contrast, TREM2 overexpression driven by the *CD11b* promoter results in decreased levels of p-tau in a P301S tau model, which is associated with decreased levels of the tau kinases CDK5 and GSK3β[483]. Conversely,

levels of p-tau is increased when TREM2 expression is knocked down in the same tau model[471]. In AD brains, TREM2 protein levels correlate with the degree of tau pathology in the temporal cortex[458]. Moreover, CSF levels of sTREM2 and tau also correlate in early AD[484]. TREM2 p.R47H AD cases have elevated CSF levels of p-tau compared to the common variant[485,486]. These evidence indicate that TREM2 levels may reflect ongoing neuroinflammation that correlate with the degree of tau pathology in AD.

1.6.5.7 TREM2 and synaptic/neuronal loss

Considering the potential role of TREM2 in modulating amyloid and tau pathology as well as neuritic dystrophy, it is not surprising that TREM2 is also associated with synaptic and neuronal loss. TREM2-deficient AD mice exhibit decreased numbers of neurons in cortical layer V[438]. In contrast, TREM2 overexpression rescues neuronal loss in amyloid[417] and tau[483] mouse models of AD. However, in human AD brains, elevated levels of TREM2 protein positively correlate with cleaved caspase 3 (apoptotic marker) and negatively correlate with SNAP25 (presynaptic marker) in the temporal cortex, indicating increased neurodegeneration[458]. Furthermore, TREM2 expression levels negatively correlate with grey matter volume[426]. Interestingly, TREM2 p.R47H AD cases also exhibit decreased grey matter volume in the temporal cortex and hippocampus[486,487], which is associated with cognitive deficits in old age[110]. While increased TREM2 expression appears to be neuroprotective in mouse models, TREM2 levels in AD seem to reflect the activity of microglia in the clearance of apoptotic neurons in vulnerable brain regions during AD.

1.6.6 TREM2 and phagocytosis

Numerous studies have shown that TREM2 is involved in phagocytosis. TREM2 deficiency *in vitro* impairs phagocytosis of various substrates including apoptotic neurons[106,384,412,429], components of bone[418,488], whole bacteria or bacterial components[381,432,442,452] and lipids[108,393]. In addition, primary microglia with TREM2 deficiency also exhibit dysfunctional phagocytosis of bacteria, fluorescent beads and $A\beta_{1-42}$ fibrils[417,452]. TREM2-deficiency in N9 microglial cells and bone marrow-derived macrophages (BMDM) also impair uptake and clearance of $A\beta_{1-42}$ and amyloid plaques from brain slice cultures from AD mice[489].

Conversely, increased TREM2 signalling by ligand binding or overexpression enhances phagocytosis[384,394,417]. TREM2 levels appear to correlate with phagocytosis of $A\beta_{1–40}$ in BV2 microglia with TREM2 knock down or overexpression[428]. Moreover, TREM2-deficient primary microglia are ineffective at phagocytosing lipoproteins such as ApoJ/clusterin and LDL[108]. By extension, phagocytosis of $A\beta_{1–42}$ fibrils complexed to clusterin or LDL by these microglia is also decreased[108]. Monocyte-derived macrophages from AD patients with TREM2 p.R62H have lower uptake of Aβ-LDL complexes and Aβ fibrils than those without the variant[108]. Interestingly, the loss of TREM2 function can be rescued by anti-inflammatory TGF-β stimulation. TREM2-deficient primary microglia treated with TGF-β have comparable levels of phagocytosis of apoptotic cells and Aβ to cells with intact TREM2[438,490].

Together, these findings suggest that TREM2-mediated phagocytosis may require lipoprotein interaction with the phagocytic substrate for efficient uptake and may be affected by microglial activation state. However, there are conflicting evidence that TREM2 activation alone is sufficient to trigger phagocytosis independent of substrate. TREM2 activation by Hsp60 increase phagocytosis of bacteria[442], indicating that specificity of phagocytosis could be mediated by other receptors. Supporting this, MerTK, Fc-gamma receptor (FcγR) and components of the complement cascade which are implicated in phagocytosis are associated with TREM2 expression[402,465]. Studies that stimulated TREM2-deficient N9 microglia or BMDM with antibodies against fibrillar $A\beta_{1–42}$ observe increased FcγR-mediated phagocytosis but this did not return to TREM2 WT levels[489]. Besides that, C1q expression increase with phagocytosis in TREM2-deficient alveolar macrophages[491]. Thus, TREM2 is not the only receptor involved in phagocytosis and is likely to function in concert with other receptors to to mediate clearance of pathology.

TREM2-mediated phagocytosis appears to be modulated by proinflammatory signals. On LPS treatment, the correlation between TREM2 expression and phagocytosis of Aβ by BV2 microglia is lost[428]. Similarly, in an *in vivo* model of sepsis, LPS treatment result in the failure for injected myeloid cells overexpressing TREM2 to enhance phagocytosis of bacteria compared to untreated mice[492]. Curiously, phagocytosis through TREM2 can be dependent on the cell type. BMDM from TREM2-deficient mice have decreased phagocytosis but TREM2-deficient alveolar macrophages appear to have increased phagocytosis of

bacteria[491].

Disease-associated variants largely impair TREM2 function including phagocytosis. In microglia, the p.R47H[435] and p.R62H[108] variants has been reported to impair phagocytosis. Evidence suggests that there may be variant-specific effects on the phagocytosis of different substrates. TREM2 p.Y38C, p.R47H and p.T66M variants impair phagocytosis of polystyrene beads whereas p.Y38C and p.T66M but not p.R47H impair phagocytosis of *E. coli* particles[452].

There are some studies that suggest TREM2 may be involved in lysosomal degradation of phagocytosed substrates. Gene network analyses have shown that lysosomal-associated genes are co-regulated with TREM2 in the brain and in monocyte-derived macrophages[402]. In addition, the uptake of myelin debris by TREM2-deficient microglia is not impaired but the debris remain in the cells longer than TREM2-expressing microglia in a study using models of demyelination[493]. Furthermore, bacterial uptake is unaffected by TREM2 deficiency in macrophages but they are unable to kill and degrade the bacteria[399]. Even so, degradation of $A\beta_{1-42}$ appears not to be altered by TREM2-deficient primary microglia[417], suggesting that impaired phagocytosis by the loss of TREM2 function may be dependent on the ligand and phagocytic substrate.

1.6.7 TREM2 and modulation of inflammatory responses

TREM2 expression is found to be co-regulated with the expression of pro- and anti-inflammatory-associated genes in the brain[402]. Proinflammatory stimulation *in vitro* using TNF-α[369,380], IL-1β[369,380,485], ROS[369,494], IFN-γ[495], TLR agonists including LPS[380,381,405,427,494–497], CpGs[498] and other ligands[377,408,409,427], mitochondrial lysates[499] and bacteria[491] decrease TREM2 expression. Conversely, anti-inflammatory mediators such as vasoactive intestinal peptide[500] and IL-4[495] increase TREM2 expression.

On the other hand, *in vitro* knockdown of TREM2 expression increase levels of proinflammatory mediators including iNOS, TNF-α, IL-1β and IL-6[435] after cells are stimulated with neuronal debris[384], $A\beta_{1-42}$[417] and TLR activation[381,394,495,497,501]. Interestingly, ROS production in response to bacteria is lower with TREM2 knockdown[399,447]. Likewise, *in vitro* LPS treatment of TREM2-deficient primary microglia lead to exaggerated release of

proinflammatory cytokines like IL-1β and TNF-α compared to TREM2-expressing primary microglia[496].

In *in vivo* models, increased TREM2 expression is generally associated with inflammatory responses. Inflammatory stimuli such as cigarette smoke, bacterial and viral infection, and acute injury in the lungs increase TREM2 expression in alveolar macrophages[421,491,500,502–506]. Besides that, high fat diet is associated with increased numbers of Iba-1- and CD68-expressing cells in the brain[507] as well as increased immune-related gene expression (*CCL5*, *CD97*, *IL10RB*) in adipose tissue which coincides with increased TREM2[508]. Increased TREM2 expression is also observed in numerous other proinflammatory conditions including sepsis[492], rheumatoid arthritis[509], corneal infection[395], macular degeneration[369], glioma[510], cancers of the mouth[511], oesophagus[512] and liver[513], after prosthetic joint implants[514], osteoporosis[515], mucosal injury of the colon[516], colitis[517], gastrointestinal mucositis[518] and muscular sarcoidosis[519]. Furthermore, in neurological diseases other than AD, TREM2 levels are increased in traumatic brain injury (TBI)[520,521], stroke[429,522], spinal nerve transection[523], amyotrophic lateral sclerosis[355], Parkinson's disease[524], prion disease[415,525], demyelination[394,410,437,526,527] and also after Aβ vaccination[528]. Moreover, TREM2 expression is also positively correlated with aging in mice[433,529] and humans[402]. This is likely because aging is associated with chronic systemic inflammation[530].

Loss of TREM2 function in *in vivo* models appears to result in different immune responses depending on disease. TREM2 knockdown in a tau model of AD and an aging mouse model increase levels of proinflammatory cytokines[460,529]. A TREM2-deficient model of colonic mucosal injury also increase the production of IFN-γ, TNF-α and iNOS[516]. On the other hand, decreased expression of proinflammatory cytokines is observed in other TREM2-deficient models of AD amyloid[239,438,468], TBI[520], stroke[522], lung infection[491,502] and demyelination[437]. Conflicting observations are also seen in studies overexpressing TREM2. TREM2 overexpressed in *in vitro* and *in vivo* models of AD decrease expression of proinflammatory cytokines[417,483]. Despite this, activation of TREM2 *in vitro* in a macrophage cell line increase NO levels[380] and *in vivo* after spinal nerve injury increase levels of TNF-α and IL-1β[523]. Likewise, TREM2 overexpression in mice result in increased expression of IL-6, TNF-α and MCP-1 in adipose tissue[393]. These suggest that TREM2 may differentially affect the regulation of inflammatory responses depending on the underlying

pathology, potentially mediated by the different ligands that bind TREM2 in these diseases.

There are limited studies that looked at the effects of TREM2 variants on inflammatory responses. The p.R47H variant increase proinflammatory *Il6* and *Tnf* mRNA expression in response to LPS compared to WT TREM2 in BV2 microglia[435]. Similarly, RANTES and IFN-γ are increased in AD cases with the p.R47H variant compared to normal TREM2[455].

Other studies have suggested that TREM2 may modulate astrocyte function. TREM2-deficient mouse models of AD[239,468] and demyelination[493] exhibit decreased astrocyte activation as measured by GFAP levels. However, GFAP is unaltered in a TREM2-deficient TBI mouse model[520], suggesting that TREM2 may have disease-specific effects on astrocyte activation. Additionally, expression of TREM2 may be associated with the activation of the adaptive immune system. Myeloid cells with elevated levels of TREM2 are more effective at inducing T cell proliferation[428]. Gene network analyses also found that TREM2 co-enriched with genes associated with T cell- and B cell-mediated adaptive immunity[402]. However, TREM2 activation did not lead to increased expression of antigen presentation-associated proteins[394,531], suggesting that TREM2 may require other signals to activate adaptive immune responses.

In summary, TREM2 function appears to mediate and modulate numerous inflammatory responses. In various *in vivo* models of diseases associated with proinflammatory responses, the level of TREM2 is increased, likely reflecting microglial activity. However, TREM2 deficiency in mouse models result different inflammatory responses depending on disease context. The TREM2 p.R47H variant seem to result in increased proinflammatory responses, similar to the effects of *in vitro* TREM2 deficiency. TREM2 appear to affect the activity of other cell types including astrocytes and T cells but further investigation is required to confirm the role of TREM2 in modulating their activation in context of disease.

1.6.8 TREM2 and chemotaxis/migration

The loss of TREM2 function also impairs chemotaxis. TREM2 knockdown decrease chemotactic response in BV2 microglia in a scratch assay[428]. TREM2 deficiency in glioma also impair chemotaxis towards serum and downregulated genes involved in tissue invasion such as CXCL10, CXCR3, MMP2 and MMP9[510]. Likewise, TREM2-deficient primary microglia

are found to downregulate chemotaxis-related genes relative to TREM2-expressing primary microglia[532]. Furthermore, chemotaxis of TREM2-deficient microglia towards AD mouse brain slice cultures when co-cultured together is impaired[532]. TREM2 deficiency also decrease migration of N9 microglia towards CCL2 and C5a in transwell assays[532]. In contrast, TREM2 activation by antibody stimulation increase CCR7-mediated chemotaxis[380,384,385]. Additionally, network analyses revealed TREM2 co-enriched with genes involved in purinergic signalling which is implicated in mediating microglial chemotaxis[402], although TREM2 regulation of purinergic receptor-mediated chemotaxis has yet to be investigated. DOCK2 and DOCK8, associated with tissue transmigration, are also co-expressed with TREM2[402]. However, other studies found conflicting evidence for the role of TREM2 in chemotaxis. Chemotaxis is not impaired in osteoclasts derived from NHD patients with TREM2 variants[418]. PBMC derived from similar patients exhibit mixed expression of genes involved in chemotaxis as well[405]. These suggest that TREM2-mediated chemotaxis may be dependent on cell type.

TREM2-deficient mice with middle cerebral artery occlusion have decreased microglial infiltration associated with decreased levels of CCL2[522]. Similarly, DAP12-deficient mice have decreased recruitment of peripheral macrophages into the lungs in response to cigarette smoke or intranasal CCL2 treatment[421]. These effects are ameliorated by the introduction of a TREM2–DAP12 fusion construct[421], suggesting that immune cell recruitment could be mediated by TREM2 signalling.

1.6.9 TREM2 and cell survival/proliferation

Knockdown of TREM2 in primary microglia lower cell survival in culture[496]. In *in vivo* models, TREM2-deficient AD mice have decreased total brain myeloid cells[241,438], which is linked to the loss of plaque-associated myeloid cells[468,470]. This change could be due to increased apoptosis and/or decreased proliferation. The lack of TREM2 in various cell types including osteoclasts[397], BMDM[426], hepatic cancer[513] and glioma[510] increase the levels of caspase 3, Bax, Annexin V and TUNEL positive staining that are markers of apoptosis. Likewise, plaque-associated microglia in TREM2-deficient AD mice have increased expression of apoptotic markers[438]. However, PBMC-derived osteoclasts with the NHD-associated TREM2 E14X variant that results in the loss of functional TREM2

do not appear more vulnerable to apoptosis[418]. Correspondingly, primary microglia and BV2 microglia with decreased TREM2 expression have lower cell survival associated with decreased levels of Wnt/β-catenin signalling components[533]. Furthermore, decreased TREM2 expression in microglia[533], glioma[510] and hepatic cancer cells[513] results in cell cycle arrest.

Cell proliferation may be modulated by TREM2 as well. TREM2 deficiency in osteoclast precursor cells prevents CSF1R-mediated proliferation[397], a key signalling pathway for proliferation of myeloid cell types[383]. Myeloid cell proliferation is decreased in TREM2-deficient *in vivo* models of AD[241,468], demyelination[437,493], colonic mucosal injury[516], TBI[520], ischaemia[429,522] and aging[437]. These suggest that loss of TREM2 function can lower cell survival, resulting in increased apoptosis as well as reduce proliferation to decrease overall cell density.

1.6.10 Soluble TREM2

sTREM2 is produced from cleavage of TREM2 by ADAM10 and ADAM17[380,452,456,534]. Similar to APP, the remaining membrane-bound fragment after ADAM10/17 processing can be cleaved by γ-secretase[534] to produce carboxy-terminal fragments (CTFs). NHD-associated TREM2 variants p.Y38C and p.T66M appear to dramatically decrease sTREM2 release *in vitro*[452,535], potentially due to impaired protein trafficking to the cell membrane[378,379,432,452,453]. On the other hand, the AD-associated TREM2 variant p.R47H exhibit an intermediate phenotype relative to the p.Y38C and p.T66M variants with slightly decreased sTREM2 release[382,452], which the mechanism remain unclear. It has been suggested that the p.R47H variant partially impairs protein trafficking compared to the p.Y38C and p.T66M variants and result in intermediate protein degradation[382]. Interestingly, the AD-associated TREM2 variant p.H157Y[361] is located at the recently identified ADAM10/17 cleavage site of TREM2[456]. ADAM10/17 has an increased preference for tyrosine at the P1' position of its cleavage site and therefore the p.H157Y variant may enhance proteolytic cleavage of TREM2 to release sTREM2. This suggests a potential loss of TREM2 function due to decreased availability of membrane-bound TREM2 to mediate innate immune signalling.

The physiological role of sTREM2 is yet to be elucidated. sTREM2 may act as a decoy receptor to negatively regulate TREM2 signalling[452,527]. Supporting this, osteoclastogenesis, which is dependent on TREM2 signalling is inhibited by a chimaeric TREM2-Fc protein used to model sTREM2[536]. Besides that, sTREM2 appear to enhance cell survival. Treatment of sTREM2 on microglia with or without TREM2 expression[537] and TREM2-deficient BMDM[489] improve cell survival which is not associated with increased cell proliferation. sTREM2 is found to activate Akt–GSK3β–β-catenin and NFκB signalling pathways to mediate microglial cell survival[537]. sTREM2 also appears to modulate inflammatory responses. *In vitro* treatment of sTREM2 on primary microglia results in increased expression of proinflammatory cytokine genes such as *Il1b*, *Il6*, *Il10* and *Tnf* but not anti-inflammatory related genes like *Arg1* and *Ym1*[537]. Similar treatment on TREM2-deficient primary microglia also results in the same observations[537], indicating that sTREM2-mediated activation is independent of full length TREM2 expression and there may be an endogeneous receptor for sTREM2. AD-associated TREM2 p.R47H and p.R62H variants also appear to impair sTREM2-mediated proinflammatory activation and survival[537]. It is further suggested that intracellular cleavage by-products of TREM2 may have a functional role in regulating inflammatory activation. TREM2 CTFs promote TREM2-mediated anti-inflammatory signalling in response to LPS[501]. Alternatively, these fragments could negatively regulate TREM2 signalling by sequestering DAP12 and decreasing DAP12 association with receptors[534]. This leads to a decrease in overall DAP12 phosphorylation and lower activation of downstream signalling pathways[534,538].

So far, established fluid biomarkers for AD include $A\beta_{1–42}$ and tau levels in the CSF. The earliest detectable change in AD is the decrease in CSF $A\beta_{1–42}$ level[539] associated with its incorporation into amyloid plaques[540]. This can occur many years before symptoms of dementia show[539] (Figure 1.5). On the other hand, CSF tau and p-tau correlate with the progression of tau pathology in the brain which is indicative to neuronal damage and cognitive deficits[541]. Recently, studies have suggested that the proteolytic cleavage of TREM2 to produce sTREM2 reflect ongoing inflammation in AD associated with the transition of pre-clinical to symptomatic AD[452,527] (Figure 1.5). CSF sTREM2 levels are increased in AD patients and positively correlate with CSF tau and p-tau but not $A\beta_{1–42}$[484,535,542,543] (Figure 1.5). This seems contrary to the functional consequences of TREM2 deficiency on amyloid burden and implies that CSF sTREM2 level is associated

with neuronal damage rather than amyloid plaque deposition[362]. In pre-clinical AD, CSF sTREM2 level appears normal but is increased in patients with AD-associated MCI[484] (Figure 1.5). CSF sTREM2 is also increased after deposition of Aβ and coincide with changes in hippocampal volume, precuneus glucose metabolism and cognitive performance[484]. Moreover, CSF sTREM2 level is elevated in familial AD cases with cognitive deficits but not in cognitive normal cases[484]. Further implication of CSF sTREM2 level and neuroinflammation is seen in MS patients treated with an antibody inhibiting T cell migration into the CNS, which result in decreased CSF sTREM2 and inflammation as well as improvements in clinical outcome[544]. CSF sTREM2 level appears to be elevated in AD patients with the TREM2 variant p.R47H but not in p.R62H when compared to cognitively normal controls[535]. However, this study was performed in a small cohort and cases with TREM2 variants were a mixture of symptomatic AD and cognitively normal individuals[535]. There are some studies that reported contradicting findings on CSF sTREM2 level in AD which are unchanged[452] or decreased[545] compared to control cases. It could be that CSF sTREM2 increases in early clinical AD and fall off in the later stages of AD[484] (Figure 1.5).

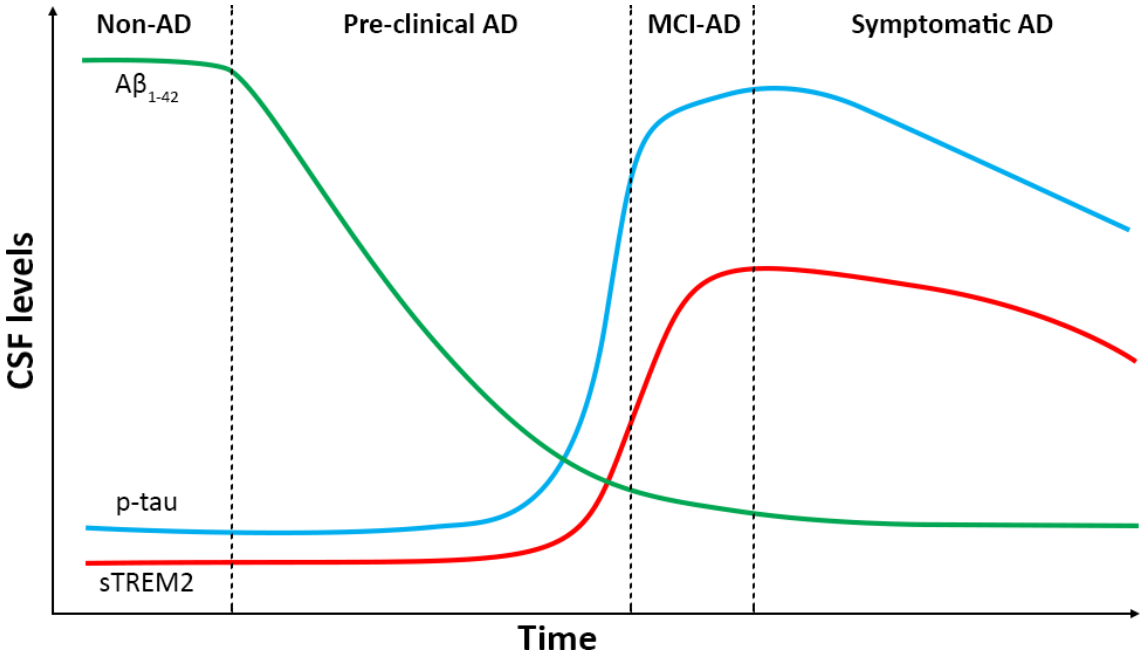

Figure 1.5. CSF levels of $A\beta_{1-42}$, p-tau and sTREM2 changes throughout the progression of AD.
CSF $A\beta_{1-42}$ decrease as amyloid deposition begin in the brain while p-tau and sTREM2, in correlation, increase with neuronal damage, neuroinflammation and progression of cognitive deficits.
Figure adapted from Ulrich *et al.* (2017)[362].

1.6.11 Conclusion

TREM2 appears to be involved in various microglial-mediated innate immune responses that occur in AD. Some of these responses, particularly those that are related to immunoregulation towards anti-inflammatory effects and clearance of pathology and cellular debris by phagocytosis appear to be beneficial by suppressing cytotoxic proinflammatory responses. Studies investigating TREM2 dysfunction found that disease-associated TREM2 variants, which increases the risk of developing neurodegenerative diseases like AD result in a similar phenotype to TREM2-deficient models. This suggests that most of these variants convey a loss or decreased TREM2 function. However, protein structure and tracking studies observed that the variants have different effects on TREM2, either affecting ligand binding, protein folding, post-transcriptional modifications or protein cleavage. Apart from the variants that cause loss of functional TREM2 expression on the cell membrane, it is unclear how these variants impact signalling pathways downstream of TREM2 and lead to dysfunctional inflammatory responses. Although there is an increasing number of studies exploring the role of TREM2, studies that use experimental models endogeneously expressing the TREM2 variants to study their effects on AD pathogenesis have been limited. Furthermore, to my knowledge, there has not been any studies investigating the effects of these variants on the signalling pathways downstream of TREM2.

Thus, this project will explore and generate an *in vitro* model carrying the disease-associated TREM2 variants with endogeneous downstream signalling pathways suitable for use in screening assays. The cell model will then be characterised for changes in key proteins of the signalling pathways downstream of TREM2 to elucidate differences caused by the disease-associated variants. This will pave the way for these cells to be used to screen therapeutic compounds that can take advantage of the beneficial effects of TREM2 function.

1.7 Aims and objectives

Overall aim

To generate an *in vitro* model carrying disease-associated TREM2 variants with endogeneous downstream signalling components. The generated cells will be characterised for changes in key signalling proteins downstream of TREM2 as well as functional phenotype due to disease-associated TREM2 variants. These cells can then be used to screen disease-modifying therapeutic compounds.

Specific aims

1. To identify a suitable cell model for use in large scale or high-throughput experiments and introduce the AD-associated TREM2 variants into the cells.
   (a) To choose a cell type relevant for TREM2 function and AD.
   (b) To use the most effective method to perform genome editing.
2. To study the effects of disease-associated TREM2 variants on microglia in the hippocampus of AD brains.
   (a) To assess abundance and morphological activation of microglia expressing commonly used functional microglial markers between disease-associated TREM2 variant carriers and normal TREM2 carriers.
   (b) To establish microglial markers from dysfunction conveyed by disease-associated TREM2 variants in people, which can be used to characterise the generated *in vitro* TREM2 model.
3. To characterise the generated *in vitro* TREM2 model.
   (a) To confirm that CRISPR/Cas9-mediated editing of *Trem2* in the generated cell line resulted in the expected functional expression of TREM2 protein.
   (b) To investigate changes in the activation of key signalling mediators downstream of TREM2 and compare functional microglial markers identified from people with disease-associated TREM2 variants in the generated cell model.

Chapter 2

Materials and methodology

2.1 Materials

2.1.1 Reagents

Reagent	Catalog #	Manufacturer
100 bp DNA Ladder	15628-019	Thermo Fisher Scientific
Acetic acid, glacial	20102	VWR Chemicals
Adenosine 5'-triphosphate (ATP)	P0756	New England Biolabs
Aluminium potassium sulfate dodecahydrate	10647411	Acros Organics
Ammonium acetate (7.5M)	A2706	Sigma-Aldrich
Avidin biotin complex horseradish peroxidase solution, VECTASTAIN Elite ABC HRP Kit (Peroxidase, Standard)	PK-6100	Vector Laboratories
Bicinchoninic acid (BCA) protein assay	10678484	Thermo Fisher Scientific
BlueJuice Gel Loading Buffer (10×)	10816015	Thermo Fisher Scientific
Boric acid	B7660	Sigma-Aldrich
Bovine serum albumin (BSA)	sc-2323	Santa Cruz
Cell Line Nucleofector Kit L	VCA-1005	Lonza
Cell Line Optimization Nucleofector Kit for Nucleofector 2b Device	VCO-1001N	Lonza
CellTracker Red CMTPX Dye	C34552	Thermo Fisher Scientific
Chloroform (99+%, stabilised with amylene)	AC167735000	Acros Organics
Dabco 33-LV	290734	Sigma-Aldrich
3,3'-diaminobenzidine tetrahydrochloride (DAB)	D5905	Sigma-Aldrich
DPX new	100579	Merck
Dulbecco's Modified Eagle Medium (DMEM), high glucose, GlutaMAX, pyruvate	31966	Thermo Fisher Scientific
Dimethyl sulfoxide (DMSO)	D5879	Sigma-Aldrich
DL-Dithiothreitol (DTT)	D0632	Sigma-Aldrich
Dulbecco's phosphate-buffered saline (DPBS)	14190	Thermo Fisher Scientific
EndoFree Plasmid Maxi Kit	12362	QIAGEN
Ethanol, absolute	E7023	Sigma-Aldrich
Ethylenediaminetetraacetic acid (EDTA, 0.5 M)	03690	Sigma-Aldrich
Ethylenediaminetetraacetic acid disodium salt dihydrate	E4884	Sigma-Aldrich
FastDigest BpiI (BbsI)	FD1014	Thermo Fisher Scientific
Filter paper, grade 3 qualitative	1003-917	GE Healthcare
Foetal bovine serum (FBS), heat inactivated	10500064	Thermo Fisher Scientific
Formic acid (80%)	20315	VWR Chemicals
Formalin solution, neutral buffered (NBF, 10%)	HT501128	Sigma-Aldrich
FuGENE 6 Tranfection Reagent	E2693	Promega
GelRed nucleic acid stain (10,000×)	BT41003	Biotium
Glycerol	G5516	Sigma-Aldrich
Glycine	sc-29096B	Santa Cruz
Haematoxylin monohydrate	115938	Merck
Hoechst 33342, trihydrochloride, trihydrate solution in water	H3570	Thermo Fisher Scientific
Hydrochloric acid (HCl, 5 M)	10695872	Fisher Chemical

Reagent	Catalog #	Manufacturer
Hydrogen peroxide (H_2O_2, 30%)	23615	VWR Chemicals
Industrial methylated spirit (IMS, 99%)	IMS005	Solmedia Ltd
Isopropanol	20839.297	VWR Chemicals
KASP V4.0 2× Master mix, High ROX	KBS-1016-022	LGC Genomics
LB agar, powder (Lennox L Agar)	22700	Thermo Fisher Scientific
LB broth base	12780	Thermo Fisher Scientific
Lipofectamine 2000 transfection reagent	11668	Thermo Fisher Scientific
Lipofectamine 3000 transfection reagent	L3000	Thermo Fisher Scientific
Methanol	MET005	Solmedia Ltd
MicroAmp Clear Adhesive Film	4306311	Thermo Fisher Scientific
MicroAmp Optical Adhesive Film	4311971	Thermo Fisher Scientific
Mowiol 4-88	81381	Sigma-Aldrich
Nitrocellulose membrane, Amersham Protran NC	15259804	GE Healthcare
Nocodazole, Ready Made Solution	SML1665	Sigma-Aldrich
Normal goat serum	X0907	Dako
Normal swine serum	X0901	Dako
Nuclease-free water (not DEPC-treated)	AM9937	Ambion
NuPAGE Antioxidant	NP0005	Thermo Fisher Scientific
NuPAGE LDS Sample Buffer (4×)	NP0007	Thermo Fisher Scientific
NuPAGE MOPS SDS Running Buffer (20×)	NP0001	Thermo Fisher Scientific
NuPAGE 4-12% Bis-Tris Midi Protein Gels, 26-well	WG1403BOX	Thermo Fisher Scientific
NuPAGE Sample Reducing Agent (10×)	NP0004	Thermo Fisher Scienfitic
One Shot Stbl3 chemically competent *E. coli*	C737303	Thermo Fisher Scientific
One*Taq* Hot Start 2× Master Mix with Standard Buffer	M0484	New England Biolabs
Opti-MEM I Reduced Serum Medium	31985047	Thermo Fisher Scientific
Penicillin-streptomycin	15140122	Thermo Fisher Scientific
Phenol/chloroform/isoamyl alcohol (25:24:1 mixture, pH 8.0)	10306413	Fisher BioReagents
Phosphatase inhibitor tablets, PhosSTOP	4906845001	Roche
PolyFect Transfection Reagent	301105	QIAGEN
Ponceau S	P3504	Sigma-Aldrich
Protease inhibitor cocktail, cOmplete ULTRA Tablets, Mini, EDTA-free, *EASYpack*	5892791001	Roche
Precision Plus Protein All Blue Prestained Protein Standards	1610373	Bio-Rad
Protein Deglycosylation Mix	P6039S	New England Biolabs
Protein Deglycosylation Mix II	P6044S	New England Biolabs
Puromycin dihydrochloride	sc-108071	Santa Cruz
QIAamp DNA Mini Kit	51306	QIAGEN
QIAGEN Plasmid Plus Midi Kit	12945	QIAGEN
QIAprep Spin Miniprep Kit	27106	QIAGEN
QIAquick Gel Extraction Kit	28706	QIAGEN
QIAquick PCR Purification Kit	28106	QIAGEN
QIAvac 24 Plus	19413	QIAGEN
QIAzol Lysis Reagent	79306	QIAGEN
Quick-Load 100 bp DNA Ladder	N0467	New England Biolabs

Reagent	Catalog #	Manufacturer
Radioimmunoprecipitation assay (RIPA) buffer	R0278	Sigma-Aldrich
RNeasy Plus Universal Mini Kit	73404	QIAGEN
Roswell Park Memorial Institute (RPMI) 1640 medium	21875	Thermo Fisher Scientific
Sodium chloride (NaCl)	71376	Sigma-Aldrich
Tri-sodium citrate dihydrate	10448610	Fisher Chemical
Sodium dodecyl sulfate (SDS, 10%)	71736	Sigma-Aldrich
Sodium iodate	S4007	Sigma-Aldrich
Sudan Black B	199664	Sigma-Aldrich
SuperScript IV Reverse Transcriptase	18090200	Thermo Fisher Scientific
T4 DNA ligase	EL0014	Thermo Fisher Scientific
T4 polynucleotide kinase	M0201	New England Biolabs
Tris base	30-20-60	Severn Biotech Ltd
Tris-borate-EDTA (TBE) buffer (10×)	T4415	Sigma-Aldrich
Tris-HCl (1 M)	T2694	Sigma-Aldrich
Triton X-100	X100	Sigma-Aldrich
Trypsin-EDTA (0.25%), phenol red	25200	Thermo Fisher Scientific
TurboFect transfection reagent	R0533	Thermo Fisher Scientific
Tween 20	P5927	Sigma-Aldrich
UltraPure Agarose	16500	Thermo Fisher Scientific
Xylene	XYL005	Solmedia Ltd

2.1.2 Solutions

Solution	Reagent	Amount	Stock conc.	Working conc.
100 bp DNA Ladder (10 ng/µL)	100 bp DNA Ladder	1 µL	1 µg/µL	10 ng/µL
	10× BlueJuice Gel Loading Buffer	10 µL	10×	1×
	ddH_2O	Up to 100 µL		
Acid alcohol (1% v/v)	HCl (5 M)	3 mL	-	1% v/v
	IMS	210 mL	-	70% v/v
	dH_2O	Up to 300 mL		
Antibody stripping buffer	Glycine	7.5 g	-	200 mM
	SDS (10%)	5 mL	-	0.1% v/v
	Tween 20	5 mL	-	1% v/v
	HCl (5 M)	∼10.5 mL	(or to pH 2.2)	
	ddH_2O	Up to 500 mL		
Citrate-buffered saline (CBS, 10×, pH 6.0)	Tri-sodium citrate dihydrate	29.4 g	100 mM	10 mM
	HCl (5 M)	∼4 mL	(or up to pH 6.0)	
	ddH_2O	Up to 1 L		
Direct-Lyse lysis buffer (0.5×)	Tris base	0.61 g	-	10 mM
	EDTA	0.37 g	-	2.5 mM
	NaCl	5.85 g	-	200 mM
	SDS (10%)	7.5 mL	-	0.15% v/v
	Tween 20	1.5 mL	-	0.3% v/v
	ddH_2O	Up to 500 mL		
DNA extraction cell lysis buffer (1×)	Tris-HCl (1 M)	5 mL	-	10 mM
	EDTA (0.5 M)	25 mL	-	25 mM
	NaCl	2.19 g	-	75 mM
	SDS (10%)	25 mL	-	0.5% v/v
	ddH_2O	Up to 500 mL		
Harris' haematoxylin	Haematoxylin monohydrate	5 g	-	15.6 mM
	Absolute ethanol	50 mL	-	-
	Aluminium potassium sulfate dodecahydrate	100 g	-	210 mM
	ddH_2O	950 mL		
	Sodium iodate	370 mg	-	1.87 mM
	Glacial acetic acid	4 mL	-	70 mM
Mowiol hard set aqueous mounting medium	Mowiol 4-88	2.4 g	-	-
	Glycerol	6 g/ 4.75 mL	-	-
	ddH_2O	6 mL		
	Tris-Cl (0.2 M, pH 8.5)	12 mL	-	-
	Dabco 33-LV	Variable	-	2.5% v/v
Ponceau S staining solution	Ponceau S	2.5 g	-	0.5% w/v
	ddH_2O	495 mL		
	Glacial acetic acid	5 mL	-	1% v/v

Solution	Reagent	Amount	Stock conc.	Working conc.
Sodium boric acid (SBA) buffer (20×)	Boric acid	45 g	730 mM	36.5 mM
	Sodium hydroxide	8 g	200 mM	10 mM
	ddH_2O	Up to 1 L		
Transfer buffer (10×)	Tris base	30.29 g	250 mM	25 mM
	Glycine	144.13 g	1.92 M	192 mM
	ddH_2O	Up to 1 L		
Transfer buffer (1×, working solution)	10× transfer buffer	100 mL	10×	1×
	Methanol	200 mL	-	20% v/v
	ddH_2O	Up to 1 L		
Tris-acetate-EDTA (TAE, 50×, pH 8.3)	Tris base	242 g	2.0 M	40 mM
	EDTA (0.5 M)	100 mL	50 mM	1 mM
	Glacial acetic acid	57.1 mL	2.0 M	40 mM
	ddH_2O	Up to 1 L		
Tris-buffered saline (TBS, 10×, pH 7.6)	Tris base	60.45 g	500 mM	50 mM
	NaCl	87.66 g	1.5 M	150 mM
	HCl (5 M)	∼81.5 mL	(or to pH 7.6)	
	ddH_2O	Up to 1 L		
TBS-T 0.1%	10× TBS	100 mL	10×	1×
	Tween 20	1 mL	-	0.1% v/v
	ddH_2O	Up to 1 L		
TBS-Tx 0.1%	10× TBS	10 mL	10×	1×
	Tritox X-100	100 µL	-	0.1% v/v
	ddH_2O	Up to 100 mL		
TBS-Tx 0.25%	10× TBS	10 mL	10×	1×
	Tritox X-100	250 µL	-	0.25% v/v
	ddH_2O	Up to 100 mL		

2.1.3 Primers and oligonucleotides

2.1.3.1 PCR primers

PCR primer	Primer sequence (5'→3')	Annealing temp.
mTREM2_Ex2_M13F(-21)_F1	TGTAAAACGACGGCCAGTATTCTAGAGCCCGTCAGGGA	65°C
mTREM2_Ex2_M13R_R1	CAGGAAACAGCTATGACTCCCCCTGAAAAAGTCCCAC	

Table 2.1. All PCR primers used. Red font: sequencing primer M13F or M13R.

2.1.3.2 RT-PCR primers

RT-PCR primer	Primer sequence (5'→3')	Annealing temp.
mAIF1F1	GATGAGGATCTGCCGTCCAAA	54°C
mAIFR1	AGTAGCTGAACGTCTCCTCG	
mCD68F1	CACAGTGGACATTCATGGCG	55°C
mCD68R1	GCAAGAGAAACATGGCCCGA	
mCIITAF1	CTGGGGAGGAGGAGATCGAA	55°C
mCIITAR1	AAGAGGTCCTTGCTCAGGC	
mCX3CR1F1	CGTGAGACTGGGTGAGTGAC	54°C
mCX3CR1R1	CCGGTTGTTCATGGAGTTGG	
mDAP12F1	GCCCAGAGTGACACTTTCCC	56°C
mDAP12R1	GGGAGGTACCCTGTGGATCT	
mHexbF1	CGACCCAGACTGGAAGGTTG	54°C
mHexbR1	GCCATGGCATCCAGAGTTTT	
mIL1bF1	TGCCACCTTTTGACAGTGATG	53°C
mIL1bR1	TTCTTGTGACCCTGAGCGAC	
mIL6F1	TCTCTGCAAGAGACTTCCATCC	54°C
mIL6R1	TAACGCACTAGGTTTGCCGA	
mP2RY12F1	TACCCTACAGAAACACTCAAGGC	54°C
mP2RY12R1	CAGGGTGTAGGGAATCCGTG	
mTNFaF1	TCTTCTCATTCCTGCTTGTGG	52°C
mTNFaR1	AGGGTCTGGGCCATAGAACT	
mTREM2F1	CGGAATGGGAGCACAGTCAT	55°C
mTREM2R1	CTTGATTCCTGGAGGTGCTGT	
mTREM2F4	AACTGCTTCCAAGCAAGTGGC	53°C
mTREM2R4	GATCTCCAGCATCTTGGTCATCTA	
mTREM2_cDNA_seq_F1 (M13F)	TGTAAAACGACGGCCAGTATGGGACCTCTCCACCAGTT	66°C
mTREM2_cDNA_seq_R1 (M13R)	CAGGAAACAGCTATGACGGAGGTGCTGTGTTCCACTT	

Table 2.2. All RT-PCR primers used. Red font: sequencing primer M13F or M13R.

2.1.4 Antibodies

Primary antibody	Catalog #	Manufacturer
Anti β-actin (clone C4), mouse, monoclonal	sc-47778	Santa Cruz
Anti amyloid-$\beta_{1\text{-}16}$ (clone 6E10) Alexa Fluor 488, mouse, monoclonal	803013	BioLegend
Anti amyloid-$\beta_{17\text{-}24}$ (clone 4G8), mouse, monoclonal	800701	BioLegend
Anti human CD68 (clone PG-M1), mouse, monoclonal	M087601-2	Dako
Anti mouse CD68/macrosialin (clone FA-11), rat, monoclonal	137001	BioLegend
Anti Erk1/2 (p44/42 MAPK, clone L34F12), mouse, monoclonal	4696	Cell Signalling Technology
Anti phospho-Erk1/2 (p44/42 MAPK) Thr202, Tyr204 (clone D13.14.4E), rabbit, monoclonal	4370	Cell Signalling Technology
Anti GAPDH, rabbit, polyclonal	sc-25778	Santa Cruz
Anti human HLA-DP, DQ, DR (clone CR3/43), mouse, monoclonal	M0775	Dako
Anti I-A/I-E (MHC class II, clone M5/114.15.2), rat, monoclonal	107601	BioLegend
Anti Iba-1, rabbit, polyclonal	019-19741	Wako
Anti Pyk2 (clone 5E2), mouse, monoclonal	3480	Cell Signalling Technology
Anti phospho-Pyk2 Tyr402, rabbit, polyclonal	3291	Cell Signalling Technology
Anti Syk (clone 6A464), mouse, monoclonal	sc-73089	Santa Cruz
Anti phospho-Syk Tyr525, Tyr526 (clone C87C1), rabbit, monoclonal	2710	Cell Signalling Technology
Anti tau, rabbit, polyclonal	A0024	Dako
Anti phospho-tau Ser202, Thr205 (clone AT8), mouse, monoclonal	MN1020	Thermo Fisher Scientific
Anti human TREM2, goat, polyclonal	AF1828	R&D Systems
Anti human TREM2, rabbit, polyclonal	HPA012571	Atlas Antibodies
Anti human/mouse TREM2 (clone 237920), rat, monoclonal	MAB17291	R&D Systems
Anti mouse TREM2, rabbit, polyclonal	sc-48765	Santa Cruz
Anti mouse TREM2, sheep, polyclonal	AF1729	R&D Systems
IgG_{2B} isotype control, rat, monoclonal	MAB0061	R&D Systems

Table 2.3. All primary antibodies used for immunohistochemistry, immunofluorescence, and Western blotting.

Secondary antibody	Catalog #	Manufacturer
Anti mouse IgG, goat, polyclonal, biotinylated	E0433	Dako
Anti rabbit IgG, swine, polyclonal, biotinylated	E0353	Dako
Anti mouse IgG, goat, polyclonal, Alexa Fluor 488	A11001	Thermo Fisher Scientific
Anti mouse IgG, goat, polyclonal, Alexa Fluor 568	A11004	Thermo Fisher Scientific
Anti mouse IgG, goat, polyclonal, Alexa Fluor 680	A21057	Thermo Fisher Scientific
Anti rabbit IgG, goat, polyclonal, Alexa Fluor 488	A11008	Thermo Fisher Scientific
Anti rabbit IgG, goat, polyclonal, Alexa Fluor 594	A11012	Thermo Fisher Scientific
Anti rat IgG, goat, polyclonal, Alexa Fluor 488	A11006	Thermo Fisher Scientific
Anti sheep IgG, donkey, polyclonal, Alexa Fluor 488	A11015	Thermo Fisher Scientific

Table 2.4. All secondary detection antibodies used for immunohistochemistry, immunofluorescence, and Western blotting.

2.2 Methodology for Chapter 3

2.2.1 sgRNA and HDR template design

2.2.1.1 sgRNA

sgRNA sequences were designed using the CRISPR Design Tool (http://crispr.mit.edu) where mouse *Trem2* Exon 2 was used as the input to search for viable sgRNA sequences. sgRNA targeting sequences, while relatively flexible, require a NGG protospacer adjacent motif (PAM) sequence next to the 20 nt sgRNA sequence[546]. A double Cas9 nickase (Cas9n) design was used and this requires a sgRNA for each nickase. Therefore, a pair of sgRNA sequences were designed to flank the target region for the knock-in mutation, with each sgRNA targeting opposite DNA strands to induce a double-stranded DNA (dsDNA) break[546]. For this project, 4 design strategies with iterative improvements were employed.

For CRISPR v1, the CRISPR/Cas9 strategy used was based on a published protocol and adapted for BV2 using the double Cas9 nickase design[546]. The sgRNA pairs used were designed to target the AD-associated rs75932628 (human and mouse c.140G>A, p.R47H) TREM2 variant in mouse (Table 2.5). The location and orientation of the sgRNA targeting sequences are shown in Figure 2.1.

For CRISPR v2, a new sgRNA pair targeting the p.R47H variant were designed slightly further apart to check if CRISPR v1 sgRNA pair was ineffective in inducing HDR activity (Table 2.6, Figure 2.2).

CRISPR v1 sgRNA		Sequence (5'→3')
mTREM2_R47H_sgRNA-A_R1a	Top	CACCGCGTCTCCCCCAGTGCTTCA
	Bottom	AAACTGAAGCACTGGGGGAGACGC
	Duplex	CACCGCGTCTCCCCCAGTGCTTCA.... ....CGCAGAGGGGGTCACGAAGTCAAA
mTREM2_R47H_sgRNA-B_F1a	Top	CACCGCAAGGCCTGGTGTCGGCAGC
	Bottom	AAACGCTGCCGACACCAGGCCTTGC
	Duplex	CACCGCAAGGCCTGGTGTCGGCAGC.... ....CGTTCCGGACCACAGCCGTCGCAAA

Table 2.5. CRISPR v1 sgRNA pair targeting the *Trem2* p.R47 codon.
Top and bottom ssDNA oligonucleotides were phosphorylated and annealed into dsDNA fragments for cloning.
Blue font: sgRNA sequences; red font: additional G-C for compatibility with U6 promoter.

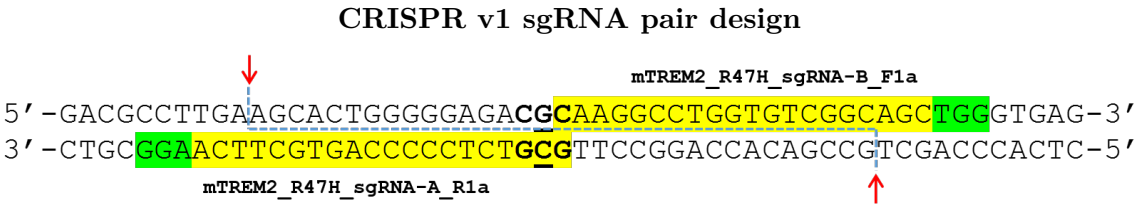

Figure 2.1. CRISPR v1 sgRNA pairs targeted sequences flanking the *Trem2* p.R47 codon to nick on both DNA strands and create a 5' DNA overhang.
A region of mouse *Trem2* Exon 2 sequence showing the sgRNA pair targeting sequences for CRISPR v1.
Yellow highlight: sgRNA sequence, green highlight: PAM sequence, bold font: targeted p.R47 codon, underlined font: targeted c.140G, red arrows: Cas9n nicks, and blue dotted lines: DNA separation after double nicking.

CRISPR v2 sgRNA		Sequence (5'→3')
mTREM2_R47H_sgRNA-A_R2a	Top	CACCGATAAGTACATGACACCCTCA
	Bottom	AAACTGAGGGTGTCATGTACTTATC
	Duplex	CACCGATAAGTACATGACACCCTCA.... ....CTATTCATGTACTGTGGGAGTCAAA
mTREM2_R47H_sgRNA-B_F1a	Top	CACCGCAAGGCCTGGTGTCGGCAGC
	Bottom	AAACGCTGCCGACACCAGGCCTTGC
	Duplex	CACCGCAAGGCCTGGTGTCGGCAGC.... ....CGTTCCGGACCACAGCCGTCGCAAA

Table 2.6. CRISPR v2 sgRNA pair targeting *Trem2* p.R47 codon.
Blue font: sgRNA sequences; red font: additional G-C for compatibility with U6 promoter.

CRISPR v2 sgRNA pair design

Figure 2.2. CRISPR v2 sgRNA pairs target sequences flanking the *Trem2* p.R47 codon.
A region of mouse *Trem2* Exon 2 sequence showing the sgRNA pair targeting sequences for CRISPR v2.
Yellow highlight: sgRNA sequence, green highlight: PAM sequence, bold font: targeted p.R47 codon, underlined font: targeted c.140G, red arrows: Cas9n nicks, and blue dotted lines: DNA separation after double nicking.

For CRISPR v3, sgRNA pairs targeting other dementia-associated rs104894002 (human c.97C>T, p.Q33X and mouse c.97AG>TA p.R33X) and rs142232675 (human and mouse c.259G>A, p.D87N) TREM2 variants in mouse were designed to test if the lack of HDR was unique to the p.R47 loci on *Trem2* (v3a). Additionally, a second set (v3b) of sgRNA pairs targeting the sgRNA-blocking mutations introduced by the v3a HDR templates (see Chapter 2.2.1.2: HDR template) for p.R47H, p.Q33X and p.D87N variants were designed to explore the possibility to revert the sgRNA-blocking mutations back to the WT sequence as described by Paquet *et al*[547] (Table 2.7, Figure 2.3).

For CRISPR v4, only the sgRNA pair targeting the p.R47H variant from CRISPR v2/v3a were used.

CRISPR v3 sgRNA		**Sequence (5'→3')**
mTREM2_R47H_sgRNA-A_R2a	Top	CACCGATAAGTACATGACACCCTCA
	Bottom	AAACTGAGGGTGTCATGTACTTATC
	Duplex	CACCGATAAGTACATGACACCCTCA.... ....CTATTCATGTACTGTGGGAGTCAAA
mTREM2_R47H_sgRNA-B_F1a	Top	CACCGCAAGGCCTGGTGTCGGCAGC
	Bottom	AAACGCTGCCGACACCAGGCCTTGC
	Duplex	CACCGCAAGGCCTGGTGTCGGCAGC.... ....CGTTCCGGACCACAGCCGTCGCAAA
mTREM2_R47H_sgRNA-A_R2b	Top	CACCGATAAGTACATGACACTCTCA
	Bottom	AAACTGAGAGTGTCATGTACTTATC
	Duplex	CACCGATAAGTACATGACACTCTCA.... ....CTATTCATGTACTGTGAGAGTCAAA
mTREM2_R47H_sgRNA-B_F1b	Top	CACCGCAAGGCCTGGTGTCGCCAGC
	Bottom	AAACGCTGGCGACACCAGGCCTTGC
	Duplex	CACCGCAAGGCCTGGTGTCGCCAGC.... ....CGTTCCGGACCACAGCGGTCGCAAA
mTREM2_Q33X_sgRNA-A_R1a	Top	CACCGGCCATGCCCTGCAGCACCG
	Bottom	AAACCGGTGCTGCAGGGCATGGCC
	Duplex	CACCGGCCATGCCCTGCAGCACCG.... ....CCGGTACGGGACGTCGTGGCCAAA

Continued on next page...

CRISPR v3 sgRNA		Sequence (5'→3')
mTREM2_Q33X_sgRNA-B_F1a	Top	CACCGATGACGCCTTGAAGCACTGG
	Bottom	AAACCCAGTGCTTCAAGGCGTCATC
	Duplex	CACCGATGACGCCTTGAAGCACTGG.... ....CTACTGCGGAACTTCGTGACCCAAA
mTREM2_Q33X_sgRNA-A_R1b	Top	CACCGGCCATGCCCTGCAGGACCG
	Bottom	AAACCGGTCCTGCAGGGCATGGCC
	Duplex	CACCGGCCATGCCCTGCAGGACCG.... ....CCGGTACGGGACGTCCTGGCCAAA
mTREM2_Q33X_sgRNA-B_F1b	Top	CACCGATGACGCCTTGAAGCATTGG
	Bottom	AAACCCAATGCTTCAAGGCGTCATC
	Duplex	CACCGATGACGCCTTGAAGCATTGG.... ....CTACTGCGGAACTTCGTAACCCAAA
mTREM2_D87N_sgRNA-A_R1a	Top	CACCGTGCTCCCATTCCGCTTCTTC
	Bottom	AAACGAAGAAGCGGAATGGGAGCAC
	Duplex	CACCGTGCTCCCATTCCGCTTCTTC.... ....CACGAGGGTAAGGCGAAGAAGCAAA
mTREM2_D87N_sgRNA-B_F1a	Top	CACCGATCGCAGATGACACCCTTGC
	Bottom	AAACGCAAGGGTGTCATCTGCGATC
	Duplex	CACCGATCGCAGATGACACCCTTGC.... ....CTAGCGTCTACTGTGGGAACGCAAA
mTREM2_D87N_sgRNA-A_R1b	Top	CACCGTGCTCCCATTCCGCTTTTTC
	Bottom	AAACGAAAAAGCGGAATGGGAGCAC
	Duplex	CACCGTGCTCCCATTCCGCTTTTTC.... ....CACGAGGGTAAGGCGAAAAAGCAAA
mTREM2_D87N_sgRNA-B_F1b	Top	CACCGATCGCAGATAACACACTTGC
	Bottom	AAACGCAAGTGTGTTATCTGCGATC
	Duplex	CACCGATCGCAGATAACACACTTGC.... ....CTAGCGTCTATTGTGTGAACGCAAA

Table 2.7. CRISPR v3 sgRNA pairs targeting p.R47H, p.Q33X and p.D87N variants in mouse *Trem2*.
Blue font: sgRNA sequences; red font: additional G-C for compatibility with U6 promoter; green font: sgRNA-blocking mutations.

(a) CRISPR v3 Q33X

(b) CRISPR v3 D87N

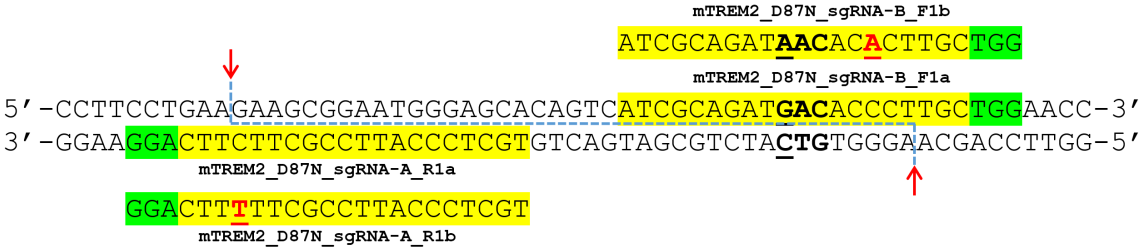

(c) CRISPR v3 R47H

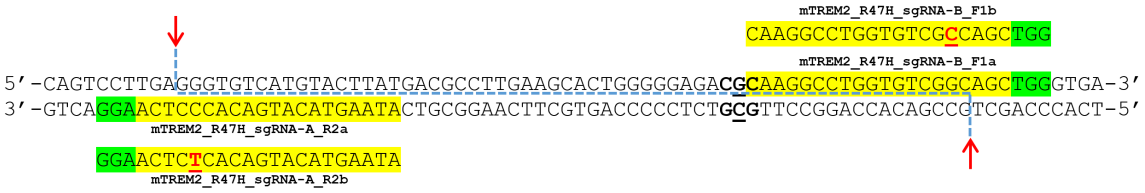

Figure 2.3. CRISPR v3 sgRNA pairs targeted sequences flanking *Trem2* p.Q33X, p.D87N and p.R47H variants.
Regions within mouse *Trem2* Exon 2 sequence showing sgRNA pairs targeting the **(a)** p.Q33X, **(b)** p.D87N, and **(c)** p.R47H variants for CRISPR v3a and v3b.
Yellow highlight: sgRNA sequence, green highlight: PAM sequence, bold font: targeted codon, underlined font: targeted base for knock-in mutation, red font: sgRNA-blocking mutation, red arrows: Cas9n nicking, and blue dotted lines: DNA separation after double nicking.

2.2.1.2 HDR template

HDR templates used were single-stranded DNA (ssDNA) oligonucleotides with the knock-in mutation in the middle with at least 40 nt flanking homology arms as recommended by Ann Ran *et al*[546]. These can correspond to the sense or anti-sense orientation of mouse *Trem2* genomic DNA (gDNA) sequence. The R47H and D87N HDR templates were 181 nt long (90 nt flanking homology arms) and the Q33X was 113 nt long (56 nt flanking homology arms), which were ordered as Ultramer oligonucleotides from Integrated DNA Technologies. Upon receiving these, they were reconstituted to 100 µM with nuclease-free water or endotoxin-free TE buffer.

For CRISPR v1, the HDR template used did not contain any modifications other than the intended knock-in mutation for the p.R47H variant (Table 2.8). The sense and anti-sense orientations were made. For CRISPR v2, silent mutations were added into the HDR template at the PAM sequence (PAM-blocking mutations) to prevent Cas9 from re-targeting HDR-edited gDNA[547] alongside the intended knock-in mutation for the p.R47H variant (Table 2.8). The sense and anti-sense orientations were used.

For CRISPR v3, instead of PAM-blocking mutations, sgRNA blocking mutations were used in the HDR templates targeting the p.Q33X, p.D87N and p.R47H variants (v3a). Similar to PAM-blocking mutations, these prevent Cas9 from re-targeting HDR-edited gDNA. Paquet *et al*[547] reported that the location of the knock-in mutation relative to the cut site is crucial for HDR incorporation. Therefore, the sgRNA-blocking mutations were introduced as close as possible to the nick locations for each of the sgRNA pairs (Table 2.8, Figure 2.3). Additionally, to revert the sgRNA-blocking mutations back to the WT sequence, a second set (v3b) of HDR templates targeting the p.Q33X and p.D87N variants were designed to only contain the intended knock-in mutation, similar to CRISPR v1. The HDR template targeting the p.R47H variant was re-used from CRISPR v1 (Table 2.8). To decrease the amount of clones to screen, only the anti-sense orientation for v3a and v3b HDR templates were designed. It has been reported that the using the anti-sense HDR template would result in at least similar or better HDR efficiency to the sense orientation[548–551].

For CRISPR v4, the v3a anti-sense HDR template targeting the p.R47H variant was reused (Table 2.8).

CRISPR design	HDR template	Sequence (5'→3')
CRISPR v1	mTREM2_R47H_HDR-sense_v1	AAGCCCTCAACACCACGGTGCTGCAGGGCATGGCCGGCCAG TCCTTGAGGGTGTCATGTACTTATGACGCCTTGAAGCACTG GGGGAGACACAAGGCCTGGTGTCGGCAGCTGGGTGAGGAGG GCCCATGCCAGCGTGTGGTGAGCACACACGGTGTGTGGCTG CTGGCCTTCCTGAAGAA
	mTREM2_R47H_HDR-a.sense_v1	TTCTTCAGGAAGGCCAGCAGCCACACACCGTGTGTGCTCAC CACACGCTGGCATGGGCCCTCCTCACCCAGCTGCCGACACC AGGCCTTGTGTCTCCCCCAGTGCTTCAAGGCGTCATAAGTA CATGACACCCTCAAGGACTGGCCGGCCATGCCCTGCAGCAC CGTGGTGTTGAGGGCTT
CRISPR v2	mTREM2_R47H_HDR-sense_v2	AAGCCCTCAACACCACGGTGCTGCAGGGCATGGCCGGCCAG TCTTTGAGGGTGTCATGTACTTATGACGCCTTGAAGCACTG GGGGAGACACAAGGCCTGGTGTCGGCAGCTCGGTGAGGAGG GCCCATGCCAGCGTGTGGTGAGCACACACGGTGTGTGGCTG CTGGCCTTCCTGAAGAA
	mTREM2_R47H_HDR-a.sense_v2	TTCTTCAGGAAGGCCAGCAGCCACACACCGTGTGTGCTCAC CACACGCTGGCATGGGCCCTCCTCACCGAGCTGCCGACACC AGGCCTTGTGTCTCCCCCAGTGCTTCAAGGCGTCATAAGTA CATGACACCCTCAAAGACTGGCCGGCCATGCCCTGCAGCAC CGTGGTGTTGAGGGCTT
CRISPR v3a	mTREM2_R47H_HDR-a.sense_v3a	TTCTTCAGGAAGGCCAGCAGCCACACACCGTGTGTGCTCAC CACACGCTGGCATGGGCCCTCCTCACCCAGCTGGCGACACC AGGCCTTGTGTCTCCCCCAGTGCTTCAAGGCGTCATAAGTA CATGACACTCTCAAGGACTGGCCGGCCATGCCCTGCAGCAC CGTGGTGTTGAGGGCTT
	mTREM2_Q33X_HDR-a.sense_v3a	ACACCAGGCCTTGCGTCTCCCCCAATGCTTCAAGGCGTCAT AAGTACATGACACCTACAAGGACTGGCCGGCCATGCCCTGC AGGACCGTGGTGTTGAGGGCTTGGGACAGGG
	mTREM2_D87N_HDR-a.sense_v3a	CTCGGCCTCGGAGACTCTGACACTGGTAGAGGCCCGCGTCA CCGGCTTGGAGGTTCTTCAGAGTGATGGTGACGGTTCCAGC AAGTGTGTTATCTGCGATGACTGTGCTCCCATTCCGCTT TTTCAGGAAGGCCAGCAGCCACACACCGTGTGTGCTCACCA CACGCTGGCATGGGCCCTC

Continued on next page...

CRISPR design	HDR template	Sequence (5'→3')
CRISPR v3b	mTREM2_R47H_HDR-a.sense_v1	TTCTTCAGGAAGGCCAGCAGCCACACACCGTGTGTGCTCAC CACACGCTGGCATGGGCCCTCCTCACCCAGCTGCCGACACC AGGCCTT**GTG**TCTCCCCCAGTGCTTCAAGGCGTCATAAGTA CATGACACCCTCAAGGACTGGCCGGCCATGCCCTGCAGCAC CGTGGTGTTGAGGGCTT
	mTREM2_Q33X_HDR-a.sense_v3b	ACACCAGGCCTTGCGTCTCCCCCAGTGCTTCAAGGCGTCAT AAGTACATGACAC**CTA**CAAGGACTGGCCGGCCATGCCCTGC AGCACCGTGGTGTTGAGGGCTTGGGACAGGG
	mTREM2_D87N_HDR-a.sense_v3b	CTCGGCCTCGGAGACTCTGACACTGGTAGAGGCCCGCGTCA CCGGCTTGGAGGTTCTTCAGAGTGATGGTGACGGTTCCAGC AAGGGT**GTT**ATCTGCGATGACTGTGCTCCCATTCCGCTTCT TCAGGAAGGCCAGCAGCCACACACCGTGTGTGCTCACCACA CGCTGGCATGGGCCCTC
CRISPR v4	mTREM2_R47H_HDR-a.sense_v3a	TTCTTCAGGAAGGCCAGCAGCCACACACCGTGTGTGCTCAC CACACGCTGGCATGGGCCCTCCTCACCCAGCTG**GCG**ACACC AGGCCTT**GTG**TCTCCCCCAGTGCTTCAAGGCGTCATAAGTA CATGACAC**TCT**CAAGGACTGGCCGGCCATGCCCTGCAGCAC CGTGGTGTTGAGGGCTT

Table 2.8. HDR template sequences used in all CRISPR/Cas9 designs. Underlined font: knock-in mutations, blue font: target AD-associated variant codon, green font: PAM/sgRNA-blocking mutation codon.

2.2.2 Cloning sgRNA into sgRNA-Cas9 expression plasmids

To prepare the sgRNA fragments for cloning into the sgRNA-Cas9 expression plasmids, ssDNA oligonucleotides were phosphorylated and annealed into dsDNA fragments. To do this, 1 µL 100 µM (100 pmol) top strand and 1 µL 100 µM (100 pmol) bottom strand was mixed in a 0.2 mL PCR tube with 1× T4 DNA Ligase Buffer, 1 µL (10 units) T4 polynucleotide kinase (PNK), and nuclease-free water up to 10 µL (Table 2.9). The reaction mixture was then incubated in a thermocycler at 37°C for 30 min, 95°C for 5 min, and allowed to cool to RT. The phosphorylated and annealed sgRNA duplex was diluted 1:200 with nuclease-free water to 0.5 µM to prepare for cloning.

The sgRNA-Cas9 expression plasmids containing the eGFP selection marker (pSpCas9n(BB)-2A-GFP) and puromycin resistance selection marker (pSpCas9n(BB)-2A-Puro) were gifts from Feng Zhang (Addgene plasmids #48140 and #48141, respectively)[546]. The reported plasmid maps for pSpCas9n(BB)-2A-GFP and pSpCas9n(BB)-2A-Puro are shown in Figure 2.4. sgRNA pairs were cloned into the respective plasmids at the BpiI restriction sites (GAAGAC(2/6)^, Figure 2.5) and the combinations are detailed in Table 2.10.

To clone the sgRNA duplex into pSpCas9n(BB), 100 ng pSpCas9n(BB), 2 µL 0.5 µM sgRNA duplex (1 pmol), 1 µL 10 mM ATP (10 nmol), 2 µL 10× FastDigest buffer, 1 µL FastDigest BpiI, 0.5 µL T4 DNA Ligase (2.5 Weiss U), and nuclease-free water up to 20 µL was prepared in a 0.2 mL PCR tube (Table 2.11). The reaction mixture was incubated in a thermocycler for 6 cycles of 37°C for 5 min and 21°C for 5 min.

Reagent	**Amount**	**Working amount/ concentration**
sgRNA top (100 µM)	1 µL	100 pmol
sgRNA bottom (100 µM)	1 µL	100 pmol
T4 DNA Ligase Buffer (10×)	1 µL	1×
T4 PNK (10,000 units/mL)	1 µL	10 units
Nuclease-free water	6 µL	

Table 2.9. Reaction mixture to phosphorylate and anneal sgRNA top and bottom single-stranded DNA oligonucleotides into dsDNA fragments.

(a)

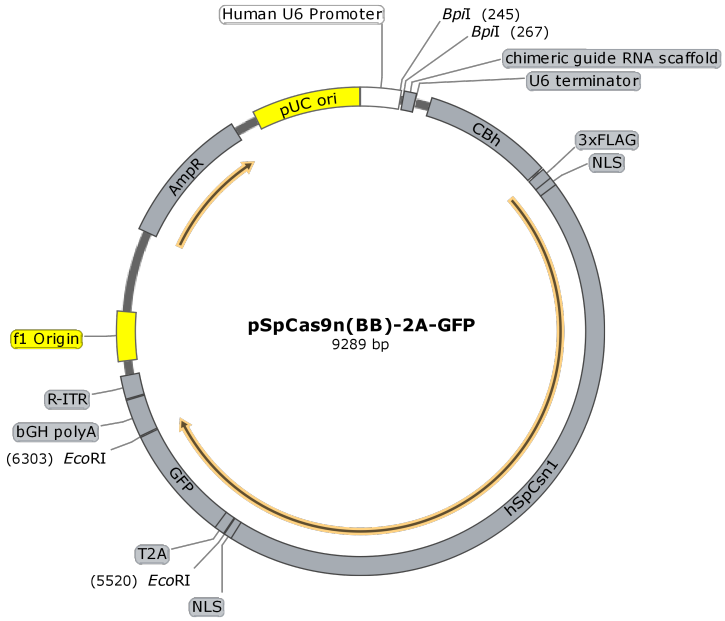

(b)

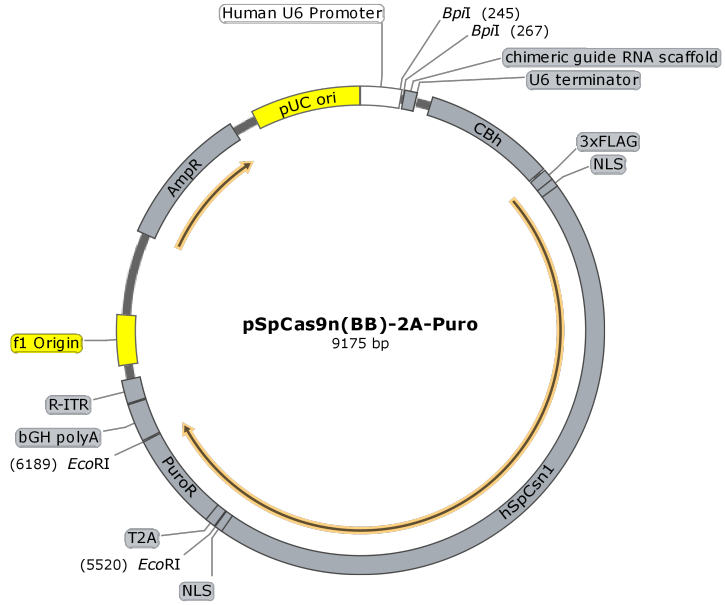

Figure 2.4. Plasmid maps for (a) pSpCas9n(BB)-2A-GFP and (b) pSpCas9n(BB)-2A-Puro.
sgRNA dsDNA fragments were inserted between the BpiI restriction sites.
CBh: hybrid CMV enhancer/chicken β-actin promoter, NLS: nuclear localisation sequence, hSpCsn1: human codon-optimised *Streptococcus pyogenes*-derived Cas9 with D10A mutation gene, T2A: *Thoseaasigna* virus 2A self-cleaving peptide, GFP: enhanced GFP gene, PuroR: puromycin resistance gene, bGH polyA: bovine growth hormone polyadenylation terminator signal, R-ITR: R-inverted terminal repeat, AmpR: ampicillin resistance gene, pUC ori: pUC origin of replication.

Figure 2.5. BpiI restriction sites, GAAGAC(2/6)ˆ, within pSpCas9n(BB) where the sgRNA dsDNA fragments will be cloned.
Green font: part of U6 promoter, red font: part of sgRNA scaffold, bold font: BpiI restriction sites, red arrows and blue dotted lines: DNA digestion.

pSpCas9n(sgRNA)
CRISPR v1
pSpCas9n(mTREM2_R47H_sgRNA-A_R1a)-2A-GFP
pSpCas9n(mTREM2_R47H_sgRNA-B_F1a)-2A-Puro
CRISPR v2
pSpCas9n(mTREM2_R47H_sgRNA-A_R2a)-2A-GFP
pSpCas9n(mTREM2_R47H_sgRNA-B_F1a)-2A-Puro
CRISPR v3a
pSpCas9n(mTREM2_R47H_sgRNA-A_R2a)-2A-GFP
pSpCas9n(mTREM2_R47H_sgRNA-B_F1a)-2A-mCherry2
pSpCas9n(mTREM2_Q33X_sgRNA-A_R1a)-2A-GFP
pSpCas9n(mTREM2_Q33X_sgRNA-B_F1a)-2A-mCherry2
pSpCas9n(mTREM2_D87N_sgRNA-A_R1a)-2A-GFP
pSpCas9n(mTREM2_D87N_sgRNA-B_F1a)-2A-mCherry2
CRISPR v3b
pSpCas9n(mTREM2_R47H_sgRNA-A_R2b)-2A-GFP
pSpCas9n(mTREM2_R47H_sgRNA-B_F1b)-2A-mCherry2
pSpCas9n(mTREM2_Q33X_sgRNA-A_R1b)-2A-GFP
pSpCas9n(mTREM2_Q33X_sgRNA-B_F1b)-2A-mCherry2
pSpCas9n(mTREM2_D87N_sgRNA-A_R1b)-2A-GFP
pSpCas9n(mTREM2_D87N_sgRNA-B_F1b)-2A-mCherry2
CRISPR v4
pSpCas9n(mTREM2_R47H_sgRNA-A_R2a)-2A-GFP
pSpCas9n(mTREM2_R47H_sgRNA-B_F1a)-2A-mCherry2

Table 2.10. List of all cloned pSpCas9n(sgRNA) plasmids that were used in CRISPR v1, v2, v3 and v4.

Reagent	Amount	Working amount/ concentration
pSpCas9n(BB)	Variable	100 ng
sgRNA dsDNA fragments (0.5 µM)	2 µL	1 pmol
ATP (10 mM)	1 µL	10 nmol
FastDigest buffer (10×)	2 µL	1×
FastDigest BpiI	1 µL	-
T4 DNA Ligase (5 Weiss U/µL)	0.5 µL	2.5 Weiss U
Nuclease-free water	Up to 20 µL	

Table 2.11. Reaction mixture to clone sgRNA dsDNA fragments into pSpCas9n(BB) at the BpiI restriction sites.

2.2.3 *E. coli* transformation

Transformation of competent Stbl3 *E. coli* (Thermo Fisher Scientific) was performed following the manufacturer's protocols with slight modifications. A 50 µL vial was thawed on ice and split into two 25 µL aliquots in 1.5 mL microfuge tubes, each for individual transformations. 2 µL of pSpCas9(sgRNA), sgRNA inserted into pSpCas9n(BB), from Chapter 2.2.2 was added into 25 µL Stbl3 *E. coli* and gently mixed. The *E. coli* were incubated on ice for 10 min, heat-shocked for 45 s at 42°C, and incubated on ice again for 2 min. 125 µL SOC medium (at RT) was added to each microfuge tube. 75 µL of each transformated *E. coli* was plated on a pre-warmed LB agar plate with 100 µg/mL ampicillin, reserving the remaining cells at 4°C as back up. The LB agar plates were incubated inverted at 37°C overnight.

The following day, 3 colonies for each pSpCas9n(sgRNA) were picked using a sterile pipette tip and inoculated on a reference LB agar plate with 100 µg/mL ampicillin and in a 30 mL Universal tube containing 3 mL LB broth with 100 µg/mL ampicillin. The reference plate and LB broth culture were incubated overnight at 37°C with the reference plate inverted and the liquid culture shaking at ∼300 rpm. The next day, reference plates were wrapped with Parafilm and stored at 4°C. The liquid culture was harvested by pelleting the cells at 6800 ×g for 3 min at RT to check for successful sgRNA insertion.

2.2.4 Validation of successful sgRNA insertion

pSpCas9n(sgRNA) plasmids were extracted and purified using the QIAprep Spin Miniprep Kit (QIAGEN) according to the manufacturer's protocols. The *E. coli* pellet was re-suspended in 250 µL Buffer P1 containing RNase A and LyseBlue reagent in a 1.5 mL microfuge tube. 250 µL Buffer P2 was added and mixed by inverting tube until the cell suspension turned homogenously blue. 350 µL Buffer N3 was added and mixed immediately by inverting tube until the cell suspension became colourless. The cell suspension was centrifuged at 14,500 ×g for 10 min. The supernatant was transferred onto a QIAprep spin column and centrifuged at 14,500 ×g for 1 min, discarding the flow-through. 0.5 mL Buffer PB was added to the spin column and centrifuged at 14,500 ×g for 1 min, discarding the flow-through. 0.75 mL Buffer PE with ethanol was added to the spin column and centrifuged at 14,500 ×g for 1 min, discarding the flow-through. The spin column was centrifuged again at 14,500 ×g for 1 min, discarding the flow-through. 50 µL Buffer EB was added to the spin column and after 1 min, plasmids were eluted into a clean 1.5 mL microfuge tube by centrifugation at 14,500 ×g for 1 min.

The purified pSpCas9n(sgRNA) plasmids were Sanger sequenced by contract to GENEWIZ using the U6-Fwd primer (`GAGGGCCTATTTCCCATGATTCC`) (Figure 2.4).

2.2.5 Expansion of transformed *E. coli* and plasmid DNA extraction

Initially, for CRISPR v1 and v2, plasmids were harvested using the QIAGEN Plasmid Plus Midi Kit (QIAGEN). Plasmids for CRISPR v3 were harvested using the EndoFree Plasmid Maxi Kit (QIAGEN). Both kits were used following the manufacturer's protocols.

For the QIAGEN Plasmid Plus Midi Kit, one colony for each validated pSpCas9n(sgRNA) was picked from the reference plate using a sterile pipette tip and inoculated into 3 mL LB broth with 100 µg/mL ampicillin in a 30 mL Universal tube as the starter culture. The starter culture was incubated at 37°C for ∼8 h with ∼300 rpm shaking. 500 µL of the starter culture was transferred into 500 µL 50% glycerol with LB broth in a cryovial and frozen at -80°C for long-term storage. The remaining starter culture was transferred into 50 mL LB broth with 100 µg/mL ampicillin and incubated at 37°C overnight with ∼300 rpm shaking. *E. coli* was harvested by centrifugation at 6,000 ×g for 15 min at 4°C. Pelleted *E. coli* was resuspended in 4 mL Buffer P1 containing RNase A and LyseBlue reagent. 4 mL Buffer P2 was added and mixed by inverting the tube until the cell suspension turned homogenously blue. This was incubated for 3 min at RT. 4 mL Buffer S3 was added and mixed immediately by inverting the tube until the cell suspension became completely colourless. The lysate was immediately transferred to a QIAfilter cartridge and incubated for 10 min at RT. The cell lysate was passed through the QIAfilter cartridge into a new tube. 2 mL Buffer BB was added to the filtered lysate and mixed by inverting. The lysate was transferred into a QIAGEN Plasmid Plus Midi spin column with a tube extender attached to a QIAvac 24 Plus (QIAGEN) vacuum manifold. The lysate was passed through the spin column by vacuum suction. The tube extenders were discarded and the spin columns were transferred into 2 mL collection tubes. 0.7 mL Buffer ETR was added to the spin column and centrifuged at 10,000 ×g for 1 min, discarding the flow-through. 0.7 mL Buffer PE was added to the spin column and centrifuged at 10,000 ×g for 1 min, discarding the flow-through. The spin column was centrifuged again at 10,000 ×g for 1 min to completely remove residual wash buffer. 200 µL Buffer EB was added to the spin column and after 1 min, eluted into a 1.5 mL microfuge tube by centrifugation at 10,000 ×g for 1 min. Plasmid DNA concentration and purity was determined by 260 nm absorbance on a NanoDrop spectrophotometer.

For the EndoFree Plasmid Maxi Kit, validated colonies were inoculated into a starter culture and cryopreserved bacterial stocks were prepared from the starter culture as described above. The remaining starter culture was transferred into 250 mL LB broth with 100 µg/mL ampicillin. The culture was incubated and pelleted as described above. Pelleted *E. coli* was resuspended in 10 mL Buffer P1 containing RNase A and LyseBlue reagent. 10 mL Buffer P2 was added and mixed by inverting until the cell suspension turned homogenously blue. This was incubated for 5 min at RT. 10 mL cold Buffer P3 was added and immediately mixed by inverting until the lysate became completely colourless. The lysate was immediately decanted into the barrel of a QIAfilter cartridge and incubated for 10 min at RT. The lysate was then passed through the cartridge using the provided plunger into a 50 mL centrifuge tube. 2.5 mL Buffer ER was added to the filtered lysate and mixed by inverting, followed by incubation for 30 min on ice. A QIAGEN-tip 500 was equilibrated by applying 10 mL Buffer QBT and emptied by gravity flow. The filtered lysate was then transferred into the QIAGEN-tip and passed through by gravity flow. The QIAGEN-tip was washed with 2× 30 mL Buffer QC and DNA was eluted with 15 mL Buffer QN into a 30 mL endotoxin-free centrifuge tube. DNA was precipitated with 10.5 mL isopropanol and centrifuged at 15,000 ×g for 30 min at 4°C, discarding the supernatant. The DNA pellet was washed with 5 mL endotoxin-free 70% ethanol and centrifuged at 15,000 ×g for 10 min, discarding the supernatant. The DNA pellet was air-dried for 5–10 min and DNA reconstituted in endotoxin-free Buffer TE. Plasmid DNA concentration and purity was determined by 260 nm absorbance on a NanoDrop spectrophotometer.

2.2.6 Generation of pSpCas9n(BB)-2A-mCherry2

pSpCas9n(BB)-2A-mCherry2 was made by replacing the puromycin resistance gene in pSpCas9n(BB)-2A-Puro with the mCherry2 fluorescent protein gene. This was contracted to GENEWIZ. Briefly, the T2A-puromycin resistance gene was excised from the plasmid at the EcoRI sites flanking the region (Figure 2.4b) by EcoRI restriction endonuclease digestion, leaving sticky ends. T2A-mCherry2 sequence with compatible sticky ends was ligated into the linearised plasmid. Successful cloning was validated by GENEWIZ through Sanger sequencing. Prepared pSpCas9n(BB)-2A-mCherry2 was received as a endotoxin-free Maxi-scale purified plasmid. The plasmid map is shown in Figure 2.6.

The expression of mCherry2 protein from the plasmid was validated by electroporation of 5 µg pSpCas9n(BB)-2A-mCherry2 into BV2 cells as described in Chapter 2.2.14.

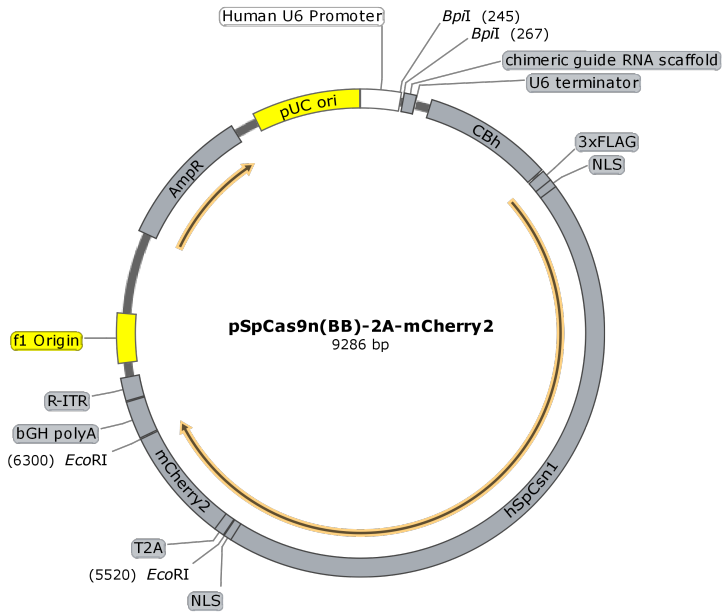

Figure 2.6. Plasmid map for pSpCas9n(BB)-2A-mCherry2.
sgRNA dsDNA fragments were inserted between the BpiI restriction sites.
CBh: hybrid CMV enhancer/chicken β-actin promoter, NLS: nuclear localisation sequence, hSpCsn1: human codon-optimised *Streptococcus pyogenes*-derived Cas9 with D10A mutation gene, T2A: *Thoseaasigna* virus 2A self-cleaving peptide, mCherry2: mCherry2 fluorescent protein gene, bGH polyA: bovine growth hormone polyadenylation terminator signal, R-ITR: R-inverted terminal repeat, AmpR: ampicillin resistance gene, pUC ori: pUC origin of replication.

2.2.7 Cell culture

BV2 immortalised mouse microglia cell line[552] was a kind gift from Dr Jennifer Pocock (UCL). BV2 were cultured in RPMI-1640 w/ 10% FBS + 1% PS and passaged at a 1:50 split when cells reach ∼80% confluency. To passage, cells were gently rinsed with DPBS and detached by incubating cells with 0.25% trypsin-EDTA for 5 min at 37°C, followed by gentle tapping of the culture vessel. Trypsin was inactivated by adding at least an equal volume of warm RPMI-1640 w/ 10% FBS + 1% PS. Detached cells were pelleted by centrifugation at 200 ×g for 5 min, discarding the supernatant. The cell pellet was resuspended in warm RPMI-1640 w/ 10% FBS + 1% PS and seeded into new culture vessels as appropriate. BV2 cultures were maintained up to passage 25 before discarding, as their growth characteristics become noticably poorer after this point.

HEK293A human embryonic kidney cell line[553] was cultured in DMEM, high glucose, GlutaMAX, pyruvate w/ 10% FBS + 1% PS and passaged at 1:10 split when cells reach confluency. Passaging protocols were performed similar to BV2.

2.2.8 DNA extraction and phenol/chloroform/isoamyl alcohol purification

$\sim 1 \times 10^6$-cell pellets were resuspended in 600 µL DNA extraction cell lysis buffer and briefly vortexed. 600 µL phenol/chloroform/isoamyl alcohol (PCI) was added and briefly vortexed to mix. The mixture was then centrifuged at 14,500 ×g for 15 min. 500 µL of the top aqueous layer was transferred into a new 1.5 mL microfuge tube. 500 µL chloroform was added to the aqueous layer and briefly vortexed to mix. The mixture was centrifuged at 14,500 ×g for 15 min. 400 µL of the top aqueous layer was transferred into a new 1.5 mL microfuge tube. 200 µL 7.5 M ammonium acetate and 800 µL ice-cold 100% ethanol was added to the aqueous layer and incubated for at least 1 h at -20°C to precipitate DNA. DNA was pelleted by centrifugation at 14,500 ×g for 15 min at 4°C. The supernatant was discarded and the DNA pellet was washed with 150 µL 70% ethanol. Loose DNA was collected by centrifugation at 14,500 ×g for 2 min at 4°C, discarding the supernatant. The DNA pellet was air-dried for 10 min at RT and resuspended in 20 µL Buffer EB (QIAGEN). DNA concentration and purity were determined by 260 nm absorbance on a NanoDrop spectrophotometer.

2.2.9 Polymerase chain reaction

PCR reagents per reaction were set up as described in Table 2.12 with the primer pairs mTREM2_Ex2_M13F(-21)_F1 and mTREM2_Ex2_M13R_R1 (Table 2.13). These were transferred to a thermocycler and incubated with the cycling conditions described in Table 2.14.

Reagents	**Amount**	**Working conc.**
One*Taq* Hot Start 2× Master Mix with Standard Buffer	5.0 µL	1×
Forward primer (10 µM)	0.2 µL	200 nM
Reverse primer (10 µM)	0.2 µL	200 nM
Nuclease-free water	3.6 µL	
Template DNA (10 ng/µL)	1.0 µL	1 ng/µL
Total volume	10.0 µL	

Table 2.12. PCR reagent setup per reaction using the One*Taq* Hot Start 2× Master Mix with Standard Buffer.

PCR primer	**Primer sequence (5'→3')**
mTREM2_Ex2_M13F(-21)_F1	TGTAAAACGACGGCCAGTATTCTAGAGCCCGTCAGGGA
mTREM2_Ex2_M13R_R1	CAGGAAACAGCTATGACTCCCCCTGAAAAAGTCCCAC

Table 2.13. PCR primers used to amplify *Trem2* Exon 2.
Red font: sequencing primer M13F or M13R as indicated.

Step	**Temperature**	**Time**	**Cycles**
Initial denaturation	94°C	30 s	–
Denaturation	94°C	30 s	
Annealing	65°C	60 s	40
Extension	68°C	60 s	
Final extension	68°C	5 min	–
Hold	4°C	Until collection	–

Table 2.14. Thermocycling conditions for PCR.

2.2.10 Agarose gel electrophoresis and Sanger sequencing

Agarose gel was prepared by dissolving 2 g UltraPure Agarose in 100 mL 1× sodium boric acid (SBA), Tris-acetate-EDTA (TAE), or Tris-borate-EDTA (TBE) buffer to obtain a 2% gel. 3 µL 10,000× GelRed was added to the dissolved agarose. The agarose gel was cast and allowed to set for 30 min at RT or 10 min at 4°C. Once set, the gel was transferred into the electrophoresis tank containing the same buffer used to make the gel. Unless indicated otherwise, 1 µL PCR products were mixed with 4 µL 1.25× BlueJuice Gel Loading Buffer before loading into the wells alongside 100 ng 100 bp DNA Ladder (Thermo Fisher Scientific) or 2 µL Quick-Load 100 bp DNA Ladder (New England Biolabs) for DNA size reference. Electrophoresis was performed at 300 V (15 V/cm) for 45 min for SBA buffer, 100 V (5 V/cm) for 60 min for TAE buffer, or 200 V (10 V/cm) for 90 min for TBE buffer. DNA bands were visualised and imaged on a ChemiDoc XRS+ System (Bio-Rad).

For sequencing, remaining PCR product was purified using the QIAquick PCR Purification Kit according to the manufacturer's protocols or purified by contract to GENEWIZ before Sanger sequencing, also by GENEWIZ.

2.2.11 RNA extraction and purification

RNA was extracted and purified using the RNeasy Plus Universal Mini Kit (QIAGEN) according to the manufacturer's protocols. BV2 cell pellets or C57BL/6 mouse brain tissue were lysed in 900 µL QIAzol Lysis Reagent, vortexed for 1 min and incubated for 5 min at RT. 100 µL gDNA Eliminator Solution was added and mixed vigorously for 15 s. 180 µL chloroform was added and mixed vigorously for 15 s. The sample was incubated for 2-3 min at RT before centrifuging at 12,000 ×g for 15 min at 4°C. 600 µL of the top aqueous layer was transferred into a new 1.5 mL microfuge tube, to which 600 µL 70% ethanol was added and briefly vortexed. 700 µL of the mixture was transferred into an RNeasy Mini spin column in a 2 mL collection tube, centrifuged at 8,000 ×g for 15 s at RT, discarding the flow-through. The remaining sample was similarly passed through the spin column. 700 µL Buffer RWT was added to each spin column, centrifuged at 8,000 ×g for 15 s, discarding the flow-through. 500 µL Buffer RPE was added to each spin column, centrifuged at 8,000 ×g for 15 s, discarding the flow-through. Another 500 µL Buffer RPE was added to each spin column, centrifuged at 8,000 ×g for 2 min and collection tube discarded. The spin columns were placed in a new 2 mL collection tube and centrifuged at 14,500 ×g for 1 min. Spin columns were transferred into new 1.5 mL microfuge tubes. 30 µL RNase-free water was added to each spin column and centrifuged at 8,000 ×g for 1 min. Another 30 µL RNase-free water was added to each spin column and centrifuged again to collect any remaining column-bound RNA. RNA concentration and purity were determined by 260 nm absorbance on a NanoDrop spectrophotometer.

2.2.12 Reverse transcription-polymerase chain reaction

5 µg of total purified RNA was converted into cDNA using SuperScript IV Reverse Transcriptase (Thermo Fisher Scientific) according to the manufacturer's protocol. 5 µg total RNA template was added to 1 µL 50 ng/µL random hexamers, 1 µL 10 mM dNTP mix and nuclease-free water up to a total volume of 13 µL. These were gently mixed and briefly centrifuged to collect. The mixture was incubated for 5 min at 65°C and then transferred onto ice to chill for at least 1 min. Meanwhile, the reverse transcriptase reaction mixture was prepared by combining 4 µL 5× SSIV Buffer, 1 µL 100 mM DTT, 1 µL 40 U/µL RNaseOUT, and 1 µL SuperScript IV Reverse Transcriptase per reaction. 7 µL of the reaction mixture was added to each chilled RNA template, gently mixed and briefly centrifuged. The reaction was incubated at 23°C for 10 min, 50°C for 10 min, 80°C for 10 min, and held at 4°C until collection.

Targets of interest were amplified by PCR as described in Chapter 2.2.9, in a 10 µL reaction volume. 1 µL cDNA was used as the template. Primer pairs and annealing temperatures used are listed in Table 2.15. RT-PCR products were resolved by agarose gel electrophoresis as described in Chapter 2.2.10.

Primer ID	Annealing temperature	Primer sequence (5'→3')
mAIF1F1	54°C	GATGAGGATCTGCCGTCCAAA
mAIF1R1		AGTAGCTGAACGTCTCCTCG
mCD68F1	55°C	CACAGTGGACATTCATGGCG
mCD68R1		GCAAGAGAAACATGGCCCGA
mCIITAF1	55°C	CTGGGGAGGAGGAGATCGAA
mCIITAR1		AAGAGGTCCTTGCTCAGGC
mCX3CR1F1	54°C	CGTGAGACTGGGTGAGTGAC
mCX3CR1R1		CCGGTTGTTCATGGAGTTGG
mDAP12F1	56°C	GCCCAGAGTGACACTTTCCC
mDAP12R1		GGGAGGTACCCTGTGGATCT
mHexbF1	54°C	CGACCCAGACTGGAAGGTTG
mHexbR1		GCCATGGCATCCAGAGTTTT
mIL1bF1	53°C	TGCCACCTTTTGACAGTGATG
mIL1bR1		TTCTTGTGACCCTGAGCGAC
mIL6F1	54°C	TCTCTGCAAGAGACTTCCATCC
mIL6R1		TAACGCACTAGGTTTGCCGA
mP2RY12F1	54°C	TACCCTACAGAAACACTCAAGGC
mP2RY12R1		CAGGGTGTAGGGAATCCGTG
mTNFaF1	52°C	TCTTCTCATTCCTGCTTGTGG
mTNFaR1		AGGGTCTGGGCCATAGAACT
mTREM2F1	55°C	CGGAATGGGAGCACAGTCAT
mTREM2R1		CTTGATTCCTGGAGGTGCTGT

Table 2.15. RT-PCR primers used to analyse mouse gene expression in BV2.

2.2.13 Transfection into BV2 by chemical-based transfection reagents

Lipofectamine 2000 (Thermo Fisher Scientific), Lipofectamine 3000 (Thermo Fisher Scientific), TurboFect (Thermo Fisher Scientific), PolyFect (QIAGEN), and FuGENE 6 (Promega) were explored as possible transfection reagents. $\sim 4 \times 10^5$ BV2 cells were seeded into each well of a 12-well culture plate containing 1 mL warm RPMI-1640 w/ 10% FBS and allowed to adhere for a few hours in a humidified incubator at 37°C/5% CO_2. Transfection was performed according to the manufacturer's protocols using the CRISPR v1 pSpCas9n(mTREM2_R47H_sgRNA-A_R1a)-2A-GFP plasmid. Table 2.16 shows the setup for the transfection reagents. When used in other culture well plate sizes, the amount of cells, transfection reagents, and plasmid DNA was scaled linearly relative to the surface area of wells.

After the transfection reagents were prepared, transfection complexes were left to incubate for 20 min at RT. During the incubation, old culture medium was replaced with fresh warm 1 mL RPMI-1640 w/ 10% FBS. After the incubation, transfection complexes were added dropwise directly into the respective wells. The 12-well culture plate was gently gyrated to ensure even coverage of transfection complexes and incubated in a humidified incubator at 37°C/5% CO_2 overnight. Transfection efficiency was assessed by counting the number of GFP-positive cells counterstained with DAPI at 10× objective magnification field of view.

Transfection reagent	**DNA:transfection reagent ratio**	**Diluent**
Lipofectamine 2000	1 µg plasmid DNA:3 µL Lipofectamine 2000	100 µL Opti-MEM
Lipofectamine 3000	1 µg plasmid DNA:2 µL P3000 Reagent: 3 µL Lipofectamine 3000	100 µL Opti-MEM
TurboFect	1 µg plasmid DNA:2 µL TurboFect	100 µL Opti-MEM
PolyFect	1 µg plasmid DNA:10 µL PolyFect	50 µL Opti-MEM
FuGENE 6	1 µg plasmid DNA:3 µL FuGENE 6	100 µL Opti-MEM

Table 2.16. 12-well culture plate setup of transfection reagents used to optimise the best transfection conditions for BV2.
pSpCas9n(mTREM2_R47H_sgRNA-A_R1a)-2A-GFP was transfected into BV2.

2.2.14 Transfection into BV2 by electroporation

The Nucleofector 2b (Lonza) system was used for electroporation with the Cell Line Optimization Nucleofector Kit for Nucleofector 2b Device (Lonza) to determine optimal electroporation parameters according to the manufacturer's protocol.

During optimisation (CRISPR v1 and v2), 1×10^6 cells were resuspended in 100 µL Nucleofector Solution L or V. 2 µg pmaxGFP alone or 5 µg of each plasmid pair (total 10 µg) was combined and added with 100 pmol sense or anti-sense HDR template to the cell suspension. The cell suspension was transferred into a Nucleofector cuvette and electroporated using the recommended programs A-030, A-033, A-020 or D-023.

After optimisation (CRISPR v3 onwards), 2×10^6 cells were resuspended in 100 µL Nucleofector Solution L and electroporated with 2.5 µg of each plasmid pair (total 5 µg) combined with 100 pmol anti-sense HDR template using program A-030.

After electroporation, 500 µL warm RPMI-1640 w/ 10% FBS was gently added to the cuvettes and incubated for 10 min at 37°C. The cell suspension was transferred into 6-well culture plates containing 1.5 mL warm RPMI-1640 w/ 10% FBS and incubated in a humidified incubator at 37°C/5% CO_2 overnight. Transfection efficacy was estimated by observing GFP expression by fluorescence microscopy or by flow cytometry.

2.2.15 Puromycin treatment

24 h post-transfection of BV2 or HEK293A with sgRNA-Cas9 expression plasmid pairs and HDR template using Lipofectamine 3000, old cell culture medium was replaced with fresh warm culture medium containing puromycin dihydrochloride between 0–5 µg/mL. Cells were incubated with puromycin for 48 h in a humidified incubator at 37°C/5% CO_2. After the incubation period, cells were imaged at 100× magnification and cell viability was compared to determine optimal puromycin concentration.

2.2.16 Nocodazole treatment

5×10^5 BV2 cells were seeded into each well of a 6-well culture plate and allowed to adhere for 7 h in a humidified incubator at 37°C/5% CO_2. Old culture medium was replaced with 0 ng/mL, 10 ng/mL, 100 ng/mL, 200 ng/mL, 500 ng/mL, or 1000 ng/mL nocodazole in warm RPMI-1640 w/ 10% FBS. Cells were incubated with nocodazole for 17 h in a humidified incubator at 37°C/5% CO_2. Culture medium containing nocodazole was discarded and cells were immediately electroporated as described in Chapter 2.2.14.

2.2.17 Nuclei staining in BV2

1.6×10^5 electroporated BV2 cells were seeded onto 13 mm diameter coverslips in 24-well culture plates with RPMI-1640 w/ 10% FBS + 1% PS and allowed to adhere. Culture medium was replaced with 200 µL of 5 µM CellTracker Red CMTPX Dye in RPMI-1640 and incubated for 45 min in a humidified incubator at 37°C/5% CO_2. Stained cells were fixed with 500 µL 10% neutral buffered formalin (NBF) for 5 min and gently rinsed 3× 5 min with DPBS. Fixed cells were stained with 1 µg/mL Hoechst 33342 in water for 5 min and gently washed with dH_2O for 5 min. The coverslips were mounted onto glass slides with Mowiol hard set aqueous mounting medium and allowed to set for at least 30 min at RT. Slides were viewed and imaged using a Leica DM5000 B fluorescence microscope.

2.2.18 Fluorescence-activated cell sorting

Before performing FACS, transfected cells were gently rinsed with DPBS, detached with 0.25% trypsin-EDTA and pelleted at 200 ×g for 5 min, discarding the culture medium supernatant. Cell pellet was resuspended in 1 mL warm 10% FBS in DPBS or 500 µL warm phenol red-free RPMI-1640. Cells were passed through a 40 µm cell strainer and kept on ice until FACS.

Transfection efficiency was determined by the percentage of GFP^{hi} (excitation laser 488 nm, emission detection 525/50 nm) and/or $mCherry2^{hi}$ (excitation laser 561 nm, emission detection 610/20 nm) cells during FACS on a BD FACS Aria (BD Biosciences). Gates were set according to untransfected controls.

For CRISPR v1 and v2, 24 h post-electroporation, transfected cells were clonally isolated by single-cell sorting GFP^{hi} cells into each well of a 96-well culture plate with 100 µL RPMI-1640 w/ 10% FBS + 1% PS. The clonal cells were incubated in a humidified incubator at 37°C /5% CO_2. Each well was monitored regularly to ensure growth from a single cell. Only wells with cell that grew from a single cell were subsequently investigated. On average, it took 2 weeks for each BV2 clonal line to reach confluency in a 96-well culture plate.

For CRISPR v3 onwards when pSpCas9n(sgRNA)-2A-Puro was replaced with pSpCas9n (sgRNA)-2A-mCherry2, at 24 h post-electroporation, transfected cells were first enriched by sorting GFP^{hi} and $mCherry2^{hi}$ double-positive cells into 1 mL RPMI-1640 w/ 10% FBS + 1% PS (Figure 2.7b). Enriched cells were allowed to recover in T75 flasks with 15 mL RPMI-1640 w/ 10% FBS + 1% PS for a week in a humidified incubator at 37°C /5% CO_2. Before single-cell sorting, cells were detached and pelleted as described above. Just before resuspension in warm phenol red-free RPMI-1640, cells were resuspended in 1 mL 5 µg/mL Hoechst 33342 in RPMI-1640 + 10% FBS + 1% PS and incubated for 15 min at 37°C. Excess Hoechst 33342 was removed by pelleting the cells again and discarding the supernatant. Mononucleated cells were then single-cell sorted by forward scatter $(FSC)^{lo}$ and side scatter $(SSC)^{lo}$ only (Figure 2.7c) or in combination with $Hoechst^{lo}$ (Figure 2.8) into 96-well culture plates as described above.

(a) Untransfected BV2 **(b) CRISPR v3 transfected BV2**

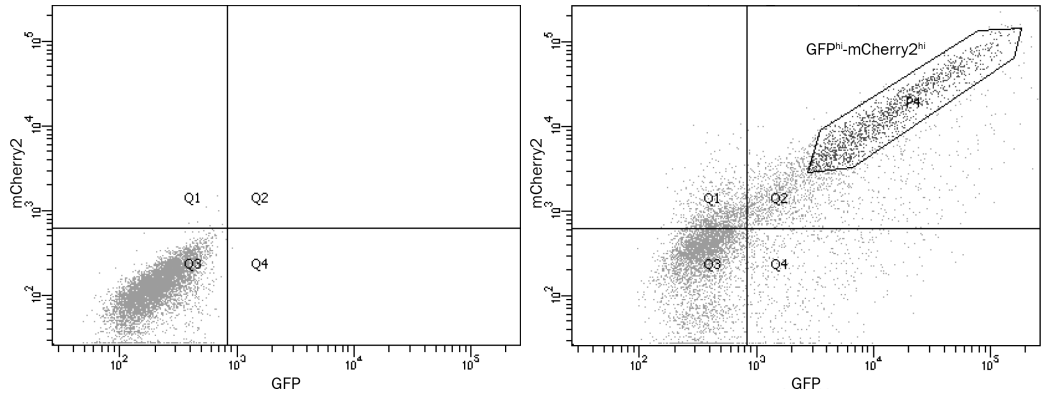

(c) Mononucleated cells

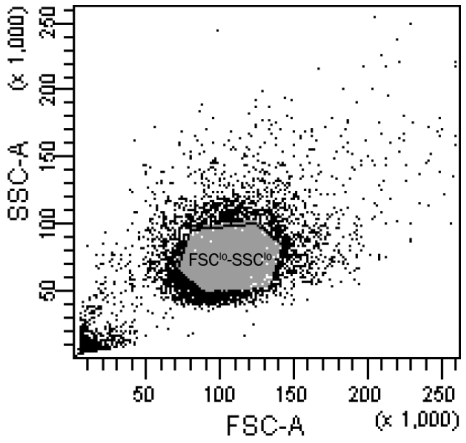

Figure 2.7. Gating parameters for FACS used in CRISPR v3.
(a) Untransfected BV2 to establish threshold for GFP^{hi} and $mCherry2^{hi}$ gating. **(b)** GFP^{hi} and $mCherry2^{hi}$ BV2 transfected with CRISPR v3 plasmids and HDR templates. **(c)** FSC^{lo}-SSC^{lo} gating to single-cell sort mononucleated cells.

(a) Total cell population

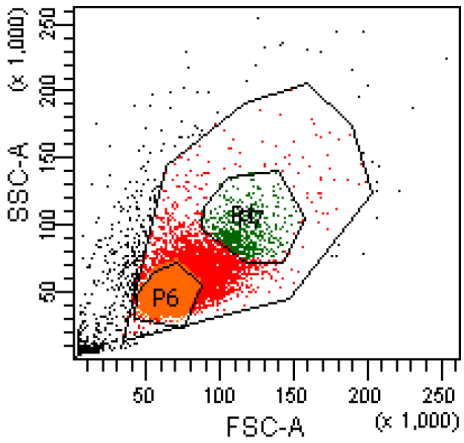

(b) Mononucleated cell population

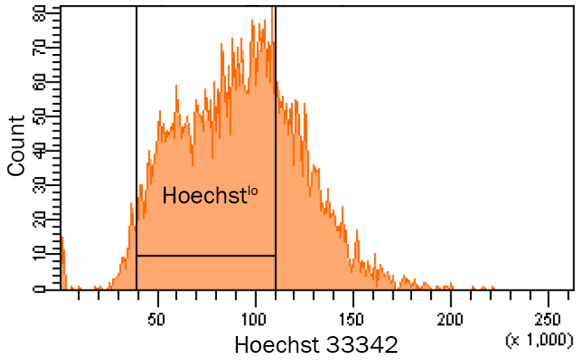

(c) Multinucleated cell population

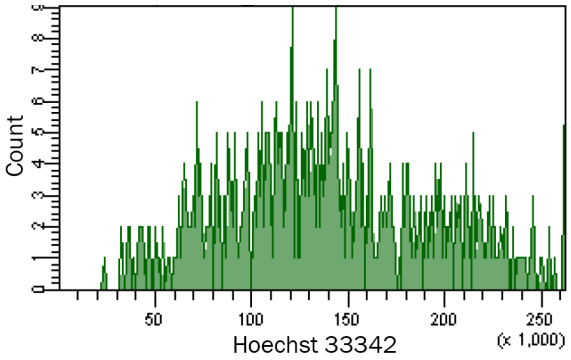

Figure 2.8. Gating parameters for mononucleated cells using Hoechst 33342 by FACS.
(a) Smaller and less granulated mononucleated cells (FSC^{lo}-SSC^{lo}, orange) were gated from the total cell population (red). **(b)** Hoechst^{lo} cells were gated from FSC^{lo}-SSC^{lo} cells and single-cell sorted. **(c)** Larger and more granulated cells (green) were more likely to be multinucleated with higher Hoechst 33342 fluorescence intensity.

2.2.19 Cryopreservation in 96-well culture plates

Old culture medium was discarded and cells were gently rinsed with DBPS. DPBS was discarded and cells in the 96-well culture plate were detached by incubation with 25 µL 0.25% trypsin-EDTA for 5 min at 37°C, followed by gentle tapping. The cell suspension was gently mixed by pipetting to break cell clumps and 20 µL was transferred into 20 µL 2× freezing medium (20% DMSO in FBS) in a replicate 96-well culture plate. The remaining 5 µL cell suspension was transferred into 10 µL 0.5× Direct-Lyse lysis buffer in a replicate 96-well PCR plate for crude DNA extraction (Chapter 2.2.20). Both plates were sealed with MicroAmp Clear Adhesive Film (Thermo Fisher Scientific) plate sealing films. The 96-well culture plate was covered with its lid and wrapped in a thick layer of paper towels before transferring into a thick polystyrene box. The polystyrene box was transferred into a -80°C freezer. Cells cryopreserved in this manner were found to be viable for up to a month, allowing sufficient time for successfully edited clonal lines to be screened for further expansion and characterisation.

2.2.20 Crude DNA extraction

This crude DNA extraction protocol was adapted from Ramlee *et al.* (2015)[554]. The 5 µL cell suspension in 10 µL 0.5× Direct-Lyse lysis buffer in 96-well PCR plates from Chapter 2.2.19 were incubated in a thermocycler according to the conditions in Table 2.17. The lysates were diluted with 40 µL nuclease-free water.

Temperature (°C)	**Time (min)**
65	0:30
8	0:30
65	1:30
97	3:00
8	1:00
65	3:00
97	1:00
65	1:00
80	10:00

Table 2.17. Thermocycling conditions for crude DNA extraction from cells in 96-well PCR plates.

2.2.21 DNA purification of crude DNA extracts

Crude DNA extracts were purified using the QIAamp DNA Mini Kit (QIAGEN) following the manufacturer's protocols. Crude DNA extracts were reconstituted to 200 µL with DPBS and transferred to individual 1.5 mL microfuge tube containing 20 µL proteinase K. 200 µL Buffer AL was added and mixed by vortexing for 15 s. Samples were incubated for 10 min at 56°C and briefly centrifuged. 200 µL ethanol was added to the samples, mixed by vortexing for 15 s and briefly centrifuged. Samples were transferred into a QIAamp Mini spin column in a 2 mL collection tube and centrifuged at 6,000 ×g for 1 min, discarding the flow-through. 500 µL Buffer AW1 was added to the spin column and centrifuged at 6,000 ×g for 1 min, discarding the flow-through. 500 µL Buffer AW2 was added to the spin column and centrifuged at 14,500 ×g for 3 min, discarding the flow-through. The spin column was centrifuged again at 14,500 ×g for 1 min and transferred into a clean 1.5 mL microfuge tube. 200 µL Buffer AE was added into the spin column and incubated for 1 min at RT, followed by centrifugation at 6,000 ×g for 1 min to elute DNA.

2.2.22 Competitive allele specific PCR

A custom competitive allele specific PCR (KASP) assay kit (KASP on Demand + KASP V4.0 2×Master mix, High ROX) was designed and validated by LGC Genomics to genotype the rs75932628 R47H variant in mouse *Trem2*. The assay was performed following the manufacturer's protocols. Positive control DNA was prepared by using combinations of the HDR templates in the sense or anti-sense orientation with the WT or R47H variant (CRISPR v1, Table 2.8) at the appropriate molar ratios to simulate the homozygous WT (GG) alleles, homozygous R47H variant (AA) alleles, or the heterozygous R47H variant (GA) alleles (Table 2.18). These positive control DNA were validated to work with the primers of the custom KASP assay.

The assay reagents: 2.5 µL DNA template of various formats (e.g. undiluted crude DNA, 1:10 diluted crude DNA, 1:10 diluted *Trem2* amplicons), 2.5 µL KASP V4.0 2× Master mix, High ROX, and 0.07 µL KASP on Demand primers per reaction, were prepared in 384-well PCR plates (Table 2.19). The plate was sealed using a MicroAmp Optical Adhesive Film (Thermo Fisher Scientific). The assay was performed and read on a 7900HT Real-Time PCR System (Applied Biosystems) with the recommended 61-55°C Touchdown thermocycling condition (Table 2.20).

Control genotype	**HDR template**	**Molar ratio**
GG	WT sense	2
	WT anti-sense	2
AA	R47H sense	2
	R47H anti-sense	2
GA	WT sense	1
	WT anti-sense	1
	R47H sense	1
	R47H anti-sense	1

Table 2.18. Molar ratios of the individual ssDNA HDR template used to make up positive control DNA for the KASP genotyping assay.
These simulate the mouse *Trem2* homozygous WT (GG) alleles, homozygous p.R47H variant (AA) alleles, or heterozygous p.R47H variant (GA) alleles.

Reagents	Volume
DNA template	2.5 µL
KASP V4.0 2× Master mix, High ROX	2.5 µL
KASP on Demand primers	0.07 µL

Table 2.19. Reagent setup per reaction for KASP assay in a 384-well PCR plate format.

Description	Temperature	Duration	No. of cycles
Hot-start Taq activation	94°C	15 min	1
Touchdown	94°C	20 s	10
	61°C decreasing 0.6°C per cycle to 55°C	60 s	
Amplification	94°C	20 s	26
	55°C	60 s	
Cool	24 °C	60 s	1

Table 2.20. Recommended thermocycling conditions for KASP assay.

2.2.23 Karyotyping

Cells were prepared at ∼40–50% confluency in T25 flasks and shipped to Cell Guidance Systems Ltd filled to the neck with warm RPMI-1640 w/ 10% FBS + 1% PS for karyotyping. Karyotyping reports and representative images were received and analysed.

2.2.24 Expansion and cryopreservation of clonal cell lines

Cryopreserved clonal cell lines of interest in 96-well culture plates were thawed in a 37°C incubator for ∼10 min. After thawing, the outside of the plates was sprayed with 70% IMS. 200 µL warm RPMI-1640 w/ 10% FBS + 1% PS was added to each well to dilute DMSO from the freezing medium. The cells were allowed to recover overnight in a 37°C/5% CO_2 incubator. The following day, culture medium was replaced with 100 µL fresh warm RPMI-1640 w/ 10% + 1% PS. Clonal lines were allowed to grow to confluence in the 96-well culture plate.

Old culture medium was discarded and cells were gently rinsed with DPBS. Cells were detached by incubation with 25 µL 0.25% trypsin-EDTA for 5 min at 37°C, followed by tapping of the plate. Cell suspension was directly transferred into 25 mL warm RPMI-1640 w/ 10% FBS + 1% PS in a T175 flask. Clonal lines were allowed to expand until confluent in the T175 flasks in a humidified incubator at 37°C/5% CO_2, replacing culture medium as necessary.

After reaching confluency, old culture medium from each flask was transferred into individual 50 mL centrifuge tubes to collect non-adherent cells. Remaining adherent cells were gently rinsed with DPBS and the DPBS was transferred into the respective 50 mL centrifuge tubes. Cells were detached with 0.25% trypsin-EDTA and incubated for 5 min at 37°C, followed by tapping of the flask. Cell suspension was transferred into the respective 50 mL centrifuge tubes and centrifuged at 200 ×g for 5 min, discarding the supernatant. Cell pellets were resuspended at 1×10^6 cells/mL in RPMI-1640 w/ 10% FBS + 1% PS + 10% DMSO. 1 mL aliquots were added into cryovials, which were transferred into Mr Frosty (Thermo Fisher Scientific) freezing containers containing isopropanol. The freezing containers were kept at -80°C overnight and the cryovials were transferred into liquid nitrogen for storage.

2.3 Methodology for Chapter 4

2.3.1 Source of brain tissue and selection criteria

Hippocampal brain sections were obtained from various tissue banks, including the MRC London Neurodegenerative Diseases Brain Bank (King's College London, UK), Queen Square Brain Bank for Neurological Disorders (University College London, UK), Oxford Brain Bank (John Radcliffe Hospital, UK), Southampton Brain Bank (BRAIN UK), and the Netherlands Brain Bank (Netherlands Institute for Neuroscience, Royal Netherlands Academy of Arts and Sciences).

The inclusion criteria was that all cases with disease-associated TREM2 variants, previously identified by Dr Angela Hodges, were considered (Table 2.21). There were 6 non-AD controls with TREM2 variants that were not included in the study as meaningful statistics cannot be performed with large data variation between cases. Each AD case with TREM2 variants were pair-matched for age at death and gender with a non-AD control and an AD case without TREM2 variants.

Cases were excluded if they did not have available tissue sections containing the posterior hippocampus. Besides that, AD cases that were not Braak tau stage[77] IV–VI and non-AD controls that were not Braak tau stage 0–I were also excluded.

Following the inclusion and exclusion criteria, 16 AD cases with disease-associated TREM2 variants (AD/TREM2$^{\text{var}}$), 21 AD cases (AD/TREM2$^{\text{wt}}$) and 18 non-AD control cases (Control/TREM2$^{\text{wt}}$) without disease-associated TREM2 variants were selected.

Informed consent was obtained from all tissue donors in accordance with the Declaration of Helsinki (1991) and protocols and procedures were approved by the relevant local ethical committee at each site.

Subject ID	Inclusion/Exclusion (reason)	Disease-associated TREM2 variant (SNP ID)	Diagnosis	Age at death (y)	Sex	Source
A220/11	Include	p.R47H (rs75932628)	AD Braak IV	71	Female	MRC London
A166/04	Include	p.R47H (rs75932628)	AD Braak VI	43	Male	MRC London
A191/07	Include	p.Q33X (rs104894002)	AD Braak VI	69	Female	MRC London
A341/11	Include	p.R47H (rs75932628)	AD Braak VI	76	Male	MRC London
P03_09	Include	p.R47H (rs75932628)	AD Braak VI	64	Male	QSBB
P07_09	Include	p.R47H (rs75932628)	AD Braak VI	66	Female	QSBB
P1405/06	Include	p.R47H (rs75932628)	AD Braak VI	76	Female	BRAIN UK
P19_06	Include	p.D87N (rs142232675)	AD Braak VI	71	Male	QSBB
P59_03	Include	p.R47H (rs75932628)	AD Braak VI	41	Female	QSBB
S00/318	Include	p.D39E (rs200392967)	AD Braak VI	72	Female	TNBB
S05/265	Include	p.G58A (novel)	AD Braak VI	64	Male	TNBB
S96/204	Include	p.D87N (rs142232675)	AD Braak VI	91	Female	TNBB
A013/03	Include	p.R47H (rs75932628)	AD Braak V–VI	89	Male	MRC London
A025/03	Include	p.T96K (rs2234253), p.W191X (rs2234258), p.L211P (rs2234256)	AD Braak V–VI	72	Female	MRC London
A112/96	Include	p.R98W (rs147564421)	AD Braak V–VI	78	Female	MRC London
C33/88	Include	p.R47H (rs75932628)	AD Braak V–VI	76	Female	OBB
A228/96	Exclude (non-AD, no hippocampus)	p.T96K (rs2234253), p.W191X (rs2234258), p.L211P (rs2234256)	Control	81	Female	MRC London
A008/97	Exclude (non AD)	p.A105V (rs145080901)	Control	33	Female	MRC London
A358/99	Exclude (non AD)	p.R47H (rs75932628)	Control	55	Female	MRC London
C19_93	Exclude (non AD)	p.R47H (rs75932628)	Control	82	Male	QSBB

Subject ID	Inclusion/Exclusion (reason)	Disease-associated TREM2 variant (SNP ID)	Diagnosis	Age at death (y)	Sex	Source
P23_07	Exclude (non AD)	p.R47H (rs75932628)	Control	77	Male	QSBB
05/023	Exclude (non AD)	p.R47H (rs75932628), p.D87N (rs142232675)	MCI	80	Female	OBB
S01/283	Exclude (no hippocampus)	p.D87N (rs142232675)	AD Braak IV	86	Female	TNBB
04/021	Exclude (no hippocampus)	p.R47H (rs75932628)	AD Braak VI	93	Female	OBB
93/1074	Exclude (no hippocampus)	p.R47H (rs75932628)	AD Braak V–VI	78	Female	OBB

Table 2.21. Cases with disease-associated TREM2 variants previously identified by Dr Angela Hodges prior to this project.
6 non-AD controls with TREM2 variants were not included as meaningful statistics cannot be performed with large data variation between cases. Cases were excluded if hippocampal tissue were unavailable. AD cases that were not Braak tau stage IV–VI or non-AD controls that were not Braak tau stage 0–I were also excluded.
MRC London: MRC London Neurodegenerative Diseases Brain Bank (King's College London, UK); QSBB: Queen Square Brain Bank for Neurological Disorders (University College London, UK); BRAIN UK: Southampton Brain Bank (BRAIN UK); TNBB: the Netherlands Brain Bank (Netherlands Institute for Neuroscience, Royal Netherlands Academy of Arts and Sciences); OBB: Oxford Brain Bank (John Radcliffe Hospital, UK).

2.3.2 Immunohistochemistry

5–7 µm thick formalin-fixed paraffin-embedded (FFPE) sections of the entorhinal cortex containing the hippocampus were cut from tissue blocks and mounted on charged microscope slides by the various tissue bank providers. Sections were deparaffinised with xylene for 2× 5 min and rehydrated in decreasing concentrations of industrial methylated spirit (IMS; 100%, 95%, 70% v/v) for 5 min each. Endogenous peroxidase were quenched with 0.7% v/v hydrogen peroxide (H_2O_2) in methanol for 30 min. Sections were washed in running tap water and distilled water (dH_2O) for 5 min each. Heat-induced epitope retrieval (HIER) was performed with citrate-buffered saline (CBS, pH 6.0) in a microwave for 15 min followed by washing in running tap water until the slides were cool. For Aβ staining, sections were also treated with 80% v/v formic acid for 1 h followed by washing in running tap water for 10 min. Sections were washed in dH_2O for 5 min while a hydrophobic barrier was drawn around the sections. Sections were washed in 1× TBS-T 0.1% for 2× 5 min. Non-specific binding was blocked with 10% v/v normal serum (from the same species that the secondary antibodies were raised in) in 1× TBS-Tx 0.25% for 1 h at RT. Blocking solution was discarded and the primary antibody solution with 1% v/v blocking serum in TBS-Tx 0.1% was immediately applied and incubated overnight at 4°C. Sections were washed in 1× TBS-T 0.1% for 2× 5 min. The secondary antibody solution in TBS-T 0.1% was applied on the sections and incubated for 1 h at RT. Sections were washed in 1× TBS-T 0.1% for 2× 5 min. Sections were visualised with the VECTASTAIN Elite ABC HRP Kit (Vector Laboratories) for 1 h, washed in 1× TBS-T 0.1% for 2× 5 min, followed by incubation with activated 3,3'-diaminobenzidine tetrahydrochloride (DAB; 0.024% H_2O_2 in DAB dissolved in 1× TBS-T 0.1%). Sections were washed in running tap water and dH_2O for 5 min each. Sections were counterstained in Harris' haematoxylin for 40 s, washed in running tap water to remove excess staining, differentiated in 1% acid alcohol, and followed by blueing of haematoxylin in running tap water for 5 min. Sections were washed in dH_2O for 5 min. Sections were dehydrated in increasing concentrations of IMS (70%, 95%, 100%, 100% v/v) for 5 min each and cleared with xylene for 2× 5 min. Sections were coverslipped with DPX and left to set overnight.

Combinations of blocking, primary antibody and secondary antibody solutions used are shown in Table 2.22.

Blocking solution	Primary antibody	Dilution	Manufacturer	Cat#	Secondary antibody	Dilution	Manufacturer	Cat#
NGS	Anti human CD68 (clone PG-M1), mouse	1:50	Dako	M087601-2	Anti mouse IgG, goat, biotinylated	1:200	Dako	E0433
NGS	Anti human HLA-DP, DQ, DR (clone CR3/43), mouse	1:100	Dako	M0775	Anti mouse IgG, goat, biotinylated	1:200	Dako	E0433
NSS	Anti Iba-1, rabbit	1:1000	Wako	019-19741	Anti rabbit IgG, swine, biotinylated	1:200	Dako	E0353
NGS	Anti amyloid-$\beta_{17\text{-}24}$ (clone 4G8), mouse	1:1200	BioLegend	800701	Anti mouse IgG, goat, biotinylated	1:200	Dako	E0433
NGS	Anti phospho-tau Ser202, Thr205 (clone AT8), mouse	1:1000	TFS	MN1020	Anti mouse IgG, goat, biotinylated	1:200	Dako	E0433

Table 2.22. Combinations of blocking solution, primary antibodies, and secondary antibodies that were used for immunohistochemistry.
NGS: normal goat serum, NSS: normal swine serum, TFS: Thermo Fisher Scientific.

2.3.3 Immunofluorescence

Adjacent FFPE sections used in immunohistochemistry were used for immunofluorescence. Sections were deparaffinised with xylene for 2× 5 min and rehydrated in decreasing concentrations of IMS (100%, 95%, 70% v/v) for 5 min each. Sections were washed in dH_2O for 5 min. HIER was performed with CBS in a microwave for 15 min followed by washing in running tap water until the slides were cool. For Aβ staining, sections were also treated with 80% v/v formic acid for 1 h followed by washing in running tap water for 10 min. Sections were washed in dH_2O for 5 min while a hydrophobic barrier was drawn around the sections. Sections were washed in 1× TBS-T 0.1% for 2× 5 min. Non-specific binding was blocked with 10% v/v normal serum (from the same species that the secondary antibodies were raised in) in 1× TBS-Tx 0.25% for 1 h at RT. Blocking solution was discarded and the primary antibody solution with 1% v/v blocking serum in TBS-Tx 0.1% was immediately put on and incubated overnight at 4°C. Sections were washed in 1× TBS-T 0.1% for 2× 5 min. The secondary antibody solution in TBS-T 0.1% was put on the sections and incubated for 1 h at RT. Sections were washed in 1× TBS-T 0.1% for 2× 5 min. Autofluorescence was quenched in 0.3% Sudan Black B in 70% IMS for 10 min. Sections were washed in 1× TBS-T 0.1% for 2× 5 min. Nuclei were stained with 1 µg/mL Hoechst 33342 in dH_2O for 10 min. Sections were washed in dH_2O for 5 min. Sections were coverslipped with Mowiol hard set aqueous mounting medium and left to set in the dark overnight at RT.

Combinations of blocking, primary antibody and secondary antibody solutions applied sequentially or simultaneously for multiplex staining are shown in Table 2.23. For sequentially applied antibodies, the first primary and secondary antibodies were applied as usual, followed by application of the second blocking and primary antibody solutions.

Blocking solution	Primary antibody	Dilution	Manufacturer	Cat#	Secondary antibody	Dilution	Manufacturer	Cat#
Simultaneously applied antibodies								
NGS	Anti human CD68 (clone PG-M1), mouse	1:50	Dako	M087601-2	Anti mouse IgG, goat, AF488	1:200	TFS	A11001
	Anti Iba-1, rabbit	1:1000	Wako	019-19741	Anti rabbit IgG, goat, AF594	1:200	TFS	A11012
NGS	Anti human HLA-DP, DQ, DR (clone CR3/43), mouse	1:50	Dako	M0775	Anti mouse IgG, goat, AF488	1:200	TFS	A11001
	Anti Iba-1, rabbit	1:1000	Wako	019-19741	Anti rabbit IgG, goat, AF594	1:200	TFS	A11012
NGS	Anti human CD68 (clone PG-M1), mouse	1:50	Dako	M087601-2	Anti mouse IgG, goat, AF568	1:200	TFS	A11004
	Anti tau, rabbit	1:1000	Dako	A0024	Anti rabbit IgG, goat, AF488	1:200	TFS	A11008
NGS	Anti human HLA-DP, DQ, DR (clone CR3/43), mouse	1:50	Dako	M0775	Anti mouse IgG, goat, AF568	1:200	TFS	A11004
	Anti tau, rabbit	1:1000	Dako	A0024	Anti rabbit IgG, goat, AF488	1:200	TFS	A11008
NGS	Anti Iba-1, rabbit	1:1000	Wako	019-19741	Anti rabbit IgG, goat, AF594	1:200	TFS	A11012
	Anti phospho-tau Ser202, Thr205 (clone AT8), mouse	1:1000	TFS	MN1020	Anti mouse IgG, goat, AF488	1:200	TFS	A11001
Sequentially applied antibodies								
NGS	Anti human CD68 (clone PG-M1), mouse	1:50	Dako	M087601-2	Anti mouse IgG, goat, AF568	1:200	TFS	A11004
NMS	Anti amyloid-$\beta_{1\text{-}16}$ (clone 6E10) AF488, mouse	1:100	BioLegend	803013	–	–	–	–
NGS	Anti human HLA-DP, DQ, DR (clone CR3/43), mouse	1:50	Dako	M0775	Anti mouse IgG, goat, AF568	1:200	TFS	A11004
NMS	Anti amyloid-$\beta_{1\text{-}16}$ (clone 6E10) AF488, mouse	1:100	BioLegend	803013	–	–	–	–
NGS	Anti Iba-1, rabbit	1:1000	Wako	019-19741	Anti rabbit IgG, goat, AF594	1:200	TFS	A11012
NMS	Anti amyloid-$\beta_{1\text{-}16}$ (clone 6E10) AF488, mouse	1:100	BioLegend	803013	–	–	–	–

Table 2.23. Combinations of blocking solution, primary antibodies, and secondary antibodies that were applied simultaneously or sequentially for multiplex immunofluorescence staining.
AF: Alexa Fluor, NGS: normal goat serum, NMS: normal mouse serum, TFS: Thermo Fisher Scientific.

2.3.4 Microscopy

DAB-stained whole-slide sections were imaged using a Leica SCN400F (Leica Biosystems) slide scanner at University College London with a maximum optical magnification of 200×.

Fluorescently labelled sections were imaged using a Leica DM5000 B at the indicated magnifications. The filters used were: A4 filter for Hoechst 33342, L5 filter for GFP/AF488, and TX2 filter for mCherry2/AF568/AF594.

2.3.5 Semi-automated computerised quantification

Scanned sections were analysed using a custom-made semi-automated pipeline combining ImageJ v1.50i (National Institutes of Health, USA) macros and Python scripts as outlined in Figure 2.9.

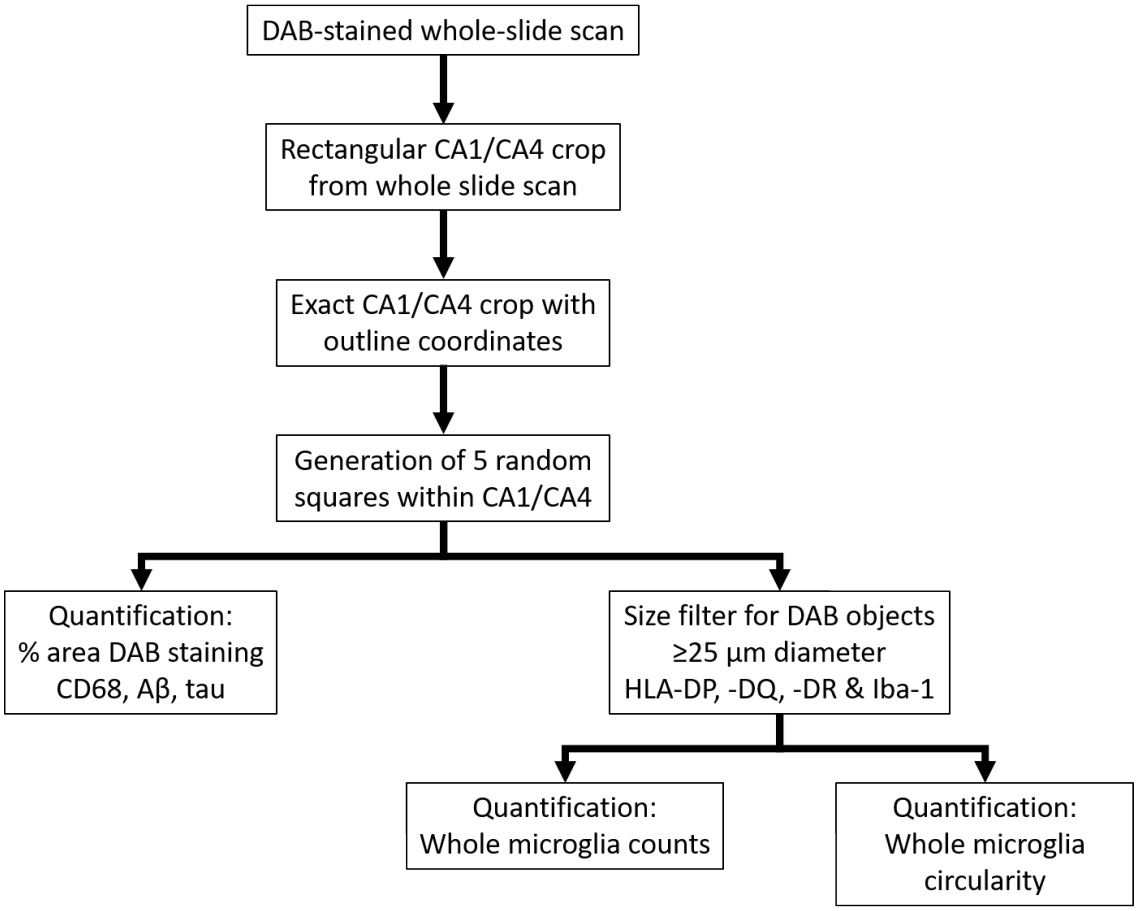

Figure 2.9. Pipeline for a custom made semi-automated quantification of DAB-stained whole-slide sections that were scanned.
$CD68^+$ microglia were quantified by % area DAB staining. HLA-DP, DQ, DR^+ and Iba-1^+ whole microglia were quantified by microglial counts. HLA-DP, DQ, DR^+ and Iba-1^+ whole microglia morphology were quantified by circularity. Aβ and tau pathology burden were quantified by % area DAB staining.

2.3.5.1 Generation of randomly sampled field of views

General rectangular regions of interest (ROI) of the hippocampal cornus ammonis (CA) 1 and CA4 were cropped out from the Leica proprietary whole slide scan image using the "Extract Image Region" function in Aperio ImageScope v12.1.0.5029 (Leica Biosystems). These regions were selected because of their vulnerability in AD and the pathological burden between AD cases are relatively consistent. Parameters used were 50% size scaling, unticking "Thumbnail", and TIF output with LZW compression. The output image has a scale of 2 pixels (px):1 µm.

After cropping, the TIF image was opened in ImageJ and the "Record..." function opened. A more granular ROI selection was done using the "Polygon selections" tool to exactly outline the CA1 or CA4. Once the polygon selection is complete, the boundary coordinates of the each specific ROI selection was obtained from the "Record..." window. Boundary coordinates were saved in separate .txt files and the ROI selection was also saved using the "ROI Manager".

The boundary coordinates were input into a Python script and used to generate coordinates for 5 random non-overlapping squares of 0.5×0.5 mm^2 for each ROI and section. The coordinates of each square were input into the "Specify..." function (Width: 1000 px, Height: 1000 px, X/Y coordinates as generated, ticked "Centered") in ImageJ to create selections of the squares. The square selections were saved using the "ROI Manager" and also cropped into individual images using the "Duplicate..." function. The cropped squares were saved as TIF images.

2.3.5.2 Quantification of % area of DAB staining

For CD68, Aβ, and tau staining, quantification was performed using % area staining. The number of $CD68^+$ microglia could not be determined because the intracellular punctate staining pattern did not delineate individual microglia.

The 5 randomly sampled square images were opened in ImageJ. A threshold filter to distinguish DAB staining from background was achieved using the "Color Threshold..." function (Hue: 0–30; Saturation: 0–255, adjusted according to background; Brightness: determined by the "Mean" option under "Thresholding method") and by clicking on the "Filtered" followed by "Select".

A size filter was applied to remove non-specific DAB staining using the "Analyze Particles..." function (Size: 10–Infinity, tick "Add to Manager"). For anti-$A\beta_{17\text{-}24}$ (clone 4G8) antibody staining, intracellular APP was excluded by using a size filter of "2000–Infinity". This step also separated discontiguous DAB staining into individual ROI selection particles to perform the size filter. The filtered individual ROI selections particles were combined again and saved using the "ROI Manager".

A binary black and white mask was created using "Create Mask". Quantification options were selected within "Set Measurements..." (tick "Area fraction" and "Limit to threshold", Decimal places: 3). % area of DAB staining was obtained using the "Measure" function. Data from the "Results" window was saved as a .txt file which can be opened in Excel (Microsoft) for data processing.

2.3.5.3 Quantification of microglial abundance

For HLA-DP, DQ, DR and Iba-1 staining, quantification was performed by counting the number of stained microglia.

Microglial counts were quantified by using a third party ImageJ plugin "Hull And Circle"[555], which has the capability to quantify shape descriptions (e.g. Feret's diameter) for individual thresholded particles*.

The 5 randomly sampled square images were opened in ImageJ. DAB staining was thresholded as described in Chapter 2.3.5.2. A binary black and white mask was created using "Create Mask". A size filter was applied to the ROI selections to remove selected non-specific DAB staining using the "Analyze Particles..." function (Size: 50–Infinity, tick "Exclude on edges", "Clear results", and "Add to Manager") and separate discontiguous DAB staining into individual ROI selection particles. The filtered individual ROI selections for each particle were saved using the "ROI Manager".

The "Hull And Circle" plugin was launched*. "Draw Circle" and "Draw Hull" was unticked in "Settings". Quantification of Feret's diameter for each particle was performed by using the "Scan Roi Manager" button. The resulting data window was saved as a .txt file.

A second size filter was applied to the saved individual ROI selections for each particle using a Python script that reads the saved data containing the Feret's diameter. It then removes particles that have Feret's diameter smaller than 50 px/25 µm from the saved individual ROI selections. 25 µm diameter was chosen as the threshold as it matches the reported smallest average size of a whole microglia[556] and therefore avoids counting microglial processes present in the plane which the section was cut.

Microglial counts was established by counting the number of remaining particles $\geqslant$25 µm from the data list using Excel.

*At time of writing the macro, I did not realise that Feret's diameter was an option in the ImageJ built-in "Measure" function. This means that for future quantification, "Hull And Circle" is not required. Instead, at the same point when "Hull And Circle" is used, Feret's diameter can be quantified by selecting "Feret's diameter" in "Set Measurements..." and using the "Measure" function. This can be combined with quantifying circularity as described in Chapter 2.3.5.4 to generate the data in one step.

2.3.5.4 Quantification of microglial morphology

Microglia are very plastic cells and can change morphology in response to immune activation. Morphological analysis was performed by measuring the circularity of microglia. Circularity values range from 0–1, with 1 representing a perfect circle and values closer to 0 indicate an increasingly elongated polygon. In other words, microglia with greater circularity values have a more amoeboid shape indicating functional activation, whereas lower circularity values represent a more ramified shape indicating a more surveillance state.

The saved individual ROI selection containing only particles $\geqslant$25 µm from Chapter 2.3.5.3 was opened with the corresponding image file in ImageJ. Quantification options were selected within "Set Measurements..." (tick "Shape descriptors", Decimal places: 3). Circularity values for each particle were obtained using the "Measure" function. Data from the "Results" window was saved as a .txt file.

2.3.6 Statistical analyses

All statistical analyses were performed using SPSS Statistics 23 (IBM). All tests were nominally significant for p-values $\leqslant 0.05$.

Differences in group demographics for age at death and gender were assessed using one-way ANOVA and binary logistic regression, respectively.

Semi-automated cell counting was compared with manual cell counting by assessing the Pearson correlation between cell counts for both methods on HLA-DP, DQ, DR-immunostained sections. Semi-automated cell counting was also compared with the commonly used % area staining quantification method by assessing the Pearson correlation between output measures from both methods in HLA-DP, DQ, DR and Iba-1 immunostained sections.

Individual group differences for % area staining, microglial counts, and circularity were assessed by calculating the mean measure of the 5 sampled squares and using one-way ANCOVA with 1000-sample bootstrapping and Sidak correction for pairwise comparisons. The effects of age at death, sex, APOE ε4 status, CD33 risk variants, years of tissue storage, and post-mortem delay on outcome measures were assessed as potential confounders. Only age at death had a significant effect and was included as a covariate in the one-way ANCOVA tests.

Group differences for amyloid and tau pathology burden were assessed with Student's t-test. The associations between microglial abundance and AD pathology were assessed using Pearson correlation.

2.4 Methodology for Chapter 5

2.4.1 Cell culture

BV2 cells, including CRISPR/Cas9-edited and control cell lines, were cultured as described in Chapter 2.2.7, unless specified otherwise. Passage number of CRISPR/Cas9-edited and control cell lines used are indicated below.

Phenotype	Clone ID	Passage number
TREM2 WT	C3bA1	22
	C3bA6	22
	C3bA8	22
	C3bA12	22
	C3bB4	22
TREM2 KO	C1G10	17
	C1E2	17
	C3bB10	20
	C3bC4	22

Table 2.24. Passage number of CRISPR/Cas9-edited and control cell lines used.

2.4.2 DNA sequence verification

$\sim 2 \times 10^6$-cell pellets were prepared in 1.5 mL microfuge tubes for each clonal line. DNA was extracted and PCI-purified as described in Chapter 2.2.8. PCR, agarose gel electrophoresis and Sanger sequencing was performed as described in Chapter 2.2.9 and 2.2.10.

2.4.3 Reverse transcription-polymerase chain reaction

Following RNA extraction (described in Chapter 2.2.11), 5 µg of total purified RNA was converted into cDNA using SuperScript IV Reverse Transcriptase (Thermo Fisher Scientific) according to the manufacturer's protocol as described in Chapter 2.2.12.

Exon 2 of protein-coding *Trem2* transcripts (NM_031254 & NM_001272078) and Intron 1–Exon 2 of retained intron *Trem2* transcript (ENSMUST00000132340.1) were amplified by PCR using primer pairs mTREM2_cDNA_seq_F1/R1 and mTREM2F4/R4, respectively

(Table 2.25), as described in Chapter 2.2.9, in a 10 µL reaction volume. 1 µL cDNA was used as the template.

RT-PCR products were resolved by agarose gel electrophoresis as described in Chapter 2.2.9.

Primer ID	Primer sequence (5'→3')	Temp.
mTREM2_cDNA_seq_F1 (M13F)	TGTAAAACGACGGCCAGTATGGGACCTCTCCACCAGTT	66°C
mTREM2_cDNA_seq_R1 (M13R)	CAGGAAACAGCTATGACGGAGGTGCTGTGTTCCACTT	
mTREM2F4	AACTGCTTCCAAGCAAGTGGC	53°C
mTREM2R4	GATCTCCAGCATCTTGGTCATCTA	

Table 2.25. RT-PCR primers used amplify cDNA generated from *Trem2* isoform 1 and 2 transcripts.
Red font: sequencing primer as indicated in brackets.

2.4.4 Protein extraction

For the validation of loss of functional TREM2 protein expression in CRISPR/Cas9-edited TREM2 clonal lines, untreated cells were harvested from T75 flasks by scraping confluent cells and pelleting them in 50 mL centrifuge tubes by centrifugation at 200 ×g for 5 min. Cell pellets were resuspended in 1 mL DPBS to wash and transferred into 1.5 mL microfuge tubes. The cell suspension was centrifuged at 14,500 ×g for 5 min at 4°C, discarding the supernatant. The cell pellet was resuspended in 100 µL (per 1×10^6 cells) of RIPA buffer supplemented with cOmplete ULTRA, EDTA-free (Roche) protease inhibitor cocktail and PhosSTOP (Roche) phosphatase inhibitor made up according to the manufacturer's protocols (1 tablet each in 10 mL RIPA buffer). Lysates were briefly vortexed to complete resuspension and incubated on ice for 3× 10 min, with brief vortexing in between incubations. Lysates were then passed through a 26-gauge needle syringe several times to shear DNA. Any remaining DNA was physically removed with the needle syringe. Lysates were further sonicated for 15 s before being centrifuged at 14,500 ×g for 10 min at 4°C to separate RIPA-insoluble debris. The supernatants were carefully transferred into new 1.5 mL microfuge tubes on ice.

Protein concentration was determined by BCA protein assay (Thermo Fisher Scientific) according to the manufacturer's protocols. The Working Reagent was prepared by combin-

ing Reagent A and Reagent B in a 50:1 ratio to a total volume of 200 µL Working Reagent per reaction. Aliquots of each sample were diluted 1:10 to bring the concentration of each protein sample within the reference standard range. 10 µL diluted standards/samples were added in duplicates to individual wells of a clear, flat-bottomed 96-well assay plate, followed by 200 µL of Working Reagent per well. The plate was covered with a plate sealer and agitated at ∼800 rpm on an orbital shaker to mix. The plate was incubated at 37°C for 30 min before measuring absorbance at 562 nm on a PHERAstar FS (BMG LABTECH) plate reader.

2.4.5 Protein lysate deglycosylation

Protein lysates were deglycosylated using the Protein Deglycosylation Mix II (New England Biolabs) with modifications to the manufacturer's protocol to maintain protein concentration at ⩾3 µg/µL to enable sufficient loading in Western blots. 90 µg protein lysate was diluted with ddH_2O to a total volume of 24 µL. 3 µL Deglycosylation Mix Buffer 2 was added and samples were heated to 100°C for 10 min to denature protein. The denatured protein lysate was chilled on ice for at least 5 min to condense any evaporation, followed by centrifugation at 14,500 ×g for 2 min at 4°C. 3 µL Protein Deglycosylation Mix II was added and gently mixed. The reaction was incubated overnight at 37°C. The following day, the deglycosylated protein lysate was again chilled on ice for at least 5 min to condense any evaporation, followed by centrifugation at 14,500 ×g for 2 min at 4°C to collect. To dissolve precipitated proteins, 10.5 µL 4× NuPAGE LDS Sample Buffer (Thermo Fisher Scientific) and 4.5 µL NuPAGE Sample Reducing Agent (Thermo Fisher Scientific) or 500 mM DTT were added and gently mixed.

2.4.6 Western blot

Samples were prepared by mixing the desired amount of protein lysate with 4× NuPAGE LDS Sample Buffer and 10× NuPAGE Sample Reducing Agent (or 500 mM DTT) to 1× working concentration at a maximum volume of 20 µL. Samples were then heated at 100°C for 10 min to denature protein. Denatured protein lysates were chilled on ice for at least 5 min to condense any evaporation, followed by centrifugation at 14,500 ×g for 2 min at 4°C to collect.

Gel electrophoresis was performed by loading the samples into a 26-well NuPAGE 4-12% Bis-Tris Midi Protein Gel alongside 3 µL Precision Plus Protein All Blue Prestained Protein Standards (Bio-Rad) in a XCell4 SureLock Midi Cell (Thermo Fisher Scientific). The Upper and Lower Buffer Chambers were filled with 1× NuPAGE MOPS SDS Running Buffer and 500 µL NuPAGE Antioxidant was added to the Upper Buffer Chamber (All NuPAGE products were from Thermo Fisher Scientific). Gel electrophoresis was performed at a constant 200 V for 55 min.

After completion of the gel electrophoresis, a wet protein transfer was performed. 4 sheets of grade 3 qualitative filter paper and 1 sheet of Amersham Protran NC nitrocellulose membrane (GE Healthcare) were cut and pre-soaked in 1× transfer buffer with 20% (v/v) methanol. The gel was trimmed to remove wells and dye front. The gel was then sandwiched next to the nitrocellulose membrane in between 2 sheets of filter paper on each side. The transfer sandwich was gently pressed to remove air bubbles and then put into a transfer cassette. Wet protein transfer was performed in a Trans-Blot Electrophoretic Transfer Cell (Bio-Rad) with 1× transfer buffer with 20% (v/v) methanol at a constant 80 V for 1 h.

Once the transfer was complete, the nitrocellulose membrane was briefly rinsed in 1× TBS-T 0.1%. The TBS-T 0.1% was discarded and Ponceau S staining solution was added and briefly incubated to visualise protein on the nitrocellulose membrane. Ponceau S was discarded and the membrane was rinsed twice with ddH_2O to improve contrast. Ponceau S protein staining was imaged on the ChemiDoc XRS+ System for reference. Ponceau S staining was removed with 3× 5 min washes in 1× TBS-T 0.1%.

The nitrocellulose membrane was incubated in 5% (w/v) BSA for 1 h at RT to block non-specific antibody binding. The blocking solution was removed before adding the

diluted primary antibody solution with 1% blocking solution in 1× TBS-T 0.1% and incubated overnight at 4°C on an orbital shaker. The following day, the primary antibody solution was removed and the membrane was washed with 3× 5 min in 1× TBS-T 0.1%. Diluted secondary antibody solution in 1× TBS-T 0.1% was added to the membrane and incubated while covered for 1 h at RT. The secondary antibody solution was removed and the membrane was washed with 3× 5 min in 1× TBS-T 0.1%. Antibody binding was visualised and imaged on the ChemiDoc XRS+ System. Detected protein band intensities were quantified using ImageJ.

Combinations of primary antibody and secondary antibody solutions used are shown in Table 2.26.

Primary antibody	Dilution	Manufacturer	Cat#	Secondary antibody	Dilution	Manufacturer	Cat#
Anti β-actin (clone C4), mouse	1:10000	Santa Cruz	sc-47778	Anti mouse IgG, goat, AF568	1:5000	TFS	A11004
				Anti mouse IgG, goat, AF680	1:5000	TFS	A21057
Anti mouse CD68/macrosialin (clone FA-11), rat	1:1000	BioLegend	137001	Anti rat IgG, goat, AF488	1:5000	TFS	A11006
Anti Erk1/2 (clone L34F12), mouse	1:2000	CST	4696	Anti mouse IgG, goat, AF488	1:5000	TFS	A11001
Anti phospho-Erk1/2 (clone D13.14.4E), rabbit	1:2000	CST	4370	Anti rabbit IgG, goat, AF594	1:5000	TFS	A11012
Anti GAPDH, rabbit	1:1000	Santa Cruz	sc-25778	Anti rabbit IgG, goat, AF594	1:5000	TFS	A11012
Anti Iba-1, rabbit	1:5000	Wako	019-19741	Anti rabbit IgG, goat, AF594	1:5000	TFS	A11012
Anti I-A/I-E (MHC class II, clone M5/114.15.2), rat	1:1000	BioLegend	107601	Anti rat IgG, goat, AF488	1:5000	TFS	A11006
Anti Pyk2 (clone 5E2), mouse	1:1000	CST	3480S	Anti mouse IgG, goat, AF488	1:5000	TFS	A11001
Anti phospho-Pyk2, rabbit	1:1000	CST	3291S	Anti rabbit IgG, goat, AF594	1:5000	TFS	A11012
Anti Syk (clone 6A464), mouse	1:1000	Santa Cruz	sc-73089	Anti mouse IgG, goat, AF488	1:5000	TFS	A11001
Anti phospho-Syk (clone C87C1), rabbit	1:1000	CST	2710S	Anti rabbit IgG, goat, AF594	1:5000	TFS	A11012
Anti human TREM2, goat	1:1000	R&D	AF1828	Anti sheep IgG, donkey, AF488	1:5000	TFS	A11015
Anti human TREM2, rabbit	1:1000	Atlas	HPA012571	Anti rabbit IgG, goat, AF488	1:5000	TFS	A11008
Anti human/mouse TREM2 (clone 237920), rat	1:1000	R&D	MAB17291	Anti rat IgG, goat, AF488	1:5000	TFS	A11006
Anti mouse TREM2, rabbit	1:1000	Santa Cruz	sc-48765	Anti rabbit IgG, goat, AF488	1:5000	TFS	A11008
Anti mouse TREM2, sheep	1:2000	R&D	AF1729	Anti sheep IgG, donkey, AF488	1:5000	TFS	A11015

Table 2.26. Combinations of primary antibodies and secondary antibodies that were used for Western blotting.
Atlas: Atlas Antibodies; CST: Cell Signalling Technology; R&D: R&D Systems; TFS: Thermo Fisher Scientific.

2.4.7 TREM2-activating antibody treatment

6-well culture plates were first coated with antibodies. 500 µL 10 µg/mL TREM2 activating antibody (MAB17291, R&D Systems) or isotype control antibody (MAB0061, R&D Systems) in sterile DPBS were added to each well. The plates were gyrated to ensure that the antibody solution covered the bottom of each well evenly. Plate lids were put on and plates wrapped in Parafilm to prevent evaporation. Plates were left to incubate overnight at 4°C on a slow orbital shaker for even coating. The next day, the antibody solutions were transferred into replicate plates. Wells of the original plates were gently rinsed with 1 mL DPBS to remove unbound antibodies and kept in DBPS until ready to use.

The replicate plates were incubated in exactly the same conditions as the original. The antibody solutions were removed and wells were gently rinsed with 1 mL DPBS to remove unbound antibodies. Non-specific binding was blocked with 500 µL 5% BSA in each well on a slow orbital shaker for 1 h. Blocking solutions were discarded and wells were gently rinsed 3 times with 1 mL DPBS. 100 µL 1:1000 anti rat IgG AF488 (A11006, Thermo Fisher Scientific) was added to each well and incubated on a slow orbital shaker for 1 h. Antibody solutions were discarded and wells were gently rinsed 3 times with 1 mL DPBS. Fluorescence intensities in each well were measured at 485 nm absorption and 520 nm emission on the PHERAstar FS plate reader.

Clonal cell lines (BV2 WT, CRISPR TREM2 WT, CRISPR TREM2 KO) were cultured in RPMI-1640 w/ 10% FBS + 1% PS in T75 flasks until 60-70% confluency. Culture medium was then replaced with RPMI-1640 without FBS to serum-deprive cells for 24 h before treatment with antibodies. When ready, cells were detached with 0.25% trypsin-EDTA, pelleted, and resuspended in warm RPMI-1640. Cell density was adjusted to 1×10^6 cells/mL with warm RPMI-1640. 1 mL cells were gently added to the side of each well (Uncoated, Isotype control, TREM2-activating) and then gyrated to ensure even dispersion of cells. The cells were left to incubate for 1 h at 37°C/5%CO_2.

At harvest, culture medium was transferred into individual 1.5 mL microfuge tubes on ice. 100 µL RIPA buffer supplemented with protease and phosphatase inhibitors was immediately added to each well on ice to harvest cells. Cells were lysed in the wells by scraping with the reverse end of a micropipette tip. Cell lysates were transferred into

individual 1.5 mL microfuge tubes on ice and briefly vortexed. Lysates were incubated for 3× 10 min on ice with brief vortexing between incubations. The reserved culture medium were centrifuged at 14,500 ×g for 10 min at 4°C to pellet any cells/debris. The culture medium supernatant was transferred into new 1.5 mL microfuge tubes on ice and frozen at -20°C for future analyses. Cell protein lysates were sonicated for 15 s and centrifuged at 14,500 ×g for 10 min at 4°C to pellet RIPA-insoluble debris. The supernatant was transferred into new 1.5 mL microfuge tubes on ice. Protein concentration was determined by BCA protein assay and Western blot performed as described in Chapter 2.4.6.

2.4.8 Statistical analyses

All statistical analyses were performed using SPSS Statistics 23 (IBM). All tests were nominally significant for p-values $\leqslant 0.05$.

Relative fluorescence intensities of plate-bound antibodies were quantified by normalising to uncoated wells (background fluorescence intensity). Group differences between uncoated, isotype control antibody and TREM2-activating antibody wells (10 wells each) were assessed using one-way ANOVA with post-hoc pairwise comparisons (Tukey HSD correction).

Activation of Syk, Pyk2 and Erk1/2 was quantified by calculating band intensity ratio of the phospho-protein:total protein in 4 different TREM2 WT and TREM KO cell lines and normalised to the relative amount of plate-bound treatment antibody (isotype control or TREM2 activating antibody) measured using secondary antibody fluorescence intensity.

CD68 and Iba-1 protein levels were quantified by quantifying protein band intensity in 4 different TREM2 WT and TREM2 KO cell lines and normalised to β-actin band intensity.

Individual group differences between untreated, isotype control and TREM2-activating antibody treatment in 4 different TREM2 WT and TREM2 KO cell lines were assessed using one-way ANOVA with post-hoc pairwise comparisons (Tukey HSD correction).

Chapter 3

CRISPR/Cas9-mediated genome editing of *Trem2* in the BV2 cell line

3.1 Introduction

This project aims to develop an *in vitro* disease cell model of TREM2 suitable for functional characterisation and drug screening. Different experimental models have advantages and disadvantages depending on the hypothesis being tested. To investigate how different cells work together in a system, animal models would be more suitable than cell culture models which tend to be of one cell type or in co-culture. On the other hand, cell culture models are ideal for investigating subcellular molecular pathways or high-throughput screening assays because they can be isolated from the influences of other cell types, specifically treated with compounds, and are easily scalable. Various primary cells and cell lines were considered for their cell type, suitability of underlying biology, and proliferative capacity to use as a model of TREM2 dysfunction. TREM2 is expressed on myeloid cells including dendritic cells, monocyte/macrophages, osteoclasts and microglia[400,557]. Among these cell types, microglia have been strongly associated with the pathogenesis of AD[362]. They have an active role in the maintenance of the CNS and is part of the innate immune system of the brain[198]. In disease, increased microglia activity has been associated with the progression and severity of AD[198,238,558]. For example, microglia respond to the hallmark pathologies of AD including neuronal debris and Aβ by releasing cytokines and chemokines as well as phagocytosis of these material[559]. Additionally, chronic activation of microglia may be involved in disease progression of AD. Blocking of microglial proliferation by inhibiting CSF1R prevents synaptic degeneration in APP/PS1 mice[238]. With the increasing amount of literature on TREM2 dysfunction in microglia contributing to the vulnerability of developing AD, microglia was used as the cell type of choice for functional characterisation and drug screening. This enables the comparison and validation of the generated disease cell model with established phenotypes of microglia with TREM2 dysfunction.

To perform functional characterisation and drug screening, the microglial model of choice would replicate the disease biology of TREM2 dysfunction conveyed by the AD-associated risk variants in people. Of the *in vitro* models, primary microglia are considered the gold standard for experimental models as they are believed to closely resemble endogeneous biology compared to cell lines that are transformed or modified to achieve immortalisation[560,561]. Primary microglia can be derived from human or rodent brains. To harvest primary human microglia, brain tissue can be obtained as biopsies from patients undergoing

brain surgery for epilepsy[562] or autopsy tissue if there is a short post-mortem delay[563–565]. Primary human microglia could be isolated from people with the TREM2 variants of interest but this is impractical as the variants are very rare (minor allele frequency [MAF] 0.0012–0.0063 in healthy populations[110] and 0.009–0.02 in AD cases[109]). While obtaining primary microglia from control human or rodent brains[566] are potential alternatives, they have limited *in vitro* proliferation capacity required for clonal expansion following genome editing to characterise and provide sufficient cells for experiments.

An alternative to primary human microglia is to generate microglia from induced pluripotent stem cells (iPSCs) derived from people with a TREM2 variant. iPSCs would have the required proliferative capacity to theoretically proliferate indefinitely, which allow the production of sufficient cells to perform various functional characterisation and drug screening assays. Even if iPSCs cannot be obtained from patients with TREM2 variants, iPSCs from control patients could be genome edited to knock-in the disease-associated variants before or after differentiation into microglia-like cells, depending on their proliferative capacity in the respective states. Genome editing of *TREM2* in iPSCs before differentiation may affect their ability to respond to differentiating factors and differentiate into microglia-like cells. Osteoclasts derived from NHD patients with TREM2 variants[418] and a TREM2-deficient macrophage cell line have impaired capability to differentiate, which was associated with a PlexinA1-dependent pathway[567]. However, microglia from TREM2 KO mice do not appear to be affected developmentally and can be detected and isolated from the brain[452,495,522], suggesting that the differentiation of microglia was not compromised by the lack of TREM2. Regardless, protocols to generate microglia from iPSCs were yet to be established at the start of the project, although a number of groups have since published successful protocols and characterisation of microglia-like cells derived from iPSCs[568–570].

Besides that, immortalised microglia cell lines also have a high rate of proliferation to theoretically provide limitless numbers of cells. They also are easier to culture compared to iPSCs. Immortalised cells are derived from spontaneously occurring cancer cells or transformed with viral oncogenes to obtain their proliferative capacities. Two immortalised human microglia cell lines derived from embryonic human microglia, CHME[571] and HMO6[572] have been previously described. Unfortunately, these cell lines were not commercially available or for academic sharing at the time of this project. A number of

rodent microglia cell lines have been extensively studied over many years, including BV2[552], N9[573], EOC[574], C8-B4[575], MG5[576], HAPI[577], MG6[578], and SIM-A9[579]. Of these, BV2 has been the most frequently used and studied. The BV2 cell line is generated from 1-week old C57BL/6 mouse primary microglia cultures and immortalised with the v-raf/v-myc carrying J2 virus[552].

Because primary microglia are considered as the gold standard for *in vitro* experimental models, immortalised microglial cell lines have been compared to primary microglia to assess their validity as an experimental model. Studies by Henn *et al.* (2009)[560] and Das *et al.* (2016)[580] have investigated and compared the regulation of the transcriptome between primary microglia and BV2 in response to LPS stimulation. Both studies have found that primary microglia regulated a far greater number of genes by up to ten times compared to BV2. There are also a relatively large number of genes, especially key inflammatory genes such as *Tnf, Cxcl10, Il1a, Il1b, Ccl4 and Ccl5*, that were similarly regulated by primary microglia and BV2. Of the 299 genes upregulated in BV2, 264 (88.3%) genes are also upregulated in primary microglia[580]. Despite this, almost all proinflammatory cytokines and chemokines are more highly induced in primary microglia than in BV2[580]. In agreement with transcriptomic data, primary microglia and BV2 release TNF-α and IL-6[581]. However, there are discrepancies in the expression of some proinflammatory cytokines such as IL-1β in BV2 although the concentration and duration of LPS treatment used were similar[581,582]. Moreover, with relevance to AD, both primary microglia and BV2 respond to fibrillar $A\beta_{1-42}$ by stimulating phagocytosis and releasing similar cytokines such as TNF-α[583–585]. Oligomeric $A\beta_{1-42}$ also induces TNF-α release but does not stimulate phagocytosis in both cells[583–585].

However, primary microglia may not represent endogeneous physiology as expected. The isolation of microglia from brain tissue exposes them to large quantities of cell debris which activate microglia and also potentially cause microglial priming. Priming causes microglia to be vulnerable to other inflammatory stimuli and result in an exaggerated response[327]. This may explain the greater number of genes regulated and the enhanced immune-related responses such as the expression of proinflammatory cytokines and chemokines by primary microglia compared to BV2 when stimulated with LPS[560,580]. On the other hand, BV2 which is immortalised by transformation with viral oncogenes almost certainly

have modified physiology due to the transformation. Nevertheless, BV2 appear to replicate most key inflammatory responses expected from endogeneous microglia such as release of cytokines/chemokines, chemotaxis and phagocytosis[552,560,580,586].

TREM2 expression has been previously detected in BV2 by others[412]. Mouse and human TREM2 have a 69% amino acid sequence homology, which appears modest, but the extracellular domain where most of the disease-associated variants are located has a 73% homology. Furthermore, most of the amino acids associated with the AD risk variants are conserved between mouse and human TREM2 (Figure 3.1), which means the introduction of human AD-associated TREM2 variants into mouse microglia is possible. Mouse and human TREM2 also share similar downstream signalling pathways, relying on the DAP12 adaptor protein to initiate phosphorylation and activation of intermediate signalling proteins[386,557].

Therefore, BV2 were used for this project because as an immortalised cell line, they are capable of providing consistent and sufficient amount of cells to perform functional characterisation and drug screening. BV2 also have exhibited key microglial properties and endogeneously express intact TREM2 signalling pathways. Thus, various functional phenotypic or protein expression markers that are affected by TREM2 dysfunction can be used as outcome measures during characterisation and drug screening. Genome editing was used to knock-in the equivalent AD-associated *TREM2* DNA variants into mouse *Trem2*. Various genome editing methods have been used in the past but the four major systems used were meganucleases, zinc-finger nucleases (ZFNs), transcription activator-like effector nucleases (TALENs) and clustered regularly interspaced short palindromic repeats (CRISPR)/Cas nuclease systems. These genome editing methods utilise the same general principle to generate modifications in the targeted genome involving two steps: first to create a double-stranded DNA break at the targeted location followed by the second step to induce endogeneous DNA repair mechanisms[587]. The DNA break is usually repaired through an error-prone non-homologous end joining (NHEJ) or a higher fidelity homology-directed repair (HDR) pathway[587] which can be used to generate indels or knock-in mutations, respectively.

Meganucleases were identified in single-cell eukaryotic introns where they mediate intron mobility. These are the first major tool used to perform directed genome editing[588]. SceI, which is derived from mitochondria of *Saccharomyces cerevisiae*, is one of the initial

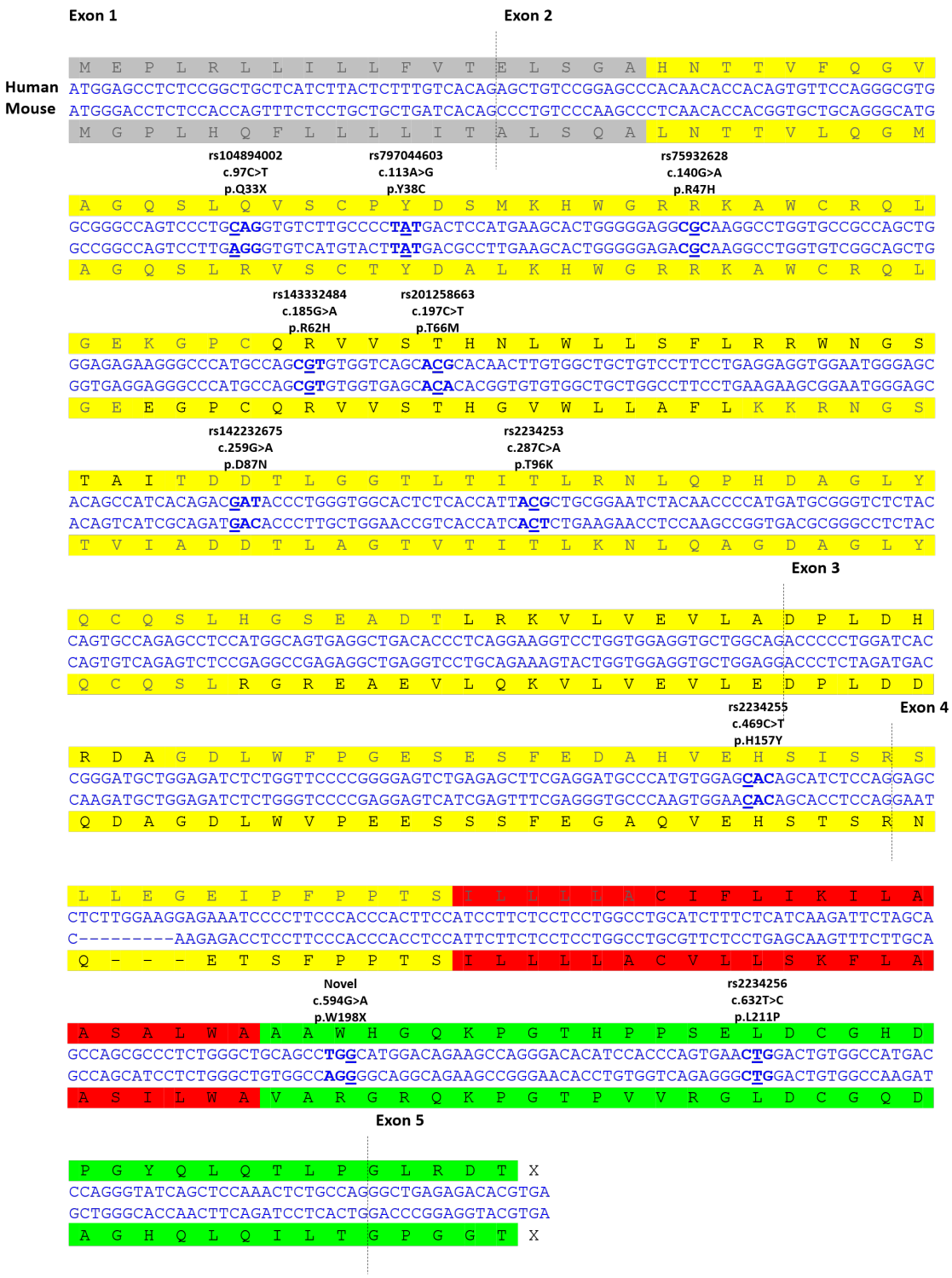

Figure 3.1. Most amino acids affected by disease-associated TREM2 variants in humans are conserved in mouse.
Aligned human and mouse *TREM2* cDNA and amino acid sequences with 69% amino acid sequence homology overall and 73% homology in the extracellular domain.
Grey: signal peptide, yellow: extracellular domain, red: transmembrane domain, green: cytoplasmic domain, bold: codon for affected amino acid variants, underline: disease-associated DNA variants.

meganucleases used[589]. However, meganucleases have limited flexibility for sequence-specific targeting as its nuclease domain is shared with the DNA-binding domain and modifications may therefore impact both functions[590].

ZFNs were described about a decade later[591]. ZFNs consist of Cys_2-His_2 zinc-finger domains, which are the most common DNA-binding motifs found in eukaryotes[592]. The use of ZFNs in genome editing involve the construction of synthetic zinc-finger proteins that can recognise 9–18 bp of DNA sequences. They are usually linked to a FokI DNA cleavage domain that performs the endonuclease activity[593,594]. Modular designs have been established by using arrays of zinc-finger domains that can recognise nearly all possible nucleotide triplets[595]. Thus, for a 18 bp target recognition, 6 zinc-finger domains in tandem are required. While ZFNs provided the first tool to target almost any sequence in the genome, this system has poor flexibility. Designing ZFN expression vectors for one target is relatively straightforward but tedious re-engineering is required to substitute the zinc-finger domains in the expression vector to target another DNA sequence.

TALENs were subsequently developed as an alternative for ZFNs. TALENs are DNA-binding proteins derived from plant pathogenic bacteria in the *Xanthomonas* genus that contain 33–35 amino acid repeat domains with each recognising a single base pair[596,597]. Similar to ZFNs, transcription activator-like effector (TALE) domains have been designed to fit into a modular construction to recognise various lengths of DNA sequences, typically 12–20 bp. They are also linked to a FokI DNA cleavage domain for nuclease activity[598]. Compared to the triplet-recognising ZFNs, the ability for TALEN to recognise single base pair sequences provided superior targeting flexibility. Moreover, unlike ZFNs, tedious re-engineering of the linkage between repeats is not required when constructing long arrays of TALEs[598]. However, the construction of repeat TALE arrays for targeting of repeated DNA sequences can be technically challenging due to the large number of identical repeat sequences required to clone into the expression vector[598]. Also, despite the various combinations of TALEs that theoretically allow for the recognition of virtually any sequence, in practice there are various restrictions such as that TALE binding sites should start with a `T` base[598].

The most recent tool in genome editing technology is the CRISPR/Cas system. It is derived from the bacterial immune system whereby foreign genetic material is recognised by RNA-

guided nucleases to excise invading DNA[599]. In bacteria, the type II CRISPR/Cas system involves short fragments of foreign DNA that are stored in the CRISPR loci and processed into RNA known as CRISPR RNA (crRNA). crRNAs anneal to 25 nt trans-activating crRNAs (tracrRNA), which are complementary to the CRISPR repeat and coded on the opposite strand upstream of the CRISPR loci. They form RNA duplexes and are processed by RNase III. The processed crRNA:tracrRNA duplexes then associate with Cas nucleases, forming ribonucleoprotein complexes that recognise DNA sequences complementary to the crRNA[599]. Unlike ZFN and TALEN, CRISPR/Cas can be easily reprogrammed by just changing the crRNA sequence without the need to synthesize large fragments of DNA oligonucleotides. The crRNA, also known as the guide/short guide RNA (gRNA/sgRNA), are usually 20 bp in size enabling them to be easily and precisely synthesized. While the crRNA can be made to target any 20 bp sequence in the genome, crRNA-binding sites on DNA require an upstream protospacer adjacent motif (PAM) for binding of the Cas nuclease[600], which in the case of Cas9, requires a `NGG` PAM sequence to be present next to the target DNA sequence[601,602]. In practice, the this is a relatively common motif in the human genome that occurs every 8 bp on average[602]. An advantage of CRISPR/Cas over previous tools for genome editing is the uncoupling of the DNA recognition system and the nuclease, which can be individually assembled. This allows the crRNA sequence to be easily substituted by simple cloning if the target DNA sequence has to be changed. Additionally, CRISPR/Cas can be multiplexed to simultaneously edit multiple targets at once by introducing an array of crRNA sequences in the expression vector.

Detailed methods and tools for the CRISPR/Cas9 system are readily available with many successful examples published[546]. Once the workflow is optimised for a cell line, changing DNA targets is expected to be easy without the need to perform tedious re-engineering and validation of expression vectors. Only 20 bp crRNA/sgRNA oligonucleotide sequences against the new target followed by a simple one-step cloning into the vector are required. Validation only requires Sanger sequencing to check for successful insertion of the crRNA/sgRNA fragment into the expression vector. Besides that, the uncoupling of CRISPR/Cas9 components mean greater flexibility in the design choice. The Cas9 nuclease can be delivered into target cells using expression vectors (plasmid, viral)[546], Cas9 mRNA[603], or protein[603] depending on the feasibility of delivery method and the desired duration of Cas9 activity. crRNA/sgRNA sequences can also be delivered through various

formats, such as incorporation of DNA sequences into an expression vector (plasmid, viral) that is subsequently transcribed into RNA or inserted together on the same Cas9 expression vector[546]. Alternatively, crRNA/sgRNA can also be pre-assembled and processed with tracrRNA for delivery with Cas9 mRNA or pre-associated to Cas9 protein and delivered as ribonucleoprotein complexes[603]. Therefore, the CRISPR/Cas9 system was chosen and used for this project.

3.2 Aims

- To generate a disease cell model of microglia carrying different AD-associated TREM2 variants suitable for functional characterisation and therapeutic drug screening.
- To introduce the variants using CRISPR/Cas9-mediated genome editing.
- To optimise methods for transfection, clonal isolation and screening.

3.3 Methodology overview

This Chapter explored and optimised various steps in the CRISPR/Cas9-mediated genome editing workflow (Figure 3.2) depending on the results of the previous CRISPR design. The different approaches are briefly described here in each method section. Detailed methods are outlined in Chapter 2.2.

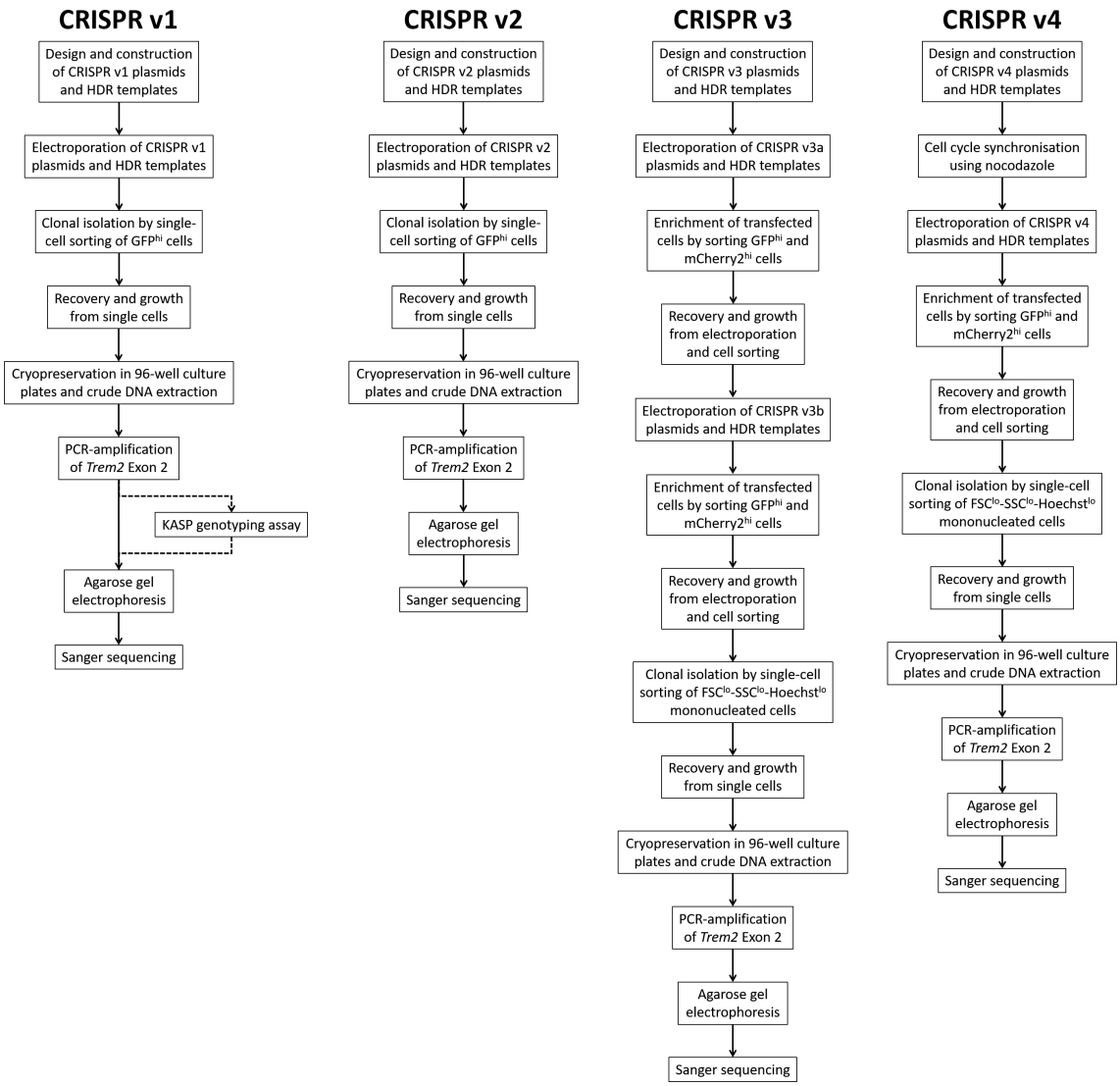

Figure 3.2. Schematic flow diagram representing the CRISPR/Cas9-mediated genome editing workflow performed on BV2.

RT-PCR

RT-PCR was performed by extracting total RNA from BV2 cell pellets and converted into cDNA by reverse transcription. Target transcripts of interest were PCR-amplified using primer pairs spanning across exons to avoid amplification of genomic DNA.

sgRNA and HDR template design

20 bp sgRNA sequences in mouse *Trem2* gene were identified using the CRISPR Design Tool (http://crispr.mit.edu). HDR templates were designed with the intended DNA variant in the middle with 56–90 nt flanking homology arms (total length 113–181 nt) corresponding to the sense or anti-sense orientation.

Preparation of sgRNA-Cas9n expression plasmids

sgRNA oligonucleotides were phosphorylated and annealed into dsDNA fragments for cloning into the expression plasmid to be expressed together with Cas9n. Each sgRNA in a pair were cloned into the pSpCas9n(BB)-2A-GFP or pSpCas9n(BB)-2A-Puro (CRISPR v1 & v2)/pSpCas9n(BB)-2A-mCherry2 (CRISPR v3 & v4). pSpCas9n(BB)-2A-mCherry2 was made by replacing the puromycin resistance gene with the mCherry2 fluorescent protein gene. Cloned sgRNA-Cas9n expression plasmids [pSpCas9n(sgRNA)] were transformed into *E. coli* for expansion. 3 colonies were selected to validate successful cloning by Miniprep and Sanger sequencing of the purified plasmids. Validated pSpCas9n(sgRNA) were expanded in large cultures and harvested by Midiprep (CRISPR v1 & v2) or EndoFree Maxiprep (CRISPR v3).

Transfection into BV2

In CRISPR v1, various transfection methods were explored for optimal co-transfection of CRISPR plasmids and HDR templates. Several chemical-based transfection reagents and electroporation were compared. Electroporation reagents and parameters were also optimised. Transfection efficiencies were established by fluorescence microscopy or during FACS. Subsequent transfections in CRISPR v2–v4 were performed by electroporation.

Puromycin treatment

In CRISPR v1, negative selection of Lipofectamine 3000-transfected BV2 and HEK293A cells with puromycin was tested as one of sgRNA-Cas9n expression plasmids contained a puromycin resistance gene [pSpCas9n(BB)-2A-Puro]. 24 h post-transfection, cells were treated with 0–5 µg/mL puromycin in culture medium for 48 h. Puromycin resistance was established by microscopy.

Nuclei staining in BV2

Before CRISPR v3, BV2 cells were stained with CellTracker Red CMTPX Dye and Hoechst 33342 to assess multinuclearity.

Nocodazole treatment

In CRISPR v4, BV2 were treated with 0–1,000 ng/mL nocodazole in culture medium for 17 h to synchronise cell cycle before electroporation.

FACS

For CRISPR v1 and v2, 24 h post-electroporation, transfected GFP^{hi} cells were clonally isolated by single-cell FACS. In CRISPR v3, CRISPR v3a-transfected GFP^{hi} and $mCherry2^{hi}$ cells were first enriched and allowed to recover for 1 week before transfection of CRISPR v3b plasmids and HDR template. CRISPR v3b-transfected cells were similarly enriched and allowed to recover before clonal isolation by single-cell FACS with or without Hoechst 33342 staining of cells. In CRISPR v4, enrichment and recovery of transfected GFP^{hi} and $mCherry2^{hi}$ cells were only performed once and followed by clonal isolation by single-cell FACS with $Hoechst^{lo}$ staining.

Screening of CRISPR/Cas9-edited clonal lines

After clonal isolation, cells were allowed to recover and grow to confluence in the 96-well culture plates. Confluent clonal lines were then split for cryopreservation and crude DNA

extraction. Clonal lines were temporarily cryopreserved in 96-well culture plates while screening was performed. Crude DNA was extracted from each clonal line and *Trem2* Exon 2 was PCR-amplified. Positive clones were screened by agarose gel electrophoresis and Sanger sequencing.

KASP genotyping

In CRISPR v1, a KASP genotyping assay was tested as an alternative screening method.

Karyotyping

Karyotyping was performed by sending a sample of early passage (P8) BV2 culture to Cell Guidance Systems Ltd.

Expansion and cryopreservation of clonal cell lines

Positive *Trem2*-edited BV2 clones with homogeneous editing (with DNA insertions or deletions) were revived from cryopreservation in the 96-well culture plates and expanded into larger cultures for proper cryopreservation and archiving in liquid nitrogen.

3.4 Results

3.4.1 Characterisation of BV2

To characterise BV2 for the expression of TREM2 and genes relevant to its function, genes co-expressed with *Trem2*, microglia-specific genes, and expression of cytokines genes were investigated by RT-PCR. In normal culture conditions, BV2 expressed transcripts from genes selected from the TREM2 co-expression network in human brain[402]: *Aif1*, *Cd68*, *Cx3cr1*, *Dap12*, *Trem2*, but not *Ciita* (Figure 3.3a). Furthermore, BV2 expressed cytokines associated with TREM2 function: *Tnf*, *Il1b*, and *Il6* (Figure 3.3a). BV2 also expressed the microglial enriched genes *Cx3cr1*, *Hexb* and *P2ry12* (Figure 3.3a) as expected by microglia derived from a young 1-week old mouse[552].

Before performing CRISPR/Cas9-mediated genome editing, the target *Trem2* gene in BV2 was sequenced to confirm it was identical to the WT mouse reference sequence. This was to ensure there were no variants which might affect the sgRNA design. Sanger sequencing revealed that *Trem2* Exon 2 in BV2 and the mm9 mouse reference sequence were identical (not shown).

3.4.2 Validation of sgRNA-Cas9 expression plasmids

Three *E. coli* colonies for each plasmid containing sgRNA were extracted and sequenced. At least one colony for each sgRNA was correctly cloned into the plasmid (Figure 3.4). These were used to make further plasmid preparations and for archiving.

(a) BV2

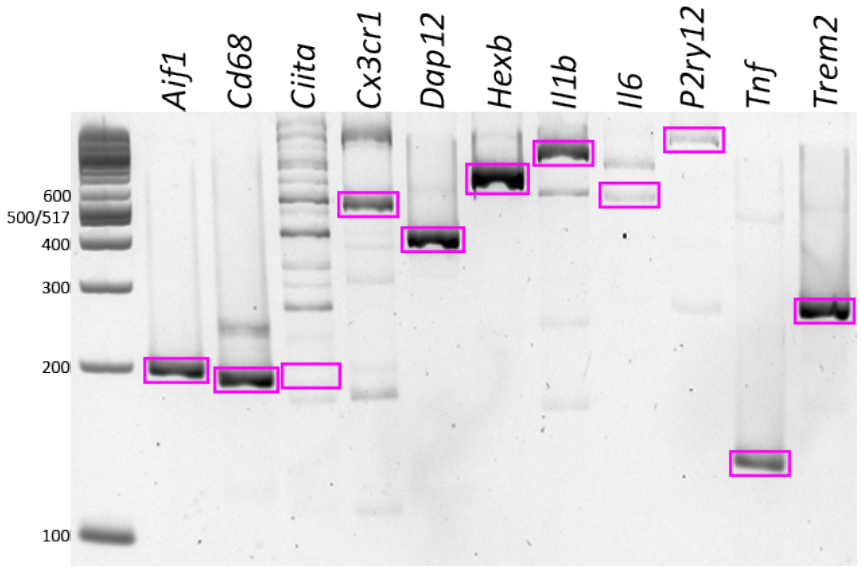

(b) WT mouse brain

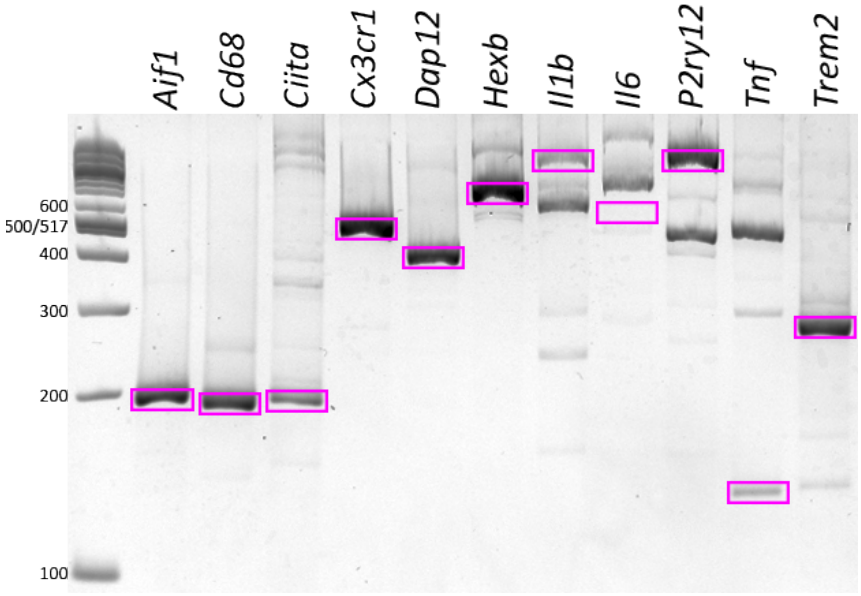

Figure 3.3. BV2 express transcripts of genes co-expressed with *TREM2* in human brain, microglia-specific genes, and cytokines associated with TREM2 function.
RT-PCR amplicons from **(a)** BV2 of genes from a *TREM2* co-expression network in human brain[402] (*Aif1*, *Cd68*, *Ciita*, *Cx3cr1*, *Dap12*, *Trem2*), cytokines that are associated with TREM2 function (*Tnf*, *Il1b*, *Il6*), or are established microglia-specific genes (*Cx3cr1*, *Hexb*, *P2ry12*). **(b)** Mouse brain was used as a positive control to identify specific RT-PCR amplicon bands as indicated in magenta boxes.
Expected amplicon sizes are *Aif1*: 193 bp, *Cd68*: 185 bp, *Ciita*: 187 bp, *Cx3cr1*: 493 bp, *Dap12*: 386 bp, *Hexb*: 673 bp, *Il1b*: 914 bp, *Il6*: 633 bp, *P2ry12*: 979 bp, *Tnf*: 130 bp, *Trem2*: 259 bp.

(a) pSpCas9n(mTREM2_R47H_sgRNA-A_R1a)-2A-GFP

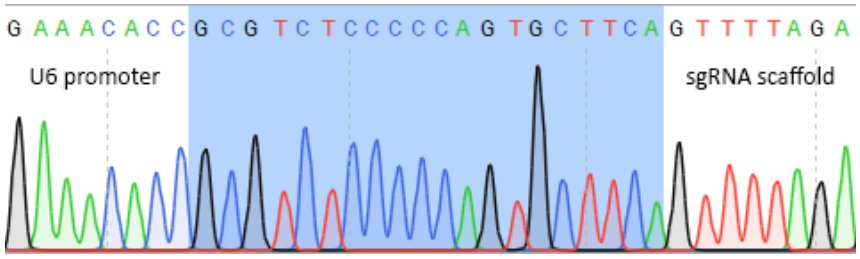

(b) pSpCas9n(mTREM2_R47H_sgRNA-B_F1a)-2A-Puro

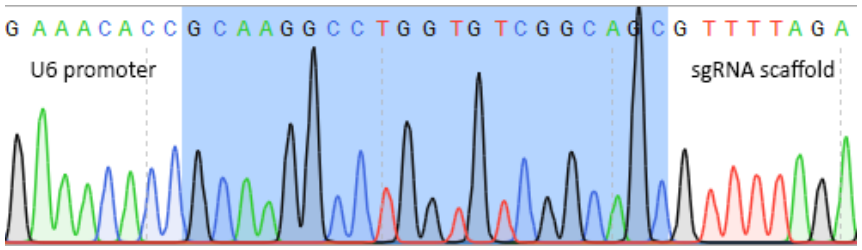

Figure 3.4. sgRNA dsDNA fragments were successfully cloned into pSpCas9n(BB).
Sequencing chromatograms of CRISPR v1 plasmids performed using the U6-Fwd primer. Blue highlighted sequence indicate the sgRNA sequence.

3.4.3 Optimisation of BV2 transfection

Optimal transfection of the sgRNA-Cas9 expression plasmids into BV2 were compared using chemical-based transfection reagents Lipofectamine 2000, Lipofectamine 3000, TurboFect, FuGENE 6, and PolyFect. Assessing GFP expression 24 h post-transfection, Lipofectamine 3000 had the highest transfection efficiency with 14 GFP^+ in ~1,000 cells (~1.4%) in a 100× magnification field of view. The transfection efficiencies of the other transfection reagents were considerably lower with PolyFect at ~0.9%, FuGENE 6 at ~0.4%, Lipofectamine 2000 at ~0.2% and TurboFect at ~0.1% (Figure 3.5, Table 3.1).

Transfection reagent	No. of GFP^+ cells	Transfection efficiency
Lipofectamine 2000	2	~0.2%
Lipofectamine 3000	14	~1.4%
TurboFect	1	~0.1%
FuGENE 6	4	~0.4%
PolyFect	9	~0.9%

Table 3.1. Lipofectamine 3000 had the highest transfection efficiency between the chemical-based transfection reagents tested.
Transfection efficiencies of CRISPR v1 pSpCas9n(mTREM2_R47H_sgRNA-A_R1a)-2A-GFP using chemical-based transfection reagents in approximately 1,000 BV2 cells.

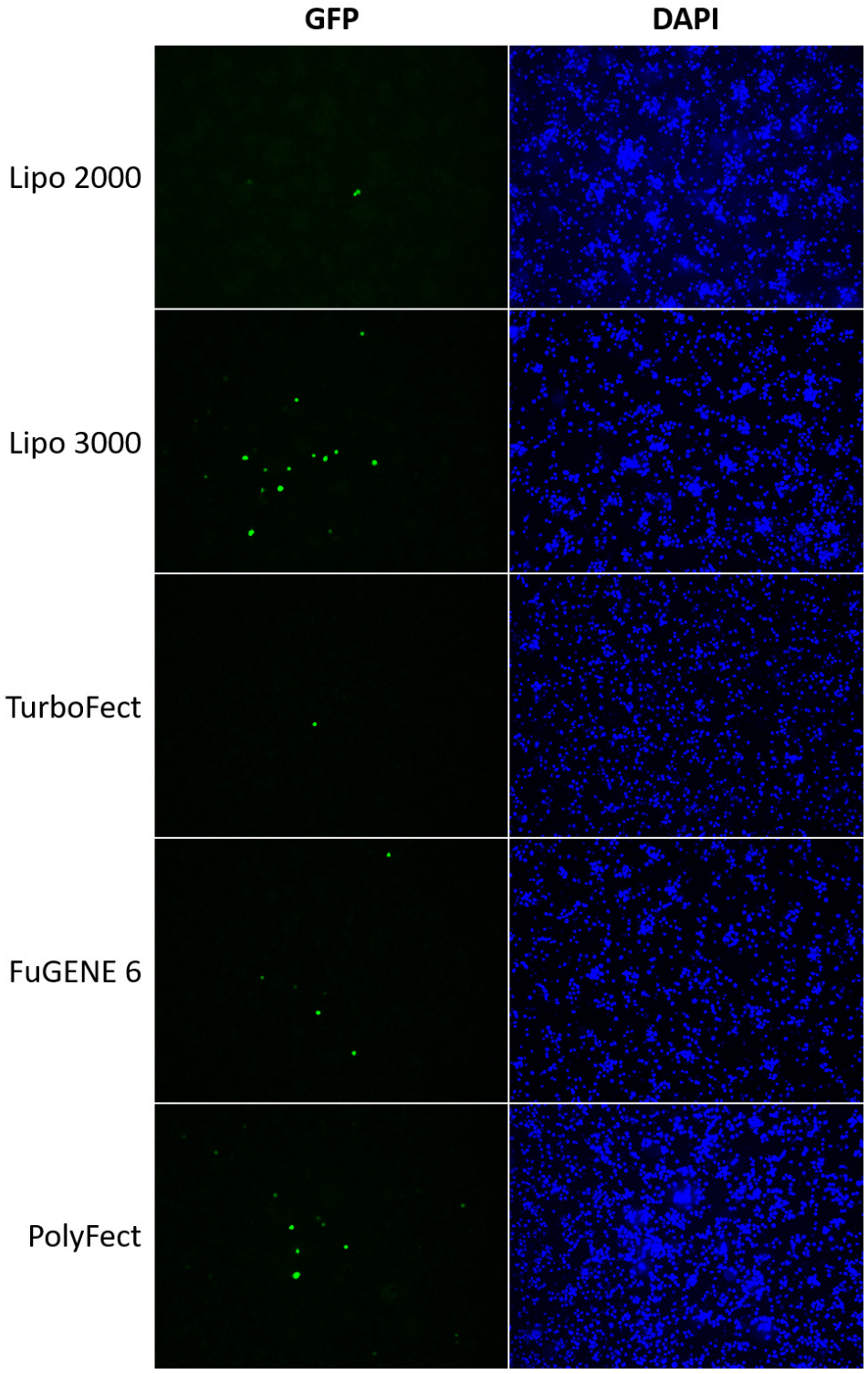

Figure 3.5. Transfection using Lipofectamine 3000 resulted in the highest number of GFP$^+$ cells compared to other transfection reagents.
BV2 cells transfected with 1 µg CRISPR v1 pSpCas9n(mTREM2_R47H_sgRNA-A_R1a)-2A-GFP using Lipofectamine 2000, Lipofectamine 3000, TurboFect, FuGENE 6, and PolyFect and nuclei stained with DAPI.
Fluorescence images were captured at 100× magnification and the number of GFP-positive cells in a single field of view were counted. There were approximately 1,000 cells in each field of view.

The transfection efficiency of Lipofectamine 3000 was still far too low to generate sufficient positive transfected cells for subsequent steps. Therefore, electroporation was explored as an alternative transfection method. Using pmaxGFP, transfection efficiency and cell viability using the recommended electroporation programs (A-030, A-033, A-020, D-023) were first compared by qualitative analysis of GFP-expressing cells in a microscopic field of view. Program A-030 resulted in the highest transfection efficiency with acceptable cell viability when used with Nucleofector Solution L and V (not shown).

Next, the transfection efficiency of the CRISPR v1 pSpCas9n(mTREM2_R47H_sgRNA-A_R1a)-2A-GFP plasmid by electroporation with Nucleofector Solution L was compared to Nucleofector Solution V using program A-030. Transfection efficiency of the plasmid with Nucleofector Solution L (14.0%) was 1.97 fold higher than with Nucleofector Solution V (7.1%) as determined by percentage of GFP^{hi} cells using flow cytometry (Figure 3.6). Hence, Nucleofector Solution L with program A-030 was used in subsequent electroporations.

(a) Nucleofector Solution L

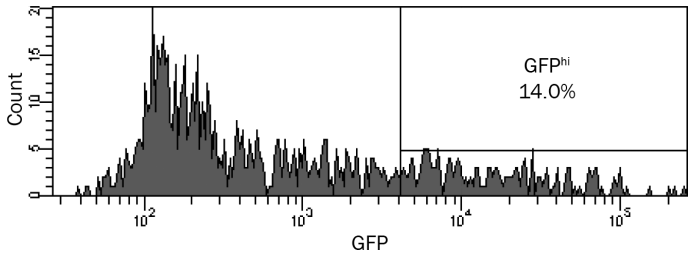

(b) Nucleofector Solution V

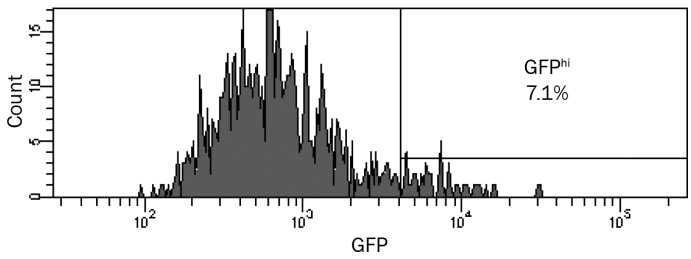

Figure 3.6. Electroporation using Nucleofector Solution L resulted in approximately two-fold higher transfection efficiency compared to Nucleofector Solution V.
Flow cytometry of BV2 transfected with CRISPR v1 pSpCas9n(mTREM2_R47H_sgRNA-A_R1a)-2A-GFP using Nucleofector Solution L or V with electroporation program A-030. Transfection efficiency was determined by the percentage of GFP^{hi} cells.

3.4.4 Optimisation of puromycin for negative selection

To enrich for BV2 cells transfected with the sgRNA-Cas9 expression plasmid, the optimal concentration of puromycin to use for negative selection was investigated. Puromycin (0–5 µg/mL) was tested on BV2 transfected with the CRISPR v1 plasmid pair and HDR templates using Lipofectamine 3000. After 48 h, only untreated BV2 remained alive whereas even the lowest (1 µg/mL) puromycin concentration resulted in almost complete cell death (not shown).

HEK293 cells transfected with the puromycin resistance gene by Lipofectamine 3000 have been reported tolerate up to 3 µg/mL puromycin over a 48–72 h treatment period[546]. Therefore, to rule out the possibility that the poor puromycin resistance in BV2 was due to the low transfection efficiency using Lipofectamine 3000, HEK293A cells were transfected with pSpCas9n(BB)-2A-Puro using Lipofectamine 3000 and 0–3 µg/mL puromycin. Although HEK293A cells had relatively higher puromycin resistance compared to transfected BV2, they too were sensitive to puromycin regardless of whether they had been transfected with a plasmid containing the puromycin resistance gene (Figure 3.7).

Subsequently, it was found that the pSpCas9n(BB)-2A-Puro plasmid obtained from Addgene contained a SNP in the puromycin resistance gene that affected its efficacy[604]. Therefore, only positive GFP^{hi} selection was used in CRISPR v1 and v2. In practice, most cells that were transfected with pSpCas9n(BB)-2A-GFP were also transfected with pSpCas9n(BB)-2A-Puro as described later. Eventually the puromycin resistance gene in pSpCas9n(BB)-2A-Puro was replaced with the mCherry2 fluorescent protein gene and used in CRISPR v3 and v4.

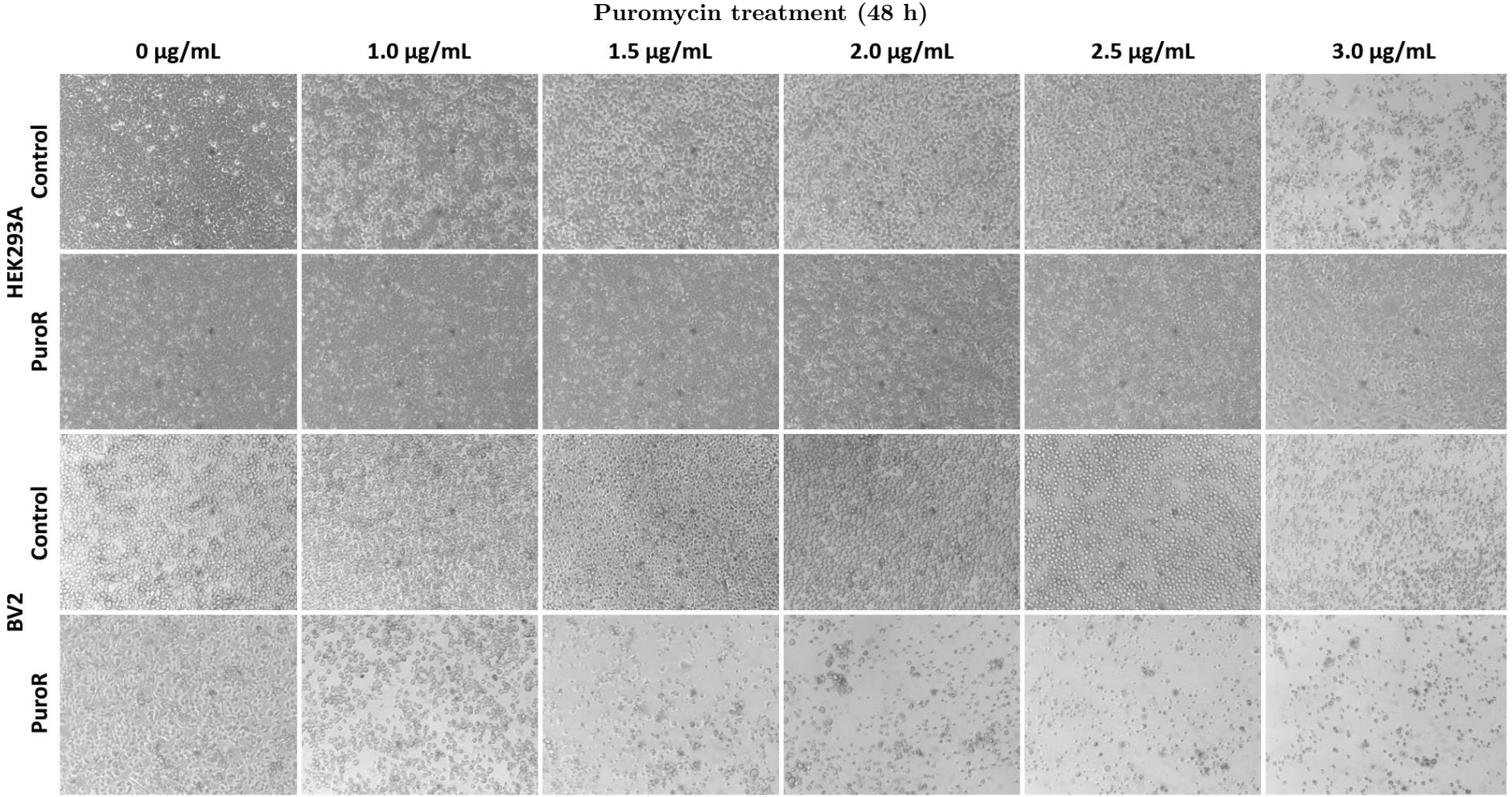

Figure 3.7. After transfection with pSpCas9n(mTREM2_R47H_sgRNA-B_F1a)-2A-Puro using Lipofectamine 3000, HEK293A and especially BV2 cells were unexpectedly vulnerable to puromycin treatment.

HEK293A or BV2 cells were treated with puromycin for 48 hours 24 hours post-transfection.

Images were captured after puromycin treatment at 100× magnification. Control: untransfected cells, PuroR: Cells transfected with pSpCas9n(mTREM2_R47H_sgRNA-B_F1a)-2A-Puro containing the puromycin resistance gene.

3.4.5 Optimisation of clone screening

The efficiency of knocking in the *Trem2* c.140G>A DNA variant to result in the p.R47H variant using CRISPR/Cas9 was expected to be low at ∼5%[605]. Therefore, a large number of clones were required to be screened. Different high-throughput screening methods were explored using CRISPR v1 plasmid pairs and HDR templates. The efficiency of HDR with the sense or anti-sense oriented HDR templates was also compared. Plasmid transfection efficiencies were slightly higher than previously achieved with the sense HDR template-transfected BV2 achieving 18.0% and the anti-sense HDR template-transfected BV2 23.8% (Figure 3.8). Overall, these transfection efficiencies were 8.2 and 10.8 fold, respectively, higher than achieved with Lipofectamine 3000 and sufficient for FACS.

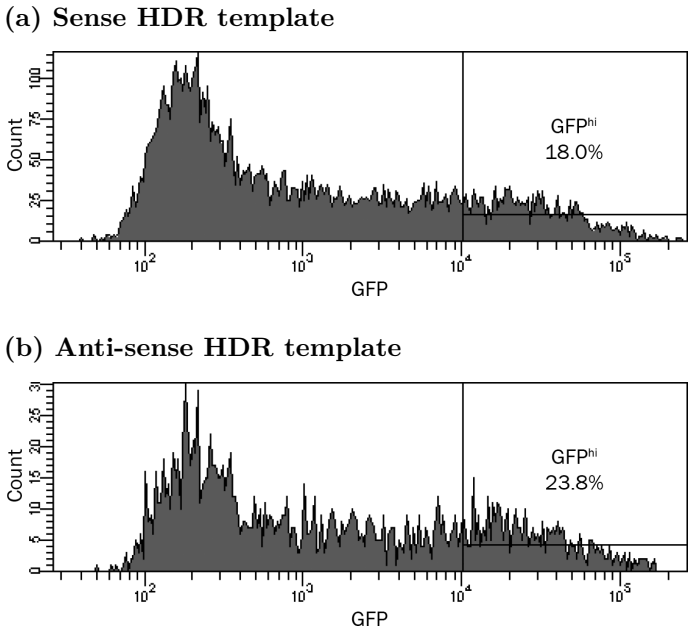

Figure 3.8. Transfection efficiency of CRISPR v1 plasmids with sense or anti-sense HDR template by electroporation were similar as expected.
Flow cytometry of BV2 transfected with CRISPR v1 plasmid pair and **(a)** sense or **(b)** anti-sense HDR template using Nucleofector Solution L with electroporation program A-030. Transfection efficiency was determined by the percentage of GFP^{hi} cells.

As standard DNA extraction and purification using PCI was not feasible in 96-well plates and with large number of clones, crude DNA from GFP^{hi}-sorted clones was prepared. Crude DNA extracts (undiluted, 1:10 diluted, and purified) were tested in PCR reactions. Undiluted crude DNA was successfully amplified without further processing (Figure 3.9) and therefore used in all subsequent screening.

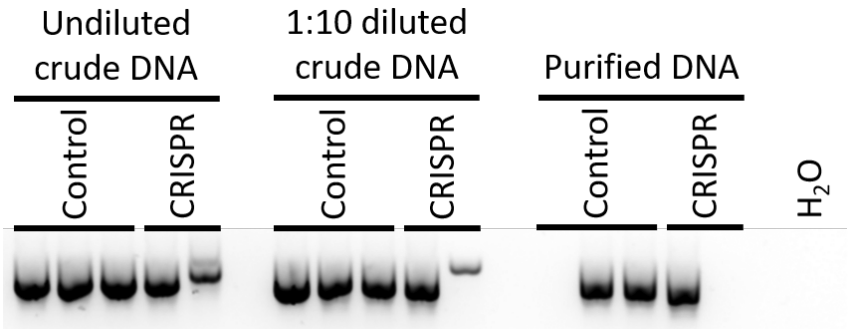

Figure 3.9. Undiluted crude DNA extracts were successfully PCR-amplified without additional processing.
Trem2 Exon 2 amplicons from various formats of crude DNA extracts resolved on a 2% TAE-agarose gel to optimise for PCR amplification.
Control: clones transfected with control plasmids without sgRNA inserted; CRISPR: clones transfected with CRISPR v1 plasmids; H_2O: no template PCR.

DNA from 96 clones transfected with the CRISPR v1 sense HDR template were genotyped with the expectation that ∼5 clones (∼5%) might carry the edited DNA variant. Agarose gel electrophoresis of *Trem2* Exon 2 amplicons revealed that most of these clones had varying amplicon sizes and were a mixture of 1–8 bands (Figure 3.10), suggesting that CRISPR/Cas9 editing was not specific as expected. To understand what had happened, they were Sanger sequenced. 90 of 96 clones were a mixture of indels (Figure 3.11), 2 clones were pure WT *Trem2* and 4 clones had homogeneous indels that resulted in a single amplicon (Table 3.2). The very high rate of clones with edited *Trem2* (94/96, 97.9%) suggested that co-transfection of both plasmids and sorting only for GFP^{hi} cells without puromycin selection was effective.

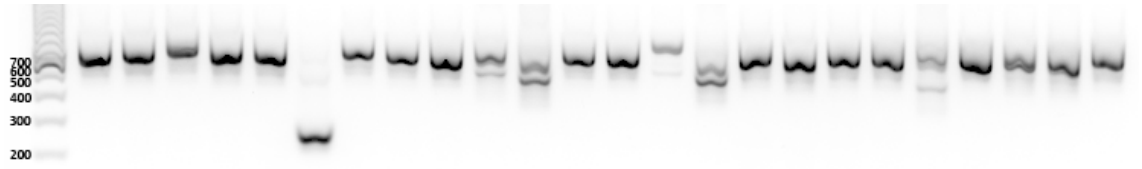

Figure 3.10. Almost all edited clones have mixed *Trem2* amplicon sizes within and between clones.
A selection of *Trem2* Exon 2 amplicons from clonal lines transfected with CRISPR v1 plasmids and sense HDR template resolved on 2% TAE-agarose gels at 100 V for 1 h. The expected amplicon size for WT *Trem2* is 646 bp. Positive and negative control lanes are not shown. DNA ladder is indicated in base pairs.

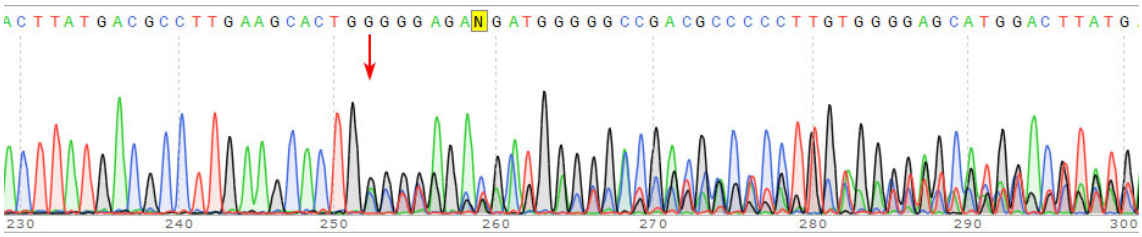

Figure 3.11. Most CRISPR v1 clones have mixed DNA sequences on Sanger sequencing chromatograms.
Example clone transfected with CRISPR v1 plasmids and sense HDR template. The boundary where the DNA sequence differed is shown (red arrow).

Clone ID	*Trem2* Exon 2 sequence (5'→3')
WT (refseq)	ATTCTAGAGCCCGTCAGGGAGTCAGTCATTAACCATCTTGCACACGCATGAGATATTCTGTTTCAAACAAAAAGTGGAAGGTACC CAAGGACCAGAACTTATCCTAATGACCATGCACACGCTATGCTCCCTGCACTCCTGGAACTGCTTCCAAGCAAGTGGCTGTCTCC TCTGCAGCCCTGTCCCAAGCCCTCAACACCACGGTGCTGCAGGGCATGGCCGGCCAGTCCTTGAGGGTGTCATGTACTTATGACG CCTTGAAGCACTGGGGGAGA**CGC**AAGGCCTGGTGTCGGCAGCTGGGTGAGGAGGGCCCATGCCAGCGTGTGGTGAGCACACACGG TGTGTGGCTGCTGGCCTTCCTGAAGAAGCGGAATGGGAGCACAGTCATCGCAGATGACACCCTTGCTGGAACCGTCACCATCACT CTGAAGAACCTCCAAGCCGGTGACGCGGGCCTCTACCAGTGTCAGAGTCTCCGAGGCCGAGAGGCTGAGGTCCTGCAGAAAGTAC TGGTGGAGGTGCTGGAGGGTGAGTACACAGTAGCTGGGTGCACCTTTGGCTGGTCCTTGTGCCAGGTCTTATTGTTGTGGGACTT TTTCAGGGGGA
C1G10	ATTCTAGAGCCCGTCAGGGAGTCAGTCATTAACCATCTTGCACACGCATGAGATATTCTGTTTCAAACAAAAAGTGGAAGGTACC CAAGGACCAGAA---------- ---------- ---------- ---------- ----------AGTCCTGCAGAAAGTACTGG TGGAGGTGCTGGAGGGTGAGTACACAGTAGCTGGGTGCACCTTTGGCTGGTCCTTGTGCCAGGTCTTATTGTTGTGGGACTTTTT CAGGGGGA
C1E2	ATTCTAGAGCCCGTCAGGGAGTCAGTCATTAACCATCTTGCACACGCATGAGATATTCTGTTTCAAACAAAAAGTGGAAGGTACC CAAGGACCAGAACTTATCCTAATGACCATGCACACGCTATGCTCCCTGCACTCCTGGAACTGCTTCCAAGCAAGTGGCTGTCTCC TCTGCAGCCCTGTCCCAAGCCCTCAACACCACGGTGCTGCAGGGCATGGCCGGCCAGTCCTTGAGGGTGTCATGTACTTATGACG CCTTG----------TGTCGGCAGCTGGGTGAGGAGGGCCCATGCCAGCGTGTGGTGAGCACACACGG TGTGTGGCTGCTGGCCTTCCTGAAGAAGCGGAATGGGAGCACAGTCATCGCAGATGACACCCTTGCTGGAACCGTCACCATCACT CTGAAGAACCTCCAAGCCGGTGACGCGGGCCTCTACCAGTGTCAGAGTCTCCGAGGCCGAGAGGCTGAGGTCCTGCAGAAAGTAC TGGTGGAGGTGCTGGAGGGTGAGTACACAGTAGCTGGGTGCACCTTTGGCTGGTCCTTGTGCCAGGTCTTATTGTTGTGGGACTT TTTCAGGGGGA
C1C4	ATTCTAGAGCCCGTCAGGGAGTCAGTCATTAACCATCTTGCACACGCATGAGATATTCTGTTTCAAACAAAAAGTGGAAGGTACC CAAGGACCAGAACTTATCCTAATGACCATGCACACGCTATGCTCCCTGCACTCCTGGAACTGCTTCCAAGCAAGTGGCTGTCTCC TCTGCAGCCCTGTCCCAAGCCCTCAACACCACGGTGCTGCAGGGCATGGCCGGCCAGTCCTTGAGGGTGTCATGTACTTATGACG CCTTGAAGC----------GGCCTGGTGTCGGCAGCTGGGTGAGGAGGGCCCATGCCAGCGTGTGGTGAGCACACACGG TGTGTGGCTGCTGGCCTTCCTGAAGAAGCGGAATGGGAGCACAGTCATCGCAGATGACACCCTTGCTGGAACCGTCACCATCACT CTGAAGAACCTCCAAGCCGGTGACGCGGGCCTCTACCAGTGTCAGAGTCTCCGAGGCCGAGAGGCTGAGGTCCTGCAGAAAGTAC TGGTGGAGGTGCTGGAGGGTGAGTACACAGTAGCTGGGTGCACCTTTGGCTGGTCCTTGTGCCAGGTCTTATTGTTGTGGGACTT TTTCAGGGGGA
C1G4	ATTCTAGAGCCCGTCAGGGAGTCAGTCATTAACCATCTTGCACACGCATGAGATATTCTGTTTCAAACAAAAAGTGGAAGGTACC CAAGGACCAGAACTTATCCTAATGACCATGCACACGCTATGCTCCCTGCACTCCTGGAACTGCTTCCAAGCAAGTGGCTGTCTCC TCTGCAGCCCTGTCCCAAGCCCTCAACACCACGGTGCTGCAGGGCATGGCCGGCCAGTCCTTGAGGGTGTCATGTACTTATGACG CCTTGAAGCACTGGGGGAGA**CGC**----------GGCAGCTGGGTGAGGAGGGCCCATGCCAGCGTGTGGTGAGCACACACGG TGTGTGGCTGCTGGCCTTCCTGAAGAAGCGGAATGGGAGCACAGTCATCGCAGATGACACCCTTGCTGGAACCGTCACCATCACT CTGAAGAACCTCCAAGCCGGTGACGCGGGCCTCTACCAGTGTCAGAGTCTCCGAGGCCGAGAGGCTGAGGTCCTGCAGAAAGTAC TGGTGGAGGTGCTGGAGGGTGAGTACACAGTAGCTGGGTGCACCTTTGGCTGGTCCTTGTGCCAGGTCTTATTGTTGTGGGACTT TTTCAGGGGGA

Table 3.2. Transfection using CRISPR v1 plasmids and sense HDR template resulted in clones with homogeneous indels within *Trem2*.
Trem2 Exon 2 sequence from positive CRISPR v1 clones.
Black font: Intronic sequence; blue font: *Trem2* Exon 2; red font: mismatch base; bold font: p.R47 codon; underlined font: target c.140G for DNA variant.

The *Trem2* c.140G>A DNA variant was not found in any of the 96 clones sequenced, which suggested HDR had not occurred and the rate of HDR is <5% and a lot more than 96 clones would need to be screened. Furthermore, the mixed DNA sequences in individual clones meant that screening for the edited DNA variant from sequencing chromatograms will be technically challenging. Together, these meant that screening by Sanger sequencing would not be time and cost efficient.

To improve the cost and efficiency of screening, a competitive allele specific PCR (KASP) genotyping assay was used to screen for clones with the DNA variant. Initially, undiluted crude DNA from 96 clones transfected with the CRISPR v1 anti-sense HDR template was tested. While the synthetic control DNA amplified, none of the sample DNA did (Figure 3.12a), suggesting inhibitors might be present in the crude DNA extracts. A 1:10 dilution of crude DNA did not improve sample amplification (not shown). Therefore, *Trem2* was pre-amplified by standard PCR from individual crude DNA and diluted by 1:10 to lower the concentration of inhibitors and PCR buffer salts. The concentration of the synthetic control DNA was also optimised to improve the assay with 1 µM resulting in better signal compared to 0.01 µM and 0.1 µM (Figure 3.12b).

Thus, using 1 µM control DNA and 1:10 diluted *Trem2* amplicons from 96 clones transfected with the CRISPR v1 anti-sense HDR template, the KASP assay successfully amplified. From this, 9 clones with homozygous DNA variant (`AA` alleles) and 11 clones with heterozygous DNA variant (`GA` alleles) were identified (Figure 3.12c). When resolved on an agarose gel, some of these clones and an additional 3 clones that failed to amplify in the KASP assay (potentially due to indels) showed mixed amplicon sizes for each clone (Figure 3.13). Subsequent Sanger sequencing of 14 amplicons thought to have a single band (Figure 3.13) revealed that all of these clones have mixed DNA sequences on the sequencing chromatogram. This meant that the method of interpreting results on the agarose gel were not optimal. Furthermore, inspection of the sequencing chromatograms suggested the different products within each clone differed by only a few base bairs which cannot be easily resolved or seen by agarose gel electrophoresis (Figure 3.14). Therefore to assess subsequent clones, 2% TBE-agarose gels were used instead of 2% TAE-agarose gels and electrophoresis were ran for much longer.

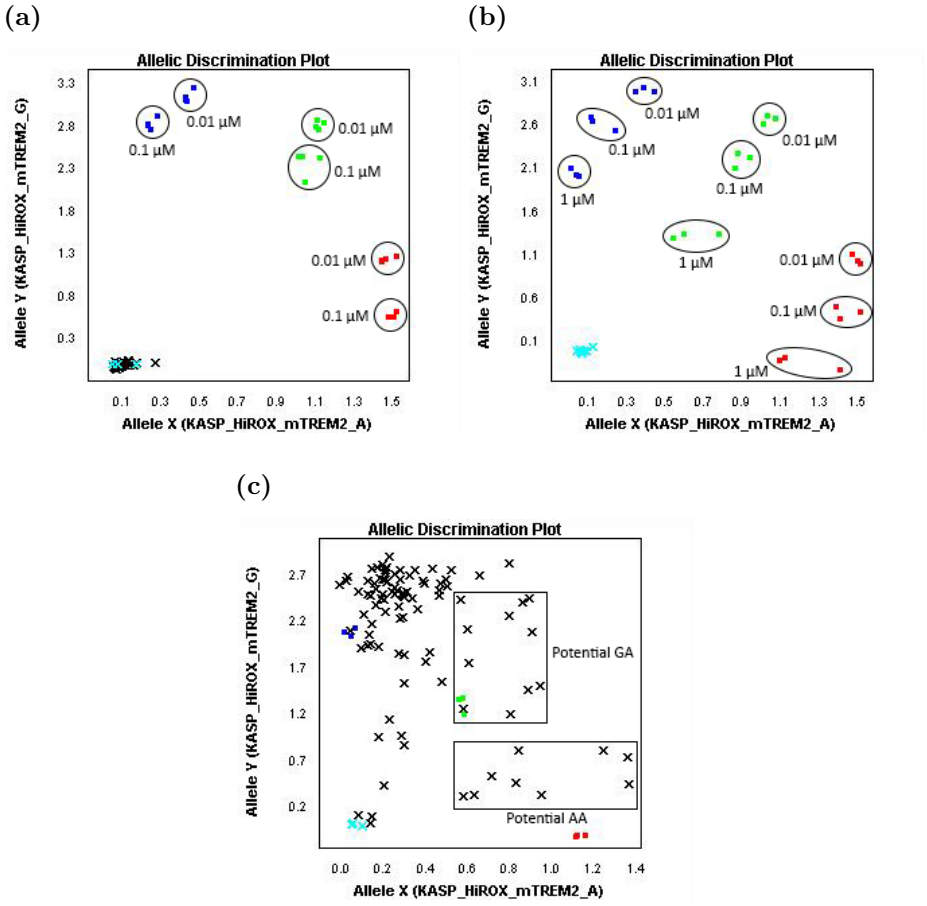

Figure 3.12. Optimisation of DNA template and control DNA in KASP genotyping assays.
(a) Undiluted crude DNA extracts from 96 clones transfected with CRISPR v1 plasmids and anti-sense HDR template failed to amplify. Two concentrations of positive control DNA were tested.
(b) 1 µM positive control DNA resulted in optimal signal. 3 concentrations of positive control DNA (0.01, 0.1, 1 µM) were compared.
(c) 1:10 diluted *Trem2* amplicons from 96 clones transfected with the CRISPR v1 plasmids and anti-sense HDR template successfully amplified. Amplicons from clones marked as potential AA and potential GA were subsequently resolved on an agarose gel and Sanger sequenced.
Blue points: homozygous WT (`GG`) control DNA, red points: homozygous DNA variant (`AA`) control DNA, green points: heterozygous DNA variant (`GA`) control DNA, cyan points: no template negative control, black points: sample DNA template.

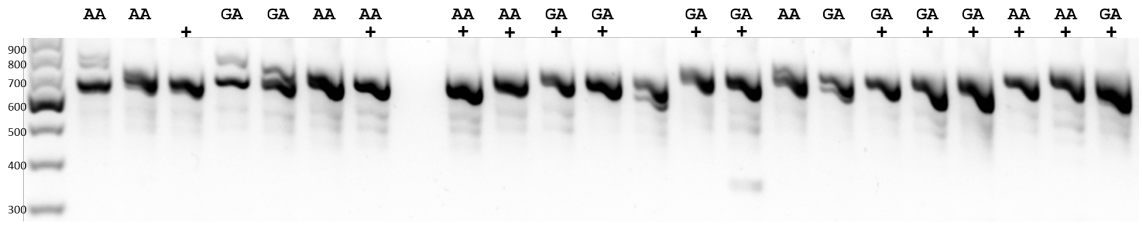

Figure 3.13. Some clones with potential homozygous (AA) and heterozygous (GA) DNA variants identified from the KASP genotyping assay and 3 additional clones that failed KASP amplification (unlabeled) had mixed *Trem2* Exon 2 amplicon sizes.
Amplicons were resolved on a 2% TAE-agarose gel at 100 V for 1 h to check for indels. Sequencing of clones thought to have a single band (+) revealed that they had heterogeneous amplicons with small indels.
Expected WT *Trem2* amplicon size is 646 bp. Positive and negative controls are not shown. DNA ladder is indicated in base pairs.

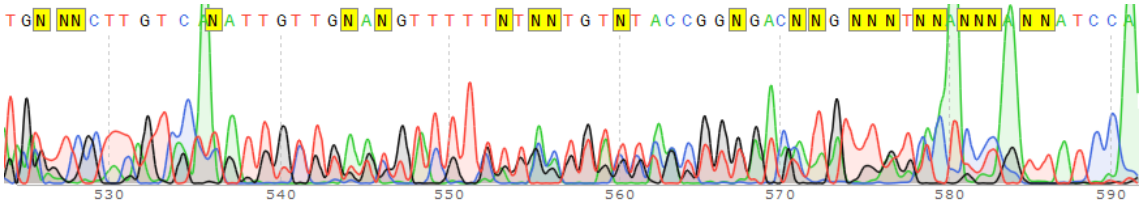

Figure 3.14. Multiple poly-A tails from sequencing chromatograms indicated mixed DNA sequences were from mixed amplicon species of varying sizes.
Although the sequence was difficult to read, it was possible to see the end of each amplicon within the mixture because the DNA polymerase adds an extra A at the end of each cycle. This example from a clone transfected with CRISPR v1 plasmids and sense HDR template shows a mixture of 4 amplicons differing by 3–55 bp.

These results also suggested cycles of repeated cut and repair events were occurring in daughter cells even after clonal isolation. It was further established that the expression of GFP persisted several days after single-cell FACS (not shown), indicating that sgRNA and Cas9n were still present and could target HDR-edited *Trem2* until NHEJ-mediated indels removed the sgRNA target sequences. It also explained why the KASP genotyping results were ambiguous and therefore the assay was not used for subsequent screening. CRISPR/Cas9 constructs and assay conditions were also redesigned to improve HDR-mediated editing and its detection.

3.4.6 Introduction of PAM-blocking mutations into HDR template (CRISPR v2 design)

The generation of BV2 expressing the TREM2 p.R47H variant was unsuccessful in CRISPR v1. Two potential options for improvement in experimental design were considered. First, to prevent Cas9 from re-targeting HDR-edited DNA and causing repeated cut and repair events, PAM-blocking silent mutations were introduced into the HDR template[547]. Second, because the relative position of the sgRNA target pairs is crucial in determining double-nicking and HDR activity[605], a new sgRNA pair targeting the p.R47H variant was designed (CRISPR v2) to test if the CRISPR v1 pair was ineffective. As expected, transfection efficiencies of the new CRISPR v2 plasmid pairs were similar to the previous electroporation experiments, achieving 20.2% for sense and 20.5% for anti-sense HDR template (Figure 3.15). 34 clones using sense HDR template and 14 clones using anti-sense HDR template were generated and screened. As seen previously, *Trem2* Exon 2 amplicons from most clones were heterogeneous. Only 3 clones had homogeneous amplicons (Figure 3.16) and subsequent Sanger sequencing revealed that 2 of these had homogeneous deletions (clone B4 and C8, Table 3.3) while the other (clone B6) had mixed amplicon sequences that was not apparent on the agarose gel. The introduction of PAM-blocking mutations did not improve the rate of homogeneous editing events nor succeeded in incorporating the targeted DNA variant.

(a) Sense HDR template

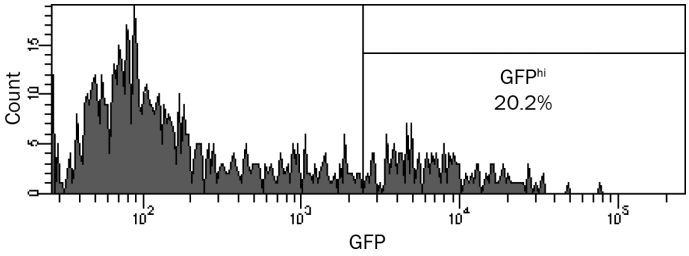

(b) Anti-sense HDR template

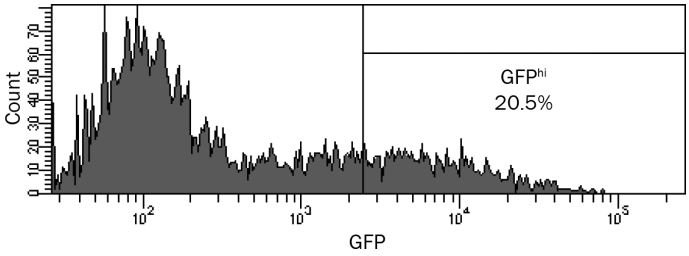

Figure 3.15. Similar to CRISPR v1, transfection efficiency of CRISPR v2 plasmids with sense or anti-sense HDR template was almost equal.
Flow cytometry of BV2 transfected with CRISPR v2 plasmid pair and **(a)** sense or **(b)** anti-sense HDR template using Nucleofector Solution L with electroporation program A-030. Transfection efficiency was determined by the percentage of GFP^{hi} cells.

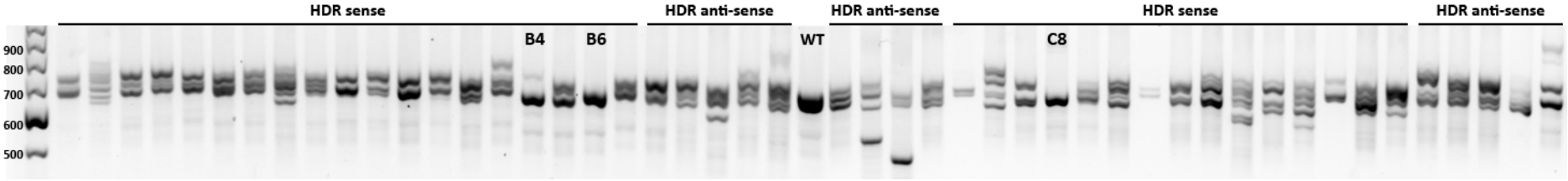

Figure 3.16. 3 clones co-transfected with CRISPR v2 plasmids with sense or anti-sense HDR template had homogeneous *Trem2* amplicons while most still resulted in mixed amplicons in each clone.

48 clonal lines were generated and screened from CRISPR v2. *Trem2* Exon 2 amplicons were resolved on a 2% TBE-agarose gel at 100 V for 3.5 h. Amplicons from clones B4, B6, and C8 which contained a single band were purified and Sanger sequenced.

WT *Trem2* amplicon (646 bp), labelled "WT", was used to compare amplicon sizes from clones. DNA ladder size is indicated in base pairs.

Clone ID	*Trem2* Exon 2 sequence (5'→3')
WT (refseq)	ATTCTAGAGCCCGTCAGGGAGTCAGTCATTAACCATCTTGCACACGCATGAGATATTCTGTTTCAAACAAAAAGTGGAAGGTACC CAAGGACCAGAACTTATCCTAATGACCATGCACACGCTATGCTCCCTGCACTCCTGGAACTGCTTCCAAGCAAGTGGCTGTCTCC TCTGCAGCCCTGTCCCAAGCCCTCAACACCACGGTGCTGCAGGGCATGGCCGGCCAGTCCTTGAGGGTGTCATGTACTTATGACG CCTTGAAGCACTGGGGGAGA**CGC**AAGGCCTGGTGTCGGCAGCTGGGTGAGGAGGGCCCATGCCAGCGTGTGGTGAGCACACACGG TGTGTGGCTGCTGGCCTTCCTGAAGAAGCGGAATGGGAGCACAGTCATCGCAGATGACACCCTTGCTGGAACCGTCACCATCACT CTGAAGAACCTCCAAGCCGGTGACGCGGGCCTCTACCAGTGTCAGAGTCTCCGAGGCCGAGAGGCTGAGGTCCTGCAGAAAGTAC TGGTGGAGGTGCTGGAGGGTGAGTACACAGTAGCTGGGTGCACCTTTGGCTGGTCCTTGTGCCAGGTCTTATTGTTGTGGGACTT TTTCAGGGGGA
C2B4	ATTCTAGAGCCCGTCAGGGAGTCAGTCATTAACCATCTTGCACACGCATGAGATATTCTGTTTCAAACAAAAAGTGGAAGGTACC CAAGGACCAGAACTTATCCTAATGACCATGCACACGCTATGCTCCCTGCACTCCTGGAACTGCTTCCAAGCAAGTGGCTGTCTCC TCTGCAGCCCTGTCCCAAGCCCTCAACACCACGGTGCTGCAGGGCATGGCCGGCCAGTCCTTGAGGGTGTCATGTACTTATGACG CCTTG----------GCCTGGTGTCGGCAGCTGGGTGAGGAGGGCCCATGCCAGCGTGTGGTGAGCACACACGG TGTGTGGCTGCTGGCCTTCCTGAAGAAGCGGAATGGGAGCACAGTCATCGCAGATGACACCCTTGCTGGAACCGTCACCATCACT CTGAAGAACCTCCAAGCCGGTGACGCGGGCCTCTACCAGTGTCAGAGTCTCCGAGGCCGAGAGGCTGAGGTCCTGCAGAAAGTAC TGGTGGAGGTGCTGGAGGGTGAGTACACAGTAGCTGGGTGCACCTTTGGCTGGTCCTTGTGCCAGGTCTTATTGTTGTGGGACTT TTTCAGGGGGA
C2C8	ATTCTAGAGCCCGTCAGGGAGTCAGTCATTAACCATCTTGCACACGCATGAGATATTCTGTTTCAAACAAAAAGTGGAAGGTACC CAAGGACCAGAACTTATCCTAATGACCATGCACACGCTATGCTCCCTGCACTCCTGGAACTGCTTCCAAGCAAGTGGCTGTCTCC TCTGCAGCCCTGTCCCAAGCCCTCAACACCACGGTGCTGCAGGGCATGGCCGGCCAGTCCTTGAGGGTGTCATGTACTTATGACG CCTTGAAGCACTGGGGGAGA**CGC**A-GG----------GCTGGGTGAGGAGGGCCCATGCCAGCGTGTGGTGAGCACACACGG TGTGTGGCTGCTGGCCTTCCTGAAGAAGCGGAATGGGAGCACAGTCATCGCAGATGACACCCTTGCTGGAACCGTCACCATCACT CTGAAGAACCTCCAAGCCGGTGACGCGGGCCTCTACCAGTGTCAGAGTCTCCGAGGCCGAGAGGCTGAGGTCCTGCAGAAAGTAC TGGTGGAGGTGCTGGAGGGTGAGTACACAGTAGCTGGGTGCACCTTTGGCTGGTCCTTGTGCCAGGTCTTATTGTTGTGGGACTT TTTCAGGGGGA

Table 3.3. Positive CRISPR v2 clones with homogeneous indels in *Trem2* Exon 2.
Their *Trem2* Exon 2 DNA sequence are as shown.
Black font: Intronic sequence; blue font: *Trem2* Exon 2; bold font: p.R47 codon, underlined font: target c.140G for DNA variant.

The presence of heterogeneous editing events in the clonal population suggested more than one copy of *Trem2* gene existed in BV2 cells. Closer investigation of BV2 revealed that there was a low frequency of multinucleated cells, with up to 4 nuclei per cell (Figure 3.17). However, this frequency did not match the rate of multiple *Trem2* amplicons occurring. Nevertheless, smaller and less granulated mononucleated cells were gated in subsequent cell sorting.

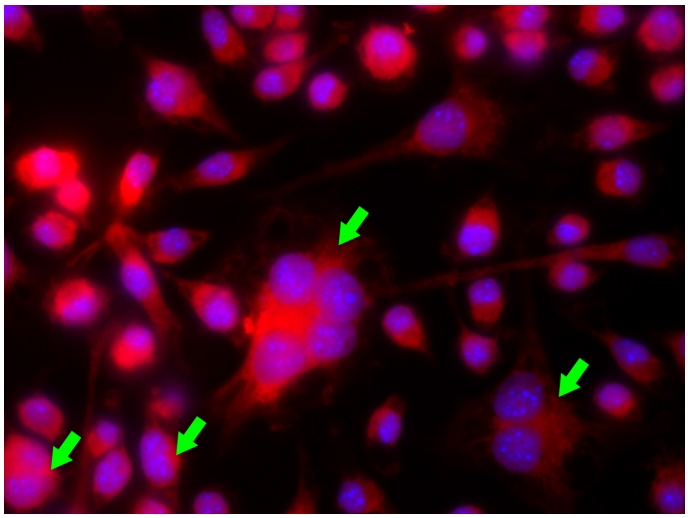

Figure 3.17. BV2 typically exhibit a low frequency of multinucleated cells in culture which slightly increases on immune activation[606].
BV2 cells were electroporated with only the HDR template and stained with CellTracker Red CMTPX Dye and Hoechst 33342.
Green arrows indicate multinucleated cells. Fluorescence microscopy images were taken at 630× magnification.

3.4.7 CRISPR/Cas9 targeting additional gene variants in *Trem2* (CRISPR v3 design)

It is possible that the targeting and editing to knock in the p.R47H variant was inefficient. Therefore, other disease-associated loci in the *Trem2* gene resulting in the p.Q33X (rs104894002) and p.D87N (rs142232675) variants were targeted. Both variants have been described in AD and Nasu-Hakola patients[109,342] with a few examples in people without AD[333]. Of these variants, only the p.D87 amino acid residue is conserved between human and mouse TREM2. Mouse TREM2 contains the p.R33 instead of p.Q33 residue but as the variant results in an early stop codon, this did not matter. The possibility to revert sgRNA-blocking mutations back to the WT sequence while retaining the intended DNA variants with a two-step editing[547] (CRISPR v3a and v3b) was also explored. Transfection efficiencies of plasmid pairs ranged between 17.6–25.6% (CRISPR v3a) and 7.2–10.4% (CRISPR v3b) (Table 3.4).

58 clones from p.Q33X-targeted CRISPR/Cas9 and 41 clones from p.D87N-targeted CRISPR/Cas9 were obtained at the end of the second editing step (CRISPR v3b). While many crude DNA extracts from these clones did not amplify, those that did still showed mixed amplicon sizes in individual clones with no single-band amplicons (Appendix Figure A2a,b), indicating that the lack of homogeneous editing is not unique to targeting the p.R47H knock-in.

Target variant	CRISPR version	Transfection efficiency
p.Q33X	v3a	23.4%
	v3b	7.2%
p.D87N	v3a	25.6%
	v3b	10.4%
p.R47H	v3a	17.6%
	v3b	8.1%

Table 3.4. Transfection efficiencies of CRISPR v3a plasmids were similar to CRISPR v1 and v2 but were lower with CRISPR v3b.
Transfection efficiency was determined by the percentage of GFP^{hi} and $mCherry2^{hi}$ cells using flow cytometry.

131 clones from the p.R47H-targeted CRISPR/Cas9 were also screened. A total of 27 single-band amplicons were identified after agarose gel electrophoresis (Appendix Figure A2c,d). Sanger sequencing revealed that only one clone had a single amplicon containing a 17 bp insertion and 11 bp deletion (net 6 bp insertion) (Table 3.5) and another clone that failed to be sequenced.

Clone ID	***Trem2* Exon 2 sequence (5'→3')**
WT (refseq)	ATTCTAGAGCCCGTCAGGGAGTCAGTCATTAACCATCTTGCACACGCATGAGATATTCTGTTTCAAACAAAAAGTGGAAGGTACC CAAGGACCAGAACTTATCCTAATGACCATGCACACGCTATGCTCCCTGCACTCCTGGAACTGCTTCCAAGCAAGTGGCTGTCTCC TCTGCAGCCCTGTCCCAAGCCCTCAACACCACGGTGCTGCAGGGCATGGCCGGCCAGTCCTTGAGGGTGTCATGTACTTATGACG CCTTGAAGCACTGGGGGAGA**CGC**AAGGCCTGGTGTCGGCAGCTGGGTGAGGAGGGCCCATGCCAGCGTGTGGTGAGCACACACGG TGTGTGGCTGCTGGCCTTCCTGAAGAAGCGGAATGGGAGCACAGTCATCGCAGATGACACCCTTGCTGGAACCGTCACCATCACT CTGAAGAACCTCCAAGCCGGTGACGCGGGCCTCTACCAGTGTCAGAGTCTCCGAGGCCGAGAGGCTGAGGTCCTGCAGAAAGTAC TGGTGGAGGTGCTGGAGGGTGAGTACACAGTAGCTGGGTGCACCTTTGGCTGGTCCTTGTGCCAGGTCTTATTGTTGTGGGACTT TTTCAGGGGGA
C3P2D10	ATTCTAGAGCCCGTCAGGGAGTCAGTCATTAACCATCTTGCACACGCATGAGATATTCTGTTTCAAACAAAAAGTGGAAGGTACC CAAGGACCAGAACTTATCCTAATGACCATGCACACGCTATGCTCCCTGCACTCCTGGAACTGCTTCCAAGCAAGTGGCTGTCTCC TCTGCAGCCCTGTCCCAAGCCCTCAACACCACGGTGCTGCAGGGCATGGCCGGCCAGTCCTTGAGGGTGTCATGTACTTATGACG CCTTGAAGCACTGGGGGAGGCGAAGCACTGGGGGAG**ACGC**AAGGC----------AGCTGGGTGAGGAGGGCCCATGCCAGCGT GTGGTGAGCACACACGGTGTGTGGCTGCTGGCCTTCCTGAAGAAGCGGAATGGGAGCACAGTCATCGCAGATGACACCCTTGCTG GAACCGTCACCATCACTCTGAAGAACCTCCAAGCCGGTGACGCGGGCCTCTACCAGTGTCAGAGTCTCCGAGGCCGAGAGGCTGA GGTCCTGCAGAAAGTACTGGTGGAGGTGCTGGAGGGTGAGTACACAGTAGCTGGGTGCACCTTTGGCTGGTCCTTGTGCCAGGTC TTATTGTTGTGGGACTTTTTCAGGGGGA

Table 3.5. Only one positive clone from CRISPR v3 R47H resulted in a net small insertion in *Trem2* Exon 2.
Trem2 Exon 2 sequence as Sanger sequenced is shown.
Black font: Intronic sequence; blue font: *Trem2* Exon 2; red font: mismatch/insertion; bold font: p.R47 codon; underlined font: target c.140G for DNA variant.

3.4.8 Improving selection of mononucleated cells using Hoechst 33342

The frequency of mixed amplicon sizes detected on agarose gels did not decrease even after sorting for smaller and less granulated cells to avoid large multinucleated cells. This suggests that cell sorting based on size (FSC) and granularity (SSC) alone was insufficient to gate for mononucleated cells. As multinucleated cells have more DNA content per cell, they are expected to have higher fluorescence intensity when stained with Hoechst 33342 compared to mononucleated cells. Hence, Hoechst 33342 was used to gate for mononucleated cells during single-cell FACS. Using CRISPR v3b p.R47H-targeted clones, there was a higher rate of single-band amplicons in Hoechst^{lo} cells (20/59, 33.9%) compared to unstained cells (23/142, 16.2%) when screened on agarose gels (Table 3.6) which initially looked promising.

Two clones with homogeneous indels were identified from the screen, one each from unstained and Hoechst^{lo} clones (Table 3.7). However, despite enriching for mononucleated cells, mixed amplicon sizes in individual clones were still present in the majority of clones and the other single bands were WT *Trem2* (Appendix Figure A3). This suggested multinuclearity is not the major contributing factor for editing events on multiple copies of *Trem2*.

Hoechst	Total clones	Single-band amplicons	Single-band rate	Indels
Unstained	142	23	16.2%	One net 142 bp insertion
Hoechst^{lo}	59	20	33.9%	One 82 bp deletion

Table 3.6. Hoechst 33342 was used to select mononucleated cells and reduced editing heterogeneity in BV2 clones.
BV2 transfected with CRISPR v3b p.R47H-targeted plasmids and HDR template were stained with Hoechst 33342 before single-cell sorting Hoechst^{lo} cells. Overall, only two clones with homogeneous indels were obtained and the remainder single amplicon clones had WT *Trem2*.

Clone ID	*Trem2* Exon 2 sequence (5'→3')
WT (refseq)	ATTCTAGAGCCCGTCAGGGAGTCAGTCATTAACCATCTTGCACACGCATGAGATATTCTGTTTCAAACAAAAAGTGGAAGGTACC CAAGGACCAGAACTTATCCTAATGACCATGCACACGCTATGCTCCCTGCACTCCTGGAACTGCTTCCAAGCAAGTGGCTGTCTCC TCTGCAGCCCTGTCCCAAGCCCTCAACACCACGGTGCTGCAGGGCATGGCCGGCCAGTCCTTGAGGGTGTCATGTACTTATGACG CCTTGAAGCACTGGGGGAGA**CGC**AAGGCCTGGTGTCGGCAGCTGGGTGAGGAGGGCCCATGCCAGCGTGTGGTGAGCACACACGG TGTGTGGCTGCTGGCCTTCCTGAAGAAGCGGAATGGGAGCACAGTCATCGCAGATGACACCCTTGCTGGAACCGTCACCATCACT CTGAAGAACCTCCAAGCCGGTGACGCGGGCCTCTACCAGTGTCAGAGTCTCCGAGGCCGAGAGGCTGAGGTCCTGCAGAAAGTAC TGGTGGAGGTGCTGGAGGGTGAGTACACAGTAGCTGGGTGCACCTTTGGCTGGTCCTTGTGCCAGGTCTTATTGTTGTGGGACTT TTTCAGGGGGA
C3bB10	ATTCTAGAGCCCGTCAGGGAGTCAGTCATTAACCATCTTGCACACGCATGAGATATTCTGTTTCAAACAAAAAGTGGAAGGTACC CAAGGACCAGAACTTATCCTAATGACCATGCACACGCTATGCTCCCTGCACTCCTGGAACTGCTTCCAAGCAAGTGGCTGTCTCC TCTGCAGCCCTGTCCCAAGCCCTCAACACCACGGTGCTGTGGGACTCTTGTTCTCATGAGTTCTTACACATTGCGATGCACGACT GTAATAAGAGACCTTTGAACTCTGATTCTTAGCATCATTTCTAGAAAAGAGAGAAAAGTGAAGAACAATGAAAATATTATTGGAA CATACCACAATTTTTTAAATACATGGGATGATTTGGTGTCGGCAGCTGGGTGAGGAGGGCCCATGCCAGCGTGTGGTGAGCACAC ACGGTGTGTGGCTGCTGGCCTTCCTGAAGAAGCGGAATGGGAGCACAGTCATCGCAGATGACACCCTTGCTGGAACCGTCACCAT CACTCTGAAGAACCTCCAAGCCGGTGACGCGGGCCTCTACCAGTGTCAGAGTCTCCGAGGCCGAGAGGCTGAGGTCCTGCAGAAA GTACTGGTGGAGGTGCTGGAGGGTGAGTACACAGTAGCTGGGTGCACCTTTGGCTGGTCCTTGTGCCAGGTCTTATTGTTGTGGG ACTTTTTCAGGGGGA
C3bC4	ATTCTAGAGCCCGTCAGGGAGTCAGTCATTAACCATCTTGCACACGCATGAGATATTCTGTTTCAAACAAAAAGTGGAAGGTACC CAAGGACCAGAACTTATCCTAATGACCATGCACACGCTATGCTCCCTGCACTCCTGGAACTGCTTCCAAGCAAGTGGCTGTCTCC TC----------G CCTTGAAGCACTGGGGGAGA**CGC**AAGGCCTGGTGTCGGCAGCTGGGTGAGGAGGGCCCATGCCAGCGTGTGGTGAGCACACACGG TGTGTGGCTGCTGGCCTTCCTGAAGAAGCGGAATGGGAGCACAGTCATCGCAGATGACACCCTTGCTGGAACCGTCACCATCACT CTGAAGAACCTCCAAGCCGGTGACGCGGGCCTCTACCAGTGTCAGAGTCTCCGAGGCCGAGAGGCTGAGGTCCTGCAGAAAGTAC TGGTGGAGGTGCTGGAGGGTGAGTACACAGTAGCTGGGTGCACCTTTGGCTGGTCCTTGTGCCAGGTCTTATTGTTGTGGGACTT TTTCAGGGGGA

Table 3.7. Two clones with a homogeneous insertion or deletion in *Trem2* following single-cell sorting of unstained or Hoechst^{lo} CRISPR v3b clones.
Trem2 Exon 2 sequence for each clone as Sanger sequenced is shown.
Black font: Intronic sequence; blue font: *Trem2* Exon 2; red font: mismatch/insertion; bold font: p.R47 codon; underlined font: target c.140G for DNA variant.

3.4.9 Determining hyperploidy in BV2 by karyotyping

Heterogeneous editing by CRISPR/Cas9 in clonal lines could also potentially result from editing of multiple copies of *Trem2* due to hyperploidy. To establish this in BV2, a sample culture was karyotyped. On average, BV2 have a triploid set of chromosomes with heterogeneity between individual cells with some missing or having additional chromosomes (Figure 3.18). More importantly, there were up to 4 copies of chromosome 17 where the mouse *Trem2* locus is, which may explain the high rate of mixed amplicon sizes in clones following CRISPR/Cas9 editing. This makes the probability of homogeneous editing, regardless of NHEJ-mediated indels or HDR-mediated knock-in mutations, very low and difficult to achieve in these cells and highlights the need for wider consideration when genome editing transformed cell lines.

(a) BV2 karyotype 1

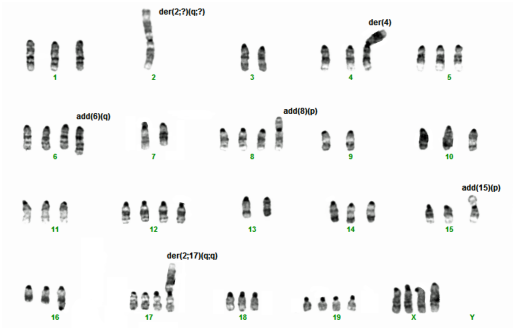

(b) BV2 karyotype 2

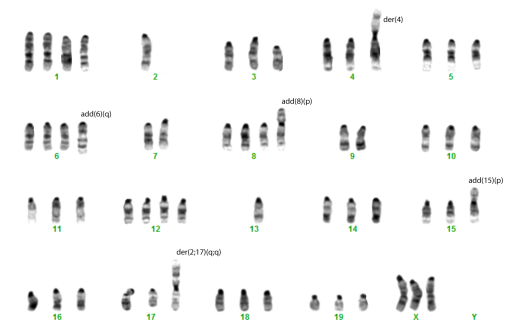

(c) BV2 karyotype 3

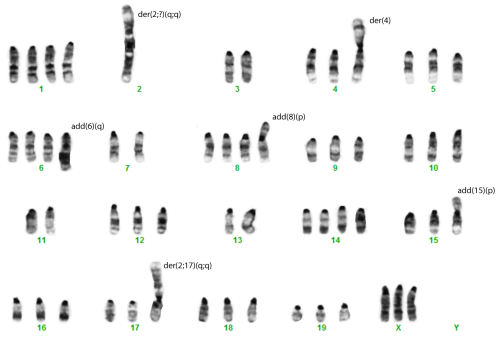

Figure 3.18. BV2 cells on average were triploid with further instability in the chromosome number between individual cells.
Chromosome 17, where the mouse *Trem2* locus is, has up to 4 copies. Karyotyped BV2 cells were cultured in normal conditions.

3.4.10 Cell cycle synchronisation of BV2 before transfection (CRISPR v4 design)

It may be possible to improve the rate of HDR so that all copies of *Trem2* in a cell would incorporate the same knock-in mutation. Lin *et al* has reported that cell cycle synchronisation using nocodazole was able to increase the efficiency of HDR by up to 31%[548]. Therefore, in a further attempt to generate BV2 with the p.R47H variant, BV2 were treated with nocodazole before electroporation. Transfection efficiencies of the plasmid pairs and HDR template for each concentration of nocodazole and untreated control cells resulted in lower transfection efficiencies than previously obtained (1.8–6.0%, Table 3.8). On screening, CRISPR/Cas9 editing was heterogeneous with mixed amplicon sizes in individual clones regardless of nocodazole treatment (Appendix Figure A4). Only untreated BV2 (4/57, 7.02%), 10 ng/mL (9/59, 15.25%), and 1000 ng/mL (11/37, 29.73%) nocodazole-treated BV2 resulted in any single-band amplicons which of those sequenced, turned out to be WT *Trem2* while 100 ng/mL (0/51), 200 ng/mL (0/16) and 500 ng/mL (0/46) nocodazole-treated BV2 resulted in mixed amplicon sizes as before (Table 3.9). Overall, cell cycle synchronisation by nocodazole treatment did not improve the rate of HDR sufficient to generate the p.R47H variant.

Nocodazole (ng/mL)	**Transfection efficiency**
0	2.0%
10	1.8%
100	6.0%
200	3.9%
500	5.8%
1000	2.8%

Table 3.8. Transfection efficiencies with CRISPR v4 plasmids and HDR template in BV2 treated with or without various concentrations of nocodazole were lower than previously achieved.
Transfection efficiency was established by percentage of GFP^{hi} and $mCherry2^{hi}$ cells using flow cytometry.

Nocodazole (ng/mL)	Total clones	Single-band amplicons	Single-band rate
0	57	4	7.02%
10	59	9	15.25%
100	51	0	0%
200	16	0	0%
500	46	0	0%
1000	37	11	29.73%

Table 3.9. Nocodazole treatment did not appear to shift cells towards a higher rate of HDR editing.
BV2 treated with different concentrations of nocodazole were transfected with CRISPR v4 R47H plasmids and HDR template. Mononucleated cells were positively gated during single-cell sorting. No clones were found to carry the p.R47H variant. Of those containing single bands which were sequenced, all were WT.

3.4.11 *Trem2*-edited BV2 clonal lines suitable for functional characterisation

The majority of 9 homogeneous *Trem2*-edited clonal BV2 cell lines containing an indel were expected to result in functional loss of TREM2 and thus were potentially useful in mechanistic and drug screening studies where a loss of TREM2 function was relevant. Although there were several clones with indels leading to frameshift generated from the different CRISPR designs, only clones from CRISPR v1 when transfected with the sense HDR template (C1G10, C1E2, C1C4, C1G4) and the CRISPR v3b clones with Hoechst 33342-mediated selection of mononucleated cells (C3bB10, C3bC4) successfully revived from cryopreservation in the 96-well culture plates (Table 3.10). Additionally, 5 WT clones which had undergone CRISPR/Cas9 editing alongside the others were revived to be used as procedure controls (Table 3.10). Characterisation of these clones is described in Chapter 5.

Clone ID	*Trem2* Exon 2 sequence (5'→3')
WT (refseq)	ATTCTAGAGCCCGTCAGGGAGTCAGTCATTAACCATCTTGCACACGCATGAGATATTCTGTTTCAAACAAAAAGTGGAAGGTACC CAAGGACCAGAACTTATCCTAATGACCATGCACACGCTATGCTCCCTGCACTCCTGGAACTGCTTCCAAGCAAGTGGCTGTCTCC TCTGCAGCCCTGTCCCAAGCCCTCAACACCACGGTGCTGCAGGGCATGGCCGGCCAGTCCTTGAGGGTGTCATGTACTTATGACG CCTTGAAGCACTGGGGGAGACGCAAGGCCTGGTGTCGGCAGCTGGGTGAGGAGGGCCCATGCCAGCGTGTGGTGAGCACACACGG TGTGTGGCTGCTGGCCTTCCTGAAGAAGCGGAATGGGAGCACAGTCATCGCAGATGACACCCTTGCTGGAACCGTCACCATCACT CTGAAGAACCTCCAAGCCGGTGACGCGGGCCTCTACCAGTGTCAGAGTCTCCGAGGCCGAGAGGCTGAGGTCCTGCAGAAAGTAC TGGTGGAGGTGCTGGAGGGTGAGTACACAGTAGCTGGGTGCACCTTTGGCTGGTCCTTGTGCCAGGTCTTATTGTTGTGGGACTT TTTCAGGGGGA
C1G10	ATTCTAGAGCCCGTCAGGGAGTCAGTCATTAACCATCTTGCACACGCATGAGATATTCTGTTTCAAACAAAAAGTGGAAGGTACC CAAGGACCAGAA---------- ---------- ---------- ---------- ----------AGTCCTGCAGAAAGTACTGG TGGAGGTGCTGGAGGGTGAGTACACAGTAGCTGGGTGCACCTTTGGCTGGTCCTTGTGCCAGGTCTTATTGTTGTGGGACTTTTT CAGGGGGA
C1E2	ATTCTAGAGCCCGTCAGGGAGTCAGTCATTAACCATCTTGCACACGCATGAGATATTCTGTTTCAAACAAAAAGTGGAAGGTACC CAAGGACCAGAACTTATCCTAATGACCATGCACACGCTATGCTCCCTGCACTCCTGGAACTGCTTCCAAGCAAGTGGCTGTCTCC TCTGCAGCCCTGTCCCAAGCCCTCAACACCACGGTGCTGCAGGGCATGGCCGGCCAGTCCTTGAGGGTGTCATGTACTTATGACG CCTTG----------TGTCGGCAGCTGGGTGAGGAGGGCCCATGCCAGCGTGTGGTGAGCACACACGG TGTGTGGCTGCTGGCCTTCCTGAAGAAGCGGAATGGGAGCACAGTCATCGCAGATGACACCCTTGCTGGAACCGTCACCATCACT CTGAAGAACCTCCAAGCCGGTGACGCGGGCCTCTACCAGTGTCAGAGTCTCCGAGGCCGAGAGGCTGAGGTCCTGCAGAAAGTAC TGGTGGAGGTGCTGGAGGGTGAGTACACAGTAGCTGGGTGCACCTTTGGCTGGTCCTTGTGCCAGGTCTTATTGTTGTGGGACTT TTTCAGGGGGA
C1C4	ATTCTAGAGCCCGTCAGGGAGTCAGTCATTAACCATCTTGCACACGCATGAGATATTCTGTTTCAAACAAAAAGTGGAAGGTACC CAAGGACCAGAACTTATCCTAATGACCATGCACACGCTATGCTCCCTGCACTCCTGGAACTGCTTCCAAGCAAGTGGCTGTCTCC TCTGCAGCCCTGTCCCAAGCCCTCAACACCACGGTGCTGCAGGGCATGGCCGGCCAGTCCTTGAGGGTGTCATGTACTTATGACG CCTTGAAGC----------GGCCTGGTGTCGGCAGCTGGGTGAGGAGGGCCCATGCCAGCGTGTGGTGAGCACACACGG TGTGTGGCTGCTGGCCTTCCTGAAGAAGCGGAATGGGAGCACAGTCATCGCAGATGACACCCTTGCTGGAACCGTCACCATCACT CTGAAGAACCTCCAAGCCGGTGACGCGGGCCTCTACCAGTGTCAGAGTCTCCGAGGCCGAGAGGCTGAGGTCCTGCAGAAAGTAC TGGTGGAGGTGCTGGAGGGTGAGTACACAGTAGCTGGGTGCACCTTTGGCTGGTCCTTGTGCCAGGTCTTATTGTTGTGGGACTT TTTCAGGGGGA
C1G4	ATTCTAGAGCCCGTCAGGGAGTCAGTCATTAACCATCTTGCACACGCATGAGATATTCTGTTTCAAACAAAAAGTGGAAGGTACC CAAGGACCAGAACTTATCCTAATGACCATGCACACGCTATGCTCCCTGCACTCCTGGAACTGCTTCCAAGCAAGTGGCTGTCTCC TCTGCAGCCCTGTCCCAAGCCCTCAACACCACGGTGCTGCAGGGCATGGCCGGCCAGTCCTTGAGGGTGTCATGTACTTATGACG CCTTGAAGCACTGGGGGAGACGC----------GGCAGCTGGGTGAGGAGGGCCCATGCCAGCGTGTGGTGAGCACACACGG TGTGTGGCTGCTGGCCTTCCTGAAGAAGCGGAATGGGAGCACAGTCATCGCAGATGACACCCTTGCTGGAACCGTCACCATCACT CTGAAGAACCTCCAAGCCGGTGACGCGGGCCTCTACCAGTGTCAGAGTCTCCGAGGCCGAGAGGCTGAGGTCCTGCAGAAAGTAC TGGTGGAGGTGCTGGAGGGTGAGTACACAGTAGCTGGGTGCACCTTTGGCTGGTCCTTGTGCCAGGTCTTATTGTTGTGGGACTT TTTCAGGGGGA
C3bB10	ATTCTAGAGCCCGTCAGGGAGTCAGTCATTAACCATCTTGCACACGCATGAGATATTCTGTTTCAAACAAAAAGTGGAAGGTACC CAAGGACCAGAACTTATCCTAATGACCATGCACACGCTATGCTCCCTGCACTCCTGGAACTGCTTCCAAGCAAGTGGCTGTCTCC TCTGCAGCCCTGTCCCAAGCCCTCAACACCACGGTGCTGTGGGACTCTTGTTCTCATGAGTTCTTACACATTGCGATGCACGACT GTAATAAGAGACCTTTGAACTCTGATTCTTAGCATCATTTCTAGAAAAGAGAGAAAAGTGAAGAACAATGAAAATATTATTGGAA CATACCACAATTTTTTAAATACATGGGATGATTTGGTGTCGGCAGCTGGGTGAGGAGGGCCCATGCCAGCGTGTGGTGAGCACAC ACGGTGTGTGGCTGCTGGCCTTCCTGAAGAAGCGGAATGGGAGCACAGTCATCGCAGATGACACCCTTGCTGGAACCGTCACCAT CACTCTGAAGAACCTCCAAGCCGGTGACGCGGGCCTCTACCAGTGTCAGAGTCTCCGAGGCCGAGAGGCTGAGGTCCTGCAGAAA GTACTGGTGGAGGTGCTGGAGGGTGAGTACACAGTAGCTGGGTGCACCTTTGGCTGGTCCTTGTGCCAGGTCTTATTGTTGTGGG ACTTTTTCAGGGGGA
C3bC4	ATTCTAGAGCCCGTCAGGGAGTCAGTCATTAACCATCTTGCACACGCATGAGATATTCTGTTTCAAACAAAAAGTGGAAGGTACC CAAGGACCAGAACTTATCCTAATGACCATGCACACGCTATGCTCCCTGCACTCCTGGAACTGCTTCCAAGCAAGTGGCTGTCTCC TC----------G CCTTGAAGCACTGGGGGAGACGCAAGGCCTGGTGTCGGCAGCTGGGTGAGGAGGGCCCATGCCAGCGTGTGGTGAGCACACACGG TGTGTGGCTGCTGGCCTTCCTGAAGAAGCGGAATGGGAGCACAGTCATCGCAGATGACACCCTTGCTGGAACCGTCACCATCACT CTGAAGAACCTCCAAGCCGGTGACGCGGGCCTCTACCAGTGTCAGAGTCTCCGAGGCCGAGAGGCTGAGGTCCTGCAGAAAGTAC TGGTGGAGGTGCTGGAGGGTGAGTACACAGTAGCTGGGTGCACCTTTGGCTGGTCCTTGTGCCAGGTCTTATTGTTGTGGGACTT TTTCAGGGGGA

Continued on next page...

Clone ID	***Trem2* Exon 2 sequence (5'→3')**
C3bA1	WT
C3bA6	WT
C3bA8	WT
C3bA12	WT
C3bB4	WT

Table 3.10. Homogeneous clones with a single insertion or deletion predicted to result in a functional TREM2 knockout and able to be grown are summarised.
Trem2 Exon 2 sequence for each clone as Sanger sequenced is shown.
Black font: Intronic sequence; blue font: *Trem2* Exon 2; red font: mismatch/insertion; bold font: p.R47 codon; underlined font: target c.140G for DNA variant.

3.5 Discussion

In CRISPR v1, multiple *Trem2* amplicons edited at a similar target site were observed on agarose gels and by sequencing. It was initially thought that the design of CRISPR v1 which did not stop Cas9n retargeting *Trem2* after successful HDR led to continuous editing until NHEJ-mediated indels disrupted the sgRNA targeting sequences. Furthermore, GFP expression in transfected BV2 was observed to last over several days (data not shown), suggesting that the sgRNA-Cas9 expression plasmid persisted long enough for extended expression of Cas9n and activity after clonal isolation by single-cell FACS. This would mean as BV2 proliferated, daughter cells that have undergone HDR would still have viable sgRNA target sequence in *Trem2* and each could undergo independent editing events from Cas9n, resulting in a genotypically heterogeneous population with slightly different indels. Thus, PAM-blocking mutations and sgRNA-blocking mutations were introduced into CRISPR v2 and v3 design, respectively. These silent blocking mutations on the HDR template would alter the sgRNA targeting sequences on *Trem2* after successful incorporation by HDR and disrupt further Cas9n targeting and editing[547,607]. Others have shown that PAM- and sgRNA-blocking mutations similarly improved accurate HDR events with no additional indels being generated in iPSCs and HEK293 cells by up to 10-fold[547].

However, multiple *Trem2* amplicons were still observed after the introduction of PAM- and sgRNA-blocking mutations in CRISPR v2 and v3, respectively. This suggested that repeated cutting was not the cause of heterogeneous editing of *Trem2*. An alternative explanation for this is that there were multiple copies of *Trem2* in each cells for Cas9n to target and cut, leading to the detection of heterogeneous NHEJ-mediated indels in clonal lines. There are two possibilities that result in multiple copies of *Trem2* to occur: multinuclearity or hyperploidy. Indeed, some multinucleated BV2 cells were observed at a low frequency when nuclei were stained in BV2 that is consistent with findings by others[606]. Microglia have been observed to form multinucleated cells upon stimulation by various inflammatory factors *in vitro*, including IL-3, IL-4, IL-13, TNF-α, granulocyte macrophage-colony stimulating factor (GM-CSF), phorbol myristate acetate (PMA), and phagocytosis of cell debris[606,608–610]. Although BV2 were not stimulated with most of these inflammatory factors and cytokines during CRISPR/Cas9-mediated genome editing, electroporation of BV2 induced a high amount of cell death (data not shown) and hence cell

debris. The rigours of FACS shortly after electroporation may also exacerbate cell stress and activation. These crucial steps in the CRISPR/Cas9 workflow may have increased the occurrence of multinucleated BV2. Unfortunately, this is unavoidable as other methods of transfection do not yield sufficient transfection efficiency.

Considering the low frequency of multinucleated cells relative to the frequency of multiple amplicons observed in each clone, it appears that multinuclearity was not the major contributing factor of multiple copies of *Trem2*. Regardless, the contribution of multinucleated cells was minimised by positively gating for mononucleated cells during FACS. Multinucleated cells induced by cell debris have been shown to have high granularity (SSC) in by flow cytometry[610] and hence, smaller and less granular cells were sorted with stricter FSC-SSC gating in CRISPR v3 and v4. However, the changes in FSC-SSC gating alone did not drastically improve the frequency of single-band amplicons observed. Additionally, segregation of multinucleated cells could be improved by using a nuclear stain such as Hoechst 33342 as they would have more intense fluorescence staining compared to mononucleated cells. The use of DNA-binding stains like Hoechst dyes to stain nuclei of live cells may impact genomic integrity as it is potentially mutagenic and carcinogenic. It can result in endoreduplication leading to polyploidy[611] and decrease in DNA synthesis[612]. Nevertheless, it has been shown that live cell staining with Hoechst 33342 for flow cytometry does not result in mutagenesis, at least in boar spermatozoa[613]. When Hoechst^{lo} cells were single-cell sorted in the present study, the rate of obtaining single homogeneous *Trem2* amplicons improved by almost two-fold compared to sorting unstained BV2 by FSC-SSC gating only.

Multiple heterogeneous editing of *Trem2* is more likely caused by hyperploidy of BV2. BV2 is a cell line infected with a v-*raf*/v-*myc* oncogene-carrying J2 retrovirus to achieve immortalisation[552]. This resulted in cancer-like proliferative properties with an indefinite and high rate of proliferation which would likely accumulate chromosomal instability in the cells[614]. These cells were established ∼27 years ago[552] and therefore likely to have accumulated chromosomal abnormalities since. Although BV2 has been widely used in the research of microglia, its genomic abnormalities and karyotype have been under-reported. Karyotyping a sample of early passage (P8) BV2 culture revealed heterogeneous aneuploidy between individual cells and importantly, there were up to 4 copies of chromosome 17 where *Trem2* is located. Most cells that were characterised had >2 copies of chromosome 17 and

this is consistent with the frequency of multiple amplicons observed after CRISPR/Cas9 editing. A recent paper described BV2 to be hypertriploid[615], similar to the observations here. Despite this, homogeneously edited clonal lines with a single edited *Trem2* amplicon were generated in the project. Considering the heterogeneity of chromosome copy numbers observed, it is possible that these cells had only one copy of chromosome 17 and hence only had one CRISPR/Cas9-mediated cut and repair event dominated by NHEJ.

In this project, it appears that CRISPR/Cas9-mediated genome editing to introduce *Trem2* gene variants by HDR was not successful. Even after 4 different experimental designs with iterative improvements, BV2 clones with the p.R47H, p.Q33X or p.D87N variants were not observed. After CRISPR v1 and v2, the p.R47H loci within *Trem2* was thought to be inefficient at inducing HDR. Thus, *Trem2* p.Q33X and p.D87N variants, in addition to p.R47H, were targeted in CRISPR v3 but this was still unsuccessful with multiple amplicons in each clone observed from agarose gels and Sanger sequencing. Some amplicons were similar in size to the WT amplicons which may be successful HDR event occurring in at least one copy of *Trem2*. Nonetheless, distinguishing the overlapping DNA sequences in sequencing chromatograms at the p.R47H (c.140G>A) loci to identify if any of the clonal lines had at least one allele with the variant was difficult. It would be possible to isolate the individual amplicons by cloning them into plasmids and sequencing. However, this would be extremely time consuming, especially when the expected frequency of HDR is extremely low. It also would not resolve the problem of having a mixed genotype in the clonal line where only some of the copies were edited with the desired variant.

Successful genome editing by CRISPR/Cas9 and HDR in immortalised cell lines have been reported, although all of them have been screened at a population level and not in clonal lines[547,548,605,616–619]. For example, HEK293 cells were frequently used as a control when editing iPSC, but were only genotyped on the population level through next generation sequencing or base mismatch endonucleases which does not account for the number of gene copies present in individual cells. HEK293 cells are known to be tetraploid[553] and if these cells were to be single-cell sorted for clonal isolation and genotyped, it is likely that multiple NHEJ-mediated indels arising from multiple edited events at a given target would be detected and homozygous HDR events in individual clones would be difficult to identify.

DNA repair by NHEJ or HDR is largely dependent on the phase of the cell cycle. NHEJ is

dominant through a large portion of the cell cycle especially in the G1, S, and G2 phases whereas HDR is limited to the late S and G2 phases after DNA replication and at the point where sister chromatids are available for use as repair templates[620]. The HDR mechanism at this point prevent telomere fusion in the M and G1 phases[621]. Because HDR is restricted to a small window and is also in competition with the dominant NHEJ in the S and G2 phases[622], it is not surprising that the rate of HDR is so low. There have been attempts to skew DNA repair occurring in the S and G2 phases from NHEJ towards HDR by suppression of NHEJ pathways using inhibitors or gene expression knockdown[623]. However, inhibition of any DNA repair mechanisms could contribute to further genomic instability and chromosomal abnormalities especially in cells already having unstable genomes due to their immortalisation.

Cell cycle synchronisation is another method that has been employed to maximise HDR efficiency for genome editing[548]. When inhibitors to different phases of the cell cycle were tested, it was surprising that nocodazole which inhibits the cell cycle at the late G2/M phase achieved the highest rate of HDR, up to 31% HDR efficiency which is higher than that achieved with inhibitors targeting the late G1/S phase when HDR begins[548]. In that publication, the authors attributed the high rate of HDR to the action of Cas9 on two sets of chromosomes in each cell during the M phase when DNA is replicated. However, in CRISPR v4 of this project, homogeneous HDR events were not detected in any clones treated with nocodazole regardless of concentration, likely due to poor transfection efficiency. The rate of HDR was measured at a population level may not directly translate to successful single cell targeting. Nonetheless, the possibility that HDR occurred at an appreciable rate cannot be ruled out because neither genotyping or sequencing could resolve where this may have happened on a subset of targets.

Future CRISPR/Cas9 designs include the addition of selectable markers on the HDR template to improve clonal cell selection. Ideally, a positive selectable marker (fluorescent protein gene) should be used instead of a negative selectable marker (antibiotic resistance gene) to avoid inducing cell death and the generation of cell debris that can activate BV2. A population of cells with successful HDR can then be enriched by FACS and clonal cell lines with the desired genotype can be established from this population. However, the selectable marker gene would need to be removed from the target gene after screening and

clone selection as it could lead to disruption of the open reading frame or dysfunctional protein folding due to the additional amino acids. The removal can be performed using the *piggyBac* system, which results in scarless excision of the selectable marker[624].

For this, the HDR template should be designed with the selectable marker gene flanked by the *piggyBac* inverted terminal repeats which will be recognised by the transposase on incorporation into gDNA alongside the intended knock-in variant. Cells with successful HDR can be enriched by FACS and followed by removal of the fluorescent protein gene using the excision-only *piggyBac* transposase. Successful excision can be gated from loss-of-fluorescence and followed by clonal isolation using single-cell FACS. While this method does not improve the rate of HDR, it greatly reduces the amount of clones to screen as it enriches for cells with successful HDR and homogeneous editing events will be more likely to be detected. Alternatively, as NHEJ-mediated indels were so prevalent, it may be possible to screen for a clonal line with at least one copy of *Trem2* with the desired variant and have the remainder copies knocked out. This would result in the functional expression of only the TREM2 variant protein and not a heterogeneous expression of WT and variant proteins. Caveats to this method is that the fluorescent protein gene would need to be incorporated directly after an endogeneous `TTAA` sequence for scarless excision of the fluorescent protein gene, which may not be present close to the targeted DNA sequences.

Moreover, instead of using immortalised rodent cell lines, microglia-like cells from human iPSCs could be established with published protocols available now[568–570]. iPSCs could be obtained from patients with a TREM2 variant to be used as the disease cell model. Isogenic control cell lines could be generated using CRISPR/Cas9-mediated genome editing to edit the variant into the WT sequence. An advantage to genome editing patient-derived iPSC is that the DNA variant provides specificity for sgRNA targeting. If the variant is heterozygous, CRISPR/Cas9 can be designed to only specifically target the variant allele and modifying it to become WT while avoiding any unwanted editing in the other WT allele. If patients with a TREM2 variant cannot be found, iPSCs from control patients could still be used. Again, genome editing can be used to introduce the variants into iPSCs similar to immortalised cell lines. A benefit to using iPSCs over immortalised cell lines is that iPSCs would be ensured to not have chromosomal abnormalities unlike immortalised

cell lines. With only two copies of *Trem2* to target and edit, it is far more likely to detect successful homogeneous HDR editing. Regardless of iPSC approach, the CRISPR/Cas9 workflow would be the same as established in this project and the suggestions made to improve screening can be implemented. Successful editing of iPSCs using CRISPR/Cas9 by others has been demonstrated[547]. Therefore, this is a promising approach to obtain a cell model that is more disease relevant as these microglia-like cells are of human origin and have a transcriptome profile and functional physiology that are highly similar to human adult microglia[568–570].

To conclude, achieving homogeneous CRISPR/Cas9-mediated genome editing of immortalised cell lines with hyperploidy and multiple copies of the target gene is challenging. Clones with homogeneous NHEJ-mediated events resulting in insertions or deletions that are predicted to result in functional loss of TREM2 were generated. On the other hand, clones with HDR-mediated knock-in of DNA variants could not be detected. This is likely due to the very low rate of HDR in combination with multiple copies of *Trem2* in each cell. Thus, obtaining clones with specific disease-associated variants was not achieved. Nevertheless, a TREM2-deficient model has a number of valuable applications such as to investigate the mechanism and signalling pathways of TREM2 function or the effects of TREM2 dysfunction in response to various ligand binding on specific phenotypic responses of microglia.

Chapter 4

Effect of Alzheimer's disease-associated TREM2 variants on microglia in post-mortem human brain hippocampal sections

4.1 Introduction

Various *in vitro* studies have implicated the loss of TREM2 function with dysfunctional phagocytosis, chemotaxis, cell survival and proliferation[383]. These are key innate immune responses mediated by microglia against disease pathology. TREM2 function also appears to modulate inflammatory responses mediated by the activation of immune receptors such as TLRs[381,394,428,495,497,501]. Consequently, TREM2 activation can skew microglia function towards anti-inflammatory responses associated with debris clearance by phagocytosis and tissue repair[384,394,412].

In vivo studies using TREM2-deficient AD mouse models reported mixed findings with amyloid and tau pathology burden depending on the AD mouse model used (Chapter 1.6.5.4 and 1.6.5.6). For example, cortical insoluble $A\beta_{1–42}$ and $A\beta_{1–40}$ load is increased in 8 m old TREM2-deficient APP/PS1 mice[468] but not in 8.5 m old TREM2-deficient 5XFAD mice[438] compared to TREM2-expressing control mice. On the other hand, hyperphosphorylated tau is decreased in 4 m old TREM2-deficient APP/PS1 mice[239] but is increased in TREM2-deficient 5XFAD mice of unreported age[241] compared to TREM2-expressing control mice. Despite differences in pathology burden that is likely due to age-dependent effects and AD mouse models, these implicate the role of dysfunctional TREM2 in microglia and how these cells may modulate the severity of pathology leading to the onset and progression of AD.

Nevertheless, TREM2 deficiency consistently decrease the density of plaque-associated microglia[239,241,438,468,470,472] and it has been shown that these microglia may be involved in limiting the neurotoxic effects of oligomeric and protofibrillar Aβ species in the periphery of amyloid plaques[470,474] (Chapter 1.6.5.3). Put together, these suggest that the role of microglia is vital in the pathogenesis of AD and its function is compromised by dysfunctional TREM2.

The various disease-associated variants appear to affect TREM2 function differently (Chapter 1.6.4). Variants such as p.R47H, p.R62H, p.D87N and p.T96K located on the exposed extracellular region of the protein affect ligand binding[106,108,378]. Besides that, variants like p.Y38C and p.T66M are located within the Ig-fold and disrupt normal protein folding of TREM2. This causes TREM2 to accumulate in the endoplasmic reticulum and increase its

degradation, which prevents its trafficking to the cell surface[378,379,432,452,453]. Additionally, some variants including the p.R47H appear to impair protein maturation by affecting post-translational modifications such as glycosylation[379,382,452] and degradation[435].

Despite the increasing number of experimental *in vitro* and *in vivo* studies on the role of TREM2 in disease, these findings need to reflect the disease in people. Studies involving people with a TREM2 variant have been very limited because of the rarity of the variants. Even the most common and established AD-associated p.R47H variant has a MAF of 0.0012–0.0063 in healthy populations[110] and 0.009–0.02 in populations with AD[109]. This means that very large AD cohorts need to be screened to identify sufficient number of cases for analysis.

A cohort consisting of 16 post-mortem cases with disease-associated TREM2 variants (9 p.R47H, 7 other variants) has been identified and requested from various UK and European brain banks by Dr Angela Hodges. These cases were identified from AD donors to the brain banks by sequencing *TREM2* Exon 2 and screened for the disease-associated TREM2 variants. In this study, the effects of disease-associated TREM2 variants on microglial dysfunction in post-mortem AD brain tissue was investigated by labelling microglia with various functional microglia-specific markers.

Traditionally, markers specific to microglial function were used to identify microglia in tissue. These markers include CD68, human leucocyte antigens (HLAs) and ionised calcium-binding adaptor molecule 1 (Iba-1). CD68 is a lysosome-associated protein and is used as a marker of phagocytosis[625,626], which is a key function of microglia to clear pathology and tissue debris. HLA genes are clustered on chromosome 6 and the cluster can be divided into 3 regions: class I, II and III. HLA class I genes consist of *HLA-A*, *HLA-B* and *HLA-C* whereas class II genes include the *HLA-DPA1*, *HLA-DPB1*, *HLA-DQA1*, *HLA-DQB1*, *HLA-DRA* and *HLA-DRB1*. On the other hand, HLA class III genes encode for several components of the complement system[627]. The HLA class II genes encode for combinations of the α- and β-subunits of the MHC class II molecule. HLA class II, especially HLA-DP, -DQ and -DR, are associated with antigen presentation[628]. Antibodies against HLA-DP, -DQ or -DR have been commonly used to label "activated" microglia[629–631], although the activation states have been poorly defined. In fact, microglia with ramified morphology, associated with a "resting" or surveillance state, were also shown to constitutively express

HLA-DR[632]. On the other hand, Iba-1 is associated as a pan-macrophage marker[633] and in normal brains include all microglia. Iba-1 is an actin-binding[634] and calcium-binding[635] protein involved in membrane ruffling and formation of phagocytic cups, which are early processes of phagocytosis[636].

Microglial activation in its most basic form is recognised as microgliosis, described by the proliferation of the local microglial population to increase cell numbers[637,638]. Activated microglia also tend to transform from a ramified into an amoeboid morphology[639,640]. These two measures can be quantified from labelled microglia in post-mortem tissue to determine their overall activation state.

Besides investigating the effects of disease-associated TREM2 variants on microglia, this study presents the opportunity to identify functional microglial markers of TREM2 dysfunction in human AD. These markers can then be used as outcome measures during characterisation of the *in vitro* TREM2 model generated in Chapter 3 to establish if its phenotype reflects TREM2 dysfunction in human AD.

4.2 Aims

- To investigate the effects of disease-associated TREM2 variants on microglia using different functional activation markers in post-mortem human brains of AD cases with and without disease-associated TREM2 variants.
- To establish microglial markers from dysfunction conveyed by disease-associated TREM2 variants in people, which can be used to characterise and compare the generated *in vitro* TREM2 model to the human disease.

4.3 Methodology overview

Detailed methods are outlined in Chapter 2.3.

AD cases with a disease-associated TREM2 variant (AD/TREM2^{var}) were identified prior to this project (A. Hodges) (Table 2.21). They were pair-matched for age at death and gender with a non-AD control (Control/TREM2^{wt}) and AD cases without a disease-associated TREM2 variant (AD/TREM2^{wt}). Cases without hippocampal tissue sections, AD cases that were not Braak tau stage IV–VI, or non-diseased controls that were not Braak tau stage 0–I were excluded from analyses.

To investigate the effects of TREM2 variants on microglia, immunohistochemistry was performed using antibodies against frequently used microglia-specific functional markers: CD68 and HLA-DP, -DQ, -DR (henceforth called HLA) as well as the pan-microglial marker Iba-1. Microglial abundance and morphology were used as measures of activation which are commonly observed changes in microgliosis. To make the groups comparable with respect to the degree of pathology, AD cases with similar Braak tau staging were selected. Additionally, sections were immunostained for amyloid and tau pathology. For high-throughput analyses, immunostained sections were imaged using a microscope slide scanner and quantification performed using a semi-automated computerised pipeline. CD68-immunostained microglia were quantified by % area staining whereas HLA- and Iba-1–immunostained microglia were quantified by cell counts.

To identify if microglia immunolabelled by CD68, HLA or Iba-1 represent similar microglial subpopulations or not, double staining immunofluorescence was performed using combinations of antibodies against these markers (Table 2.23). Additionally, to observe any dysfunction of microglial association to amyloid or tau pathology, double staining immunofluorescence was also performed on a small subset of cases using combinations of antibodies against the microglial markers with antibodies against amyloid and tau pathology (Table 2.23). Representative images of fluorescently-labelled sections were imaged on a fluorescence microscope.

4.4 Results

4.4.1 Demographics

The cases for each group in the cohort for this study were selected to match age at death, gender and Braak tau stage (IV–VI) as best as possible. Age at death was not significantly different between the 3 groups (ANOVA: F=0.731, p=0.487; Table 4.1). Gender was also comparable across the 3 groups (binomial logistic regression: χ^2=1.117, p=0.572; Table 4.1), although there was a slightly higher female:male (10:6) ratio in the AD/TREM2^{var} group. The AD/TREM2^{var} group contained cases with several different disease-associated TREM2 variants, with the p.R47H variant being the most frequent (9 cases) (Table 4.2).

Experimental group	**Median age**	**IQR**	**Gender**		**Total**
Control/TREM2^{wt}	73	66.25–78.00	Female	8	18
			Male	10	
AD/TREM2^{wt}	75	68.00–80.00	Female	11	21
			Male	10	
AD/TREM2^{var}	72	68.25–76.00	Female	10	16
			Male	6	

Table 4.1. Demographics of the research cohort used in this study.
Age at death and gender were balanced between the experimental groups.
IQR: interquartile range, Control/TREM2^{wt}: non-AD control cases without disease-associated TREM2 variants, AD/TREM2^{wt}: AD cases without disease-associated TREM2 variants, AD/TREM2^{var}: AD cases with disease-associated TREM2 variants.

Disease-associated TREM2 variants (SNP ID)	**No. of cases**
p.R47H (rs75932628)	9
p.Q33X (rs104894002)	1
p.D39E (rs200392967)	1
p.G58A (novel)	1
p.D87N (rs142232675)	2
p.R98W (rs147564421)	1
p.T96K, p.W191X, p.L211P (rs2234253, rs2234258, rs2234256)	1

Table 4.2. List of disease-associated TREM2 variants in AD/TREM2^{var}.
p.R47H was the most frequent variant. One case contained 3 variants in TREM2 which are in linkage disequilibrium.

4.4.2 Comparison between manual and semi-automated cell counting methods

While manual counting is commonly used to quantify cell abundance or density in immunostained tissue, it is laborious. Therefore, to perform high-throughput quantification of immunostained cells in a ROI, a semi-automated analysis pipeline utilising a combination of Python scripts and ImageJ macros compatible for use on scanned slide images was developed. Results were compared to manual cell counts from micrographs of the same sections and ROI performed by an experienced neuropathologist (Dr Andrew King) on HLA-immunostained images from randomly selected cases from each group in the cohort. As HLA and Iba-1 have similar staining patterns, the comparison between semi-automated quantification and manual counting was only performed on HLA-immunostained images. There was a strong correlation between the number of HLA^+ microglia counted manually and those counted by the semi-automated method (Pearson correlation: $R=0.849$, $p<0.001$, $n=110$; Figure 4.1a).

Cell counts were used to quantify HLA^+ or Iba-1^+ microglial abundance instead of the commonly used % area staining because cell counts better reflect microglial cell density. Microglia have highly dynamic morphology depending on activation states. Surveillance/resting microglia have a ramified morphology with small cell body whereas activated microglia have an amoeboid morphology and larger cell body due to retraction of microglial processes. Nevertheless, to check that cell counts were not significantly different from the commonly used % area staining and still represented cell density, semi-automated cell counts were compared to the % area staining method using HLA- and Iba-1-immunostained images. Cell counts strongly correlated with % area staining for both HLA- (Pearson correlation: $R=0.856$, $p<0.001$, $n=585$; Figure 4.1b) and Iba-1-immunostained (Pearson correlation: $R=0.941$, $p<0.001$, $n=330$; Figure 4.1c) images. These strong correlations show that these high-throughput quantification methods are comparable to commonly used methods.

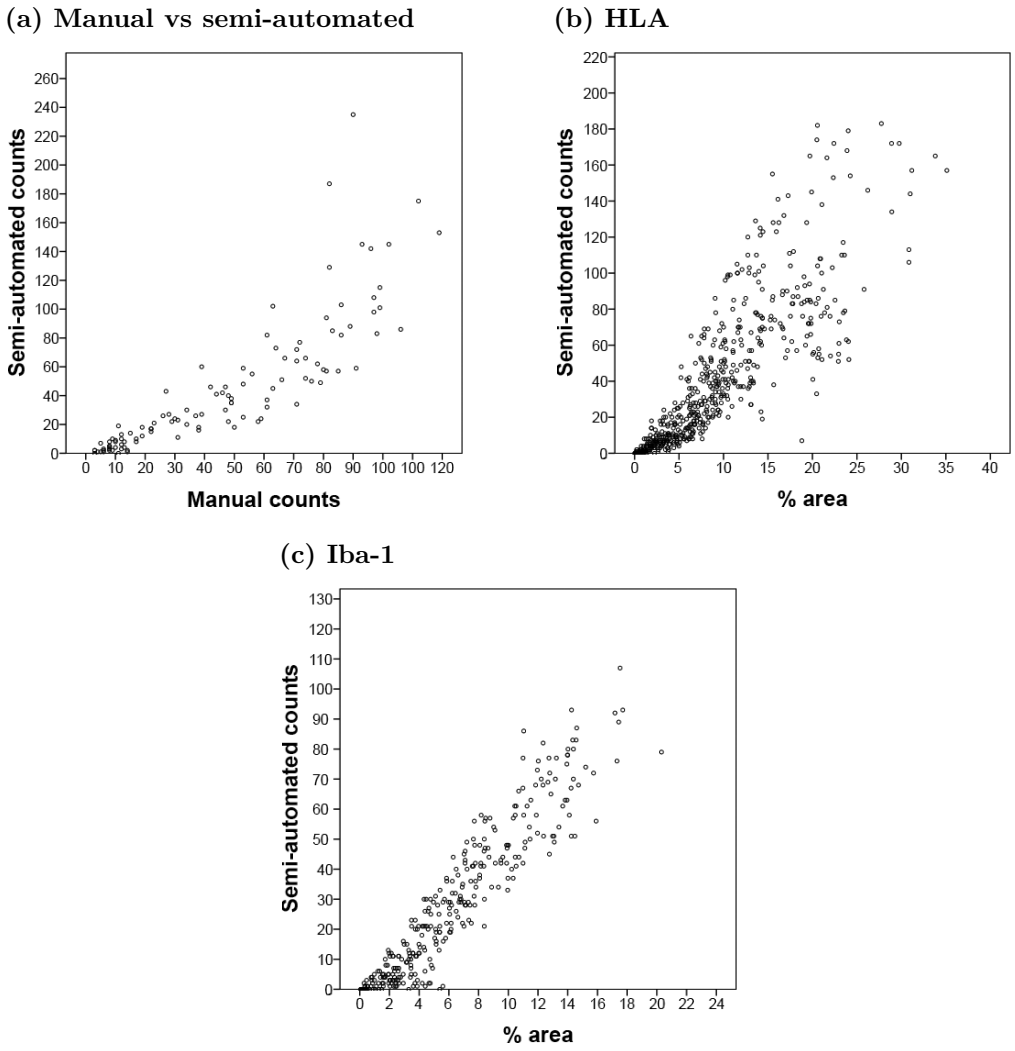

Figure 4.1. Semi-automated quantification of cell density strongly correlated with commonly used standard quantification methods in the same tissue sections.

Scatter plots showing strong correlation between **(a)** manual and semi-automated HLA$^+$ cell counts (R=0.849, p<0.001, n=110 total images across a sample of cases), **(b)** HLA % area stained and HLA$^+$ cell counts (R=0.856, p<0.001, n=585 total images across a sample of cases), **(c)** Iba-1 % area stained and Iba-1$^+$ cell counts (R=0.941, p<0.001, n=330 total images across a sample of cases).

4.4.3 AD cases with disease-associated TREM2 variants have fewer functionally activated microglia

To investigate the effects of the disease-associated TREM2 variants on the overall microglia population in the hippocampal CA1 and CA4, the abundance of cells expressing the pan-microglia marker Iba-1 were assessed. Iba-1^+ microglia abundance was not statistically different in the CA1 and CA4 between Control/$TREM2^{wt}$, AD/$TREM2^{wt}$ and AD/$TREM2^{var}$ groups. However, there was a small trend towards fewer Iba-1^+ microglia in AD/$TREM2^{var}$ cases compared to AD/$TREM2^{wt}$ in both the CA1 and CA4 (Figure 4.2).

Microglia can perform various immune-related functions when activated. Therefore, the effects of disease-associated TREM2 variants on the number of cells expressing these functional markers were investigated. Microglia have been associated with the ability to clear neuronal debris and AD pathology such as Aβ through phagocytosis. Phagocytic microglia were stained for CD68, a lysosome-associated protein marker. CD68 immunostaining resulted in a punctate pattern frequently near small and intense haematoxylin staining, which represent glial cell nuclei. There was significantly lower CD68 staining in the CA4 of AD/$TREM2^{var}$ cases compared to AD/$TREM2^{wt}$ (pairwise comparison ANCOVA: p=0.030) and Control/$TREM2^{wt}$ (pairwise comparison ANCOVA: p=0.015) (Figure 4.3b,d). There was a trend towards lower CD68 staining in the CA1 of AD/$TREM2^{var}$ compared to AD/$TREM2^{wt}$ (Figure 4.3a,c).

Activated microglia have been commonly labelled with antibodies against HLA-DP, -DQ or -DR[629–632], which function is associated with antigen presentation[628]. When immunostained for HLA, there were trends towards fewer HLA^+ microglia in the CA1 and CA4 of AD/$TREM2^{var}$ compared to AD/$TREM2^{wt}$ (Figure 4.4). The number of HLA^+ microglia in the CA1 and CA4 were similar to or lower than that of Control/$TREM2^{wt}$ (Figure 4.4). As expected, there was increased HLA^+ microglia in AD/$TREM2^{wt}$ compared to Control/$TREM2^{wt}$, which was significant in the CA1 (pairwise comparison ANCOVA: p=0.009) and a trend in the CA4 (Figure 4.4).

(a) Iba-1 CA1 **(b) Iba-1 CA4**

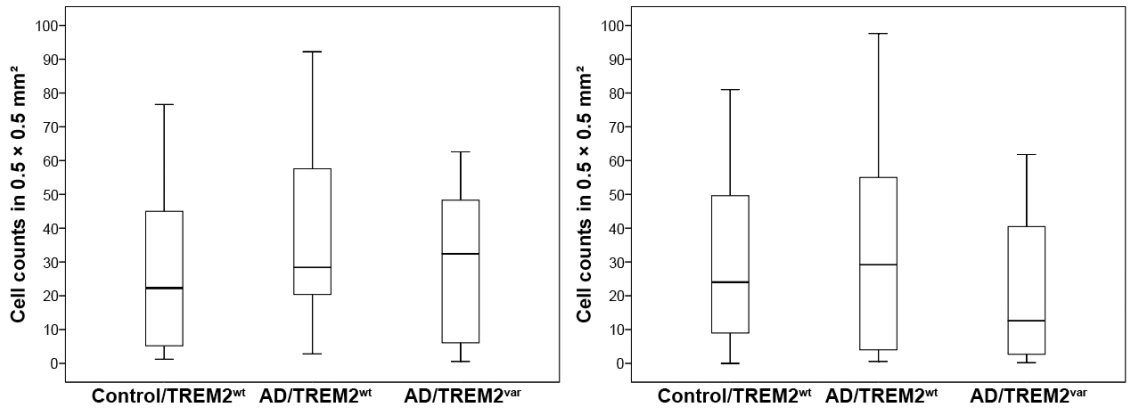

(c) Iba-1 CA1

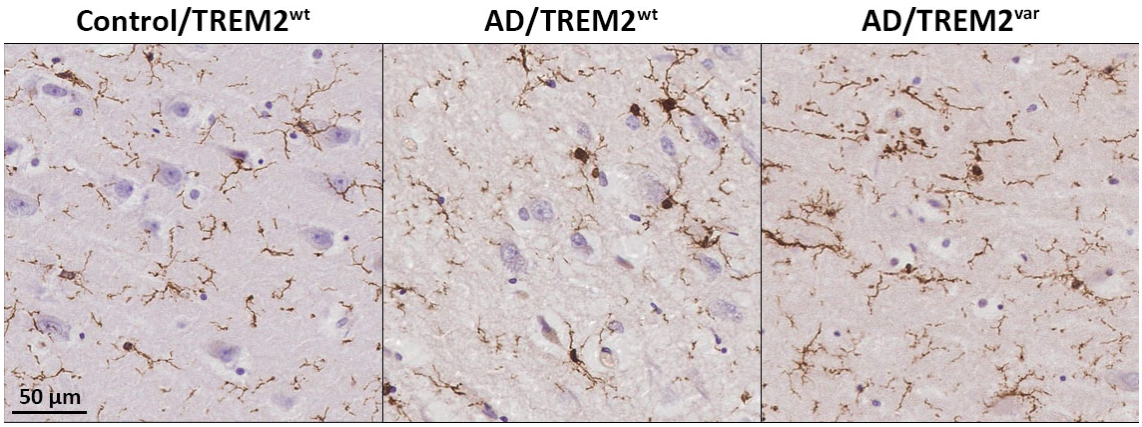

(d) Iba-1 CA4

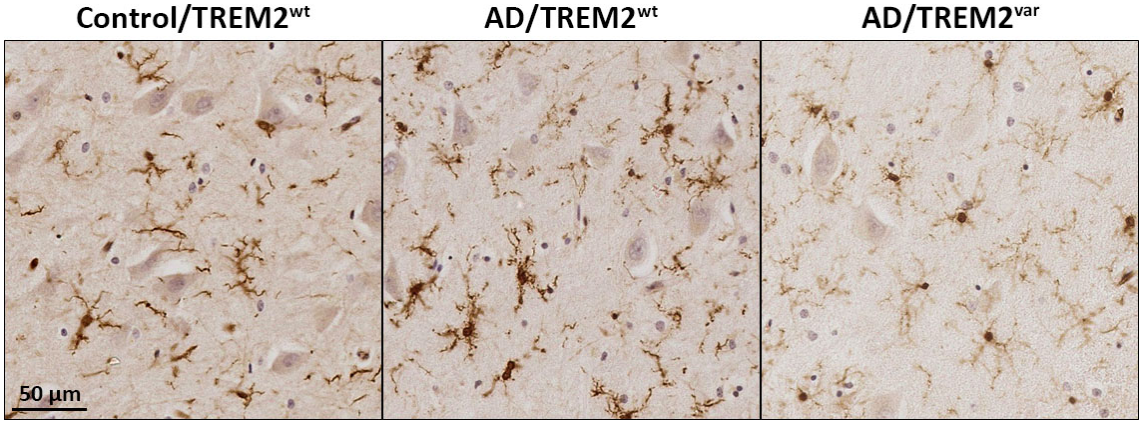

Figure 4.2. Iba-1$^+$ microglia abundance were not statistically different between the 3 experimental groups in the CA1 and CA4 but there was a small trend towards fewer Iba-1$^+$ microglia in the CA4 of AD/TREM2^{var}.
Box plots showing Iba-1$^+$ microglial abundance in the **(a)** CA1 and **(b)** CA4 of 18 Control/TREM2^{wt}, 21 AD/TREM2^{wt} and 16 AD/TREM2^{var} cases. Means and standard deviations are shown in Appendix Table A1.
Representative images from p.R47H cases illustrating Iba-1$^+$ microglial abundance in the **(c)** CA1 and **(d)** CA4 between experimental groups. Antibody binding was visualised with the dark brown DAB staining. Microscopy images are at 400× magnification.

(a) CD68 CA1 **(b) CD68 CA4**

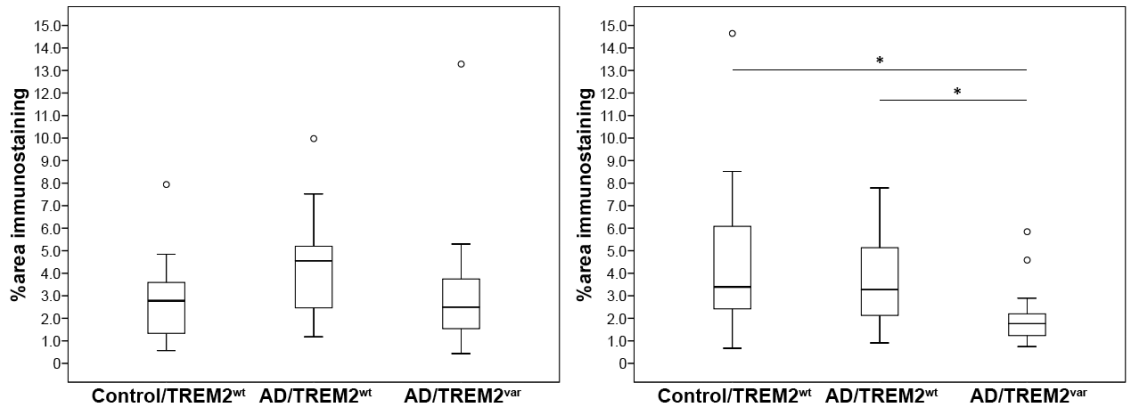

(c) CD68 CA1

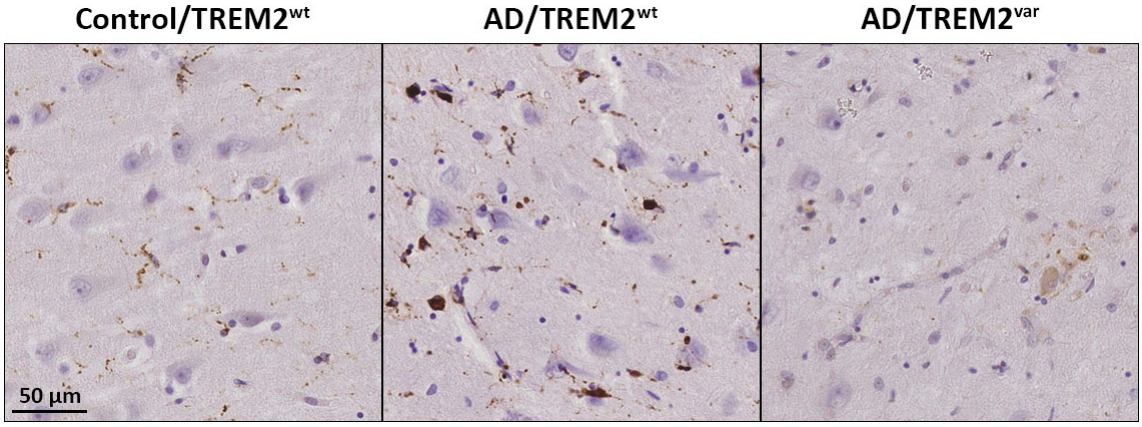

(d) CD68 CA4

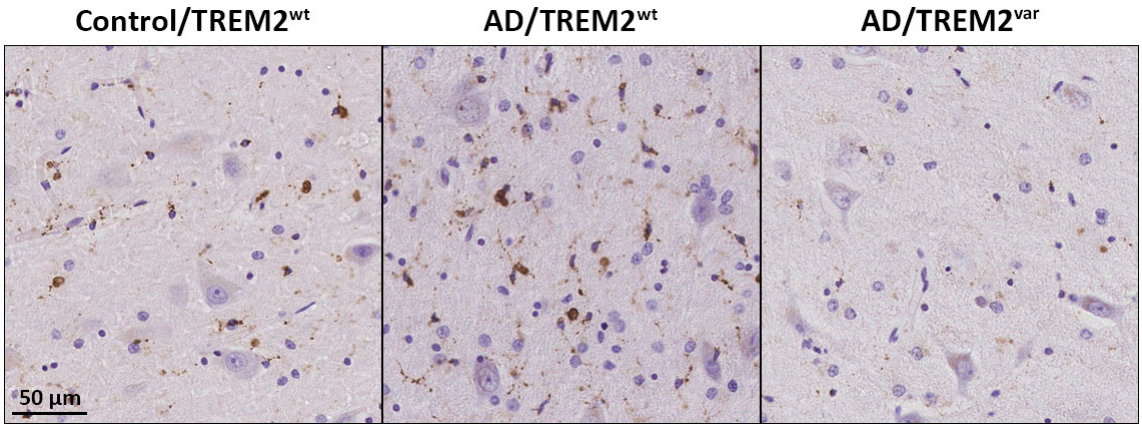

Figure 4.3. Significantly fewer CD68^{+} microglia were found in the CA4 of AD/TREM2^{var} compared to AD/TREM2^{wt} with a similar trend in the CA1. Box plots showing CD68 % area staining in the **(a)** CA1 and **(b)** CA4 of 18 Control/TREM2^{wt}, 21 AD/TREM2^{wt} and 16 AD/TREM2^{var} cases. Means and standard deviations are shown in Appendix Table A1. *: $p<0.05$
Representative images from p.R47H cases illustrating CD68 staining in the **(c)** CA1 and **(d)** CA4 between experimental groups. Antibody binding was visualised with the dark brown DAB staining. Microscopy images are at 400× magnification.

(a) HLA CA1

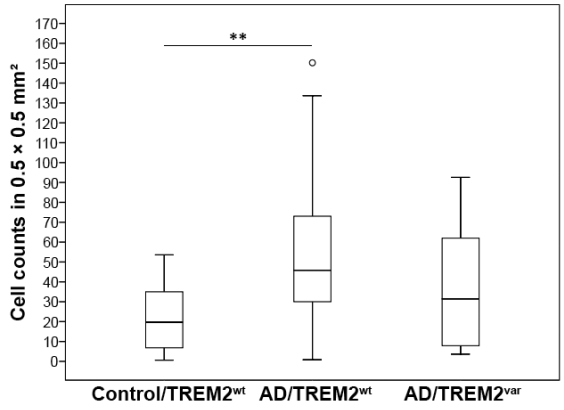

(b) HLA CA4

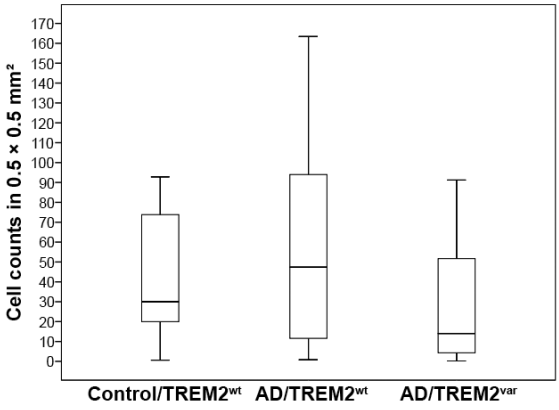

(c) HLA CA1

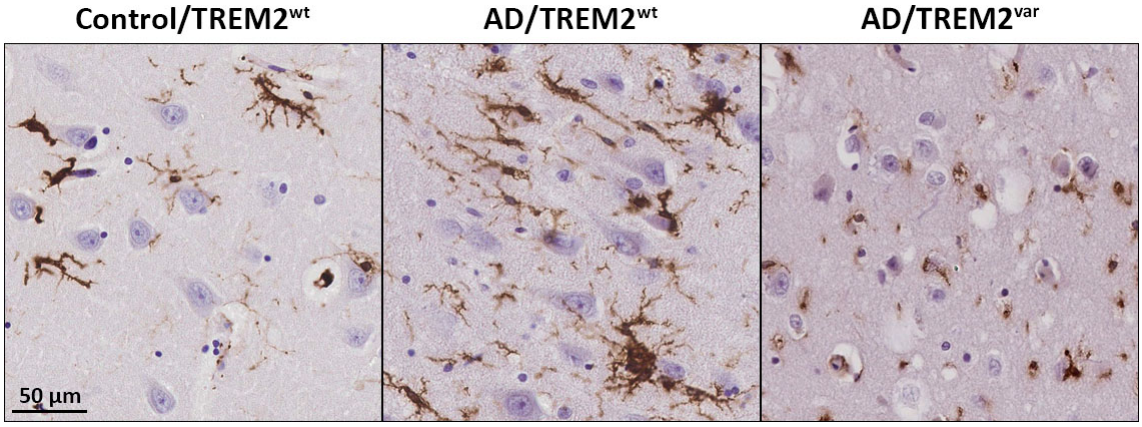

(d) HLA CA4

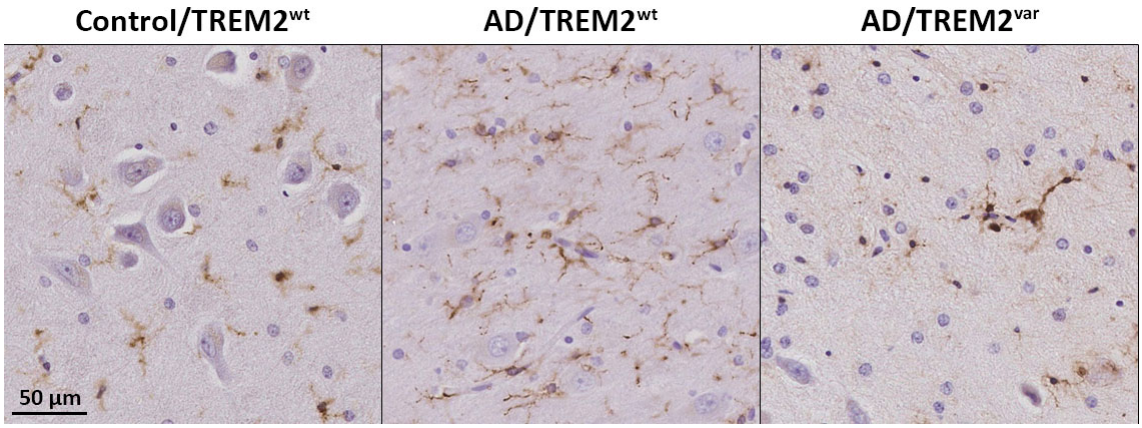

Figure 4.4. HLA$^+$ microglia abundance trended towards fewer HLA$^+$ microglia in the CA1 and CA4 of AD/TREM2^{var} compared to AD/TREM2^{wt}. Box plots showing HLA$^+$ microglial abundance in the **(a)** CA1 and **(b)** CA4 of 18 Control/TREM2^{wt}, 21 AD/TREM2^{wt} and 16 AD/TREM2^{var} cases. Means and standard deviations are shown in Appendix Table A1. **: $p<0.01$
Representative images from p.R47H cases illustrating HLA$^+$ microglial abundance in the **(c)** CA1 and **(d)** CA4 between experimental groups. Antibody binding was visualised with the dark brown DAB staining. Microscopy images are at 400× magnification.

To investigate the relationship between functional markers used to label microglia, double staining immunofluorescence was performed. Due to limitations with the species that the antibody pairs were raised in, sections could only be stained with CD68+Iba-1 and HLA+Iba-1 combinations. Many Iba-1^+ microglia were not $CD68^+$ (Figure 4.5) or HLA^+ (Figure 4.6), indicating that only a subset of cells stained with the pan-microglial Iba-1 marker were activated with a functional phenotype. Additionally, there were also $CD68^+$ and HLA^+ microglia that were not Iba-1^+ (Figure 4.5,4.6), suggesting that other cell types expressing these markers were also present. Alternatively, some of these functionally activated microglia may differentiate into a phenotype that do not express Iba-1. This may explain the different observations in the cell densities of $CD68^+$, HLA^+ and Iba-1^+ microglia between the 3 groups as they may represent different microglial subpopulations.

(a) AD/TREM2^{wt}

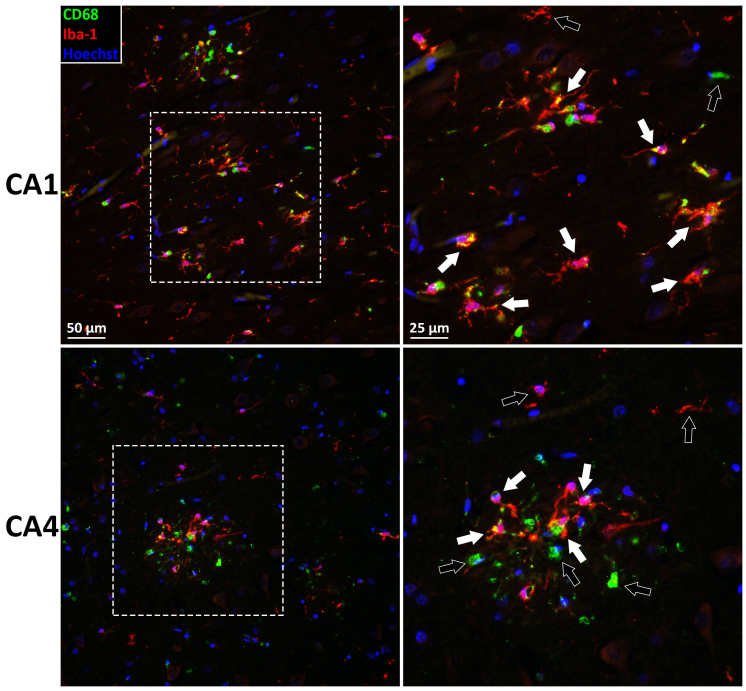

(b) AD/TREM2^{var}

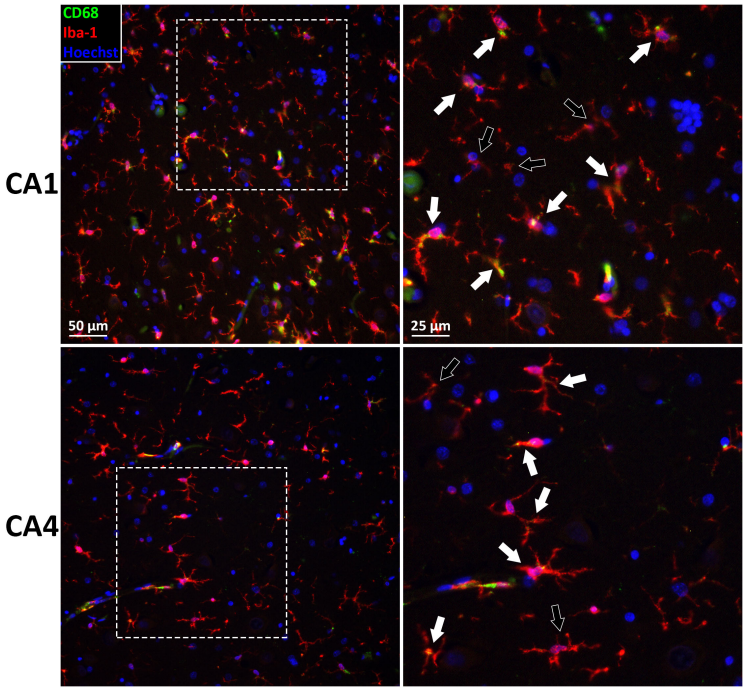

Figure 4.5. Only a subset of Iba-1$^+$ microglia were stained with CD68. Conversely, not all CD68$^+$ cells were stained with Iba-1.
Double staining immunofluorescence of CD68$^+$ (green) and Iba-1$^+$ (red) microglia subpopulations in the CA1 and CA4 of **(a)** AD/TREM2^{wt} and **(b)** AD/TREM2^{var} (p.R47H) cases.
CD68$^+$–Iba-1$^+$ microglia are indicated with filled arrows. CD68$^+$ only or Iba-1$^+$ only microglia are indicated with empty arrows. Cell nuclei were stained with Hoechst 33342 (blue). Images on the left panels were captured at 200× magnification. Right panels are images of the dotted squares at 400× magnification. Separate fluorescence channels are shown in Appendix Figure A5.

(a) AD/TREM2^{wt}

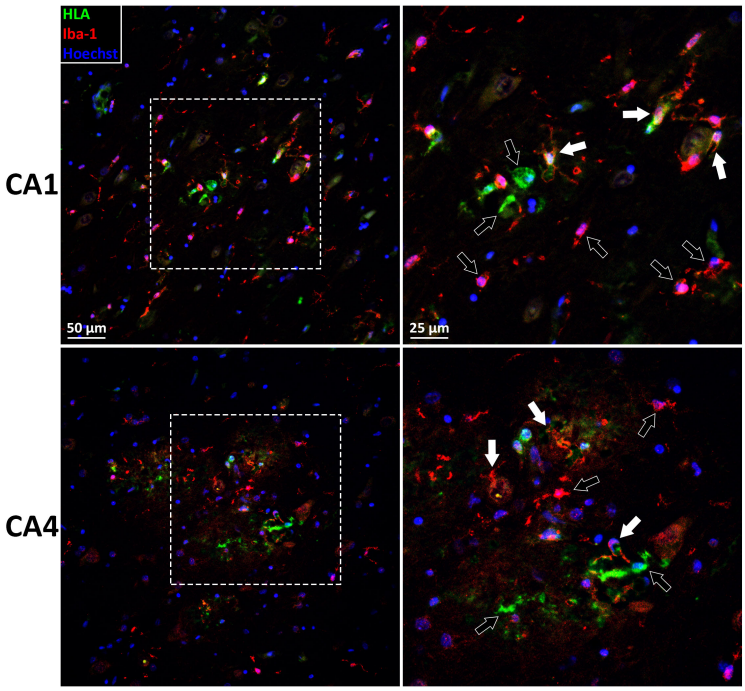

(b) AD/TREM2^{var}

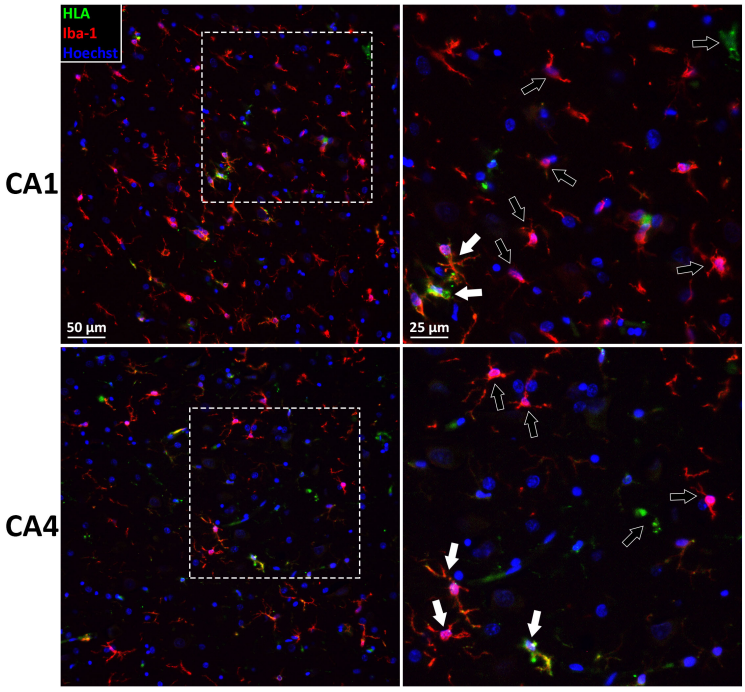

Figure 4.6. Only a subset of Iba-1$^+$ microglia were stained with HLA. Conversely, not all HLA$^+$ cells were stained with Iba-1.
Double staining immunofluorescence of HLA$^+$ (green) and Iba-1$^+$ (red) microglia subpopulations in the CA1 and CA4 of **(a)** AD/TREM2^{wt} and **(b)** AD/TREM2^{var} (p.R47H) cases.
HLA$^+$–Iba-1$^+$ microglia are indicated with filled arrows. HLA$^+$ only or Iba-1$^+$ only microglia are indicated with empty arrows. Cell nuclei were stained with Hoechst 33342 (blue). Images on the left panels were captured at 200× magnification. Right panels are images of the dotted squares at 400× magnification. Separate fluorescence channels are shown in Appendix Figure A6.

4.4.4 Microglia were morphologically activated in AD cases, including those with disease-associated TREM2 variants

To assess morphological changes in microglia that is indicative of the extent of activation[639,640], cell morphology of functionally activated HLA$^+$ microglia and pan-Iba-1$^+$ microglia was measured using circularity (cell area to perimeter ratio). Iba-1$^+$ microglia morphology was not statistically different between the 3 groups in the CA1 and CA4 (Figure 4.7a,b). However, there was a trend towards more amoeboid Iba-1$^+$ microglia in AD/TREM2^{var} cases compared to AD/TREM2^{wt} and Control/TREM2^{wt} in both hippocampal regions (Figure 4.7a,b).

Cell morphology between AD/TREM2^{wt} and AD/TREM2^{var} groups in the CA1 and CA4 were not statistically different (Figure 4.7c,d). As expected, HLA$^+$ activated microglia were significantly more amoeboid in AD/TREM2^{wt} (pairwise comparison ANCOVA in CA1: p=0.014, CA4: p=0.004) and AD/TREM2^{var} (pairwise comparison ANCOVA in CA1: p=0.011, CA4: p=0.005) compared to Control/TREM2^{wt} (Figure 4.7c,d).

As HLA and Iba-1 staining appear to label slightly different microglia, the differences in HLA$^+$ and Iba-1$^+$ cell morphology further support that they may be different microglial subpopulations. For this, only HLA$^+$ and Iba-1$^+$ microglia could be assessed as CD68 have a punctate staining pattern which does not delineate cell morphology.

(a) Iba-1 CA1 **(b) Iba-1 CA4**

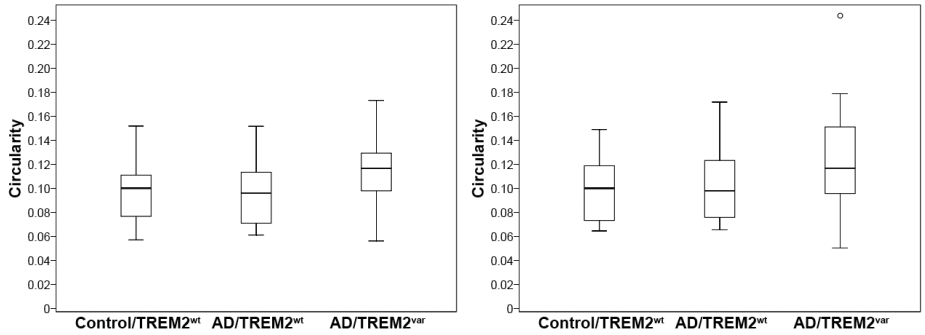

(c) HLA CA1 **(d) HLA CA4**

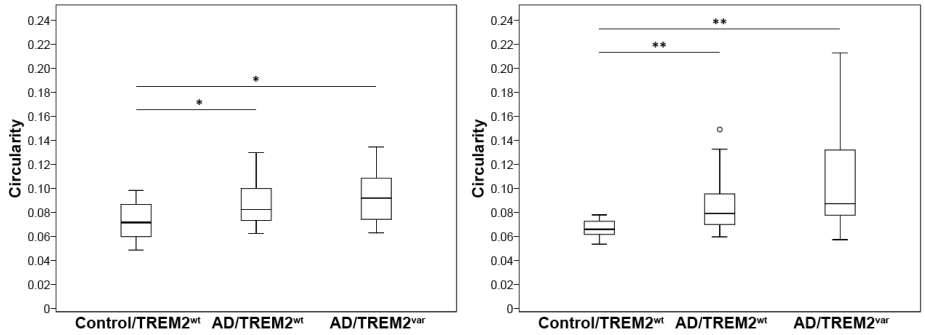

Figure 4.7. HLA$^+$ microglia, but not Iba-1$^+$ microglia, were more amoeboid in AD cases than non-AD control cases, but there was no significant difference in cell morphology in those with a TREM2 variant.

Box plots showing average circularity of **(a,b)** Iba-1$^+$ and **(c,d)** HLA$^+$ microglia in 0.5×0.5 mm^2 areas of the **(a,c)** CA1 and **(b,d)** CA4 of 18 Control/TREM2^{wt}, 21 AD/TREM2^{wt} and 16 AD/TREM2^{var} cases. Means and standard deviations are shown in Appendix Table A2.

*: $p<0.05$, **: $p<0.01$.

4.4.5 AD pathology does not appear to be affected by the presence of disease-associated TREM2 variants

AD cases with comparable pathology (Braak tau stage IV–VI) were selected for comparison. Additionally, the abundance of amyloid and hyperphosphorylated tau pathology was measured in adjacent tissue sections of the CA1 and CA4 between AD/TREM2^{wt} and AD/TREM2^{var} cases. Thus as expected, amyloid and tau pathology were not statistically different in the CA1 and CA4 between the two groups (Figure 4.8), although there was a trend towards lower tau burden in the CA4 of AD/TREM2^{var} compared to AD/TREM2^{wt} cases.

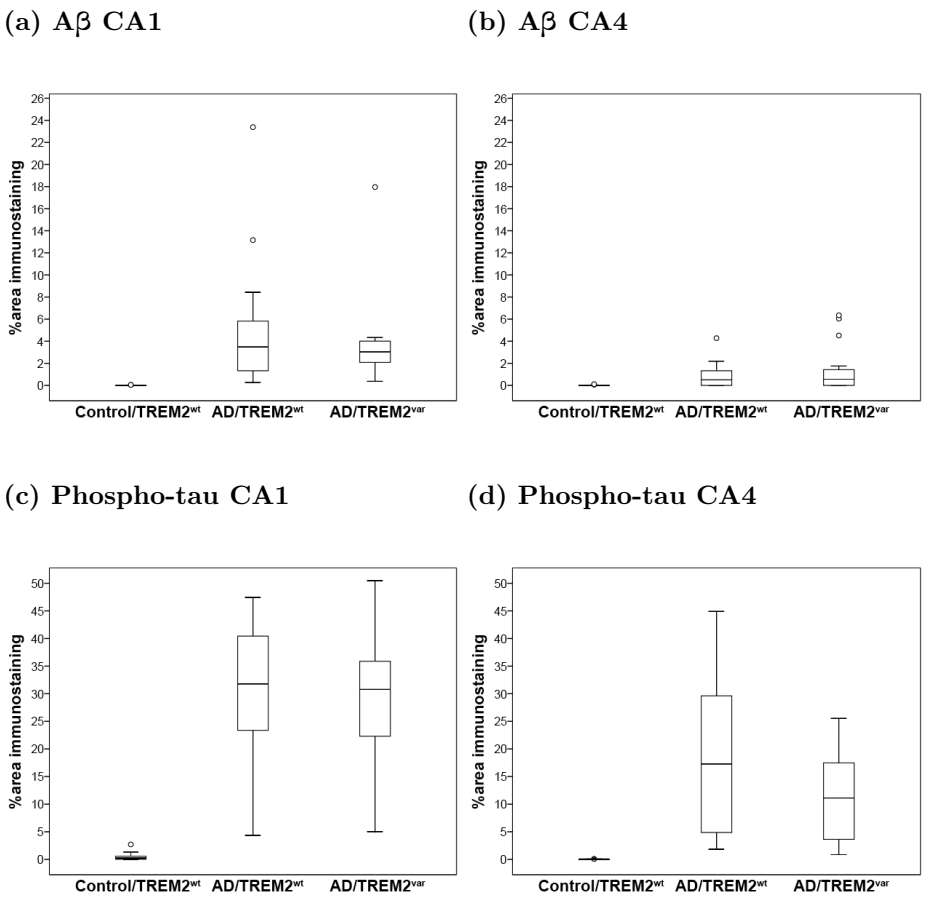

Figure 4.8. The degree of amyloid and tau pathology in the CA1 and CA4 were not affected by the disease-associated TREM2 variants.
Box plots showing AD pathology of **(a,b)** Aβ (4G8) and **(c,d)** phospho-tau (AT8) in 0.5×0.5 mm^2 areas of the **(a,c)** CA1 and **(b,d)** CA4 of 18 Control/TREM2^{wt}, 21 AD/TREM2^{wt} and 16 AD/TREM2^{var} cases. Means and standard deviations are shown in Appendix Table A3.

The abundance of microglia stained with CD68, HLA or Iba-1 was not significantly correlated with amyloid or tau burden in the AD group as a whole (Table 4.3). As TREM2 variants may influence AD pathology, this was tested for the AD/TREM2^{wt} and AD/TREM2^{var} groups separately. There was no significant correlation between microglial abundance and AD pathology, except in AD/TREM2^{wt} cases in the CA1 where there was a significant negative correlation between the number of Iba-1^{+} microglia and the degree of tau pathology (Pearson correlation: R=-0.570, p=0.007) (Table 4.3). Overall, this suggests that the number of functionally activated microglia or total microglia was not influenced by AD pathology in the hippocampus.

Correlations	**Region**	**Combined AD**		**AD/TREM2^{wt}**		**AD/TREM2^{var}**	
		R	**p**	**R**	**p**	**R**	**p**
CD68 vs tau	CA1	0.096	0.571	0.355	0.114	-0.196	0.468
	CA4	0.289	0.087	0.315	0.165	-0.311	0.260
HLA vs tau	CA1	0.169	0.324	0.235	0.305	-0.074	0.793
	CA4	0.116	0.500	0.004	0.987	0.124	0.660
Iba-1 vs tau	CA1	-0.292	0.080	-0.570	*0.007	0.016	0.954
	CA4	-0.152	0.368	-0.276	0.226	-0.124	0.648
CD68 vs Aβ	CA1	-0.029	0.863	-0.060	0.795	-0.044	0.871
	CA4	0.062	0.719	0.400	0.072	-0.226	0.418
HLA vs Aβ	CA1	0.029	0.868	0.147	0.524	-0.340	0.214
	CA4	-0.154	0.370	-0.354	0.116	0.125	0.657
Iba-1 vs Aβ	CA1	0.178	0.291	0.395	0.076	-0.311	0.260
	CA4	-0.195	0.248	-0.347	0.123	-0.027	0.922

Table 4.3. Overall microglial abundance was not affected by the degree of AD pathology in the CA1 or CA4.
Pearson correlations between microglial abundance and AD pathology burden in the CA1 and CA4 of all AD cases or separated by the presence/absence of disease-associated TREM2 variants. The only significant correlation found was between Iba-1^{+} microglia abundance and tau pathology burden in the CA1 of AD/TREM2^{wt} cases.

To visualise the the interaction between microglia and AD pathology, double staining immunofluorescence was performed. Although microglial abundance and AD pathology burden were not statistically correlated, $CD68^+$ and HLA^+ microglia were more frequently seen to cluster around amyloid plaques in the CA1 and CA4 of AD/$TREM2^{wt}$ and AD/$TREM2^{var}$ cases (Figure 4.9a,4.10a). Some Iba-1^+ microglia were also found adjacent to amyloid plaques but at a lower extent compared to $CD68^+$ and HLA^+ microglia (Figure 4.11a). Microglia co-localisation with tau pathology was less obvious. Microglia tended to only cluster around regions of intense hyperphosphorylated tau staining, which are suspected to be neuritic plaques where hyperphosphorylated tau within dystrophic neurites co-localised with amyloid plaques[641] (Figure 4.9b,4.10b,4.11b).

(a) CD68/Aβ

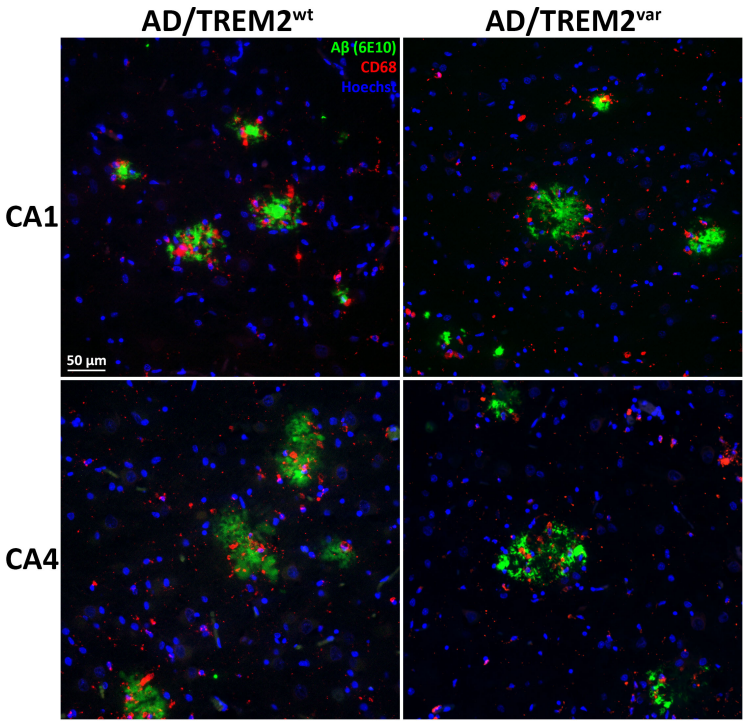

(b) CD68/tau

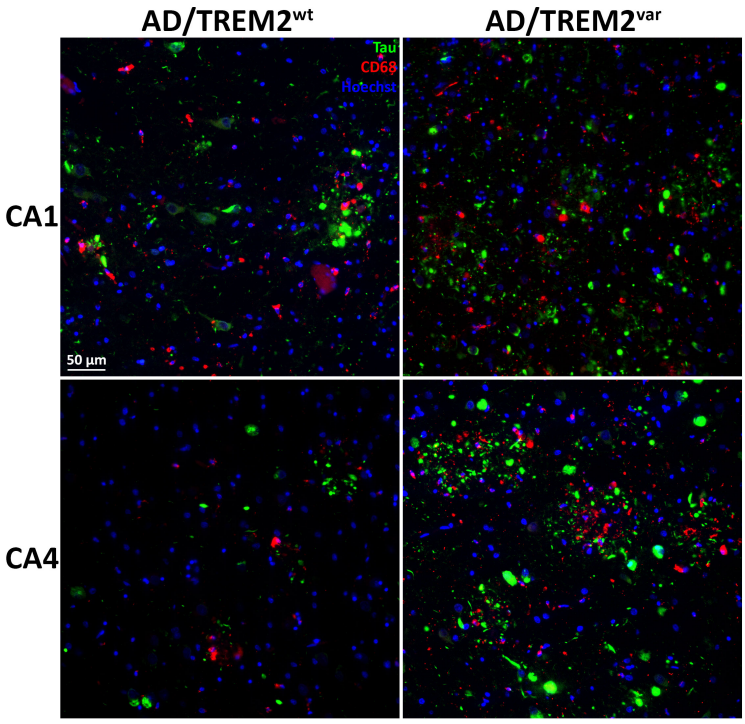

Figure 4.9. CD68$^+$ microglia were clustered around amyloid and suspected neuritic plaques in both AD/TREM2^{wt} and AD/TREM2^{var} cases.
Double staining immunofluorescence of **(a)** CD68$^+$ microglia (red) and Aβ pathology (green) or **(b)** CD68$^+$ microglia (red) and tau pathology (green) in the CA1 and CA4 of AD/TREM2^{wt} and AD/TREM2^{var} (p.R47H) cases.
Cell nuclei were stained with Hoechst 33342 (blue). Images were captured at 200× magnification.

(a) HLA/Aβ

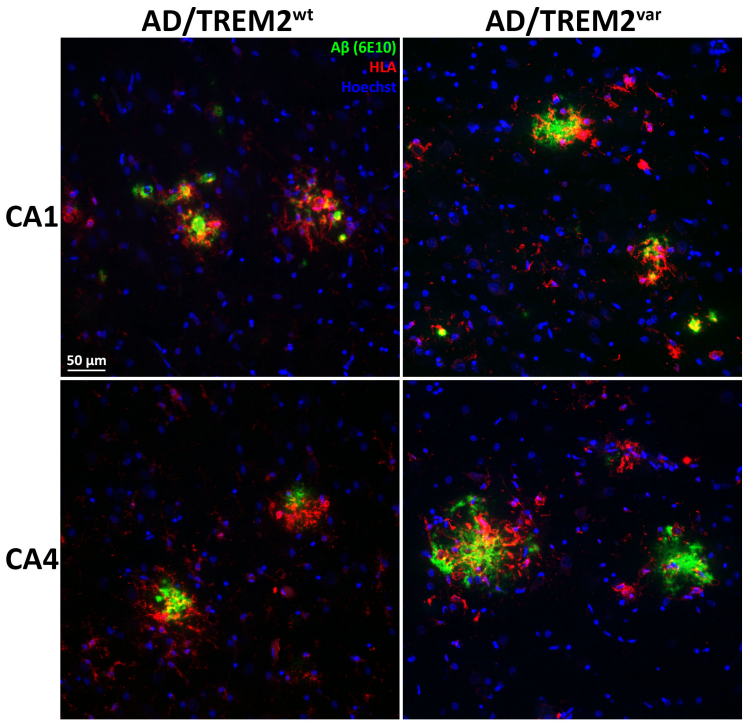

(b) HLA/tau

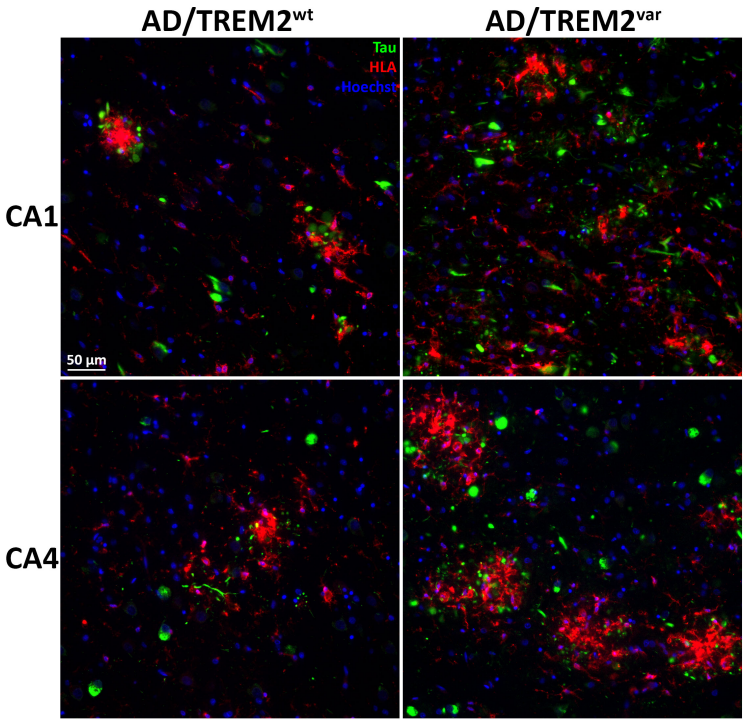

Figure 4.10. HLA$^+$ microglia strongly colocalised around amyloid and suspected neuritic plaques in both AD/TREM2^{wt} and AD/TREM2^{var} cases. Double staining immunofluorescence of **(a)** HLA$^+$ microglia (red) and Aβ pathology (green) or **(b)** HLA$^+$ microglia (red) and tau pathology (green) in the CA1 and CA4 of AD/TREM2^{wt} and AD/TREM2^{var} (p.R47H) cases.
Cell nuclei were stained with Hoechst 33342 (blue). Images were captured at 200× magnification.

(a) Iba-1/Aβ

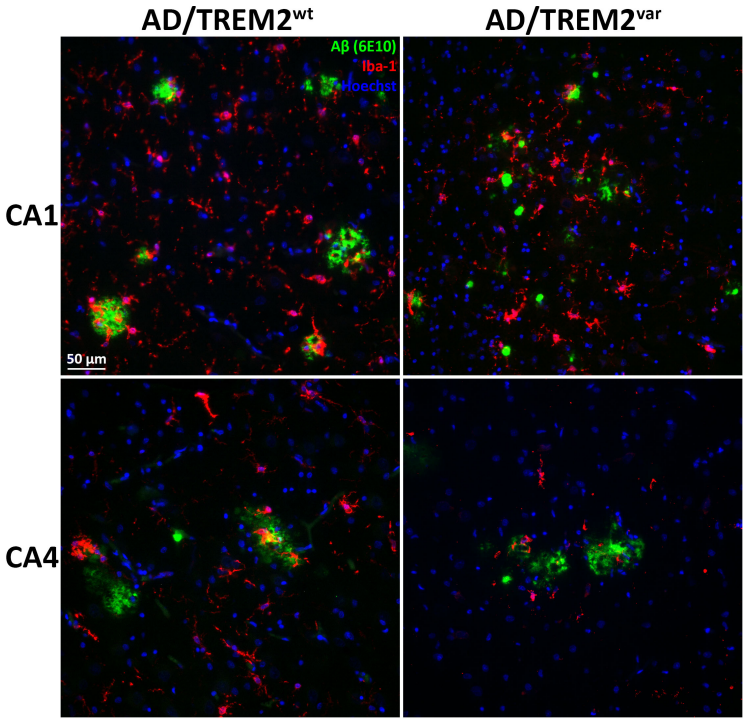

(b) Iba-1/tau

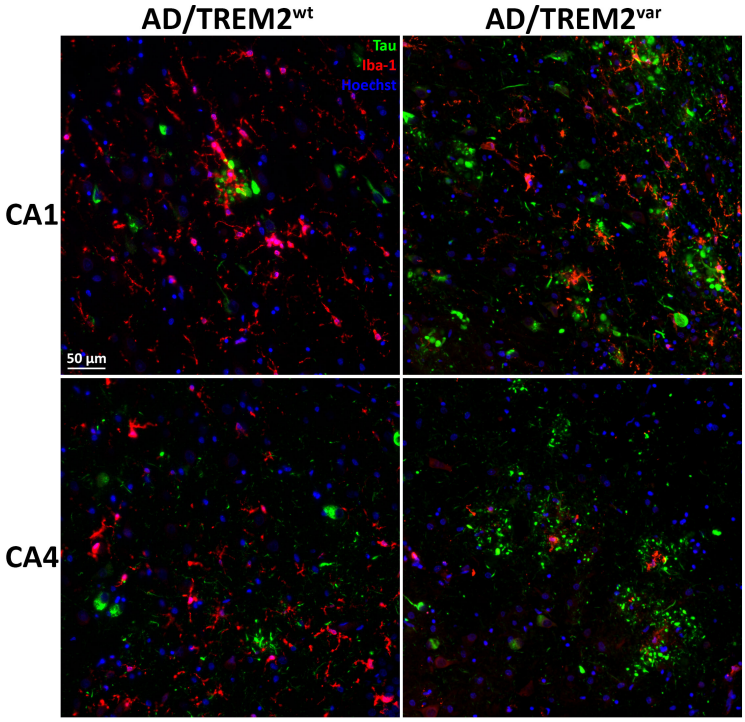

Figure 4.11. Unlike CD68^{+} and HLA^{+} microglia, Iba-1^{+} microglia were not preferentially clustered around amyloid and suspected neuritic plaques in either AD/TREM2^{wt} or AD/TREM2^{var} cases.
Double staining immunofluorescence of **(a)** Iba-1^{+} microglia (red) and Aβ pathology (green) or **(b)** Iba-1^{+} microglia (red) and tau pathology (green) in the CA1 and CA4 of AD/TREM2^{wt} and AD/TREM2^{var} (p.R47H) cases.
Cell nuclei were stained with Hoechst 33342 (blue). Images were captured at 200× magnification.

4.4.6 Analysis of AD cases with TREM2 p.R47H variant only

The different AD-associated TREM2 variants may affect the function of TREM2 and therefore AD vulnerability differently. Therefore to investigate if the effects of the most common and established AD-associated TREM2 p.R47H variant only are consistent with previous findings, analyses were repeated on these cases (AD/TREM2^{R47H}) only. In contrast to AD/TREM2^{var}, there were significantly fewer HLA^{+} microglia in the CA4 of AD/TREM2^{R47H} cases compared to AD/TREM2^{wt} (pairwise comparison ANCOVA: p=0.012) and Control/TREM2^{wt} (pairwise comparison ANCOVA: p=0.030) cases (Figure 4.12f).

Conversely, HLA^{+} microglia morphology was no longer significantly different between AD/TREM2^{R47H} and Control/TREM2^{wt} cases in the CA1 (Figure 4.13c).

Otherwise, observations between the analyses of only TREM2 p.R47H cases and all cases with a disease-associated TREM2 variant remained similar (Figure 4.12, 4.13). These findings suggest that disease-associated TREM2 variants other than the p.R47H may have different effects on HLA^{+} microglia. As the number of the other TREM2 variants were limited, this could explain the relatively small difference in the results of both analyses.

(a) Iba-1 CA1 **(b) Iba-1 CA4**

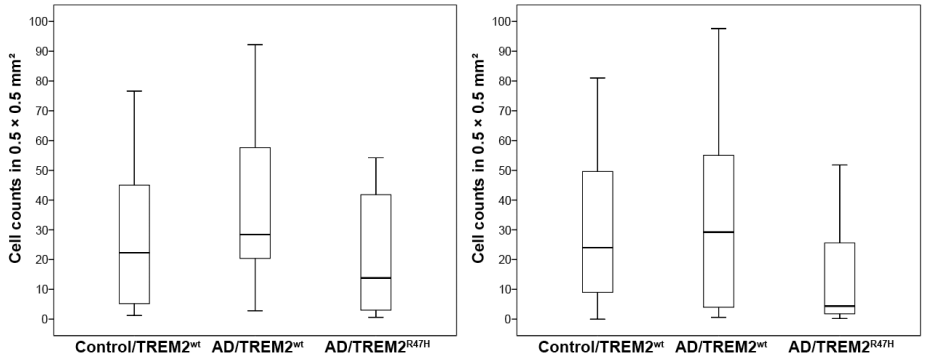

(c) CD68 CA1 **(d) CD68 CA4**

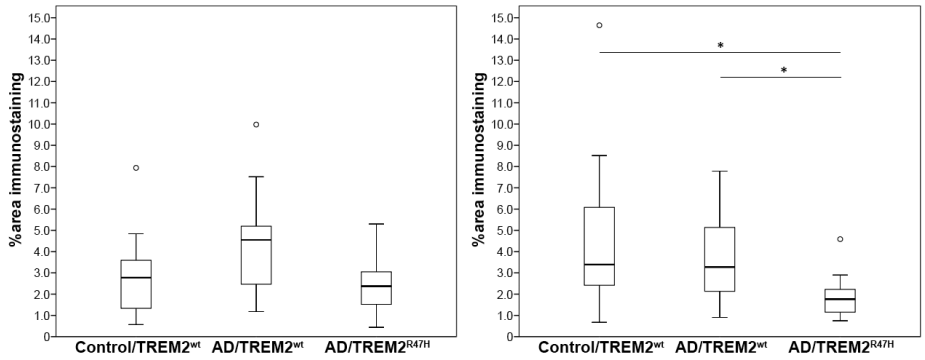

(e) HLA CA1 **(f) HLA CA4**

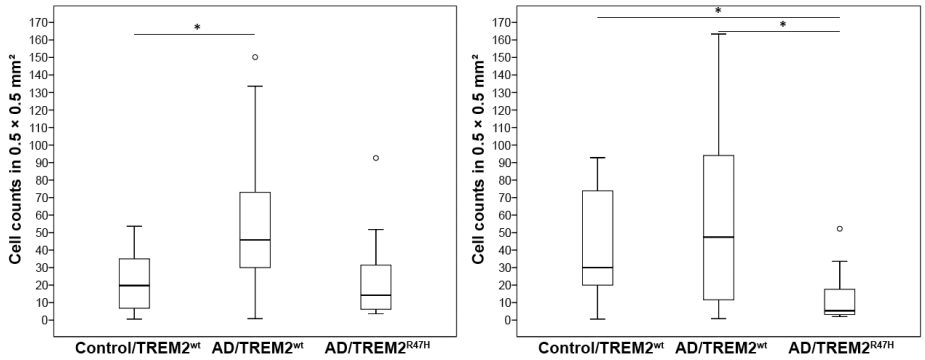

Figure 4.12. CD68$^+$ and HLA$^+$ but not Iba-1$^+$ microglia were significantly fewer in the CA4 of AD/TREM2^{R47H} compared to AD/TREM2^{wt} cases, with similar trends for Iba-1$^+$ microglia in the CA1 and CA4 as well as CD68$^+$ and HLA$^+$ microglia in the CA1.

Box plots showing **(a,b)** Iba-1$^+$, **(c,d)** CD68$^+$ and **(e,f)** HLA$^+$ microglia abundance in the **(a,c,e)** CA1 and **(b,d,f)** CA4 of 18 Control/TREM2^{wt}, 21 AD/TREM2^{wt} and 9 AD/TREM2^{R47H} cases. Means and standard deviations are shown in Appendix Table A4. *: $p<0.05$.

(a) Iba-1 CA1 **(b) Iba-1 CA4**

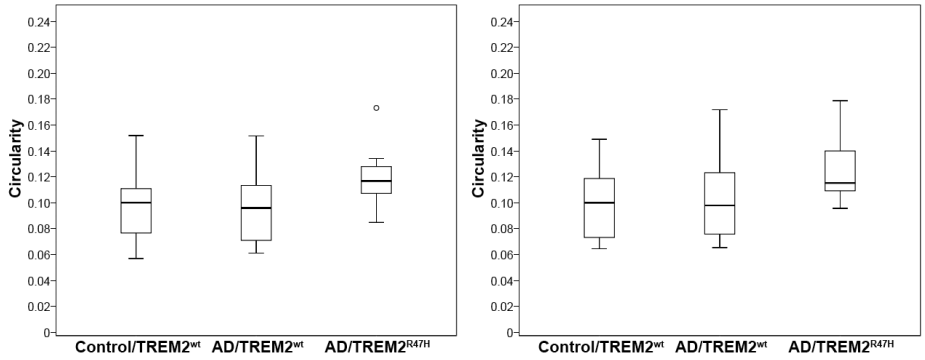

(c) HLA CA1 **(d) HLA CA4**

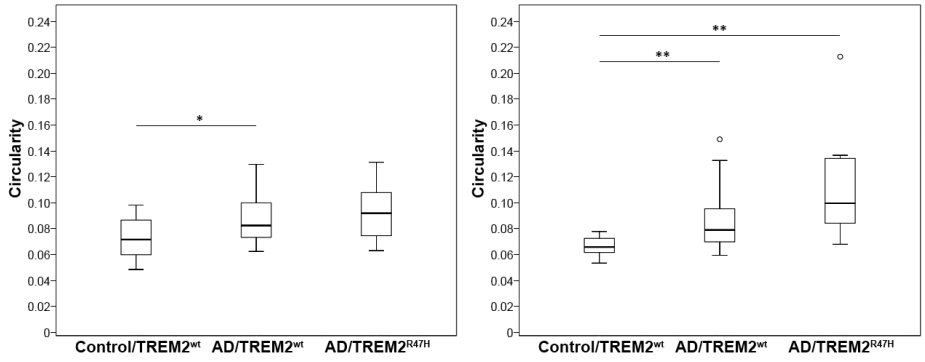

Figure 4.13. Microglial morphology in cases with the TREM2 p.R47H variant only was largely comparable to all cases including a disease-associated TREM2 variant. However, HLA$^+$ microglia in the CA1 were no longer significantly more amoeboid in AD/TREM2$^{\mathbf{R47H}}$ than Control/TREM2$^{\mathbf{wt}}$ cases.
Box plots showing average circularity of **(a,b)** Iba-1$^+$ and **(c,d)** HLA$^+$ microglia in 0.5×0.5 mm^2 areas of the **(a,c)** CA1 and **(b,d)** of 18 Control/TREM2$^{\mathrm{wt}}$, 21 AD/TREM2$^{\mathrm{wt}}$ and 9 AD/TREM2$^{\mathrm{R47H}}$ cases. Means and standard deviations are shown in Appendix Table A5. *: $p<0.05$, **: $p<0.01$.

4.5 Discussion

Microglia in end-stage AD cases in the present study appear to be activated with increased numbers of HLA-DP, -DQ, -DR-expressing microglia in the hippocampus. In contrast, AD cases with a disease-associated TREM2 variant, particularly the p.R47H variant, had significantly fewer cells expressing functionally activated markers of HLA-DP, -DQ, -DR and CD68 in the hippocampal CA4, with similar or fewer of these microglia compared to non-AD cases. Meanwhile, the overall microglia population appears to be unaffected by disease or the presence of disease-associated TREM2 variants as there were similar numbers of cells stained with the pan-microglial marker Iba-1 in the hippocampus of elderly controls and AD cases with and without disease-associated TREM2 variants. Similar findings with Iba-1-expressing microglia have been reported by others in the middle frontal gyrus of AD cases with and without the TREM2 p.R47H variant[470] and in TREM2-deficient APP/PS1 mice[468].

In contrast to the present study, Iba-1-expressing microglia in the CA1 and CA4 has also been reported to be decreased in AD cases with the TREM2 p.R47H variant compared to AD cases without TREM2 variants[473]. In addition, in TREM2-deficient 5XFAD mice, the total brain myeloid cells is also decreased compared to mice with normal TREM2[241,438]. While the inconsistencies between the studies in mice can be attributed to the different AD model used, it may be that the patient cohort studied had different demographic characteristics. Indeed, in the study that found fewer Iba-1-expressing microglia in the hippocampus, the median age at death of cases is 13.5 years older than those in the present study[473]. Moreover, % area staining and cell counts in the present study were significantly affected by age at death and were included as covariates in statistical analyses. This suggests an overall failure of microglia to respond adequately to inflammatory stimuli and undergo microgliosis despite having significant AD pathology.

Phagocytosis is one of the first functional phenotype found to be impaired by TREM2 dysfunction[384]. It is a key function of microglia to clear debris from tissue injury followed by tissue repair mediated in combination with the release of trophic factors[192,194,195]. Microglial phagocytosis can be induced through phagocytic receptors associated with pro- or anti-inflammatory responses. Activation of receptors that recognise foreign microorganisms

such as TLRs lead to the removal of invading pathogens and a proinflammatory response in these phagocytes[642]. On the other hand, stimulation of receptors like phosphatidylserine receptors that recognise apoptotic cell components result in the clearance of cell debris and the induction of anti-inflammatory responses for tissue repair[642]. Phagocytosis of material result in proteolytic degradation in the lysosome[643]. CD68 is a lysosomal/endosomal-associated glycoprotein and predominantly localises to these organelles which are present during phagocytosis[644]. Therefore, CD68 has been widely used as a marker of phagocytosis[645]. Our findings of decreased CD68 immunostaining in AD cases with a disease-associated TREM2 variant is consistent with the existing literature on the impairment of phagocytosis by the loss of TREM2 function. TREM2 deficiency has been reported to impair the phagocytosis of various substrates including apoptotic neurons[106,384,412,429], bone components[418,488], whole bacteria or bacterial components[381,432,442,452], lipids[108,393] and $A\beta_{1–42}$ fibrils[417,452,489]. Furthermore, CD68 immunostaining is lower in TREM2-deficient mouse models of AD[470] and stroke[429] compared to TREM2-expressing control mice. Conversely, increased TREM2 function and signalling result in increased phagocytosis[384,394,417]. Supporting this, it appears that TREM2 expression levels correlate with the phagocytic capabilities of microglia[428]. In studies of AD-associated TREM2 variants, the p.R47H and p.R62H have been shown to impair microglial phagocytosis[108,435]. Together, these and our findings indicate that disease-associated TREM2 variants convey a loss of function to TREM2 which negatively impacts overall levels of phagocytosis by microglia in response to AD pathology.

The increased number of HLA-DP, -DQ, -DR-expressing cells in AD cases compared to non-AD cases seen in the present study have been previously observed in various neurodegenerative diseases including AD[646–649], Parkinson's disease[649] and Huntington's disease[650] as well as in brain injury[650–652]. The number of HLA-DP, -DQ, -DR-expressing microglia in the hippocampus appear to positively correlate with the severity of AD[653]. HLA or MHC class II has been used as a marker to label activated microglia[629–631]. In AD, microglial stimulation by Aβ increase cell surface expression of MHC class II and release of proinflammatory mediators such as IL-1β, IL-6, TNF-α and IL-8[654]. This suggests that increased MHC class II expression may also be a marker of proinflammatory activation by microglia. Our findings are consistent with observations in TREM2-deficient AD mice which have decreased MHC class II expression compared to AD mice with normal TREM2[438].

Interestingly, the study by Korvatska *et al.* (2015)[473] reported that MHC class II expression in human post-mortem brain is not affected by the AD-associated TREM2 p.R47H variant. MHC class II staining is significantly increased in hippocampal CA1 and CA4 of AD cases but there is no difference between AD cases with or without the variant[473]. This is contrast to the present study with decreased numbers of HLA-DP, -DQ, -DR-expressing microglia especially in the CA4 of AD cases with the TREM2 p.R47H variant. Again, this difference may be due to their cohort being much older. Indeed, aging has been associated with the increased expression of MHC class II[655–659] and age at death was found to significantly affect the number of HLA-DP, -DQ, -DR-expressing microglia in the CA1 and CA4 in the present study.

The underlying mechanisms of TREM2 dysfunction by disease-associated variants resulting fewer HLA-DP, -DQ, -DR-expressing cells are still unknown. The loss of TREM2 function as a DAMP recognition receptor may result in microglia unable to respond to pathogenic stimuli to become activated and therefore unable to increase the expression of HLA-DP, -DQ, -DR. A network analysis study reported an association between TREM2 expression and several HLA class II genes (*HLA-DMA*, *HLA-DMB*, *HLA-DPA1*, *HLA-DPB1*, *HLA-DQA2* and *HLA-DRA*)[402]. Indeed, TREM2 signalling appears to induce MHC class II expression and antigen presenting function of dendritic cells, macrophages and microglia[430,660]. On TREM2 activation, immature dendritic cells increase the expression of antigen presenting molecules including MHC class II, CD40, B7.1, B7.2 and CCR7[380]. Microglia are also capable of expressing antigen presentation-associated adhesion or co-stimulatory molecules such as CD11a, CD40, CD54, CD58, CD80 and CD86 which are required to activate T cells[661,662]. TREM2 activation in BV2 microglia cause some of these genes to be upregulated, especially MHC class II but not CD40[660]. This suggests that TREM2 induces a different antigen presentation phenotype compared to dendritic cells. Nevertheless, an *in vitro* co-culture study using BV2 microglia overexpressing TREM2 saw increased $CD4^+$ T cell activation associated with increased MHC class II expression compared to BV2 expressing lower levels of TREM2[428].

These indicate that antigen presentation by microglia may be impaired by the loss of TREM2 function. However, there have been limited evidence for antigen presentation by microglia in the brain. Under normal physiological conditions, a very low number of T

cells are present in the CNS[663–668]. In contrast, increased T cell invasion into the brain is detected in neurodegenerative diseases, especially in multiple sclerosis and equivalent animal models[667–673]. Normally, antigen presentation to T cells does not occur within tissues[674]. Dendritic cells that phagocytose and process antigens migrate to the lymph nodes for antigen presentation to T cell receptors[660]. However, microglia do not leave the CNS and hence do not present antigens to T cells in the lymph nodes[675]. Even so, in a mouse model that antigen-presenting function is limited to injected cells, both antigen-primed dendritic cells and microglia injected intracerebrally could recruit T cells into the CNS[675], which suggests that antigen presentation can occur there. Alternatively, naive T cells that were not exposed to antigens can also migrate into the CNS attracted by chemokines released from damaged neurons, activated glia or endothelium[676]. Microglia expressing MHC molecules can then mediate antigen presentation to T cells which indicates the target antigen is nearby[677]. Besides that, it has been suggested that microglia are not the primary antigen presenting cells (APCs) to recruit T cells but instead modulate T cell effector function[678]. Supporting this, in contrast to infiltrating macrophages and dendritic cells, activated microglia are not as effective at inducing T cell proliferation which is associated with microglial production of prostaglandins and NO that inhibit proliferation and expression of MHC and co-stimulatory molecules[679,680]. Instead, activated microglia are more effective at polarising T cells towards the Th1 phenotype than infiltrating macrophages or dendritic cells[679,680]. Furthermore, microglia may be involved in resolving T cell responses. Microglia stimulated with IFN-γ or activated Th1-conditioned medium induce microglial expression of B7-H1 co-stimulatory molecule that inhibits T cell responses[681].

These suggest that there may be a role of the adaptive immune system and T cell involvement in AD but it is still underexplored. An early study observed Aβ-reactive T cells in PBMC isolated from AD patients, but plaque-associated T cells have not been detected[682]. In *in vivo* animal studies, only very few $CD4^+$ T cells are seen in the meninges of Aβ-immunised APP/HLA-DR transgenic mice[683]. In contrast, a follow up study using APP/IFN-γ transgenic mice found $CD4^+$ and $CD8^+$ T cells that co-localise with amyloid plaques and $CD11b^+$ microglia in the hippocampus[528]. The difference between these two observations can be attributed to the stimulation by IFN-γ in the latter study[528], which is found to enable T cell migration into the brain[684]. Although IFN-γ expression is experimentally induced, IFN-γ level has been reported to be elevated in the plasma of AD patients

compared to controls[685] which could facilitate T cell invasion into the brain. Additionally, in APP/PS1 mice induced with a Th2 response, plaque-associated microglia express MHC class II and surprisingly, CD11c which is a characteristic marker of dendritic cells[686]. CD11c expression is also found in microglia in several other AD mouse models[438,687–689] and in plaque-associated microglia in AD brains[690,691]. This further supports the view that microglia can transform into an APC-like phenotype. Some studies have observed co-localisation and direct contact between plaque-associated $CD11c^+$ microglia and $CD3^+$ T cells[686] or not at all[691]. This could be due to the induction of T cell responses by glatiramer acetate in the former study[686] having the same impact as IFN-γ in allowing T cell migration into the brain whereas in the latter study, the AD mice were untreated[691]. Induction of Th2 responses in AD mice results in fewer amyloid plaques and improved cognition[686], suggesting a key role for microglial antigen presentation mediated by MHC class II expression and T cell responses in the pathogenesis of AD, which could be impaired by disease-associated TREM2 variants.

Interestingly, when observed in a few AD cases with and without disease-associated TREM2 variants in the present study, HLA-DP, -DQ, -DR-expressing microglia appear to strongly colocalise with amyloid and suspected neuritic plaques regardless of TREM2 variant. However, when quantified across the tissue, AD cases with a disease-associated TREM2 variant have fewer overall microglia expressing CD68 and HLA-DP, -DQ, -DR. CD68 staining also tend to colocalise with amyloid and neuritic plaques, but it is not clear whether these are the same cells expressing HLA-DP, -DQ, -DR. Due to technical limitations of antibody species compatibility, HLA-DP, -DQ, -DR and CD68 double staining immunofluorescence could not be performed. Nevertheless, HLA-DP, -DQ, -DR- and CD68-expressing cells had partial overlap with Iba-1-expressing cells. Similar observations are also seen in AD and multiple sclerosis brains by others[692]. Surprisingly, Iba-1-expressing microglia do not appear to preferentially cluster around amyloid and neuritic plaques to the same extent as HLA-DP, -DQ, -DR- and CD68-expressing cells in the present study. This suggests that these cells better reflect functionally activated microglia responding to AD pathology compared to Iba-1-expressing cells.

In sum, our data highlight shared and distinct mechanisms in microglial response to AD pathology that involve TREM2 function. It suggests that sufficient numbers of

properly functioning microglia are required to mitigate the rapid progression of amyloid and tau pathology occurring in AD. Our findings reflect a very subtle change in microglial phenotype in individuals with disease-associated TREM2 variants. This includes a decrease in phagocytosis (lower CD68 immunostaining) and antigen presention (fewer HLA-DP, -DQ, -DR-expressing cells) by microglia which can be measured as markers to characterise the generated *in vitro* TREM2 model. Fewer HLA-DP, -DQ, -DR-expressing microglia due to disease-associated TREM2 variants may indicate a role for the adaptive immune system and T cell involvement in AD pathogenesis that has been a relatively underexplored field. Following our findings, it is important to further confirm if the lower abundance of functionally activated microglia is due to decreased cell proliferation or the impairment of resting/surveillance microglia to activate in response to pathology. Besides that, a key finding would be to check if the differences in the number of CD68- and HLA-DP, -DQ, -DR-expressing cells are directly due to TREM2 dysfunction by performing double staining immunofluorescence of these markers with an anti-TREM2 antibody. This could not be done in this study because a reliable and validated antibody against TREM2 for use in FFPE human brain tissue is not available during the project. Since then, a very recent study has successfully performed TREM2 immunostaining on these tissue[475]. Surprisingly, they did not detect any microglia expressing TREM2 but only in circulating monocytes despite careful characterisation and optimisation of immunostaining. This has strong implications on the role of TREM2 in microglia, including findings by us and others, which will require replication in our cohort as well.

4.6 Statement of collaborative work

I would like to thank Dr Kuang Lin (Institute of Psychiatry, Psychology and Neuroscience, King's College London) for co-authoring the Python script used in the semi-automated computerised quantification pipeline. I am also grateful to Dr Andrew King (Department of Clinical Neuropathology, King's College Hospital) for performing the manual cell counts for validation of the semi-automated quantification. Additionally, I would like to thank Christina Murray and Dr Tammaryn Lashley (Institute of Neurology, University College London) for providing several stained hippocampal sections and helping to scan the microscope slides at their facility.

Chapter 5

Functional characterisation of clonal TREM2-deficient BV2 microglia cell lines

5.1 Introduction

This Chapter evaluates the functional consequences of the CRISPR/Cas9-edited BV2 cell lines containing indels in *Trem2* Exon 2 which were generated in Chapter 3. These indels were either an in-frame deletion expected to cause the removal of a few amino acids at the ligand-binding site, or insertions/deletions that caused a frameshift and thus changed the amino acid sequence completely from the point of the indel. Regardless, these indels are predicted to result in the functional loss of TREM2. Further assessment of these lines is necessary to see if the predicted effect at the DNA level led to the expected changes at the transcript and protein level. Additionally, as Cas9 may still persist after screening, the clonal lines need to be checked to ensure no further Cas9 activity leading to further DNA cleavage during expansion of the cell lines.

Functional loss of TREM2 in the various clonal lines should result in the lack of activation of signalling pathways downstream of TREM2 as the cells fail to respond to stimulation by a TREM2 ligand. Activation of TREM2 has been associated with the induction of phagocytosis, cell migration, proliferation, cell survival and the production of cytokines and chemokines[383]. To mediate all of these functions, TREM2 activation leads to signalling cascades involving many different pathways which dictate the different outcomes. These signalling pathways can be activated by a number of different receptors in addition to TREM2. TREM2 acts via the adaptor protein DAP12, though DAP12 interacts with and can be activated by a range of other receptor proteins[693] such as SIRPβ1[694] and complement receptor 3 (CR3)[695] in microglia. While these receptors have diverse ligands, their functional outcomes are often similar due to convergence on common protein components downstream of receptor activation[388]. For example, activation of SIRPβ1 and CR3 have been described to mediate phagocytosis[694,695], similar to TREM2. Hence, TREM2 deficiency would not result in complete impairment of its associated functions, such as phagocytosis, if alternative DAP12- or ITAM-associated receptors become activated. Although various receptors can engage similar signalling pathways, not all of them have been implicated in disease. Therefore, disease vulnerability conveyed by the decrease in or loss of TREM2 function is expected to only result from impaired innate immune responses against TREM2 ligands.

Various ligands have been described to bind TREM2 including cell membrane lipids, lipoproteins and nucleotides (Chapter 1.6.3). However, these do not bind only to TREM2 and therefore it is difficult to differentiate their effects on different receptors (Table 5.1). For specific receptor activation, antibodies have been commonly used to simulate ligand binding. A commercially available monoclonal antibody raised against the extracellular region of TREM2 (MAB17291, R&D Systems) has been previously used and reported to result in TREM2 activation[394]. Stimulation of myeloid precursor cells transduced with TREM2 with this antibody has been shown to increase phosphorylation of Erk compared to isotype control antibodies[394]. Erk is a signalling protein known to be downstream of TREM2 activation (Figure 5.1).

TREM2 ligands	**Other known receptor(s)**	**Ref.**
Cell membrane lipids/phospholipids	CD36	696
Lipoproteins	CD36, class A scavenger receptor (SR-A)	696,697
Nucleotides	Toll-like receptor 9 (TLR9)	698

Table 5.1. Examples of TREM2 ligands that also bind other microglial receptors.

On TREM2 activation, Src-family kinases are recruited to DAP12 and phosphorylate DAP12 ITAMs[693]. The phosphorylated ITAMs in turn become docking sites for recruited Syk[699] (Figure 5.1). Syk then becomes activated and phosphorylates several downstream effectors including Vav[700], PLCγ[701] and PI3K[702], which can initiate their own signalling cascades[699,703] (Figure 5.1). The signalling pathways originating from TREM2 then start to diverge.

As numerous proteins are involved in these downstream signalling cascades, only a small number can be practically investigated without resorting to high-throughput experiments. Therefore, three key signalling proteins downstream of TREM2 that mediate important cellular functions related to immune responses associated with TREM2 function were focused on in this Chapter. Syk is a crucial signalling protein in the TREM2 signalling pathway as it transduces signals from DAP12 to trigger downstream signalling cascades (Figure 5.1). Some of these include calcium and PKC signalling, Pyk2–Rho-mediated actin-cytoskeleton reorganisation, ROS production, phagocytosis, PI3K-mediated Tec and Akt signalling, and Ras–Erk regulation of gene expression[703] (Figure 5.1). Syk is a necessary component in mediating phagocytosis as Syk deficiency result in the complete inhibition of

phagocytosis in macrophages[704]. This is associated with inability for arms of the phagocytic cup to fuse[704]. Syk is also involved in promoting cell survival through PI3K–Akt signalling to activate the Wnt–β-catenin signalling pathway[533]. Akt phosphorylates and inactivates GSK3β (Figure 5.1), which results in the stabilisation of β-catenin to regulate expression of genes associated with proliferation (c-Myc, Cyclin D1) and anti-apoptosis (Bcl-2)[533]. Moreover, Syk has a role in the induction of cytokine and chemokine production through the activation of CARD9–Erk/NFκB signalling[705] (Figure 5.1).

Besides that, Pyk2 is also an important protein in mediating TREM2–DAP12 function. Despite no direct evidence of Pyk2 activation by TREM2 signalling, signalling components downstream of TREM2 have been shown to result in Pyk2 phosphorylation. Pyk2 can be directly activated by Src-family kinases after recruitment to DAP12 upstream of Syk activation[699,706] or further downstream through Syk–Vav signalling[707] (Figure 5.1). Indeed, DAP12-deficient BMDM had impaired phosphorylation of Pyk2 when stimulated with CSF-1[708]. CSF-1 activation of its receptor CSF-1R triggers a signalling pathway that phosphorylates DAP12 ITAMs and subsequently activates Pyk2[709]. Pyk2 is a part of the intracellular calcium signalling that is involved in various immune cell responses[710–714]. Pyk2 also mediates actin-cytoskeleton reorganisation for phagocytosis[715,716] and cell polarity for chemotaxis/cell migration[717] which are established functions of TREM2[383].

Additionally, Erk1 and Erk2 mediate significant functions of TREM2. They are protein homologues that have 84% sequence homology and share many common functions[718]. Therefore, they are considered to be similar effectors here and collectively referred to as Erk1/2. They have a diverse role in mediating cellular functions as part of the MAPK signalling cascade[719]. One of these roles crucial to TREM2 function is to transmit signals from CARD9 to activate transcription factors and induce cytokine and chemokine production[705] (Figure 5.1). In addition, Erk1/2 mediates cell survival by promoting the expression of anti-apoptotic Bcl-2[720] and inhibit Bcl-2 antagonists (Bad, Bim-EL) by phosphorylation[721,722]. Erk1/2 also inhibits caspase 9 to prevent the activation of the pro-apoptotic caspase 3 and further contribute to cell survival[723].

These 3 signalling proteins are involved in almost all TREM2-related functions. Therefore, functional loss of TREM2 is expected to cause these 3 signalling proteins to not respond to TREM2 activation.

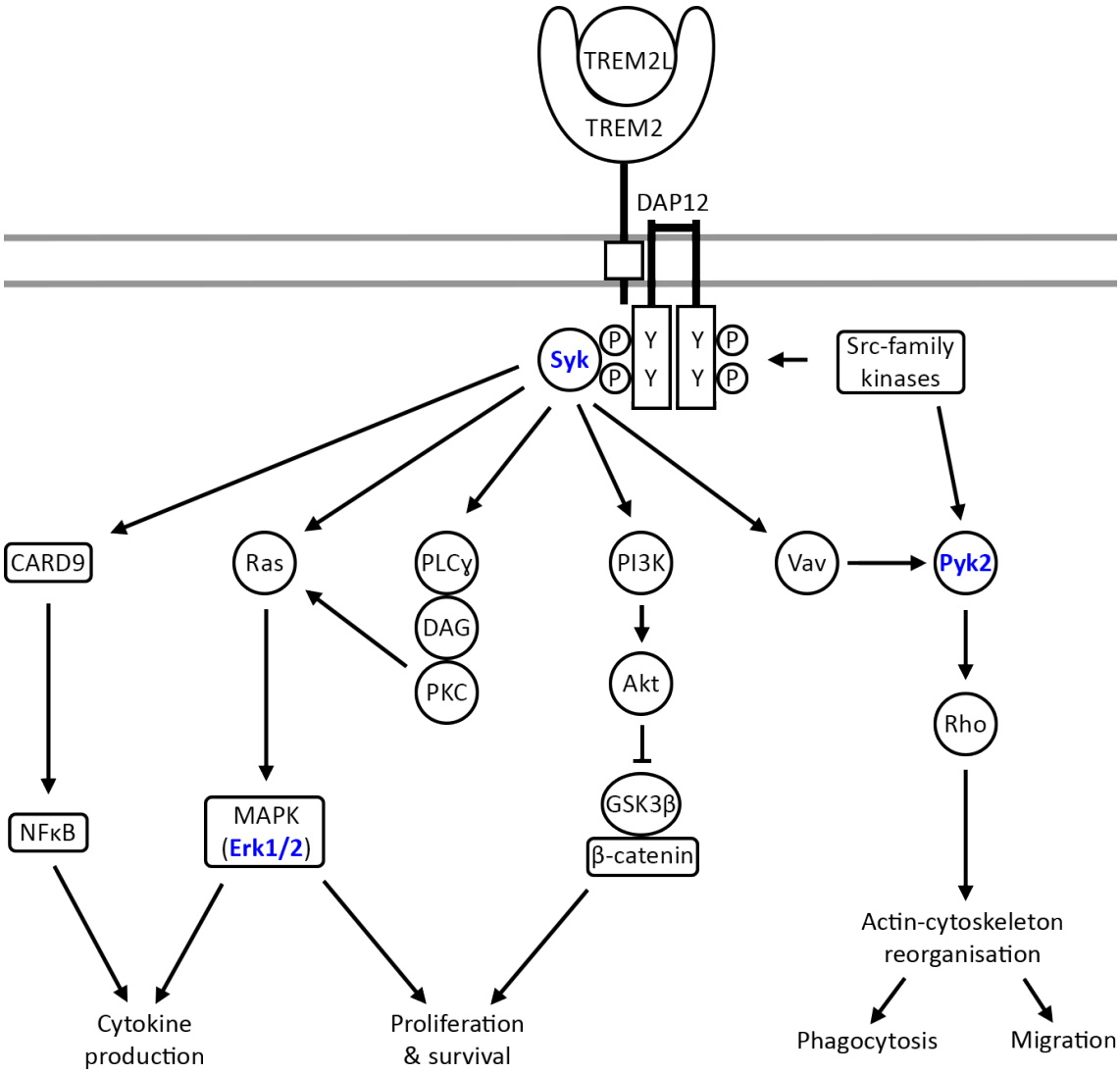

Figure 5.1. TREM2 activation initiates signalling through DAP12 to trigger further activation of various signalling cascades that mediate TREM2 function.

A simplified illustration of several signalling pathways downstream of activated TREM2. On TREM2 ligand (TREM2L) binding, Src-family kinases are recruited to DAP12 and phosphorylate tyrosine residues on DAP12 ITAMs. Syk is then recruited to the phosphorylated ITAMs and become activated. Activated Syk then further activates several intermediate signalling proteins as shown. Key signalling proteins that mediate many of TREM2 functions focused on in this Chapter are labelled in blue.

Chapter 4 showed that CD68 expression and HLA-DP, -DQ, -DR-expressing cell abundance were decreased in hippocampal CA4 of AD cases with a disease-associated TREM2 variant, particularly the p.R47H. This is despite having similar abundance of Iba-1-expressing cells between AD cases with or without a disease-associated TREM2 variant, which suggests that the variants result in loss of microglia function, particularly phagocytosis and antigen presentation. These variants have also been associated with the loss of or decreased TREM2 protein function (Chapter 1.6.4). Therefore, it is expected that the generated TREM2-deficient clonal lines would have decreased CD68 and MHC class II expression when treated with an AD-related stimulus compared to WT cells. Hence, the response of these cells can be compared with findings from Chapter 4 to determine if the clonal lines model aspects of disease due to TREM2 variants in people.

The usefulness of this *in vitro* disease model of TREM2 and its suitability for high-throughput screening to identify disease-modifying therapeutic drugs can be established through these findings. Furthermore, the initial investigation on the changes in activation of key signalling proteins downstream of TREM2 provides preliminary data on how the functional loss of TREM2 impact innate immune responses. This may then suggest potential avenues for therapeutic targeting.

5.2 Aims

- To confirm that the cell lines generated by CRISPR/Cas9-mediated editing of *Trem2* have a functional loss of TREM2 protein expression.
- To investigate the effects of TREM2 deficiency on the activation of key signalling proteins that mediate inflammatory responses associated with TREM2 function.
- To compare the effects of TREM2 deficiency in the generated cell lines with disease-associated TREM2 variants on functional microglial markers identified from Chapter 4.

5.3 Methodology overview

Detailed methods are outlined in Chapter 2.4.

Expanded cultures of *Trem2*-edited (C1G10, C1E2, C1C4, C1G4, C3bB10, C3bC4), CRISPR WT (C3bA1, C3bA6, C3bA8, C3bA12, C3bB4) clonal BV2 cell lines from Chapter 3 and BV2 WT cells were established. Cell pellets were harvested to confirm *Trem2* DNA sequence as well as transcript and protein expression. DNA were extracted and purified from all clonal lines followed by PCR amplification of *Trem2* Exon 2. Amplicons were resolved on an agarose gel to compare any change in size at the target site in *Trem2* following CRISPR/Cas9 editing. Purified amplicons were also Sanger-sequenced to confirm DNA changes and ensure clonal lines had not been mixed during handling and expansion of cultures.

For RT-PCR, RNA was extracted and converted into cDNA. Exon 2 of protein-coding transcripts (NM_031254 & NM_001272078) and Intron 1–Exon 2 of the retained Intron 1 transcript (ENSMUST00000132340.1) were PCR-amplified and amplicons resolved on an agarose gel. Protein lysates were extracted, quantified and deglycosylated. TREM2 protein expression was assessed by Western blot. Various commercially available antibodies against TREM2 were tested and validated (Table 5.2).

Primary antibody	**Immunogen**	**Manufacturer**	**Cat#**
Anti human TREM2, goat	Human TREM2 His19–Ser174	R&D Systems	AF1828
Anti human TREM2, rabbit	Human TREM2 Gln33–Pro144	Atlas Antibodies	HPA012571
Anti human/mouse TREM2 (clone 237920), rat	Mouse TREM2 Leu19–Pro168	R&D Systems	MAB17291
Anti mouse TREM2, rabbit	Mouse TREM2 Met1–Thr227	Santa Cruz	sc-48765
Anti mouse TREM2, sheep	Mouse TREM2 Leu19–Pro168	R&D Systems	AF1729

Table 5.2. Commercially available antibodies against human or mouse TREM2 used to detect functional expression of TREM2 in CRISPR/Cas9-edited clonal lines.

Clonal lines were investigated for changes in the activation of signalling mediators downstream of TREM2 and functional microglial markers identified from Chapter 4. Four TREM2 KO (C1G10, C1E2, C3bB10, C3bC4) and four TREM2 WT [three CRISPR control (C3bA1, C3bA6, C3bA8) and BV2 WT] cell lines were used. 6-well culture plates were coated with 10 µg/mL isotype control or TREM2-activating antibody (MAB17291) that binds to the extracellular region of TREM2. Clonal lines were seeded onto antibody-coated plates and incubated for 1 h. Protein lysates were harvested and changes in phosphorylation of Syk, Pyk2 and Erk1/2 as well as levels of CD68 and Iba-1 were assessed by Western blot.

5.4 Results

5.4.1 Evaluation of *Trem2* DNA sequence at CRISPR/Cas9-targeted site in expanded clonal cell lines

To ensure that the correct clonal cell lines were selected and that further Cas9 activity leading to additional DNA cleavage did not occur, *Trem2* Exon 2 DNA amplicons from expanded cultures of *Trem2*-edited (C1G10, C1E2, C1C4, C1G4, C3bB10, C3bC4) and CRISPR WT (C3bA1, C3bA6, C3bA8, C3bA12, C3bB4) clonal lines were compared by agarose gel electrophoresis and Sanger sequencing. Agarose gel resolution of amplicons from most clones (C3bA1, C3bA6, C3bA8, C3bA12, C3bB4, C1E2, C3bB10 and C3bC4) were the same as observed during screening, reflecting size differences due to indels except for clones C1C4, C1G4 and C1G10 (Figure 5.2a,b). Amplicon sizes from clones C1C4 and C1G4 appeared to be a mixed population (Figure 5.2b). For clone C1G10, in addition to the 249 bp amplicon (397 bp deletion) found in the initial *Trem2* DNA screening (Chapter 3), an amplicon smaller than the 646 bp *Trem2* WT amplicon but larger than the 619 bp amplicon (27 bp deletion) from clone C1E2 was identified (Figure 5.2a). Therefore, it is predicted to have a <27 bp deletion.

Subsequently, amplicons from these clones were Sanger sequenced. Clones C1C4 and C1G4 were not sequenced because they were no longer clonal as observed from agarose gel electrophoresis. All the sequenced cell lines retained clonality with the same changes in *Trem2* Exon 2 DNA sequence as found from clone screening in Chapter 3. Interestingly, in clone C1G10, only the smaller amplicon with 397 bp deletion but not the additional amplicon with <27 bp deletion was observed on sequencing (not shown). This meant that the exact size of this additional amplicon with <27 bp deletion could not be determined here. It was later found to have a 13 bp deletion in another copy of *Trem2* (Chapter 5.4.2). As a result from these findings, clones C1C4 and C1G4 were excluded from future experiments due to heterogeneity in *Trem2* editing.

(a) Clonal CRISPR/Cas9-edited cell lines

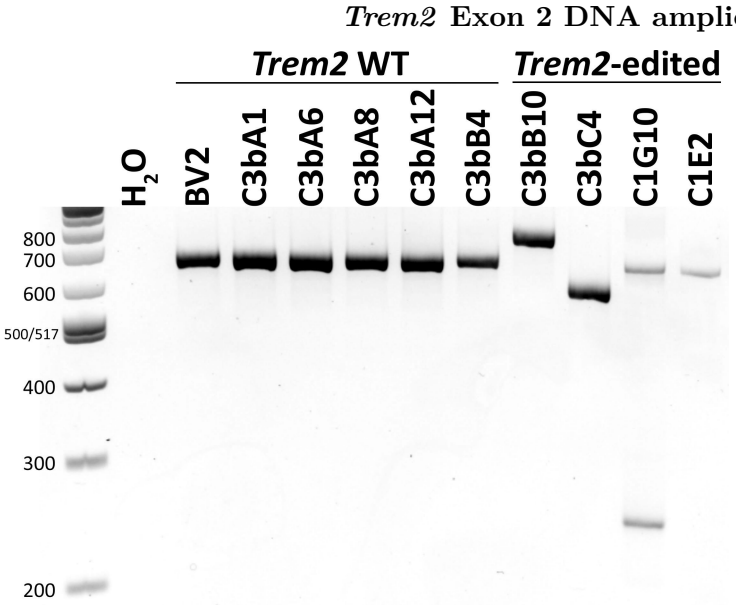

(b) C1C4 & C1G4

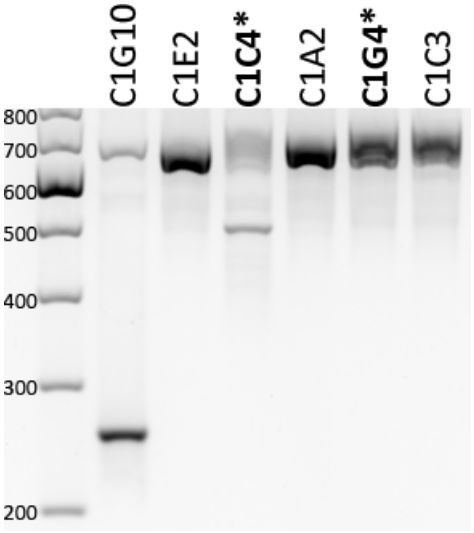

Figure 5.2. Most cell lines generated from CRISPR/Cas9 editing remained clonal after culture expansion.
(a) *Trem2* Exon 2 DNA amplicons from clonal lines on an agarose gel with expected changes in *Trem2* Exon 2 amplicon sizes after CRISPR/Cas9 editing.
Amplicon sizes are WT *Trem2*: 646 bp; C1G10: 633 bp (-13 bp), 249 bp (-397 bp); C1E2: 619 bp (-27 bp); C3bB10: 735 bp (+89 bp); C3bC4: 564 bp (-82 bp).
(b) *Trem2* Exon 2 DNA amplicon sizes from clones C1C4 and C1G4 (bold and asterisk) on an agarose gel were heterogeneous indicating loss of clonality. Negative control lane not shown.
DNA ladder sizes are indicated in base pairs.

5.4.2 Expression of *Trem2* in CRISPR/Cas9-edited clonal lines

Four mRNA isoforms are produced from murine *Trem2*. Two of these, NM_031254 and NM_001272078, are protein-coding[430]. NM_031254 translates into the full-length 227 amino acid protein. NM_001272078 uses an alternative splice site which results in a frameshift and the protein lacking the transmembrane domain. The other two isoforms are not known to translate into protein. ENSMUST00000132340.1 retains Intron 1 whereas ENSMUST00000148545.1 is a much shorter processed transcript of unknown function. To investigate the effects of indels on *Trem2* transcript expression, RT-PCR was performed. A primer pair spanning Exon 1–3 was used to detect protein-coding isoform NM_031254 and NM_001272078 transcripts (Figure 5.3). Expression of these transcripts were completely disrupted in *Trem2*-edited clones (Figure 5.4). None of the resulting cDNA amplicon sizes observed after agarose gel electrophoresis corresponded to indels generated by CRISPR/Cas9 editing. The indels generated in clones C3bB10 and C1E2 are located in Exon 2 and were not expected to disrupt transcript expression or exon splicing (Table 5.3). On the other hand, the 397 bp deletion in clone C1G10 and 82 bp deletion in clone C3bC4 start in Intron 1 and span into Exon 2 (Table 5.3), which may affect transcript splicing.

The effect of indels on ENSMUST00000132340.1 transcript with the retained Intron 1 was investigated using a primer pair spanning Intron 1–Exon 3 specific for this isoform only (Figure 5.3). Amplicons consistent with ENSMUST00000132340.1 were detected after agarose gel electrophoresis in all clones and amplicon sizes corresponded to the indels generated from CRISPR/Cas9 (Figure 5.5a). For clone C1G10, only the amplicon with the <27 bp deletion but not 397 bp deletion was detected here (Figure 5.5a). The forward primer (mTREM2F4) used is located within the 397 bp deletion and was not amplified. Therefore, this cDNA amplicon was Sanger sequenced to determine the exact deletion. This revealed a 13 bp deletion directly before the p.R47 codon (Figure 5.5b). This demonstrates that clone C1G10 has 13 bp and 397 bp deletions in two different copies of *Trem2*. Both of these deletions are predicted to result in a frameshift and a functional loss of TREM2 (Table 5.3).

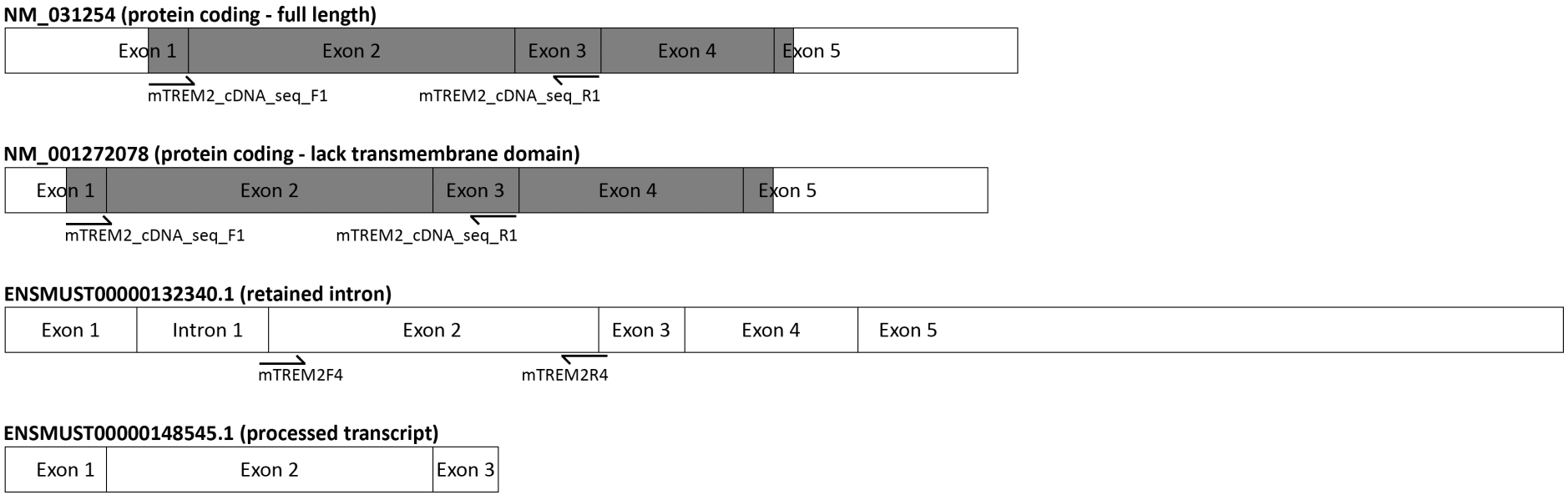

Figure 5.3. RT-PCR primers designed to specifically target protein-coding transcripts (NM_031254 & NM_001272078) and the transcript with retained Intron 1 (ENSMUST00000132340.1).

Four mRNA isoforms known to result from *Trem2*. ENSMUST00000132340.1 and ENSMUST00000148545.1 transcripts are not known to translate into protein.

Known protein-coding regions are indicated in grey. Locations of forward (⇀) and reverse (↽) primers are as indicated with the corresponding primer ID.

***Trem2* NM_031254 and NM_001272078 isoform Exon 1–3 cDNA amplicons**

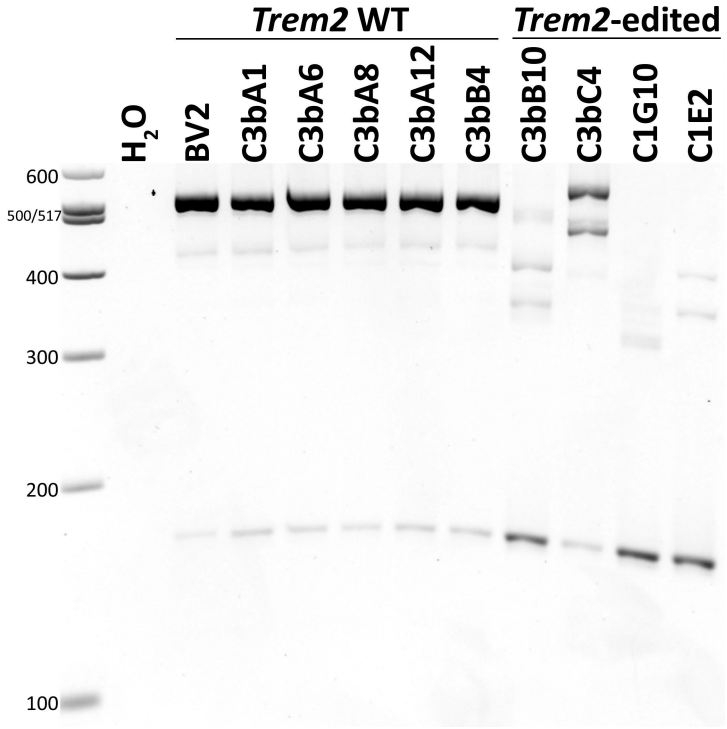

Figure 5.4. Indels in *Trem2* Exon 2 resulted in complete disruption of protein-coding NM_031254 and NM_001272078 transcripts.
None of the NM_031254 and NM_001272078 Exon 1–3 cDNA amplicon sizes from *Trem2*-edited clones on an agarose gel corresponded to the indels generated by CRISPR/Cas9 editing. Clones C1G10 and C3bC4 have deletions that start in Intron 1 which may disrupt exon splicing and transcript expression.
Expected changes in amplicon sizes are WT *Trem2*: 515 bp; C1G10: 502 bp (-13 bp), 118 bp (-397 bp); C1E2: 488 bp (-27 bp); C3bB10: 604 bp (+89 bp); C3bC4: 433 bp (-82 bp). DNA ladder sizes are indicated in base pairs.

(a) ***Trem2*** **ENSMUST00000132340.1 isoform Intron 1–Exon 2 cDNA amplicons**

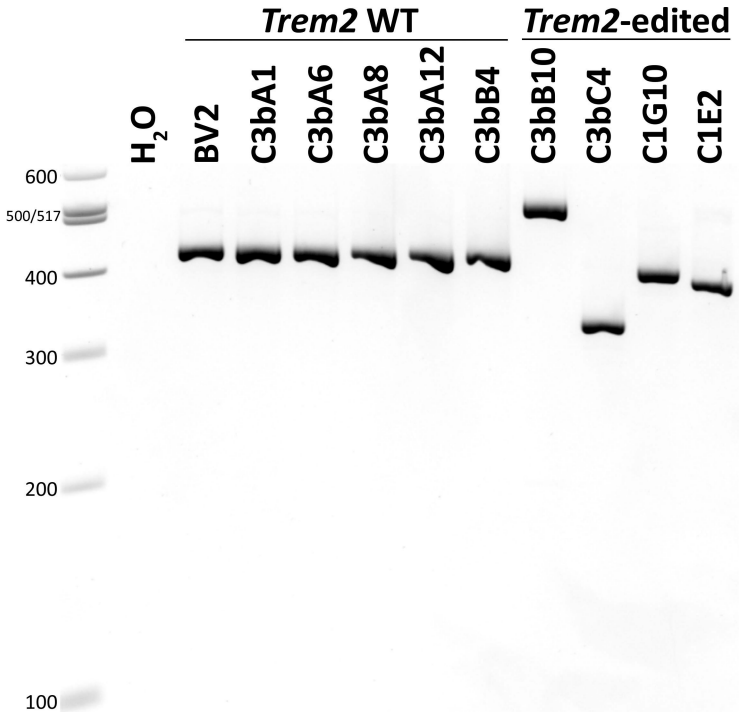

(b) C1G10

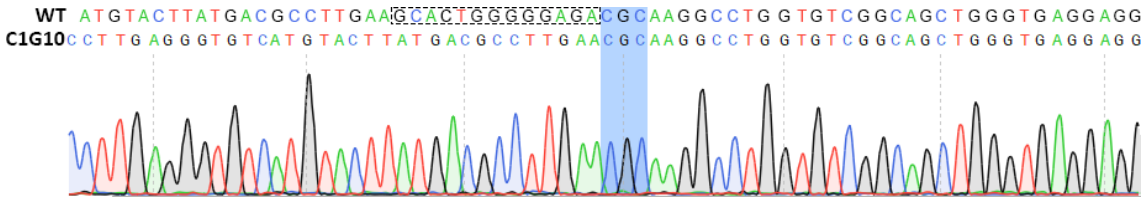

Figure 5.5. Only the amplicon with a 13 bp deletion in *Trem2* of clone C1G10 was amplified from *Trem2* cDNA ENSMUST00000132340.1.
(a) ENSMUST00000132340.1 Intron 1–Exon 2 cDNA amplicons from all clones on an agarose gel corresponded to the indels generated by CRISPR/Cas9 editing. For clone C1G10, only the amplicon with the <27 bp deletion was amplified because the forward primer (mTREM2F4) used is located within the 397 bp deletion of the other copy of *Trem2*. Expected changes in amplicon sizes are WT *Trem2*: 416 bp; C1G10: 403 bp (-13 bp); C1E2: 389 bp (-27 bp); C3bB10: 505 bp (+89 bp); C3bC4: 334 bp (-82 bp). DNA ladder sizes are indicated in base pairs.
(b) Sequencing of *Trem2* cDNA ENSMUST00000132340.1 Intron 1–Exon 2 amplicon from clone C1G10 revealed a 13 bp deletion (dotted box) directly before the p.R47 codon (highlighted blue).

5.4.3 Expression of TREM2 protein in CRISPR/Cas9-edited clonal lines

To confirm TREM2 protein expression in the CRISPR/Cas9-edited clonal lines, Western blots using various commercially available antibodies against human or mouse TREM2 were tested. Their specificity was tested in a range of protein lysates of human and mouse origin. Mature TREM2 is known to be glycosylated at two predicted N-glycosylation sites to result in a total molecular weight of ∼40–60 kDa, while unglycosylated TREM2 is predicted to be ∼25 kDa[379,452]. As the antibodies were raised against recombinant human or mouse TREM2 peptides that may not be glycosylated, the lysates were also deglycosylated to remove all N-linked glycans and expose antibody-binding epitopes. Only antibody AF1729 showed any specificity for TREM2 and only gave a weak signal at the expected molecular weight ∼25 kDa following deglycosylation of the lysates (Figure 5.6e,f). As expected, TREM2 was not expressed in N2A mouse neurons and HEK293 human kidney cell lines whereas TREM2 was detected in BV2 mouse microglia and THP-1 human monocyte cell lines of myeloid origin (Figure 5.6e,f).

Antibody AF1828 appeared to detect specific protein bands at ∼37 kDa that correspond close to the molecular weight of glycosylated TREM2 (>40 kDa). However, there was no shift in molecular weight of protein bands after deglycosylation (Figure 5.6a). This demonstrates that the protein band detected by antibody AF1828 is not a glycosylated protein and is unlikely to be TREM2. The other antibodies resulted in a large number of non-specific protein bands, with or without deglycosylation, with no distinct bands at the expected molecular weight in lysates from cells expected to express TREM2 (Figure 5.6a–d).

Therefore, antibody AF1729 was used to investigate TREM2 expression in the different *Trem2*-edited and CRISPR WT clonal lines. As expected, TREM2 protein was detected in lysates from CRISPR WT clonal lines but was undetectable in the *Trem2*-edited clonal lines that have indels predicted to cause the removal of a few amino acids or change in amino acid sequence (Figure 5.7). Interestingly, TREM2 protein was also not detected in the clonal line with a small in-frame deletion (C1E2) (Figure 5.7) which was expected to result in a loss of 9 amino acids spanning across the p.R47 residue, matching observations from protein-coding transcripts (Table 5.3).

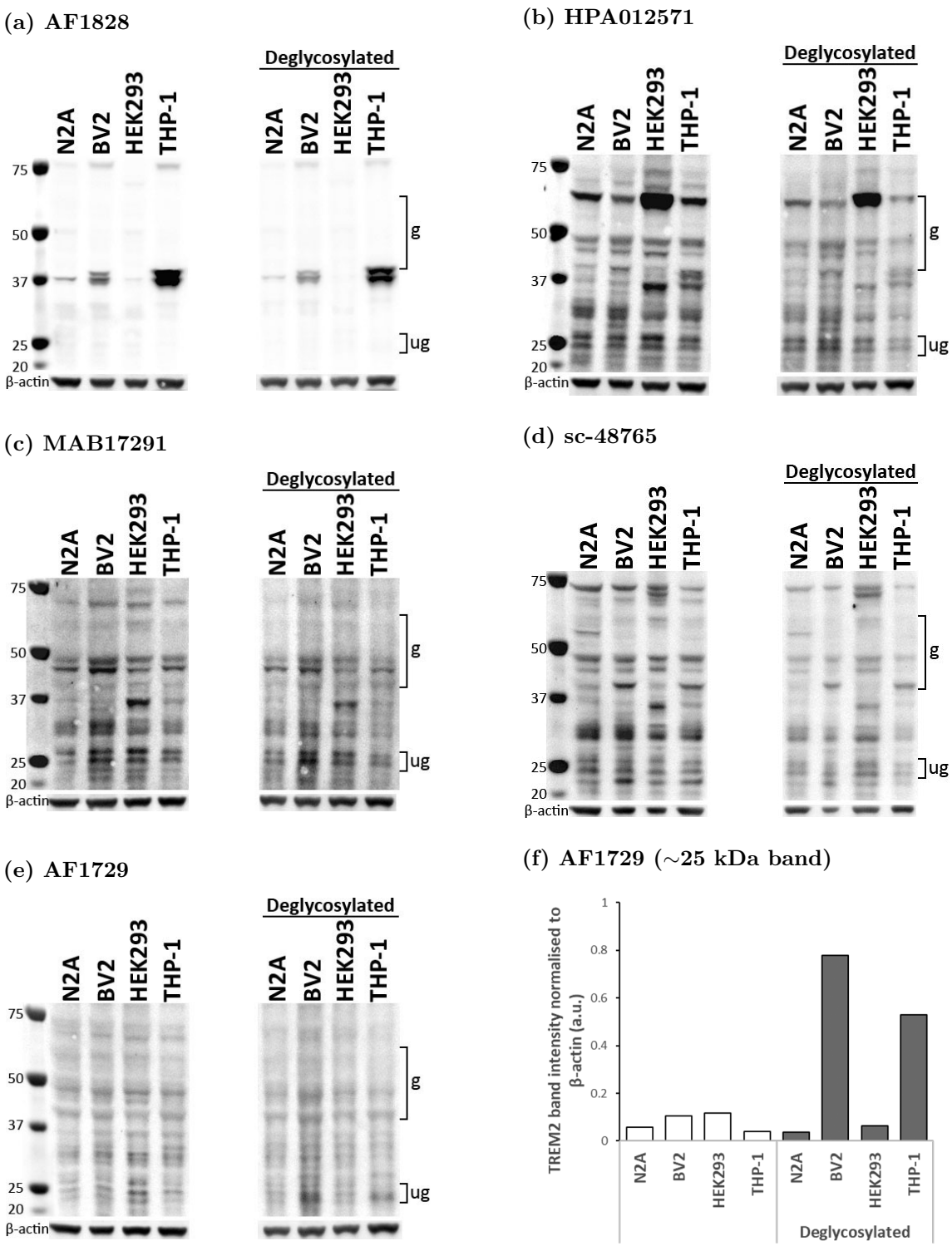

Figure 5.6. Antibody AF1729 showed specificity for TREM2 only after deglycosylation of protein lysates whereas the other antibodies were not specific for TREM2

30 µg of positive (mouse BV2 & human THP-1) and negative (mouse N2A & human HEK293), untreated and deglycosylated protein lysates were used to test the specificity of anti TREM2 antibodies **(a)** AF1828, **(b)** HPA012571, **(c)** MAB17291, **(d)** sc-48765 and **(e)** AF1729 on Western blots.

Molecular weight of glycosylated TREM2 (g): ~40–60 kDa and unglycosylated TREM2 (ug): ~25 kDa. Protein molecular weight ladder is indicated in kDa.

(f) TREM2 band intensity at ~25 kDa from deglycosylated BV2 and THP-1 lysates detected using AF1729 is distinctively higher than background in negative control lysates.

(a)

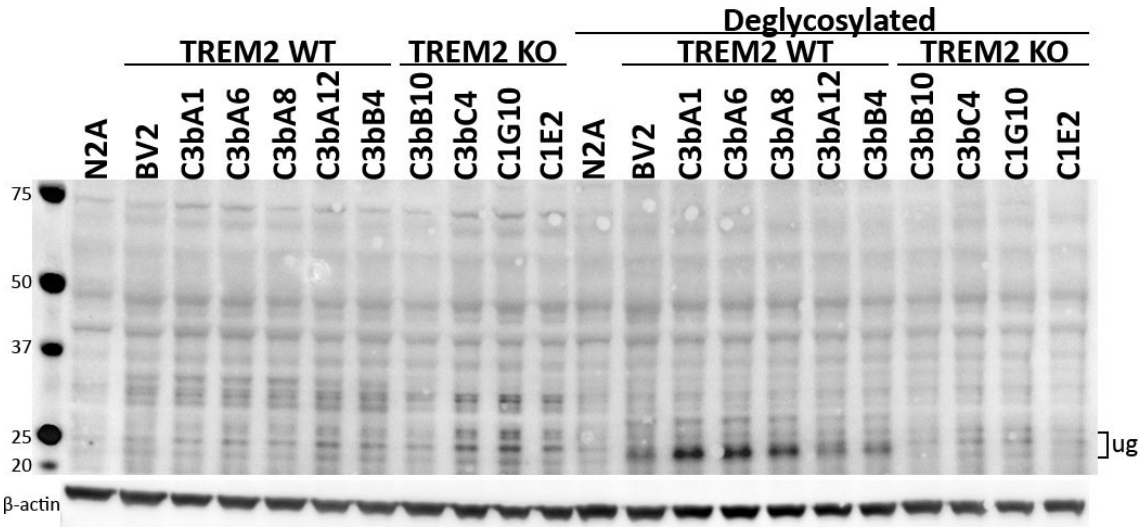

(b) Deglycosylated protein lysates (∼25 kDa band)

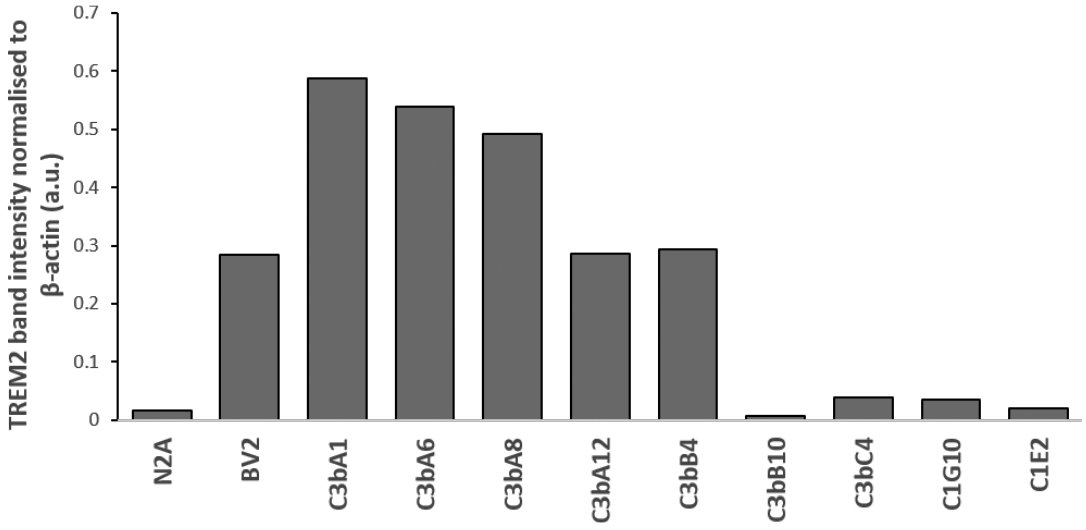

Figure 5.7. TREM2 protein was detected in CRISPR WT clonal lines but not in TREM2 KO clonal lines.
(a) 30 µg of untreated and deglycosylated protein lysates from TREM2 WT cell lines (BV2 WT and CRISPR WT clones) and TREM2 KO clonal lines were immunoblotted for TREM2 using anti-mouse TREM2 antibody AF1729. Unglycosylated mouse TREM2 (ug) is ∼25 kDa. Protein molecular weight ladder is indicated in kDa.
(b) TREM2 band intensity corresponding to blot **(a)** at ∼25 kDa from deglycosylated BV2 WT and CRISPR WT clones detected using AF1729 is distinctively higher than background in negative control lysates and TREM2 KO clonal lines.

5.4.4 Summary of CRISPR BV2 clones

Table 5.3 summarises *Trem2* Exon 2 DNA, full-length *Trem2* cDNA and TREM2 amino acid sequences of TREM2 KO and CRISPR WT clonal lines. Full-length *Trem2* cDNA sequences were predicted from Sanger-sequenced *Trem2* Exon 2 DNA or protein-coding transcripts converted into cDNA. Full-length TREM2 amino acid sequence was translated from predicted full-length *Trem2* cDNA sequence.

Clone ID	TREM2 sequence	
WT (refseq)	Exon 2 DNA (5'→3')	ATTCTAGAGCCCGTCAGGGAGTCAGTCATTAACCATCTTGCACACGCATGAGATATTCTGTTTCAAACAAAA AGTGGAAGGTACCCAAGGACCAGAACTTATCCTAATGACCATGCACACGCTATGCTCCCTGCACTCCTGGAA CTGCTTCCAAGCAAGTGGCTGTCTCCTCTGCAGCCCTGTCCCAAGCCCTCAACACCACGGTGCTGCAGGGCA TGGCCGGCCAGTCCTTGAGGGTGTCATGTACTTATGACGCCTTGAAGCACTGGGGGAGA**CGC**AAGGCCTGGT GTCGGCAGCTGGGTGAGGAGGGCCCATGCCAGCGTGTGGTGAGCACACACGGTGTGTGGCTGCTGGCCTTCC TGAAGAAGCGGAATGGGAGCACAGTCATCGCAGATGACACCCTTGCTGGAACCGTCACCATCACTCTGAAGA ACCTCCAAGCCGGTGACGCGGGCCTCTACCAGTGTCAGAGTCTCCGAGGCCGAGAGGCTGAGGTCCTGCAGA AAGTACTGGTGGAGGTGCTGGAGGGTGAGTACACAGTAGCTGGGTGCACCTTTGGCTGGTCCTTGTGCCAGG TCTTATTGTTGTGGGACTTTTTCAGGGGGA
	Full-length cDNA (5'→3')	ATGGGACCTCTCCACCAGTTTCTCCTGCTGCTGATCACAGCCCTGTCCCAAGCCCTCAACACCACGGTGCTG CAGGGCATGGCCGGCCAGTCCTTGAGGGTGTCATGTACTTATGACGCCTTGAAGCACTGGGGGAGA**CGC**AAG GCCTGGTGTCGGCAGCTGGGTGAGGAGGGCCCATGCCAGCGTGTGGTGAGCACACACGGTGTGTGGCTGCTG GCCTTCCTGAAGAAGCGGAATGGGAGCACAGTCATCGCAGATGACACCCTTGCTGGAACCGTCACCATCACT CTGAAGAACCTCCAAGCCGGTGACGCGGGCCTCTACCAGTGTCAGAGTCTCCGAGGCCGAGAGGCTGAGGTC CTGCAGAAAGTACTGGTGGAGGTGCTGGAGGACCCTCTAGATGACCAAGATGCTGGAGATCTCTGGGTCCCC GAGGAGTCATCGAGTTTCGAGGGTGCCCAAGTGGAACACAGCACCTCCAGGAATCAAGAGACCTCCTTCCCA CCCACCTCCATTCTTCTCCTCCTGGCCTGCGTTCTCCTGAGCAAGTTTCTTGCAGCCAGCATCCTCTGGGCT GTGGCCAGGGGCAGGCAGAAGCCGGGAACACCTGTGGTCAGAGGGCTGGACTGTGGCCAAGATGCTGGGCAC CAACTTCAGATCCTCACTGGACCCGGAGGTACGTGA
	Amino acid (N→C-terminus)	MGPLHQFLLLLITALSQALNTTVLQGMAGQSLRVSCTYDALKHWGR**R**KAWCRQLGEEGPCQRVVSTHGVWLL AFLKKRNGSTVIADDTLAGTVTITLKNLQAGDAGLYQCQSLRGREAEVLQKVLVEVLEDPLDDQDAGDLWVP EESSSFEGAQVEHSTSRNQETSFPPTSILLLLACVLLSKFLAASILWAVARGRQKPGTPVVRGLDCGQDAGH QLQILTGPGGT
C3bA1	WT	
C3bA6	WT	
C3bA8	WT	
C3bA12	WT	
C3bB4	WT	

Continued on next page...

Clone ID	TREM2 sequence	
C1G10-1	Exon 2 DNA (5'→3')	ATTCTAGAGCCCGTCAGGGAGTCAGTCATTAACCATCTTGCACACGCATGAGATATTCTGTTTCAAACAAAA AGTGGAAGGTACCCAAGGACCAGAA---------- ---------- ---------- ---------- ---------- ----------AGTCCTGCAGAAAGT ACTGGTGGAGGTGCTGGAGGGTGAGTACACAGTAGCTGGGTGCACCTTTGGCTGGTCCTTGTGCCAGGTCTT ATTGTTGTGGGACTTTTTCAGGGGGA
	Full-length cDNA (5'→3')	ATGGGACCTCTCCACCAGTTTCTCCTGCTGCTGATCACAG---------- ---------- ---------- ---------- ----------AGTCCTG CAGAAAGTACTGGTGGAGGTGCTGGAGGACCCTCTAGATGACCAAGATGCTGGAGATCTCTGGGTCCCCGAG GAGTCATCGAGTTTCGAGGGTGCCCAAGTGGAACACAGCACCTCCAGGAATCAAGAGACCTCCTTCCCACCC ACCTCCATTCTTCTCCTCCTGGCCTGCGTTCTCCTGAGCAAGTTTCTTGCAGCCAGCATCCTCTGGGCTGTG GCCAGGGGCAGGCAGAAGCCGGGAACACCTGTGGTCAGAGGGCTGGACTGTGGCCAAGATGCTGGGCACCAA CTTCAGATCCTCACTGGACCCGGAGGTACGTGA
	Amino acid (N→C-terminus)	MGPLHQFLLLLITGPAESTGGGAGGPSRXPRCWRSLGPRGVIEFRGCPSGTQHLQESRDLLPTHLHSSPPGL RSPEQVSCSQHPLGCGQGQAEAGNTCGQRAGLWPRCWAPTSDPHWTRRYV
C1G10-2	Exon 2 DNA (5'→3')	ATTCTAGAGCCCGTCAGGGAGTCAGTCATTAACCATCTTGCACACGCATGAGATATTCTGTTTCAAACAAAA AGTGGAAGGTACCCAAGGACCAGAACTTATCCTAATGACCATGCACACGCTATGCTCCCTGCACTCCTGGAA CTGCTTCCAAGCAAGTGGCTGTCTCCTCTGCAGCCCTGTCCCAAGCCCTCAACACCACGGTGCTGCAGGGCA TGGCCGGCCAGTCCTTGAGGGTGTCATGTACTTATGACGCCTTGAA----------**CGC**AAGGCCTGGT GTCGGCAGCTGGGTGAGGAGGGCCCATGCCAGCGTGTGGTGAGCACACACGGTGTGTGGCTGCTGGCCTTCC TGAAGAAGCGGAATGGGAGCACAGTCATCGCAGATGACACCCTTGCTGGAACCGTCACCATCACTCTGAAGA ACCTCCAAGCCGGTGACGCGGGCCTCTACCAGTGTCAGAGTCTCCGAGGCCGAGAGGCTGAGGTCCTGCAGA AAGTACTGGTGGAGGTGCTGGAGGGTGAGTACACAGTAGCTGGGTGCACCTTTGGCTGGTCCTTGTGCCAGG TCTTATTGTTGTGGGACTTTTTCAGGGGGA
	Full-length cDNA (5'→3')	ATGGGACCTCTCCACCAGTTTCTCCTGCTGCTGATCACAGCCCTGTCCCAAGCCCTCAACACCACGGTGCTG CAGGGCATGGCCGGCCAGTCCTTGAGGGTGTCATGTACTTATGACGCCTTGAA----------**CGC**AAG GCCTGGTGTCGGCAGCTGGGTGAGGAGGGCCCATGCCAGCGTGTGGTGAGCACACACGGTGTGTGGCTGCTG GCCTTCCTGAAGAAGCGGAATGGGAGCACAGTCATCGCAGATGACACCCTTGCTGGAACCGTCACCATCACT CTGAAGAACCTCCAAGCCGGTGACGCGGGCCTCTACCAGTGTCAGAGTCTCCGAGGCCGAGAGGCTGAGGTC CTGCAGAAAGTACTGGTGGAGGTGCTGGAGGACCCTCTAGATGACCAAGATGCTGGAGATCTCTGGGTCCCC GAGGAGTCATCGAGTTTCGAGGGTGCCCAAGTGGAACACAGCACCTCCAGGAATCAAGAGACCTCCTTCCCA CCCACCTCCATTCTTCTCCTCCTGGCCTGCGTTCTCCTGAGCAAGTTTCTTGCAGCCAGCATCCTCTGGGCT GTGGCCAGGGGCAGGCAGAAGCCGGGAACACCTGTGGTCAGAGGGCTGGACTGTGGCCAAGATGCTGGGCAC CAACTTCAGATCCTCACTGGACCCGGAGGTACGTGA
	Amino acid (N→C-terminus)	MGPLHQFLLLLITALSQALNTTVLQGMAGQSLRVSCTYDALNARPGVGSWVRRAHASVW**X**AHTVCGCWPSXR SGMGAQSSQMTPLLEPSPSLXRTSKPVTRASTSVRVSEAERLRSCRKYWWRCWRTLXMTKMLEISGSPRSHR VSRVPKWNTAPPGIKRPPSHPPPFFSSWPAFSXASFLQPASSGLWPGAGRSREHLWSEGWTVAKMLGTNFRS SLDPEVR

Continued on next page...

Clone ID	TREM2 sequence	
C1E2	Exon 2 DNA (5'→3')	ATTCTAGAGCCCGTCAGGGAGTCAGTCATTAACCATCTTGCACACGCATGAGATATTCTGTTTCAAACAAAA AGTGGAAGGTACCCAAGGACCAGAACTTATCCTAATGACCATGCACACGCTATGCTCCCTGCACTCCTGGAA CTGCTTCCAAGCAAGTGGCTGTCTCCTCTGCAGCCCTGTCCCAAGCCCTCAACACCACGGTGCTGCAGGGCA TGGCCGGCCAGTCCTTGAGGGTGTCATGTACTTATGACGCCTTG----------T GTCGGCAGCTGGGTGAGGAGGGCCCATGCCAGCGTGTGGTGAGCACACACGGTGTGTGGCTGCTGGCCTTCC TGAAGAAGCGGAATGGGAGCACAGTCATCGCAGATGACACCCTTGCTGGAACCGTCACCATCACTCTGAAGA ACCTCCAAGCCGGTGACGCGGGCCTCTACCAGTGTCAGAGTCTCCGAGGCCGAGAGGCTGAGGTCCTGCAGA AAGTACTGGTGGAGGTGCTGGAGGGTGAGTACACAGTAGCTGGGTGCACCTTTGGCTGGTCCTTGTGCCAGG TCTTATTGTTGTGGGACTTTTTCAGGGGGA
	Full-length cDNA (5'→3')	ATGGGACCTCTCCACCAGTTTCTCCTGCTGCTGATCACAGCCCTGTCCCAAGCCCTCAACACCACGGTGCTG CAGGGCATGGCCGGCCAGTCCTTGAGGGTGTCATGTACTTATGACGCCTTG---------- ------TGTCGGCAGCTGGGTGAGGAGGGCCCATGCCAGCGTGTGGTGAGCACACACGGTGTGTGGCTGCTG GCCTTCCTGAAGAAGCGGAATGGGAGCACAGTCATCGCAGATGACACCCTTGCTGGAACCGTCACCATCACT CTGAAGAACCTCCAAGCCGGTGACGCGGGCCTCTACCAGTGTCAGAGTCTCCGAGGCCGAGAGGCTGAGGTC CTGCAGAAAGTACTGGTGGAGGTGCTGGAGGACCCTCTAGATGACCAAGATGCTGGAGATCTCTGGGTCCCC GAGGAGTCATCGAGTTTCGAGGGTGCCCAAGTGGAACACAGCACCTCCAGGAATCAAGAGACCTCCTTCCCA CCCACCTCCATTCTTCTCCTCCTGGCCTGCGTTCTCCTGAGCAAGTTTCTTGCAGCCAGCATCCTCTGGGCT GTGGCCAGGGGCAGGCAGAAGCCGGGAACACCTGTGGTCAGAGGGCTGGACTGTGGCCAAGATGCTGGGCAC CAACTTCAGATCCTCACTGGACCCGGAGGTACGTGA
	Amino acid (N→C-terminus)	MGPLHQFLLLLITALSQALNTTVLQGMAGQSLRVSCTYDAL---------CRQLGEEGPCQRVVSTHGVWLL AFLKKRNGSTVIADDTLAGTVTITLKNLQAGDAGLYQCQSLRGREAEVLQKVLVEVLEDPLDDQDAGDLWVP EESSSFEGAQVEHSTSRNQETSFPPTSILLLLACVLLSKFLAASILWAVARGRQKPGTPVVRGLDCGQDAGH QLQILTGPGGT
C3bB10	Exon 2 DNA (5'→3')	ATTCTAGAGCCCGTCAGGGAGTCAGTCATTAACCATCTTGCACACGCATGAGATATTCTGTTTCAAACAAAA AGTGGAAGGTACCCAAGGACCAGAACTTATCCTAATGACCATGCACACGCTATGCTCCCTGCACTCCTGGAA CTGCTTCCAAGCAAGTGGCTGTCTCCTCTGCAGCCCTGTCCCAAGCCCTCAACACCACGGTGCTGTGGGACT CTTGTTCTCATGAGTTCTTACACATTGCGATGCACGACTGTAATAAGAGACCTTTGAACTCTGATTCTTAGC ATCATTTCTAGAAAAGAGAGAAAAGTGAAGAACAATGAAAATATTATTGGAACATACCACAATTTTTTAAAT ACATGGGATGATTTGGTGTCGGCAGCTGGGTGAGGAGGGCCCATGCCAGCGTGTGGTGAGCACACACGGTGT GTGGCTGCTGGCCTTCCTGAAGAAGCGGAATGGGAGCACAGTCATCGCAGATGACACCCTTGCTGGAACCGT CACCATCACTCTGAAGAACCTCCAAGCCGGTGACGCGGGCCTCTACCAGTGTCAGAGTCTCCGAGGCCGAGA GGCTGAGGTCCTGCAGAAAGTACTGGTGGAGGTGCTGGAGGGTGAGTACACAGTAGCTGGGTGCACCTTTGG CTGGTCCTTGTGCCAGGTCTTATTGTTGTGGGACTTTTTCAGGGGGA
	Full-length cDNA (5'→3')	ATGGGACCTCTCCACCAGTTTCTCCTGCTGCTGATCACAGCCCTGTCCCAAGCCCTCAACACCACGGTGCTG TGGGACTCTTGTTCTCATGAGTTCTTACACATTGCGATGCACGACTGTAATAAGAGACCTTTGAACTCTGAT TCTTAGCATCATTTCTAGAAAAGAGAGAAAAGTGAAGAACAATGAAAATATTATTGGAACATACCACAATTT TTTAAATACATGGGATGATTTGGTGTCGGCAGCTGGGTGAGGAGGGCCCATGCCAGCGTGTGGTGAGCACAC ACGGTGTGTGGCTGCTGGCCTTCCTGAAGAAGCGGAATGGGAGCACAGTCATCGCAGATGACACCCTTGCTG GAACCGTCACCATCACTCTGAAGAACCTCCAAGCCGGTGACGCGGGCCTCTACCAGTGTCAGAGTCTCCGAG GCCGAGAGGCTGAGGTCCTGCAGAAAGTACTGGTGGAGGTGCTGGAGGACCCTCTAGATGACCAAGATGCTG GAGATCTCTGGGTCCCCGAGGAGTCATCGAGTTTCGAGGGTGCCCAAGTGGAACACAGCACCTCCAGGAATC AAGAGACCTCCTTCCCACCCACCTCCATTCTTCTCCTCCTGGCCTGCGTTCTCCTGAGCAAGTTTCTTGCAG CCAGCATCCTCTGGGCTGTGGCCAGGGGCAGGCAGAAGCCGGGAACACCTGTGGTCAGAGGGCTGGACTGTG GCCAAGATGCTGGGCACCAACTTCAGATCCTCACTGGACCCGGAGGTACGTGA
	Amino acid (N→C-terminus)	MGPLHQFLLLLITALSQALNTTVLWDSCSHEFLHIAMHDCNKRPLNSDSXHHFXKREKSEEQXKYYWNIPQF FKYMGXFGVGSWVRRAHASVWXAHTVCGCWPSXRSGMGAQSSQMTPLLEPSPSLXRTSKPVTRASTSVRVSE AERLRSCRKYWWRCWRTLXMTKMLEISGSPRSHRVSRVPKWNTAPPGIKRPPSHPPPFFSSWPAFSXSFLQP ASSGLWPGAGRSREHLWSEGWTVAKMLGTNFRSSLDPEVR

Continued on next page...

Clone ID	TREM2 sequence	
C3bC4	Exon 2 DNA (5'→3')	ATTCTAGAGCCCGTCAGGGAGTCAGTCATTAACCATCTTGCACACGCATGAGATATTCTGTTTCAAACAAAA AGTGGAAGGTACCCAAGGACCAGAACTTATCCTAATGACCATGCACACGCTATGCTCCCTGCACTCCTGGAA CTGCTTCCAAGCAAGTGGCTGTCTCCTC----- ----------GCCTTGAAGCACTGGGGGAGA**CGC**AAGGCCTGGT GTCGGCAGCTGGGTGAGGAGGGCCCATGCCAGCGTGTGGTGAGCACACACGGTGTGTGGCTGCTGGCCTTCC TGAAGAAGCGGAATGGGAGCACAGTCATCGCAGATGACACCCTTGCTGGAACCGTCACCATCACTCTGAAGA ACCTCCAAGCCGGTGACGCGGGCCTCTACCAGTGTCAGAGTCTCCGAGGCCGAGAGGCTGAGGTCCTGCAGA AAGTACTGGTGGAGGTGCTGGAGGGTGAGTACACAGTAGCTGGGTGCACCTTTGGCTGGTCCTTGTGCCAGG TCTTATTGTTGTGGGACTTTTTCAGGGGGA
	Full-length cDNA (5'→3')	ATGGGACCTCTCCACCAGTTTCTCCTGCTGCTGATCACAG---------- ----------CGCCTTGAAGCACTGGGGGAGA**CGC**AAG GCCTGGTGTCGGCAGCTGGGTGAGGAGGGCCCATGCCAGCGTGTGGTGAGCACACACGGTGTGTGGCTGCTG GCCTTCCTGAAGAAGCGGAATGGGAGCACAGTCATCGCAGATGACACCCTTGCTGGAACCGTCACCATCACT CTGAAGAACCTCCAAGCCGGTGACGCGGGCCTCTACCAGTGTCAGAGTCTCCGAGGCCGAGAGGCTGAGGTC CTGCAGAAAGTACTGGTGGAGGTGCTGGAGGACCCTCTAGATGACCAAGATGCTGGAGATCTCTGGGTCCCC GAGGAGTCATCGAGTTTCGAGGGTGCCCAAGTGGAACACAGCACCTCCAGGAATCAAGAGACCTCCTTCCCA CCCACCTCCATTCTTCTCCTCCTGGCCTGCGTTCTCCTGAGCAAGTTTCTTGCAGCCAGCATCCTCTGGGCT GTGGCCAGGGGCAGGCAGAAGCCGGGAACACCTGTGGTCAGAGGGCTGGACTGTGGCCAAGATGCTGGGCAC CAACTTCAGATCCTCACTGGACCCGGAGGTACGTGA
	Amino acid (N→C-terminus)	MGPLHQFLLLLITAP**X**STGGDARPGVGSWVRRAHASVWXAHTVCGCWPSXRSGMGAQSSQMTPLLEPSPSLX RTSKPVTRASTSVRVSEAERLRSCRKYWWRCWRTLXMTKMLEISGSPRSHRVSRVPKWNTAPPGIKRPPSHP PPFFSSWPAFSXASFLQPASSGLWPGAGRSREHLWSEGWTVAKMLGTNFRSSLDPEVR

Table 5.3. *Trem2* Exon 2 DNA, predicted full-length *Trem2* cDNA and predicted full-length TREM2 amino acid sequences of TREM2 KO and CRISPR WT clones.

Trem2 Exon 2 DNA sequence was determined by Sanger sequencing. Full-length *Trem2* cDNA sequence was predicted from Sanger-sequenced *Trem2* Exon 2 DNA or cDNA. Full-length TREM2 amino acid sequence was translated from predicted full-length *Trem2* cDNA sequence. C1G10-1 and C1G10-2 represent the two different deletions identified in this cell line.

Legend:

DNA: Intron (cyan), *Trem2* Exon 2 (black), mismatch/insertion (red), p.R47 codon (bold), target c.140G for DNA variant (underline).

cDNA: Alternating exons (black/blue), mismatch/insertion (red), p.R47 codon (bold), target c.140G for DNA variant (underline).

Amino acid: Alternating exons (black/blue), residue overlap splice site (green), p.R47 residue (underline), frameshifted amino acids (orange), first stop codon (red).

5.4.5 Functional characterisation of TREM2 knockout clonal lines

To characterise the effects of TREM2 deficiency on the activation of signalling mediators downstream of TREM2, four of each TREM2 KO (C1G10, C1E2, C3bB10, C3bC4) and TREM2 WT (BV2 WT, C3bA1, C3bA6, C3bA8) cell lines were stimulated with plate-coated isotype control or TREM2-activating antibodies (MAB17291, R&D Systems) for 1 h. The amount of plate-bound antibodies in each well was checked for consistent antibody stimulation. As expected, fluorescence intensities were higher in isotype control (pairwise comparison ANOVA: $p<0.001$) and TREM2-activating antibody (pairwise comparison ANOVA: $p<0.001$) coated wells compared to uncoated wells (Figure 5.8). This indicates that the isotype control and TREM2-activating antibodies successfully bound to and coated the plates. TREM2-activating antibody-coated wells had consistently and significantly higher fluorescence intensity compared to isotype control antibody-coated wells (pairwise comparison ANOVA: $p=0.006$) (Figure 5.8), demonstrating a higher concentration of the TREM2-activating antibody than isotype control antibody were available for binding in those wells. This have implications for any direct comparison of results obtained between these two antibodies.

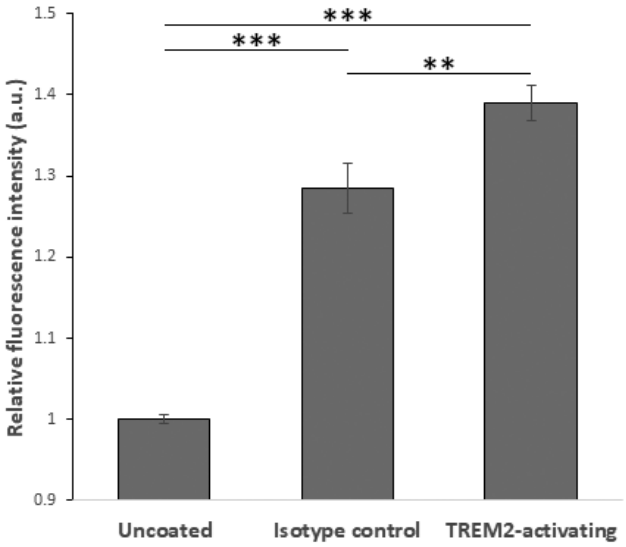

Figure 5.8. Isotype control and TREM2-activating antibody (MAB17291) successfully bound to and coated the plates.
More of the TREM2-activating antibody coated the 6-well plates compared to the isotype control antibody although the same concentration of antibodies (10 µg/mL) was used during the coating procedure. The relative amount of plate-bound antibodies was determined using fluorescent secondary antibodies against rat IgG and fluorescence intensity measured on a plate reader. Error bars indicate standard error of the mean for n=10 wells per condition.

Activation of Syk, Pyk2 and Erk1/2 (ratio of phospho-protein:total protein) between TREM2 KO and TREM2 WT cells when stimulated with the TREM2-activating antibody or isotype control antibody were not statistically different (Figure 5.9, 5.10a,b,c).

However, Pyk2 activation in TREM2 KO and TREM2 WT cells when treated with the TREM2-activating antibody were increased compared to isotype control antibody (pairwise comparison ANOVA: TREM2 KO p=0.001, TREM2 WT p=0.001; Figure 5.9, 5.10b). Similarly, Erk1/2 activation in TREM2 KO cells was significantly increased (pairwise comparison ANOVA: p=0.008) and in TREM2 WT cells showed an increasing trend when treated with the TREM2-activating antibody compared to isotype control antibody (Figure 5.9, 5.10c). Syk activation in TREM2 KO and TREM2 WT cells were not increased by treatment with TREM2-activating antibody compared to isotype control antibody (Figure 5.9, 5.10a).

Interestingly, Pyk2 activation in TREM2 KO cells when stimulated with the isotype control antibody was increased compared to uncoated wells (pairwise comparison ANOVA: p=0.006; Figure 5.9, 5.10b). Nevertheless, as expected, activation of Syk, Pyk2 and Erk1/2 in TREM2 WT cells between treatment of the isotype control antibody and uncoated wells were not statistically different (Figure 5.9, 5.10a,b,c).

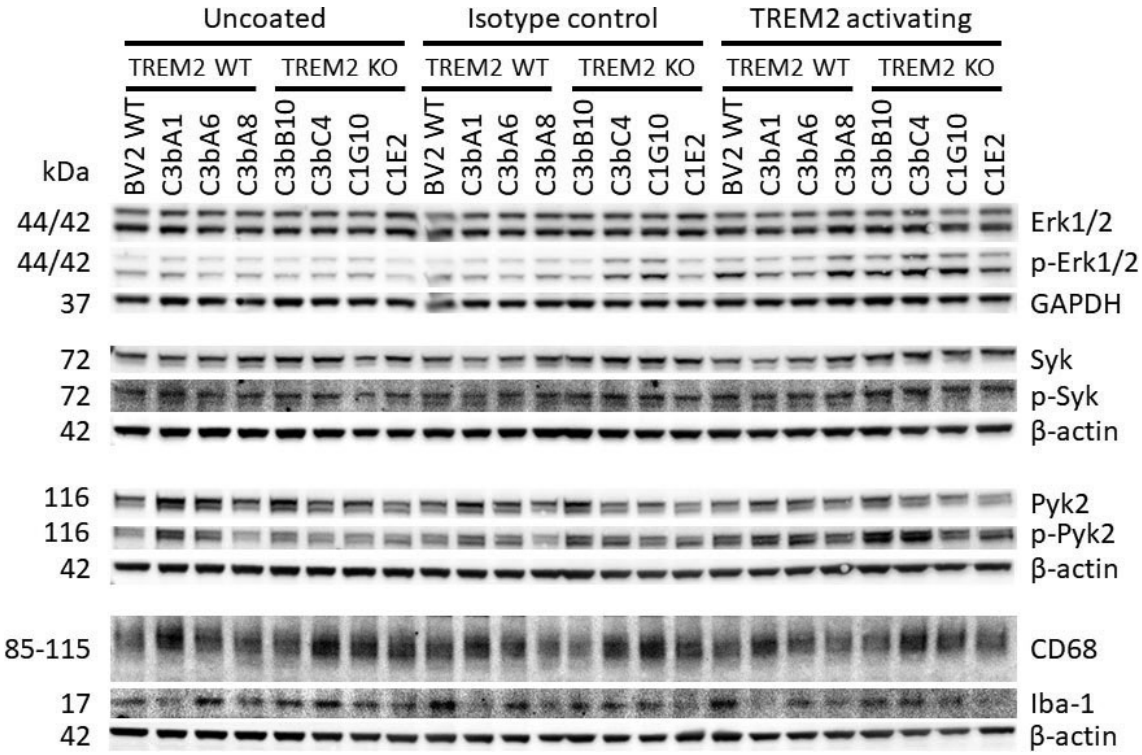

Figure 5.9. Western blots of all proteins probed from protein lysates of TREM2 KO and TREM2 WT cell lines after stimulation with the TREM2-activating antibody or isotype control antibody.

1 million cells per TREM2 WT or TREM2 KO cell line were stimulated with the antibodies for 1 h at 37°C. Total and phospho-proteins were probed on the same membrane using different fluorescent secondary antibodies for Syk, Pyk2 and Erk1/2. CD68 and Iba-1 were similarly probed on the same membrane. Exposure for each detection antibody was individually adjusted.

(a) Syk activation

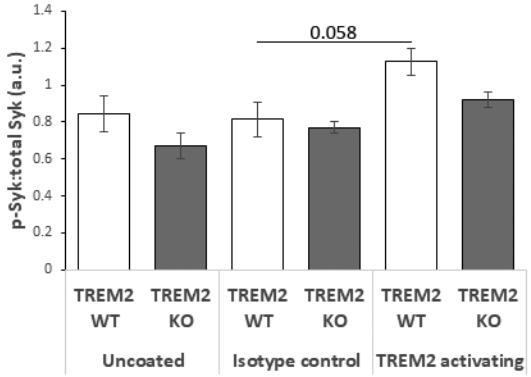

(b) Pyk2 activation

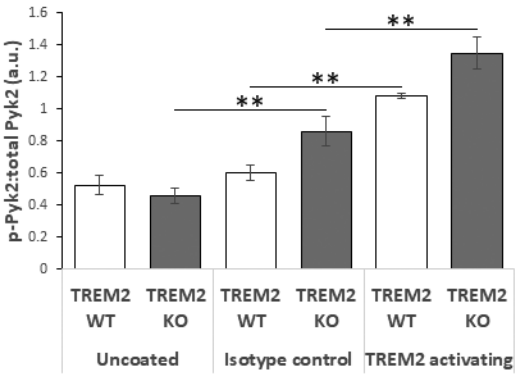

(c) Erk1/2 activation

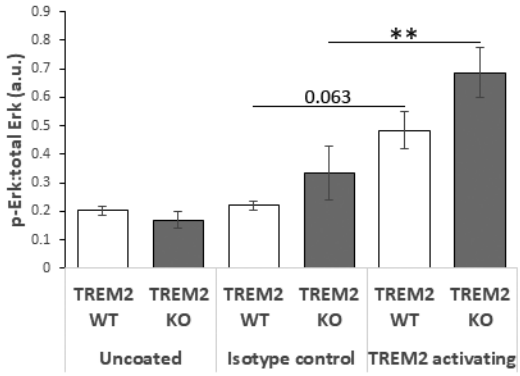

Figure 5.10. Activation of Syk, Pyk2 and Erk1/2 were not statistically different between TREM2 KO and TREM2 WT cells when stimulated with the TREM2-activating antibody.

Overall, activation of **(a)** Syk, **(b)** Pyk2 and **(c)** Erk1/2 were not statistically different between TREM2 KO and TREM2 WT cells when treated with the TREM2-activating antibody, isotype control antibody or uncoated wells.

Error bars indicate standard error of the mean for n=4 different cell lines per phenotype.
**: $p<0.01$

Differences in activation between the TREM2-activating antibody and isotype control antibody may be explained by differences in plate-bound antibody titre. Therefore, activation levels were normalised to the relative amount of plate-bound antibodies. In the normalised data, activation of Syk, Pyk2 and Erk1/2 between TREM2 KO and TREM2 WT cells when stimulated with the TREM2-activating antibody were still not statistically different (Figure 5.11a,b,c).

Pyk2 activation when treated with the isotype control antibody was higher in TREM2 KO cells compared to TREM2 WT cells (pairwise comparison ANOVA: p=0.030; Figure 5.11b). Activation of Syk and Erk1/2 when treated with the isotype control antibody were not different between TREM2 KO and TREM2 WT cells.

Pyk2 activation in TREM2 KO and TREM2 WT cells when treated with the TREM2-activating antibody remain higher than isotype control antibody (pairwise comparison ANOVA: TREM2 KO p=0.032, TREM2 WT p=0.016; Figure 5.11b). Activation of Syk and Erk1/2 in TREM2 KO and TREM2 WT cells after treatment with the TREM2-activating antibody were not different compared to isotype control antibody (Figure 5.11a,c).

(a) Syk activation

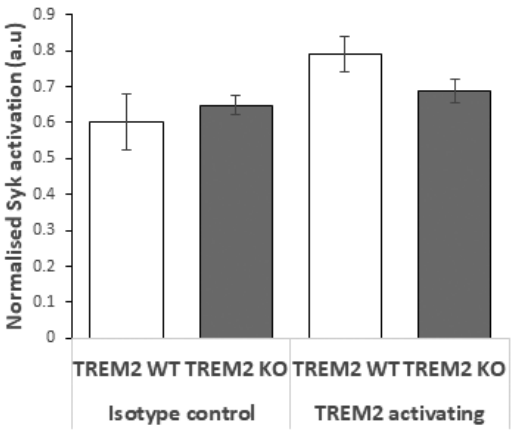

(b) Pyk2 activation

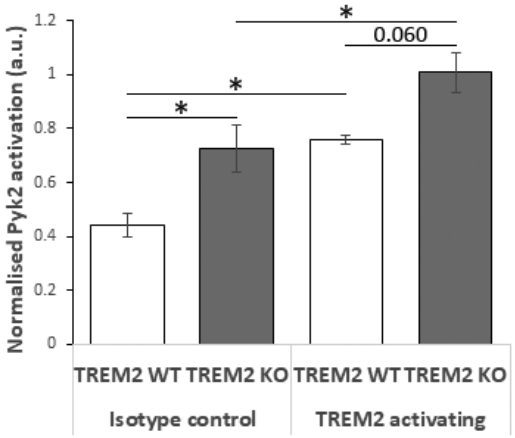

(c) Erk1/2 activation

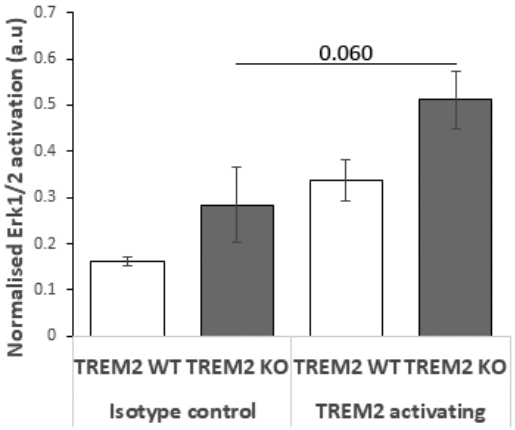

Figure 5.11. Activation of Pyk2 but not Syk and Erk1/2 in TREM2 KO and TREM2 WT cells were higher when stimulated with the TREM2-activating antibody compared to isotype control antibody.
Activation of **(a)** Syk, **(b)** Pyk2 and **(c)** Erk1/2 (phospho-protein:total protein) were normalised to the relative amount of plate-bound antibodies.
Error bars indicate standard error of the mean for n=4 different cell lines per phenotype.
*: $p<0.05$

Chapter 4 showed that CD68 expression and HLA-DP, -DQ, -DR-expressing cells were lower in hippocampal CA4 of AD cases with a TREM2 variant, particularly p.R47H, compared to AD cases without TREM2 variants. This is despite similar numbers of Iba-1-expressing cells between AD cases with or without a TREM2 variant. Therefore, mouse homologues of the same functional markers used were investigated in TREM2 KO cells to determine if the outcome of functional loss of TREM2 were comparable. CD68/macrosialin and Iba-1 expression in TREM2 KO and TREM2 WT cells when stimulated with TREM2-activating antibody, isotype control antibody or uncoated wells were similar (Figure 5.9,5.12). MHC class II expression could not be determined as the primary antibody used was unable to reliably detect MHC class II (not shown).

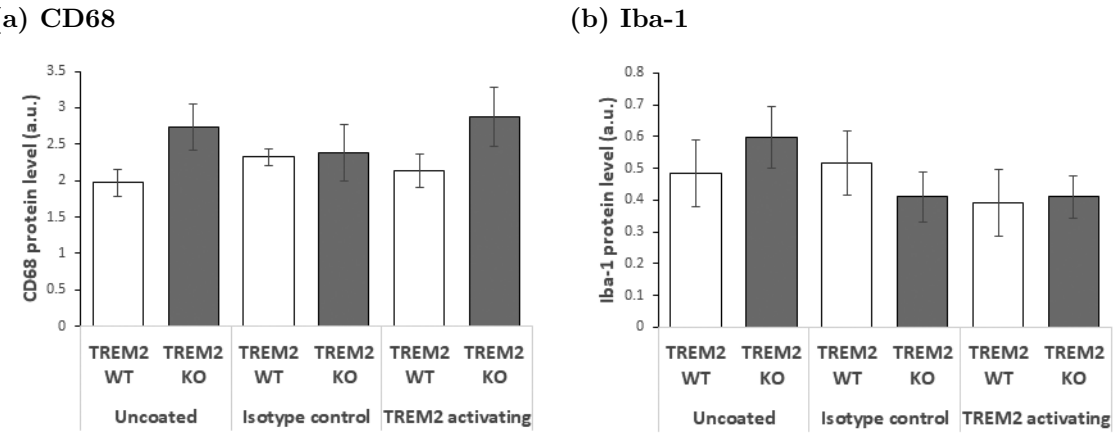

Figure 5.12. Functional microglial markers CD68 and Iba-1 in TREM2 KO and TREM2 WT cells were unaffected by stimulation with the TREM2-activating antibody or isotype control antibody.
Protein levels of **(a)** CD68 and **(b)** Iba-1 were normalised to β-actin band intensities. Error bars indicate standard error of the mean for n=4 different cell lines per phenotype.

5.5 Discussion

Four clonal microglia cell lines with functional loss of TREM2 were successfully generated. In these cell lines, indels in the *Trem2* gene led to protein-coding *Trem2* transcripts being completely disrupted and an absence of TREM2 protein expression compared to cell lines with normal *Trem2* gene.

The effects of TREM2 deficiency on the activation of Syk, Pyk2 and Erk1/2 after stimulation with a TREM2-activating antibody was then investigated. Antibody-mediated TREM2 activation additionally appeared to activate FcγR that signal through the same intermediate signalling proteins as TREM2. Stimulation of TREM2 KO cells with the TREM2-activating antibody resulted in similar activation of Syk, Pyk2 and Erk1/2 compared to TREM2 WT cells. This indicates that either the TREM2-activating antibody had no effect on activating TREM2 or it similarly activates Syk, Pyk2 and Erk1/2 through a TREM2-independent effect. Since Pyk2 activation was higher in TREM2 WT cells when stimulated with the TREM2-activating antibody compared to the isotype control antibody even after normalising for antibody titre, this demonstrates that the TREM2-activating antibody does have an effect on TREM2 activation.

Normally, non-specific IgG antibodies have limited biological function and thus have been used as isotype control antibodies in antibody-based receptor activation experiments. However, immune cells such as microglia express Fc-γ receptors (FcγR) that can bind to the Fc region of IgG antibodies and trigger FcγR responses. TREM2 and FcγR share common signal transduction mechanisms downstream of receptor activation. Like TREM2–DAP12, activated FcγR signals through ITAMs on the Fc receptor γ-chain (FcRγ; not to be confused with FcγR)[724–726]. Subsequently, Syk is also recruited to phosphorylated ITAMs on the FcRγ and activates downstream signalling cascades. As the isotype control and TREM2 activating antibody used in the present study have intact IgG Fc region, this may explain the activation of Pyk2 and Erk1/2 by the TREM2-activating antibody in TREM2 KO cells.

Unexpectedly, stimulation with the TREM2-activating antibody or isotype control antibody resulted in a slight increase (but not statistically significant) of Pyk2 activation and to a smaller extent Erk1/2 activation in TREM2 KO cells compared to TREM2 WT cells.

This suggests that not only do these antibodies appear to activate downstream signalling independent of TREM2 but this effect is enhanced by the loss of TREM2. Considering that the activation of Pyk2 and Erk1/2 by the antibodies in TREM2 KO cells can be due to FcγR signalling, the slight increase of this activation in TREM2 KO cells relative to TREM2 WT cells indicate that TREM2 deficiency enhances FcγR signalling.

This could be due to an inhibitory effect by intact TREM2. As TREM2–DAP12 and FcγR share downstream signalling proteins such as Src-family kinases and Syk, it is possible that they compete for these proteins when simultaneously activated. Without TREM2, there is a higher availability of intermediate signalling kinases to be recruited by FcγR signals to activate Pyk2 and Erk1/2. However, since TREM2–DAP12 and FcγR signalling converges at Syk and can similarly activate Pyk2 and Erk1/2, simultaneous activation of TREM2 and FcγR should still result in activation of Syk, Pyk2 and Erk1/2 regardless if the signal originated from TREM2–DAP12, FcγR or both, which is not the case here. Alternatively, expression of TREM2 and FcγR could be co-regulated. Increased signalling through FcγR suggests that the loss of TREM2 increases the expression or availability of FcγR. Although not measured here, TREM2-deficient BMDM have been reported with increased FcγR mRNA and protein expression compared to WT BMDM cells[489]. On the other hand, *Fcgr1* mRNA expression in TREM2-deficient primary adult microglia has been reported to be similar to WT primary adult microglia[532]. These differences may be due to the isolation of primary microglia involving homogenisation of brain tissue to produce a large amount of cell debris, which may activate or prime microglia to increase basal expression of FcγR. Nevertheless, the slight increase in activation of Pyk2 and Erk1/2 in TREM2 KO cells compared to TREM2 WT cells when stimulated with either the TREM2-activating antibody or isotype control antibody in the present study suggests increased FcγR expression in TREM2 KO BV2 microglia.

Even if the cells can be activated through TREM2 or FcγR with these antibodies, the lack of Syk activation by the isotype control antibody (FcγR activation only) or TREM2-activating antibody (TREM2+FcγR activation) in TREM2 WT and TREM2 KO cells is still not explained. It is possible that these treatments have a suppressive effect on the activation of Syk. An interesting property of ITAM signalling is that ligand-binding avidity affects the recruitment of signalling mediators to ITAMs. Avidity can be defined as the sum of

affinities of each ligand-binding interaction to the target receptor[727]. Strong ligand-binding avidity to receptors result in high phosphorylation of ITAMs and this leads to the commonly described recruitment of Syk. However, weak or tonic ligand-binding avidity cause only partial phosphorylation of ITAMs[728] and the recruitment of tyrosine phosphatases SHP1/2, inositol phosphatase SHIP1 or docking protein DOK3[729–731] instead of Syk (Figure 5.13). This potentially occurs through a preferential interaction between monophosphorylated ITAMs and single SH2 domain-containing phosphatases compared to dual SH2 domains of Syk[732]. The recruitment of phosphatases physically blocks other SH2 domain-containing protein including Syk from binding to ITAMs[396]. Besides that, phosphatases like SHP1 can also dephosphorylate Syk, Vav and PI3K[693,733,734] to negatively regulate ITAM-mediated signalling pathways.

In the present study, the TREM2-activating antibody binding to TREM2 is likely to have low avidity due to its monoclonal nature which binds to only one epitope site on each receptor and lead to inhibitory ITAM signalling. In agreement, stimulation of a mouse monocyte cell line with a different monoclonal antibody against TREM2 was shown to recruit SHIP1 to DAP12[396]. The inhibitory ITAM signalling can only occur with intact TREM2 which explains the lack of significant Syk activation in TREM2 WT cells when treated with the TREM2-activating antibody compared to uncoated wells in the present study. Peng *et al.* (2010) also showed that treatment of osteoclasts with a monoclonal antibody against TREM2 still resulted in phosphorylation of Syk, which was higher in SHIP1-deficient osteoclasts[396]. This suggests that the recruitment of SHIP1 does not completely prevent Syk phosphorylation. Indeed, in the present study, there was a trend towards increased Syk activation in TREM2 WT cells when stimulated with the TREM2-activating antibody (TREM2+FcγR activation) compared to the isotype control antibody (FcγR activation only).

Likewise, monomeric or multimeric IgG aggregation can affect ligand binding affinity to FcγR[735]. Dimeric or multimeric IgG aggregates have enhanced binding affinity to FcγR compared to monomeric IgG[735]. In the present study, it is not known if the plate-bound isotype control or TREM2-activating antibodies are monomeric or multimeric aggregates. As the plates were coated as evenly as possible with constant agitation, it is likely that the antibodies were coated as monomers or very small oligomers. This contrasts with

multimeric aggregations of antigen-bound IgG antibodies in immune complexes. Hence, this may explain the lack of Syk activation when stimulated with the TREM2-activating antibody in TREM2 KO cells (FcγR activation only) compared to TREM2 WT cells (TREM2+FcγR activation), which results in inhibitory ITAM signalling from FcγR (Figure 5.13).

Stimulation of macrophages with a monoclonal antibody against TREM2 also resulted in intracellular calcium flux, recruitment of PLC-γ and F-actin organisation[396]. Pyk2 is involved in this signalling pathway[703,717]. Indeed, Pyk2 was activated in TREM2 WT cells by the TREM2-activating antibody in the present study. Pyk2 can be directly activated by Src-family kinases recruited upstream of Syk activation[699,706] and circumvent the inhibitory action of phosphatase recruitment to partially phosphorylated ITAMs (Figure 5.13). This suggests that the inhibitory ITAM signalling does not significantly affect Pyk2 phosphorylation and activation.

Nevertheless, the interpretation of Syk, Pyk2 and Erk1/2 activation, even with simultaneous activation of TREM2 and FcγR when stimulated with the TREM2-activating antibody, shows that there is a difference in signalling pathways downstream of TREM2 caused by TREM2 deficiency. Furthermore, the current findings highlight the implications of functional loss of TREM2, which is the increased FcγR signalling potentially caused by increased levels of FcγR. If the loss of or decrease in TREM2 function caused by disease-associated TREM2 variants similarly result in increased expression of FcγR, it may result in exaggerated FcγR-mediated immune responses such as release of proinflammatory cytokines (e.g. TNF-α and IL-1β)[736] that can contribute to disease progression. The increased FcγR expression will need to be confirmed in the TREM2-deficient cell lines generated in this project and could also be investigated in post-mortem brain sections in cases with disease-associated TREM2 variants. Additionally, the effects of TREM2 activation will need to be separated from FcγR activation in follow-up studies. This could be done by processing the antibodies prior to use with pepsin to generate F(ab')2 fragments which lack the Fc region[385]. The cells can then be treated with non-specific F(ab')2 fragments (control treatment), TREM2-activating F(ab')2 fragments (TREM2-activating) or non-specific IgG antibody with Fc region (FcγR-activating).

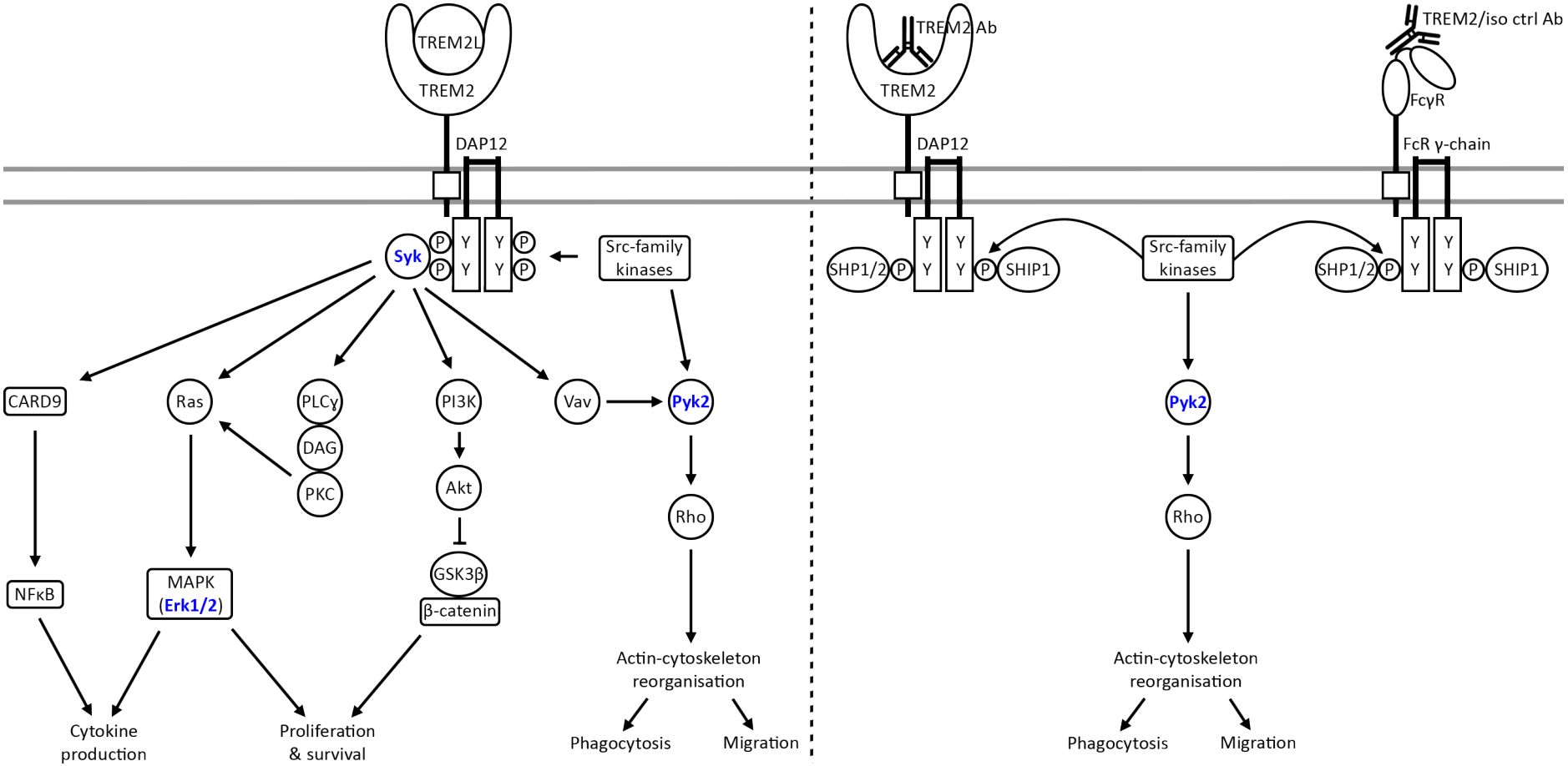

Figure 5.13. The lack of significant phosphorylation and activation of Syk and Erk1/2 in TREM2 WT cells after treatment with monoclonal TREM2-activating antibody may be due to weak ligand-binding avidity on TREM2 or FcγR that result in partial inhibitory ITAM signalling.

Unlike activating ITAM signalling (left), inhibitory ITAM signalling (right) is mediated by partial phosphorylation of ITAMs, which results in the recruitment of phosphatases such as SHP1/2 and SHIP1 to ITAMs instead of Syk. Despite the lack of Syk recruitment and activation, Pyk2 can still be phosphorylated and activated by Src-family kinases that are recruited upstream of Syk.

The present study also aimed to compare the expression of functional microglial markers CD68, HLA-DP, -DQ, -DR (MHC class II) and Iba-1 in the generated cell lines to see if they model the disease caused by TREM2 variants in people. Chapter 4 showed that AD cases with a disease-associated TREM2 variant had lower expression of CD68 and fewer HLA-DP, -DQ, -DR-expressing cells with no differences in Iba-1-expressing cell abundance compared to AD cases without TREM2 variants. Therefore, it was expected that CD68 and MHC class II expression would have a similar decrease and no difference in Iba-1 expression when stimulated with an AD pathological mimic in TREM2 KO cells compared to TREM2 WT cells. Unfortunately, the antibody against MHC class II (107601, BioLegend) used could not detect specific bands during antibody testing and optimisation. Regardless, CD68 and Iba-1 protein levels between TREM2 WT and TREM2 KO cells when stimulated with the TREM2-activating antibody were similar. The similar levels of CD68 in cells stimulated with the TREM2-activating antibody compared to uncoated wells demonstrate that CD68 expression is not induced by TREM2 or FcγR stimulation. It may be that CD68 expression is not induced without a phagocytic substrate. Therefore, the experimental setup in this study was insufficient to determine if the generated TREM2-deficient cell lines model the disease in people or not. To do so, these cells should be stimulated with an inert phagocytic substrate such as microspheres together with TREM2-activating F(ab')2 fragments. Alternatively, TREM2-activating F(ab')2 fragment-conjugated microspheres can also be used. In addition, the experiments can be combined to investigate the separate effects of TREM2 and FcγR activation in the TREM2-deficient cell lines and how they may model the disease in people. This can be done by conjugating non-specific F(ab')2 fragments, TREM2-activating F(ab')2 fragments and non-specific IgG antibody with Fc region onto microspheres and using these for cell stimulation.

In summary, this study shows that the generated *Trem2*-edited clonal lines from Chapter 3 have functional loss of TREM2 as predicted from the indels generated in in *Trem2* Exon 2. These cells can be used to investigate disease-relevant TREM2-mediated mechanisms that contribute to AD vulnerability. In addition, these TREM2-deficient microglia cell lines can also be used to screen for therapeutic compounds that ameliorate effects of the loss of TREM2 function. Stimulation of these cell lines with the TREM2-activating antibody demonstrated differences in activation of downstream signalling pathways between TREM2 KO and TREM2 WT cells. This also revealed a potential vulnerability of TREM2-

deficient cells to enhanced FcγR signalling which may lead to exaggerated and harmful FcγR-mediated immune activation.

Chapter 6

Discussions and conclusion

6.1 Overall discussion

The primary aim of this project was to generate an *in vitro* TREM2 model that endogeneously express the disease-associated variants and with intact signalling pathways downstream of TREM2. Such a model will be suitable for investigating disease-causing mechanisms conveyed by TREM2 variants and to screen therapeutic compounds. Most studies focused on elucidating TREM2 function have shown that TREM2 is involved in various innate immune responses such as phagocytosis, chemotaxis, cell survival and proliferation[383]. These studies often utilise TREM2-deficient or overexpressing models to elucidate TREM2 function.

On the other hand, studies on the TREM2 variants focused on the effects of the variants on the protein itself and how they affect functional outcomes in comparison to TREM2-deficient models. So far, disease-associated TREM2 variants have been shown to negatively impact expression of full-length protein (p.Q33X, p.W44X), protein folding (p.Y38C, p.T66M)[333,378], protein maturation (p.R47H)[379,382,452], and protein trafficking to the cell membrane (p.Y38C, p.T66M)[379,452] as well as ligand-binding (p.R47H, p.R62H, p.D87N)[106,108,378]. In these studies, expression vectors were used to overexpress TREM2 with the variants, which meant these models do not have endogeneous regulation of protein expression levels. This brings the validity of the model into question as overexpressing a misfolding protein may result in its accumulation in the endoplasmic reticulum (ER)[737]. This leads to ER stress and induce the unfolded protein response[738,739]. There are studies that used patient-derived primary myeloid cells such as peripheral blood monocytes carrying a disease-associated TREM2 variant[108]. These cells would have endogeneous expression of TREM2 with the variant and could also be used to study disease-causing mechanisms and pathways. However, they would not be suitable for screening assays because sourcing sufficient numbers of cells for the scale of such experiments would be practically and technically challenging.

Cell lines that endogeneously express TREM2 variants and can be cultured in large numbers have great value to further elucidate disease-causing mechanisms and identify therapeutic targets. However, the efficiency of knocking in TREM2 variants by CRISPR/Cas9 genome editing was far too low (Chapter 3). Furthermore, obtaining homogeneously edited clonal

lines was complicated by hyperploidy in the cell line as HDR-mediated DNA repair occurs at a rate too low to knock-in the DNA variants in all copies of *Trem2*. Also, NHEJ-mediated DNA repair is not precise and results in heterogeneous indels across different copies of *Trem2* (Chapter 3). Regardless, TREM2-deficient cell lines were successfully generated by indels in *Trem2*. These can be used to model TREM2 variants that result in the functional loss of TREM2 expression.

6.1.1 Alzheimer's disease-associated TREM2 variants may mediate inhibitory ITAM signalling

Recent studies have suggested that the disease-causing mechanism of TREM2 variants is due to decreased or loss of TREM2 protein function. However, our understanding of how disease-associated TREM2 variants impact underlying signalling pathways remain unclear. Elucidating disease-causing mechanisms and pathways conveyed by TREM2 variants may enable the identification of potential therapeutic targets, either single proteins or signalling pathways, to ameliorate the decrease or loss of TREM2 function. TREM2 is known to signal through DAP12 and its ITAMs. This leads to the recruitment of Syk and transduction of activating signals. However, it is not apparent in the TREM2 literature that TREM2 can also mediate inhibitory ITAM signalling through low ligand-binding avidity and downstream recruitment of phosphatases such as SHIP1 and SHP1/2 to DAP12 ITAMs.

Decreased CD68 expression and fewer HLA-DP, -DQ, -DR-expressing cells were observed in AD cases with disease-associated TREM2 variants, particularly p.R47H in Chapter 4. This variant has been found to decrease binding of several ligands including ApoE, proteoglycans and phospholipids[106,108,378,438]. The impairment of ligand binding is potentially due to a slight protein conformational change and change in electrostatic interactions[378]. Thus, ligands that normally bind to TREM2 would have weaker binding avidity.

In Chapter 5, the lack of Syk activation in TREM2 WT cells after treatment with a monoclonal TREM2-activating antibody suggests that that low ligand-binding avidity on TREM2 results in inhibitory signalling by recruitment of phosphatases to the ITAMs of DAP12 instead of Syk. Disease-associated TREM2 variants located on the conserved

extracellular ligand-binding basic patch (p.R47H, p.R62H and p.D87N) appear to decrease ligand-binding affinity but do not completely abolish binding[378]. This may be a disease-causing mechanism mediated by the more frequent AD-associated p.R47H and p.R62H variants to suppress innate immune activation in response to pathological ligands, such as cellular debris and protein aggregates. Thus, recognition and clearance of these ligands by TREM2-expressing cells such as microglia would be impaired.

This mechanism may have far-reaching effects beyond suppressing activation signals of TREM2 as its downstream signalling pathways are shared with many other immunoreceptors expressed on innate immune cells like microglia[699,703,732,740,741]. The phosphatases recruited to DAP12 can dephosphorylate many components of ITAM-mediated signalling and suppress signals from other receptors as well[733,734].

The suppression of activating signals by TREM2 may explain the decrease in HLA-DP, -DQ, -DR-expressing microglia in AD cases with the TREM2 p.R47H variant. Although TREM2 has not been directly implicated in antigen presentation, FcγRs are involved in antigen uptake, endosomal maturation, antigen processing and cellular activation[742]. In fact, all cell surface FcγRs, regardless of ITAM- or ITIM-carrying, are capable of internalising opsonised material or immune complexes[742]. ITAM-carrying FcγRs mediate the degradation of antigens for processing and presentation that leads to T cell activation[743,744]. On the other hand, ITIM-carrying FcγRs mediate the retention and preservation of antigens for subsequent transfer to B cells[743]. Low ligand-binding avidity by TREM2 p.R47H variant may result in phosphatase recruitment and suppress activation and signals from FcγRs, especially activating ITAM-carrying FcγRs that utilise Syk to mediate downstream signalling. Thus, suppression of antigen uptake as well as FcγR-mediated antigen processing and presentation pathways would not induce HLA-DP, -DQ, -DR expression. This is consistent with observations in post-mortem hippocampal CA4 with similar numbers of HLA-DP, -DQ, -DR-expressing cells between AD cases with a disease-associated TREM2 variant and non-AD cases (Chapter 4).

It is also possible that the decreased CD68 expression in AD cases with TREM2 p.R47H variant may be similarly affected by this. Studies so far have demonstrated increased TREM2 signalling or overexpression result in increased phagocytosis[384,394,417,428]. Moreover, other ITAM-associated receptors including FcγR, SIRPβ1 and CR3 can also induce

phagocytosis through similar ITAM-mediated signalling pathways[489,694,695,742]. Activating signals from these receptors may be suppressed by phosphatases recruited from low ligand-binding avidity of TREM2 p.R47H variant.

This overreaching effect of the TREM2 p.R47H variant on other immunoreceptor signalling pathways may explain why this rare variant has significant associations to various neurodegenerative diseases. Furthermore, ligands that have been found to bind TREM2 so far are highly implicated with pathology underlying neurodegenerative diseases. These include cell components exposed during apoptosis or released in cell debris (e.g. cell membrane lipids and nucleotides)[378,423,429,436–439] and lipoproteins significantly associated with AD (e.g. ApoE and ApoJ/clusterin)[106–108,440]. This suggests that TREM2 is highly likely to be engaged in disease and result in suppression of innate immune activation by the TREM2 p.R47H variant. Other AD risk genes further highlight the significance of this ITAM-mediated signalling pathway. *INPP5D* (SHIP1), *PTK2B* (Pyk2) and *PLCG2* (phospholipase C γ 2)[112,117] are involved in this signalling pathway whereas many other risk genes are related to functional responses to this signalling pathway such as phagocytosis and cytoskeletal organisation (Figure 1.3).

6.1.2 Decrease or loss of TREM2 function may enhance signalling of co-regulated receptors

In Chapter 5, TREM2-deficient cells had increased activation of Pyk2 by stimulation with the TREM2-activating antibody, which could only result in the activation of FcγR, compared to TREM2 WT cells. It is not clear if the increased activation is due to the loss of inhibition by TREM2 on FcγR signalling or increased expression of FcγR. Although not assessed in Chapter 5, TREM2-deficient BMDM is reported to have increased FcγR expression compared to WT BMDM[489], which may explain the increased activation of Pyk2. If the same occurs in AD patients with disease-associated TREM2 variants, the increased FcγR signalling in may result in overactivation of innate immune responses such as the release of proinflammatory TNF-α and IL-1β[736]. This may activate surrounding microglia into a M1-like state with a cytotoxic phenotype. Increased FcγR signalling is also expected to enhance antigen uptake, processing and presentation[742]. However, CD68 expression and the abundance of HLA-DP, -DQ, -DR-expressing cells were decreased in

hippocampal CA4 of AD cases with disease-associated TREM2 variants in Chapter 4. This suggests that AD-associated TREM2 variants, particularly the p.R47H variant, do not increase FcγR signalling or expression, unlike the effects seen in TREM2-deficient microglia. Nevertheless, there may be a combined effect of inhibitory ITAM signalling and increased expression of FcγR, resulting in the observations in Chapter 4.

Furthermore, the decrease or loss of TREM2 function may lead to increased expression of other receptors co-regulated by TREM2 besides FcγR. The loss of TREM2 signalling could alter basal ITAM/ITIM signalling and there may be a regulatory feedback loop to compensate for the decreased or loss of signals from TREM2. Indeed, ITAM signalling can lead to the regulation of transcription factors via the MAPK signalling pathway[719] and may enhance the expression of ITAM-associated receptors. Further confirmation is required to establish if the disease-associated TREM2 variants affect the expression of other ITAM-associated receptors.

6.2 Summary

In conclusion, 4 individual TREM2-deficient clonal microglia lines with intact signalling pathways downstream of TREM2 were generated. These cells can be used to model variants that impair trafficking of TREM2 to the cell membrane (e.g. p.Y38C, p.T66M) or variants that lead to the functional loss of TREM2 (e.g. p.W14X, p.Q33X, p.W44X). Through the generation of these cell lines, knock-in of gene variants into immortalised cell lines using CRISPR/Cas9 was found to be very difficult due to technical limitations, mainly the tendency for these cell lines to have chromosomal instability and hyperploidy. The investigation in post-mortem brain tissue revealed decreased expression of CD68 and fewer HLA-DP, -DQ, -DR-expressing microglia in the CA4 of AD cases with disease-associated TREM2 variants, particularly the p.R47H, despite no differences in the number of Iba-1-expressing microglia. Using the generated TREM2-deficient microglia cell lines, characterisation of key signalling proteins downstream of TREM2 in the presence or absence of functional TREM2 with a TREM2-activating antibody demonstrated differences in the phosphorylation of intermediate signalling proteins due to TREM2 deficiency. This also highlighted that signalling pathways downstream of TREM2 is shared with and can be activated by FcγR. Furthermore, ITAM-associated receptors including TREM2 and FcγR may suppress these signalling pathways by inhibitory ITAM signalling from low ligand-binding avidity such as by monoclonal antibody stimulation or protein variants that reduce ligand-binding avidity. In addition, TREM2 deficiency appear to enhance FcγR signalling, potentially through co-regulation with TREM2 that result in the increase of FcγR expression in the absence of TREM2. These suggest potential disease-causing mechanisms due to dysfunctional inflammatory responses. Suppression of inflammatory responses may result in the inability of immune cells to mediate clearance of pathology whereas enhanced or overactive inflammatory responses may lead to bystander damage of healthy cells. Therefore, potential therapeutic compounds may target and balance dysfunctional ITAM-mediated inflammatory responses that contribute to neurodegenerative disease vulnerability.

6.3 Future studies

The generation of *in vitro* cell models endogeneously expressing disease-associated TREM2 variants with intact downstream signalling pathways is still crucial for further investigation on the disease-causing mechanisms of these variants. Using a positive selectable marker such as a fluorescent protein gene in the HDR template may significantly improve screening efficiency for successful HDR in immortalised cell lines with multiple copies of the targeted gene. Following screening, the selectable marker gene can be removed from the target gene using transposon systems such as the *piggyBac* system to ensure scarless excision (discussed in detail in Chapter 3). Alternatively, patient-derived iPSCs can be used to generate microglia-like cells carrying the disease-associated TREM2 variant and isogenic control cell lines can be generated from these using CRISPR/Cas9. iPSCs would be initially screened to ensure that they would not have chromosomal abnormalities. Thus, to generate isogenic control lines from iPSCs carrying heterozygous variants like the AD-associated TREM2 variants, only one copy of *TREM2* needs to be targeted, which is much more likely to occur than homogeneous editing of up to four copies of *Trem2* in BV2.

The use of these cells in high-throughput assays can accelerate research on disease-causing mechanisms or pathways, which in turn allows the identification of potential therapeutic targets. For example, the effects of these variants on signalling pathways downstream of TREM2 that are shared with other ITAM-associated immunoreceptors can be studied. Besides that, expression levels of FcγR or other microglial ITAM-associated receptors can be assessed to confirm if TREM2 deficiency or the disease-associated variants lead to a compensatory increase in expression of these receptors. In addition, known ligands can be used to stimulate TREM2 with variants that affect ligand binding (e.g. p.R47H, p.R62H, p.D87N). Subsequently, downstream signalling pathways would be assessed to confirm if the variant leads to recruitment of phosphatases to DAP12 ITAMs and inhibitory ITAM signalling compared to normal TREM2 without the variant. Furthermore, other ITAM-associated receptors like FcγR can also be simultaneously stimulated to investigate if the inhibitory signalling by TREM2 p.R47H can suppress signals from these receptors and impair innate immune responses such as phagocytosis, chemotaxis and antigen presentation. Following confirmation of disease-causing mechanism, therapeutic compounds exploiting this signalling pathway can be identified using the generated *in vitro* TREM2 model in

high-throughput drug screening assays.

Moreover, markers of potential disease-causing mechanisms identified *in vitro* can be investigated in post-mortem tissue to establish if they also occur in the disease in people. For example, from the results in Chapter 5, the expression levels of FcγR as well as phosphorylation of Syk, Pyk2 and Erk1/2 can be compared between AD cases with and without disease-associated TREM2 variants. This will confirm if the disease-causing mechanisms identified *in vitro* is replicated in the disease in people. This will also establish that the model represents the disease in people when used to screen for therapeutic compounds.

Appendix

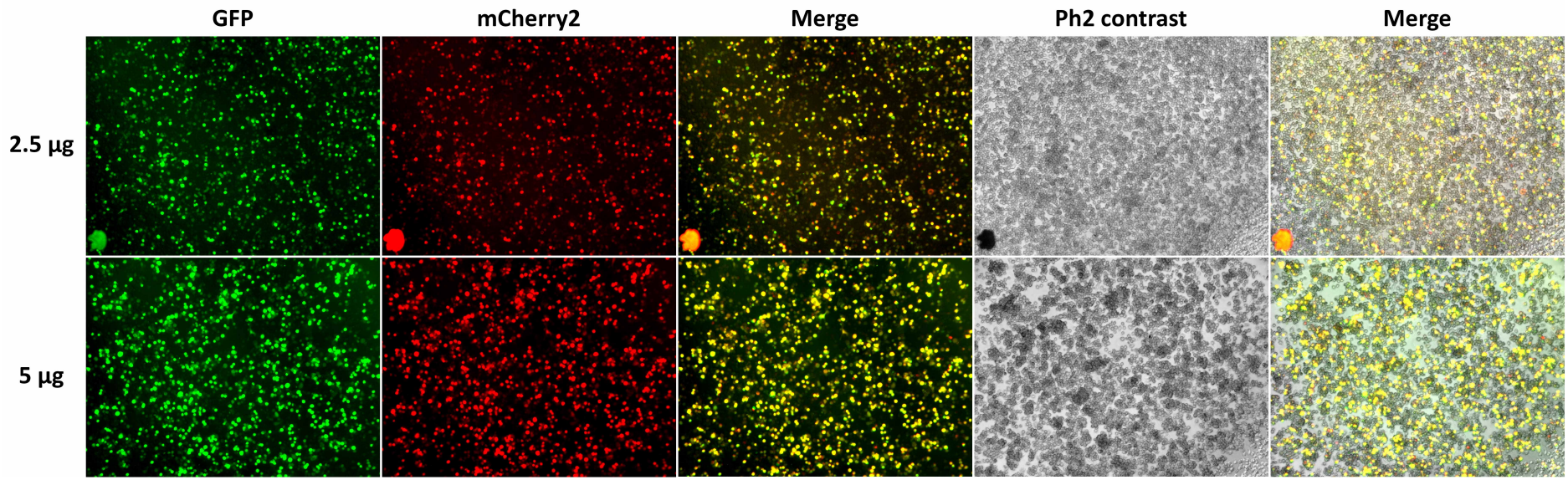

Figure A1. Comparison of transfection efficiency and cell viability between 2.5 µg and 5 µg of each sgRNA-Cas9 expression plasmid pairs (total 5 µg and 10 µg, respectively) when electroporated together with 100 pmol HDR template into 2×10^6 BV2 cells. Fluorescence microscopy images were taken at 100× magnification.

(a) Q33X

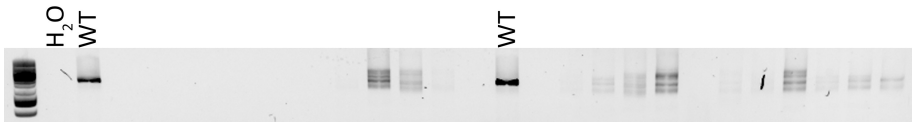

(b) D87N

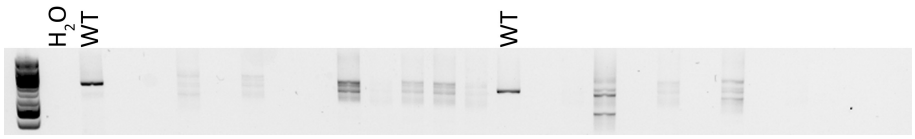

(c) R47H (Plate 1)

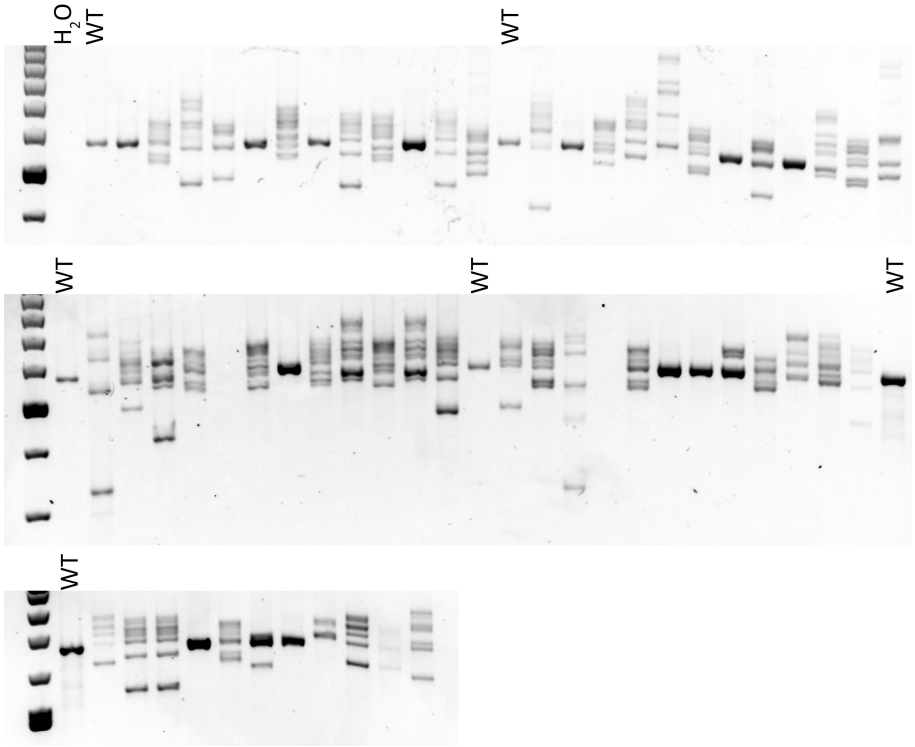

(d) R47H (Plate 2)

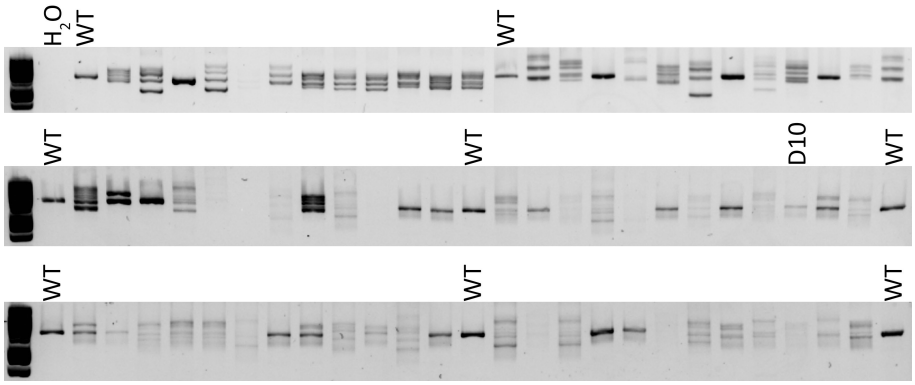

Figure A2. Agarose gel screening of CRISPR v3b **(a)** Q33X, **(b)** D87N and **(c,d)** R47H clones. Clones with single-band amplicons were Sanger sequenced.
TREM2 Exon 2 amplicons from unmodified BV2, labelled "WT", was used as a size reference (646 bp) against indels in clonal lines.

(a) Unstained clones

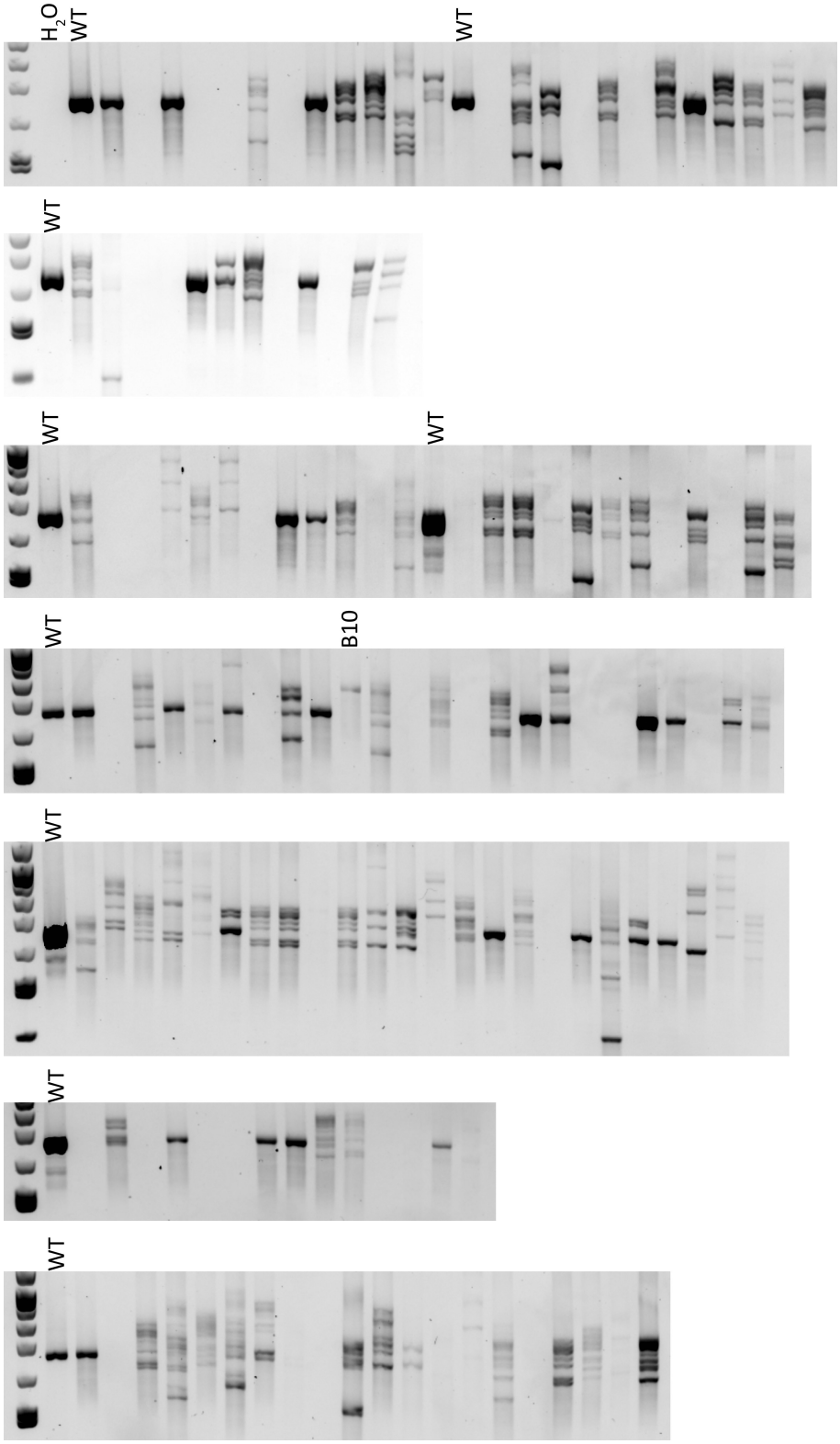

(b) Hoechst^{lo} clones

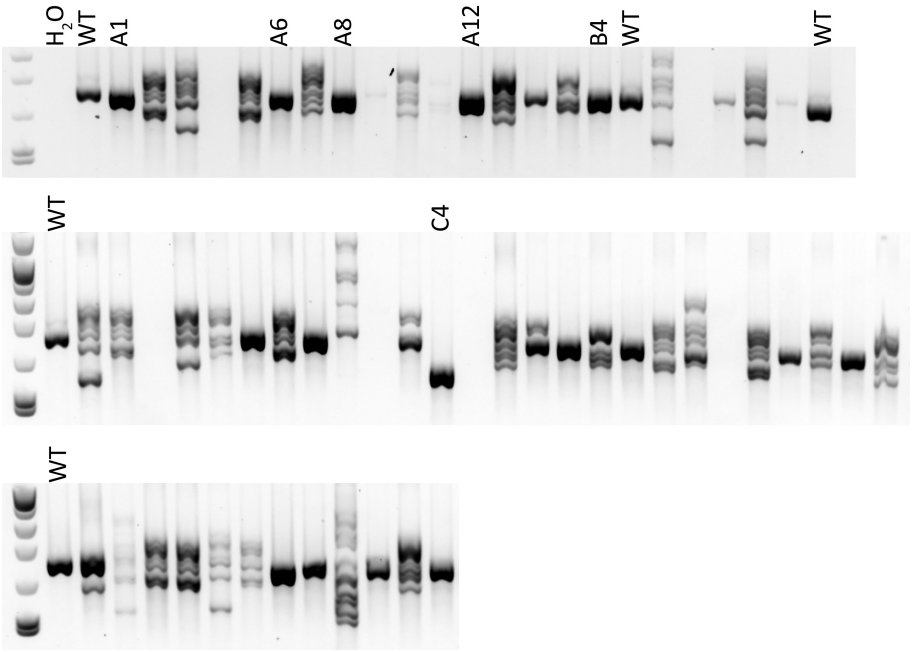

Figure A3. Agarose gel screening of **(a)** unstained or **(b)** Hoechst^{lo} CRISPR v3b clones. Clones with single-band amplicons were Sanger sequenced. Labelled amplicons indicate clones that were selected for functional characterisation.
TREM2 Exon 2 amplicons from unmodified BV2, labelled "WT", was used as a size reference (646 bp) against indels in clonal lines.

(a) 0 ng/mL nocodazole

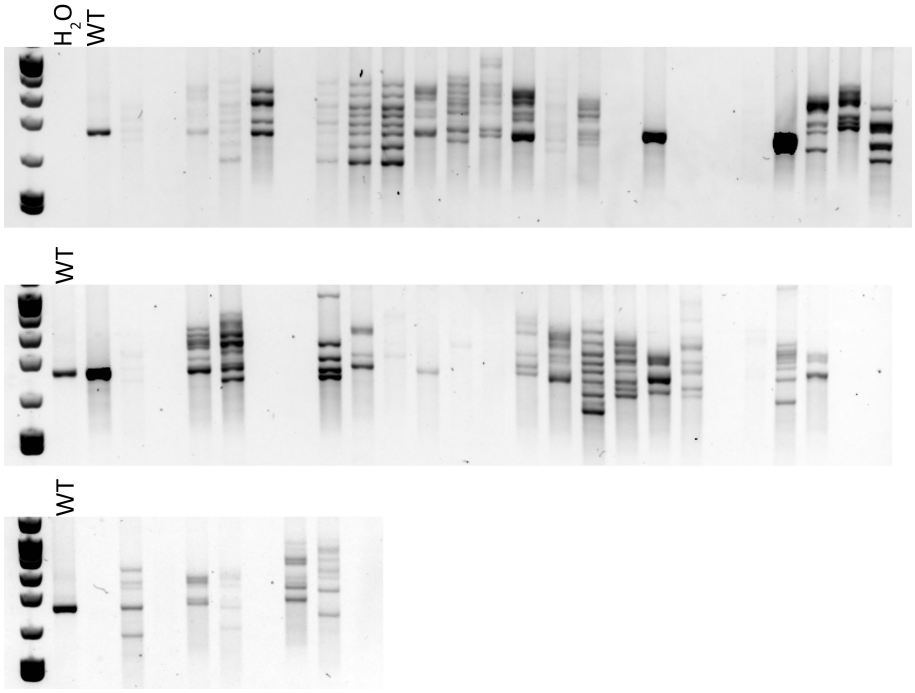

(b) 10 ng/mL nocodazole

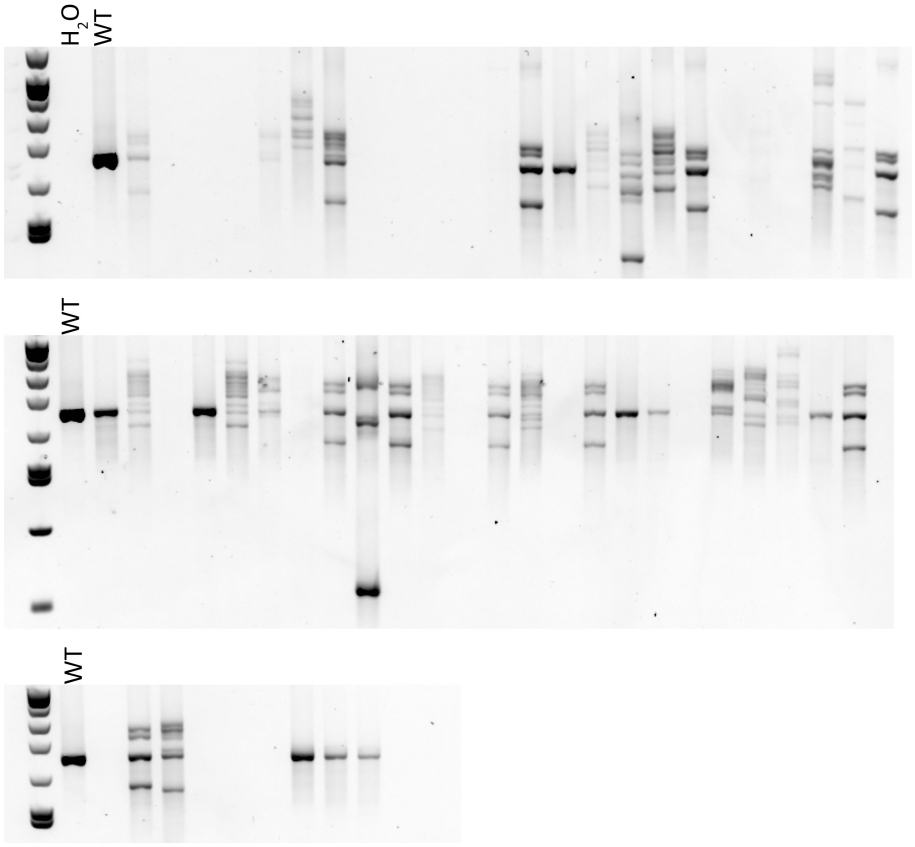

(c) 100 ng/mL nocodazole

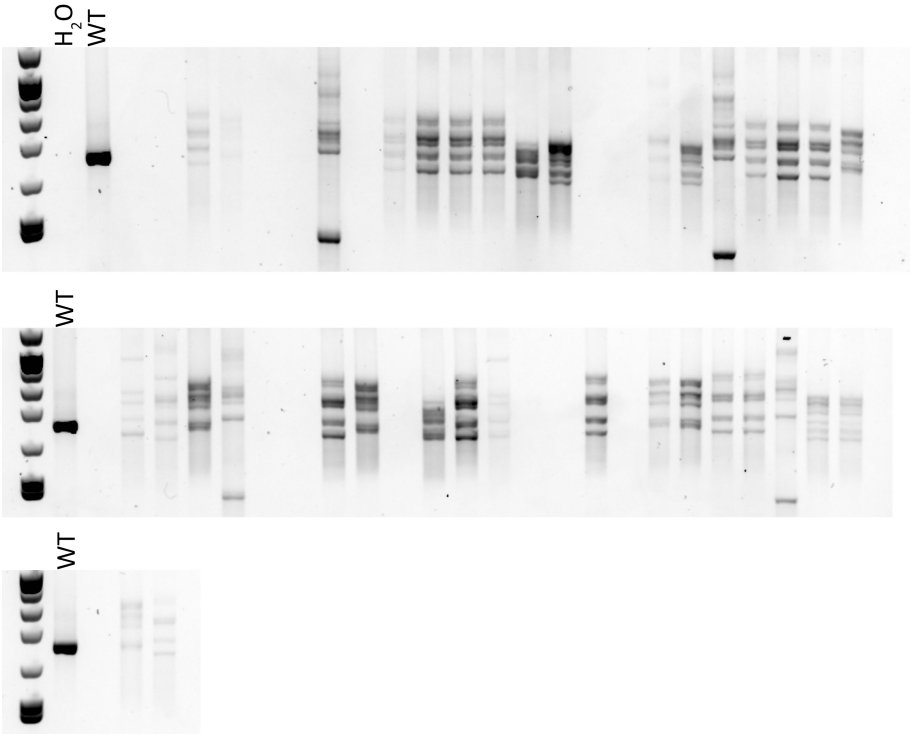

(d) 200 ng/mL nocodazole

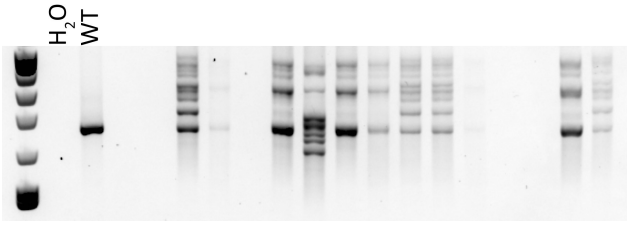

(e) 500 ng/mL nocodazole

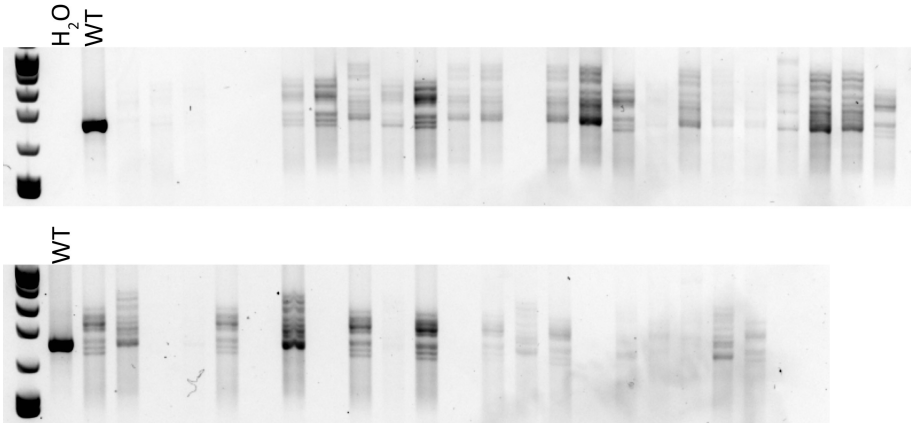

(f) 1000 ng/mL nocodazole

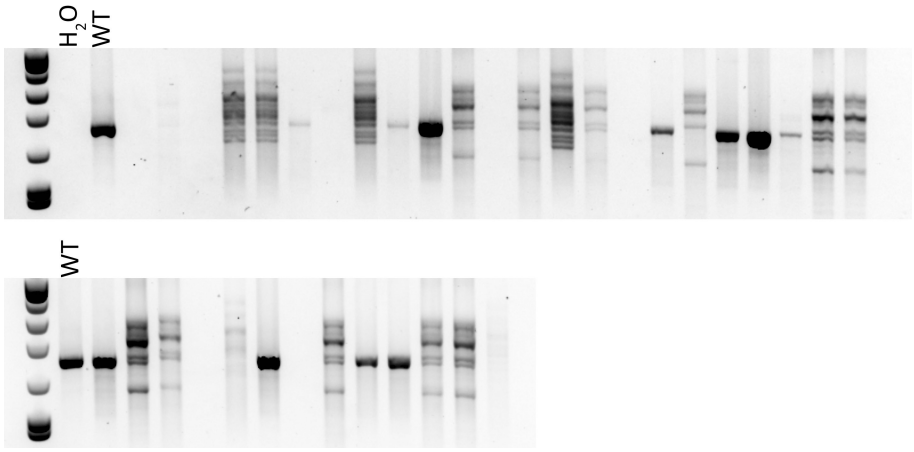

Figure A4. Agarose gel screening of CRISPR v4 clones treated with **(a)** 0 ng/mL, **(b)** 10 ng/mL, **(c)** 100 ng/mL, **(d)** 200 ng/mL, **(e)** 500 ng/mL or **(f)** 1000 ng/mL nocodazole. *TREM2* Exon 2 amplicons from unmodified BV2, labelled "WT", was used as a size reference (646 bp) against indels in clonal lines.

Stain	Region	Group	Mean (95% CI)	SD
Iba-1	CA1	Control/TREM2^{wt}	26.50 (16.31–38.83)	24.14
		AD/TREM2^{wt}	38.56 (29.65–47.69)	23.58
		AD/TREM2^{var}	29.51 (17.93–40.48)	22.13
	CA4	Control/TREM2^{wt}	29.44 (18.32–42.17)	25.15
		AD/TREM2^{wt}	34.89 (20.85–49.43)	31.81
		AD/TREM2^{var}	21.43 (11.83–31.99)	21.38
CD68	CA1	Control/TREM2^{wt}	2.91 (2.09–3.78)	1.79
		AD/TREM2^{wt}	4.20 (3.31–5.41)	2.24
		AD/TREM2^{var}	3.28 (2.19–4.69)	2.99
	CA4	Control/TREM2^{wt}	4.51 (3.21–6.10)	3.40
		AD/TREM2^{wt}	3.75 (2.90–4.65)	2.06
		AD/TREM2^{var}	2.12 (1.54–2.77)	1.40
HLA	CA1	Control/TREM2^{wt}	21.73 (14.29–30.08)	17.69
		AD/TREM2^{wt}	54.82 (38.53–73.71)	40.83
		AD/TREM2^{var}	36.61 (19.62–52.72)	32.50
	CA4	Control/TREM2^{wt}	42.32 (28.45–57.19)	31.06
		AD/TREM2^{wt}	58.53 (35.85–81.94)	51.68
		AD/TREM2^{var}	31.07 (14.46–48.68)	34.16

Table A1. Means and standard deviations of Iba-1$^+$ cell counts, CD68 % area immunostaining and HLA$^+$ cell counts in 0.5×0.5 mm^2 areas of the CA1 and CA4 for Control/TREM2^{wt}, AD/TREM2^{wt} and AD/TREM2^{var} groups.
CI: confidence interval, SD: standard deviation.

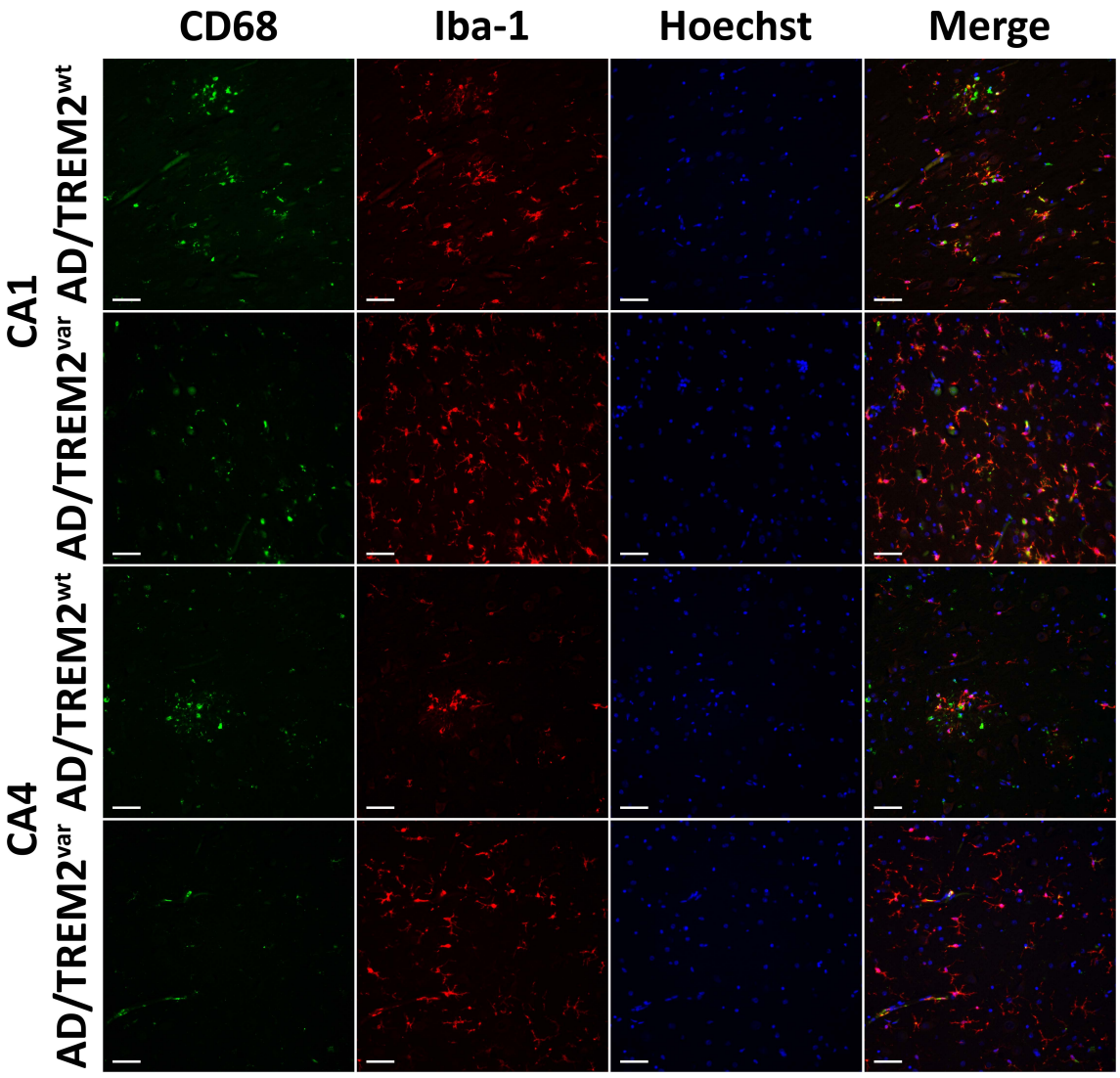

Figure A5. Images separated into individual channels from double staining immunofluorescence of CD68 and Iba-1 in AD/TREM2^{wt} and AD/TREM2^{var} cases.

These images correspond to Figure 4.5. Images were captured at 200× magnification. Scale bars indicate 50 µm.

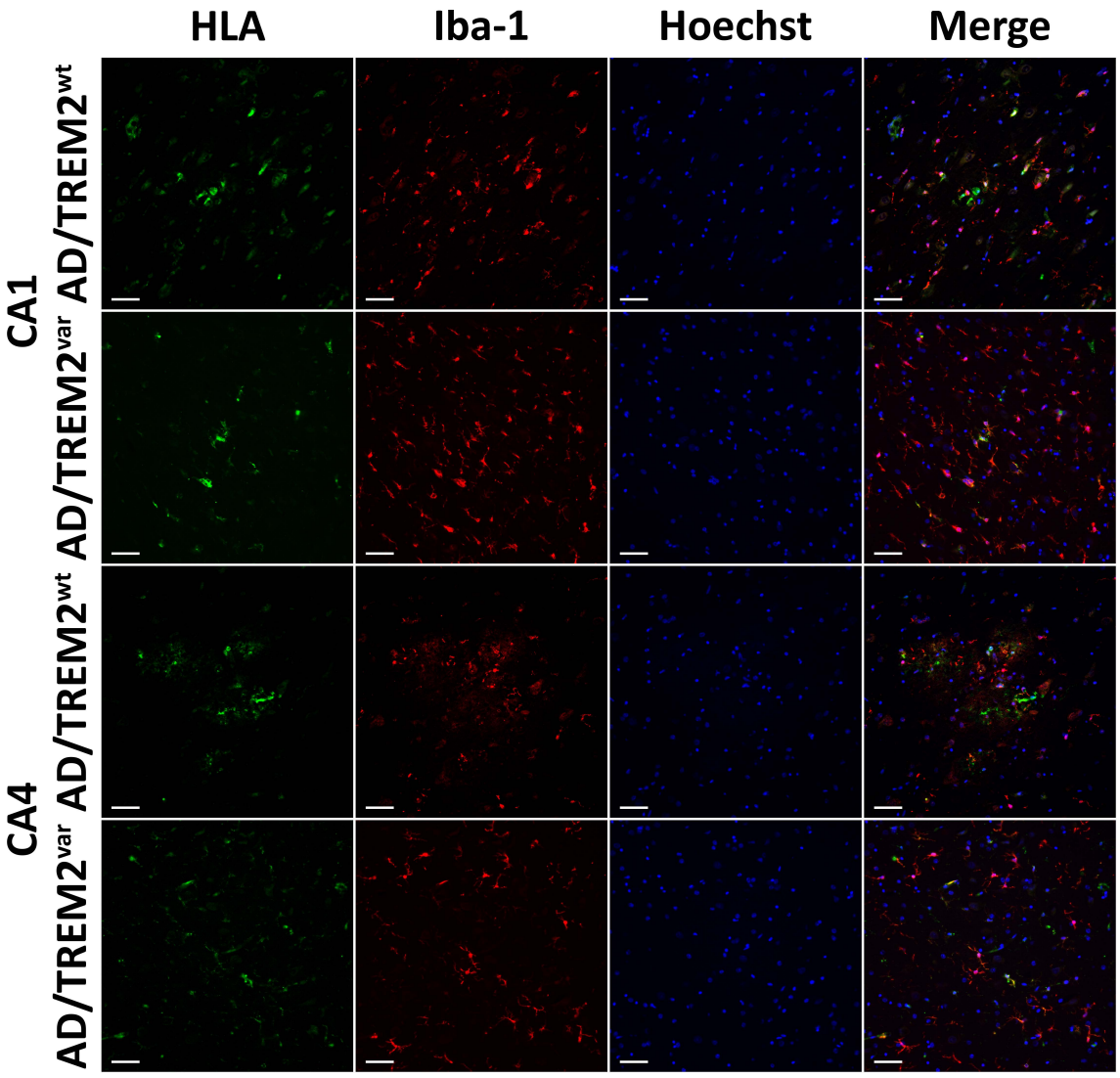

Figure A6. Images separated into individual channels from double staining immunofluorescence of HLA and Iba-1 in AD/TREM2^{wt} and AD/TREM2^{var} cases.

These images correspond to Figure 4.6. Images were captured at 200× magnification. Scale bars indicate 50 µm.

Stain	Region	Group	Mean (95% CI)	SD
Iba-1	CA1	Control/TREM2^{wt}	0.097 (0.083–0.113)	0.028
		AD/TREM2^{wt}	0.098 (0.086–0.112)	0.028
		AD/TREM2^{var}	0.113 (0.098–0.129)	0.030
	CA4	Control/TREM2^{wt}	0.099 (0.084–0.114)	0.025
		AD/TREM2^{wt}	0.112 (0.091–0.135)	0.052
		AD/TREM2^{var}	0.141 (0.109–0.183)	0.079
HLA	CA1	Control/TREM2^{wt}	0.073 (0.066–0.081)	0.016
		AD/TREM2^{wt}	0.088 (0.080–0.097)	0.020
		AD/TREM2^{var}	0.093 (0.082–0.104)	0.023
	CA4	Control/TREM2^{wt}	0.066 (0.063–0.070)	0.008
		AD/TREM2^{wt}	0.087 (0.077–0.099)	0.025
		AD/TREM2^{var}	0.104 (0.085–0.125)	0.042

Table A2. Means and standard deviations of Iba-1$^+$ and HLA$^+$ microglia circularity in 0.5×0.5 mm^2 areas of the CA1 and CA4 for each experimental group.
CI: confidence interval, SD: standard deviation.

Stain	Region	Group	Mean (95% CI)	SD
Aβ (4G8)	CA1	AD/TREM2^{wt}	4.82 (2.96–6.89)	5.33
		AD/TREM2^{var}	3.72 (2.34–5.81)	3.97
	CA4	AD/TREM2^{wt}	0.83 (0.40–1.37)	1.09
		AD/TREM2^{var}	1.39 (0.40–2.54)	2.19
Phospho-tau (AT8)	CA1	AD/TREM2^{wt}	31.55 (26.24–36.25)	11.50
		AD/TREM2^{var}	28.75 (22.57–34.55)	11.76
	CA4	AD/TREM2^{wt}	18.33 (12.71–23.56)	14.04
		AD/TREM2^{var}	11.05 (7.58–14.68)	7.73

Table A3. Means and standard deviations of Aβ or tau % area staining in 0.5×0.5 mm^2 areas of the CA1 and CA4 for AD/TREM2^{wt} and AD/TREM2^{var} cases.
CI: confidence interval, SD: standard deviation.

Stain	Region	Group	Mean (95% CI)	SD
Iba-1	CA1	Control/TREM2^{wt}	26.50 (15.90–39.18)	24.14
		AD/TREM2^{wt}	38.56 (28.78–49.49)	23.58
		AD/TREM2^{R47H}	22.11 (9.15–36.22)	20.80
	CA4	Control/TREM2^{wt}	29.44 (19.12–41.07)	25.15
		AD/TREM2^{wt}	34.89 (21.95–47.99)	31.81
		AD/TREM2^{R47H}	15.04 (4.46–28.99)	17.93
CD68	CA1	Control/TREM2^{wt}	2.911 (2.120–3.870)	1.794
		AD/TREM2^{wt}	4.204 (3.150–5.320)	2.242
		AD/TREM2^{R47H}	2.654 (1.595–3.983)	1.611
	CA4	Control/TREM2^{wt}	4.512 (3.195–6.145)	3.398
		AD/TREM2^{wt}	3.749 (2.972–4.539)	2.058
		AD/TREM2^{R47H}	1.937 (1.218–2.818)	1.218
HLA	CA1	Control/TREM2^{wt}	21.73 (14.16–30.33)	17.69
		AD/TREM2^{wt}	54.82 (37.80–75.36)	40.83
		AD/TREM2^{R47H}	25.96 (9.26–49.34)	29.34
	CA4	Control/TREM2^{wt}	42.32 (27.56–57.45)	31.06
		AD/TREM2^{wt}	58.53 (37.20–81.04)	51.68
		AD/TREM2^{R47H}	14.96 (5.53–26.24)	17.28

Table A4. Means and standard deviations of Iba-1^{+} microglial abundance, CD68 staining, and HLA^{+} microglial abundance in 0.5×0.5 mm^{2} areas of the CA1 and CA4 for AD/TREM2^{wt} and AD/TREM2^{R47H} cases.
CI: confidence interval, SD: standard deviation.

Stain	Region	Group	Mean (95% CI)	SD
Iba-1	CA1	Control/TREM2^{wt}	0.097 (0.084–0.111)	0.028
		AD/TREM2^{wt}	0.098 (0.086–0.109)	0.028
		AD/TREM2^{var}	0.121 (0.102–0.141)	0.028
	CA4	Control/TREM2^{wt}	0.099 (0.088–0.110)	0.025
		AD/TREM2^{wt}	0.112 (0.092–0.135)	0.052
		AD/TREM2^{var}	0.127 (0.109–0.149)	0.029
HLA	CA1	Control/TREM2^{wt}	0.073 (0.065–0.082)	0.016
		AD/TREM2^{wt}	0.088 (0.079–0.099)	0.020
		AD/TREM2^{var}	0.092 (0.079–0.105)	0.022
	CA4	Control/TREM2^{wt}	0.066 (0.063–0.070)	0.008
		AD/TREM2^{wt}	0.087 (0.078–0.098)	0.025
		AD/TREM2^{var}	0.115 (0.090–0.143)	0.047

Table A5. Means and standard deviations of Iba-1$^+$ and HLA$^+$ microglia circularity in 0.5×0.5 mm^2 areas of the CA1 and CA4 for each experimental group.
CI: confidence interval, SD: standard deviation.

References

[1] Hippius H, Neundörfer G. The discovery of Alzheimer's disease. *Dialogues in Clinical Neuroscience*. 2003;5(1):101.

[2] Alois A. Über eine eigenartige Erkrankung der Hirnrinde [About a peculiar disease of the cerebral cortex]. *Allgemeine Zeitschrift fur Psychiatrie und Psychisch-Gerichtlich Medizin*. 1907;64(1-2):146–148.

[3] Glenner G, Wong C. Alzheimer's disease: initial report of the purification and characterization of a novel cerebrovascular amyloid protein. *Alzheimer Disease & Associated Disorders*. 1988;2(2):134.

[4] Grundke-Iqbal I, Iqbal K, Quinlan M, Tung YC, Zaidi MS, Wisniewski HM. Microtubule-associated protein tau. A component of Alzheimer paired helical filaments. *Journal of Biological Chemistry*. 1986;261(13):6084–6089.

[5] Goate A, Chartier-Harlin MC, *et al*. Segregation of a missense mutation in the amyloid precursor protein gene with familial Alzheimer's disease. *Nature*. 1991;349(6311):704.

[6] Sherrington R, Rogaev E, Liang Ya, Rogaeva E, Levesque G, Ikeda M, *et al*. Cloning of a gene bearing missense mutations in early-onset familial Alzheimer's disease. *Nature*. 1995;375(6534):754–760.

[7] Levy-Lahad E, Wasco W, Poorkaj P, Romano DM, Oshima J, Pettingell WH, *et al*. Candidate gene for the chromosome 1 familial Alzheimer's disease locus. *Science*. 1995;p. 973–977.

[8] Corder E, Saunders A, Strittmatter W, Schmechel D, Gaskell P, Small Ga, *et al*. Gene dose of apolipoprotein E type 4 allele and the risk of Alzheimer's disease in late onset families. *Science*. 1993;261(5123):921–923.

[9] Rogers SL, Friedhoff LT. The efficacy and safety of donepezil in patients with Alzheimer's disease: results of a US multicentre, randomized, double-blind, placebo-controlled trial. *Dementia and Geriatric Cognitive Disorders*. 1996;7(6):293–303.

[10] Klunk WE, Engler H, Nordberg A, Wang Y, Blomqvist G, Holt DP, *et al.* Imaging brain amyloid in Alzheimer's disease with Pittsburgh Compound-B. *Annals of Neurology*. 2004;55(3):306–319.

[11] Sperling RA, Aisen PS, Beckett LA, Bennett DA, Craft S, Fagan AM, *et al.* Toward defining the preclinical stages of Alzheimer's disease: Recommendations from the National Institute on Aging-Alzheimer's Association workgroups on diagnostic guidelines for Alzheimer's disease. *Alzheimer's & Dementia*. 2011;7(3):280–292.

[12] McKhann GM, Knopman DS, Chertkow H, Hyman BT, Jack CR, Kawas CH, *et al.* The diagnosis of dementia due to Alzheimer's disease: Recommendations from the National Institute on Aging-Alzheimer's Association workgroups on diagnostic guidelines for Alzheimer's disease. *Alzheimer's & Dementia*. 2011;7(3):263–269.

[13] Gao S, Hendrie HC, Hall KS, Hui S. The relationships between age, sex, and the incidence of dementia and Alzheimer disease: a meta-analysis. *Archives of General Psychiatry*. 1998;55(9):809–815.

[14] Tomlinson B, Blessed G, Roth M. Observations on the brains of demented old people. *Journal of the Neurological Sciences*. 1970;11(3):205–242.

[15] Corsellis JAN. Mental illness and the ageing brain: the distribution of pathological change in a mental hospital population. Oxford University Press; 1962.

[16] Katzman R. The prevalence and malignancy of alzheimer disease. *Alzheimer's & Dementia: the Journal of the Alzheimer's Association*. 2008;4(6):378–380.

[17] Alzheimer's Society. Facts for the media; 2018. Available from: `https://www.alzheimers.org.uk/info/20027/news_and_media/541/facts_for_the_media`.

[18] Prince M, Bryce R, Albanese E, Wimo A, Ribeiro W, Ferri CP. The global prevalence of dementia: a systematic review and metaanalysis. *Alzheimer's & Dementia*. 2013;9(1):63–75.

[19] Scheltens P, Blennow K, Breteler MM, de Strooper B, Frisoni GB, Salloway S, *et al.* Alzheimer's disease. *Lancet.* 2016;388(10043):505–517.

[20] Wimo A, Prince M. World Alzheimer Report 2010: The Global Economic Impact of Dementia; 2010.

[21] Karran E, Hardy J. A critique of the drug discovery and phase 3 clinical programs targeting the amyloid hypothesis for Alzheimer disease. *Annals of Neurology.* 2014;76(2):185–205.

[22] Selkoe DJ. The molecular pathology of Alzheimer's disease. *Neuron.* 1991;6(4):487–498.

[23] Hardy JA, Higgins GA. Alzheimer's disease: the amyloid cascade hypothesis. *Science.* 1992;256(5054):184.

[24] Hardy J, Selkoe DJ. The amyloid hypothesis of Alzheimer's disease: progress and problems on the road to therapeutics. *Science.* 2002;297(5580):353–356.

[25] Selkoe DJ, Hardy J. The amyloid hypothesis of Alzheimer's disease at 25 years. *EMBO Molecular Medicine.* 2016;8(6):595–608.

[26] Kuhn PH, Wang H, Dislich B, Colombo A, Zeitschel U, Ellwart JW, *et al.* ADAM10 is the physiologically relevant, constitutive α-secretase of the amyloid precursor protein in primary neurons. *The EMBO Journal.* 2010;29(17):3020–3032.

[27] Vassar R. Bace 1. *Journal of Molecular Neuroscience.* 2004;23(1-2):105–113.

[28] Thinakaran G, Koo EH. Amyloid precursor protein trafficking, processing, and function. *Journal of Biological Chemistry.* 2008;283(44):29615–29619.

[29] O'Brien RJ, Wong PC. Amyloid precursor protein processing and Alzheimer's disease. *Annual Review of Neuroscience.* 2011;34:185–204.

[30] Selkoe DJ, Wolfe MS. Presenilin: running with scissors in the membrane. *Cell.* 2007;131(2):215–221.

[31] Mattson MP, Cheng B, Culwell AR, Esch FS, Lieberburg I, Rydel RE. Evidence for excitoprotective and intraneuronal calcium-regulating roles for secreted forms of the β-amyloid precursor protein. *Neuron.* 1993;10(2):243–254.

[32] Ring S, Weyer SW, Kilian SB, Waldron E, Pietrzik CU, Filippov MA, *et al.* The secreted β-amyloid precursor protein ectodomain APPsα is sufficient to rescue the anatomical, behavioral, and electrophysiological abnormalities of APP-deficient mice. *Journal of Neuroscience*. 2007;27(29):7817–7826.

[33] Citron M, Oltersdorf T, Haass C, McConlogue L, Hung AY, Seubert P, *et al.* Mutation of the β-amyloid precursor protein in familial Alzheimer's disease increases β-protein production. *Nature*. 1992;360(6405):672–674.

[34] Cai XD, Golde TE, Younkin SG. Release of Excess Amyloid Protein from a Mutant Amyloid Protein Precursor. *Science*. 1993;259:514–514.

[35] Suzuki N, Cheung TT, Cai XD, Odaka A, Otvos Jr L, Eckman C, *et al.* An increased percentage of long amyloid beta protein secreted by familial amyloid beta protein precursor (betaAPP717) mutants. *Science*. 1994;264(5163):1336–1341.

[36] Scheuner D, Eckman C, Jensen M, Song X, Citron M, Suzuki N, *et al.* Secreted amyloid β–protein similar to that in the senile plaques of Alzheimer's disease is increased in vivo by the presenilin 1 and 2 and APP mutations linked to familial Alzheimer's disease. *Nature medicine*. 1996;2(8):864–870.

[37] Wisniewski T, Ghiso J, Frangione B. Peptides homologous to the amyloid protein of Alzheimer's disease containing a glutamine for glutamic acid substitution have accelerated amyloid fibril formation. *Biochemical and Biophysical Research Communications*. 1991;179(3):1247–1254.

[38] De Strooper B, Saftig P, Craessaerts K, Vanderstichele H, *et al.* Deficiency of presenilin-1 inhibits the normal cleavage of amyloid precursor protein. *Nature*. 1998;391(6665):387.

[39] Wolfe MS, Xia W, Ostaszewski BL, Diehl TS, *et al.* Two transmembrane aspartates in presenilin-1 required for presenilin endoproteolysis and gamma-secretase activity. *Nature*. 1999;398(6727):513.

[40] Rovelet-Lecrux A, Hannequin D, Raux G, Le Meur N, Laquerrière A, Vital A, *et al.* APP locus duplication causes autosomal dominant early-onset Alzheimer disease with cerebral amyloid angiopathy. *Nature Genetics*. 2006;38(1):24.

[41] Prasher V, Farrer MJ, Kessling AM, Fisher E, West R, Barber P, *et al.* Molecular mapping of Alzheimer-type dementia in Down's syndrome. *Annals of Neurology.* 1998;43(3):380–383.

[42] Hardy J, Duff K, Hardy KG, Perez-Tur J, Hutton M. Genetic dissection of Alzheimer's disease and related dementias: amyloid and its relationship to tau. *Nature Neuroscience.* 1998;1(5).

[43] Lewis J, Dickson DW, Lin WL, Chisholm L, Corral A, Jones G, *et al.* Enhanced neurofibrillary degeneration in transgenic mice expressing mutant tau and APP. *Science.* 2001;293(5534):1487–1491.

[44] Ballard C, Gauthier S, Corbett A, Brayne C, Aarsland D, Jones E. Alzheimer's disease. *Lancet.* 2011;377(9770):1019–1031.

[45] McKhann G, Drachman D, Folstein M, Katzman R, Price D, Stadlan EM. Clinical diagnosis of Alzheimer's disease Report of the NINCDS-ADRDA Work Group* under the auspices of Department of Health and Human Services Task Force on Alzheimer's Disease. *Neurology.* 1984;34(7):939–939.

[46] Albert MS, DeKosky ST, Dickson D, Dubois B, Feldman HH, Fox NC, *et al.* The diagnosis of mild cognitive impairment due to Alzheimer's disease: Recommendations from the National Institute on Aging-Alzheimer's Association workgroups on diagnostic guidelines for Alzheimer's disease. *Alzheimer's & Dementia.* 2011;7(3):270–279.

[47] Dubois B, Feldman HH, Jacova C, Hampel H, Molinuevo JL, Blennow K, *et al.* Advancing research diagnostic criteria for Alzheimer's disease: the IWG-2 criteria. *Lancet Neurology.* 2014;13(6):614–629.

[48] Knopman DS, DeKosky ST, Cummings J, Chui H, Corey-Bloom J, Relkin N, *et al.* Practice parameter: Diagnosis of dementia (an evidence-based review) Report of the Quality Standards Subcommittee of the American Academy of Neurology. *Neurology.* 2001;56(9):1143–1153.

[49] Catafau AM, Bullich S. Amyloid PET imaging: applications beyond Alzheimer's disease. *Clinical and Translational Imaging.* 2015;3(1):39–55.

[50] James OG, Doraiswamy PM, Borges-Neto S. PET imaging of tau pathology in Alzheimer's disease and tauopathies. *Frontiers in Neurology*. 2015;6.

[51] Arora A, Bhagat N. Insight into the molecular imaging of Alzheimer's disease. *Journal of Biomedical Imaging*. 2016;2016:2.

[52] Drago V, Babiloni C, Bartrés-Faz D, Caroli A, Bosch B, Hensch T, *et al.* Disease tracking markers for Alzheimer's disease at the prodromal (MCI) stage. *Journal of Alzheimer's Disease*. 2011;26(s3):159–199.

[53] Frisoni GB, Fox NC, Jack CR, Scheltens P, Thompson PM. The clinical use of structural MRI in Alzheimer disease. *Nature Reviews Neurology*. 2010;6(2):67–77.

[54] Coimbra A, Williams DS, Hostetler ED. The role of MRI and PET/SPECT in Alzheimer's disease. *Current topics in medicinal chemistry*. 2006;6(6):629–647.

[55] Blennow K, Hampel H. CSF markers for incipient Alzheimer's disease. *Lancet Neurology*. 2003;2(10):605–613.

[56] Jack CR, Albert MS, Knopman DS, McKhann GM, Sperling RA, Carrillo MC, *et al.* Introduction to the recommendations from the National Institute on Aging-Alzheimer's Association workgroups on diagnostic guidelines for Alzheimer's disease. *Alzheimer's & Dementia*. 2011;7(3):257–262.

[57] Schott JM, Petersen RC. New criteria for Alzheimer's disease: which, when and why? *Brain*. 2015;138(5):1134–1137.

[58] Price JL, Morris JC. Tangles and plaques in nondemented aging and" preclinical" Alzheimer's disease. *Annals of Neurology*. 1999;45(3):358–368.

[59] Förstl H, Peng FC. Does Alzheimer's Disease Really Exist? *International Psychogeriatrics*. 2010;22(5):848.

[60] Zubenko GS, Maher B, Hughes HB, Zubenko WN, Stiffler JS, Kaplan BB, *et al.* Genome-wide linkage survey for genetic loci that influence the development of depressive disorders in families with recurrent, early-onset, major depression. *American Journal of Medical Genetics Part B: Neuropsychiatric Genetics*. 2003;123(1):1–18.

[61] Ducharme JK, Geldmacher DS. Family quality of life in dementia: a qualitative approach to family-identified care priorities. *Quality of Life Research*. 2011;20(8):1331–1335.

[62] Goedert M, Sisodia SS, Price DL. Neurofibrillary tangles and β-amyloid deposits in Alzheimer's disease. *Current Opinion in Neurobiology*. 1991;1(3):441–447.

[63] Forman MS, Trojanowski JQ, Lee VM. Neurodegenerative diseases: a decade of discoveries paves the way for therapeutic breakthroughs. *Nature Medicine*. 2004;10(10):1055–1063.

[64] Dickson DW, Crystal HA, Bevona C, Honer W, Vincent I, Davies P. Correlations of synaptic and pathological markers with cognition of the elderly. *Neurobiology of Aging*. 1995;16(3):285–298.

[65] Buée L, Bussière T, Buée-Scherrer V, Delacourte A, Hof PR. Tau protein isoforms, phosphorylation and role in neurodegenerative disorders. *Brain Research Reviews*. 2000;33(1):95–130.

[66] Liu F, Gong CX. Tau exon 10 alternative splicing and tauopathies. *Molecular Neurodegeneration*. 2008;3(1):8.

[67] Lee G, Neve RL, Kosik KS. The microtubule binding domain of tau protein. *Neuron*. 1989;2(6):1615–1624.

[68] Mandelkow EM, Mandelkow E. Biochemistry and cell biology of tau protein in neurofibrillary degeneration. *Cold Spring Harbor Perspectives in Medicine*. 2012;2(7):a006247.

[69] Grundke-Iqbal I, Iqbal K, Tung YC, Quinlan M, Wisniewski HM, Binder LI. Abnormal phosphorylation of the microtubule-associated protein tau (tau) in Alzheimer cytoskeletal pathology. *Proceedings of the National Academy of Sciences*. 1986;83(13):4913–4917.

[70] Iqbal K, Grundke-Iqbal I. Alzheimer neurofibrillary degeneration: significance, etiopathogenesis, therapeutics and prevention. *Journal of Cellular and Molecular Medicine*. 2008;12(1):38–55.

[71] Köpke E, Tung YC, Shaikh S, Alonso AdC, Iqbal K, Grundke-Iqbal I. Microtubule-associated protein tau. Abnormal phosphorylation of a non-paired helical filament pool in Alzheimer disease. *Journal of Biological Chemistry*. 1993;268(32):24374–24384.

[72] Terry RD, Masliah E, Salmon DP, Butters N, DeTeresa R, Hill R, *et al.* Physical basis of cognitive alterations in Alzheimer's disease: synapse loss is the major correlate of cognitive impairment. *Annals of Neurology*. 1991;30(4):572–580.

[73] DeKosky ST, Scheff SW, Styren SD. Structural correlates of cognition in dementia: quantification and assessment of synapse change. *Neurodegeneration*. 1996;5(4):417–421.

[74] Coleman PD, Yao PJ. Synaptic slaughter in Alzheimer's disease. *Neurobiology of Aging*. 2003;24(8):1023–1027.

[75] Sperling R, Mormino E, Johnson K. The evolution of preclinical Alzheimer's disease: implications for prevention trials. *Neuron*. 2014;84(3):608–622.

[76] Braak H, Braak E. Neuropathological stageing of Alzheimer-related changes. *Acta Neuropathologica*. 1991;82(4):239–259.

[77] Alafuzoff I, Arzberger T, Al-Sarraj S, Bodi I, Bogdanovic N, Braak H, *et al.* Staging of neurofibrillary pathology in Alzheimer's disease: a study of the BrainNet Europe Consortium. *Brain Pathology*. 2008;18(4):484–496.

[78] Thal DR, Rüb U, Orantes M, Braak H. Phases of Aβ-deposition in the human brain and its relevance for the development of AD. *Neurology*. 2002;58(12):1791–1800.

[79] Lehmann J, Nagy J, Atmadja S, Fibiger H. The nucleus basalis magnocellularis: the origin of a cholinergic projection to the neocortex of the rat. *Neuroscience*. 1980;5(7):1161–1174.

[80] Braak H, Braak E, Bohl J. Staging of Alzheimer-related cortical destruction. *European Neurology*. 1993;33(6):403–408.

[81] Nestor PJ, Scheltens P, Hodges JR. Advances in the early detection of Alzheimer's disease. *Nature Reviews Neuroscience*. 2004;5:S34–S41.

[82] Braak H, Thal DR, Ghebremedhin E, Del Tredici K. Stages of the pathologic process in Alzheimer disease: age categories from 1 to 100 years. *Journal of Neuropathology & Experimental Neurology*. 2011;70(11):960–969.

[83] Holtzman DM, Morris JC, Goate AM. Alzheimer's disease: the challenge of the second century. *Science Translational Medicine*. 2011;3(77):77sr1.

[84] Guerreiro RJ, Gustafson DR, Hardy J. The genetic architecture of Alzheimer's disease: beyond APP, PSENs and APOE. *Neurobiology of Aging*. 2012;33(3):437–456.

[85] Cruchaga C, Chakraverty S, Mayo K, Vallania FL, Mitra RD, Faber K, *et al.* Rare variants in APP, PSEN1 and PSEN2 increase risk for AD in late-onset Alzheimer's disease families. *PloS ONE*. 2012;7(2):e31039.

[86] Benitez BA, Karch CM, Cai Y, Jin SC, Cooper B, Carrell D, *et al.* The PSEN1, p. E318G variant increases the risk of Alzheimer's disease in APOE-ε4 carriers. *PLoS Genetics*. 2013;9(8):e1003685.

[87] Jin SC, Pastor P, Cooper B, Cervantes S, Benitez BA, Razquin C, *et al.* Pooled-DNA sequencing identifies novel causative variants in PSEN1, GRN and MAPT in a clinical early-onset and familial Alzheimer's disease Ibero-American cohort. *Alzheimer's Research & Therapy*. 2012;4(4):34.

[88] Jonsson T, Atwal JK, Steinberg S, Snaedal J, Jonsson PV, Bjornsson S, *et al.* A mutation in APP protects against Alzheimer's disease and age-related cognitive decline. *Nature*. 2012;488(7409):96–99.

[89] Kim M, Suh J, Romano D, Truong MH, Mullin K, Hooli B, *et al.* Potential late-onset Alzheimer's disease-associated mutations in the ADAM10 gene attenuate α-secretase activity. *Human molecular genetics*. 2009;18(20):3987–3996.

[90] Suh J, Choi SH, Romano DM, Gannon MA, Lesinski AN, Kim DY, *et al.* ADAM10 missense mutations potentiate β-amyloid accumulation by impairing prodomain chaperone function. *Neuron*. 2013;80(2):385–401.

[91] Strittmatter WJ, Weisgraber KH, Huang DY, Dong LM, Salvesen GS, Pericak-Vance M, *et al.* Binding of human apolipoprotein E to synthetic amyloid beta peptide:

isoform-specific effects and implications for late-onset Alzheimer disease. *Proceedings of the National Academy of Sciences*. 1993;90(17):8098–8102.

[92] Saunders AM, Strittmatter WJ, Schmechel D, George-Hyslop PS, Pericak-Vance M, Joo S, *et al.* Association of apolipoprotein E allele ε4 with late-onset familial and sporadic Alzheimer's disease. *Neurology*. 1993;43(8):1467–1467.

[93] Bu G. Apolipoprotein E and its receptors in Alzheimer's disease: pathways, pathogenesis and therapy. *Nature Reviews Neuroscience*. 2009;10(5):333.

[94] Sando SB, Melquist S, Cannon A, Hutton ML, Sletvold O, Saltvedt I, *et al.* APOE ε4 lowers age at onset and is a high risk factor for Alzheimer's disease; A case control study from central Norway. *BMC Neurology*. 2008;8(1):9.

[95] Riley KP, Snowdon DA, Saunders AM, Roses AD, Mortimer JA, Nanayakkara N. Cognitive function and apolipoprotein E in very old adults: findings from the Nun Study. *The Journals of Gerontology Series B: Psychological Sciences and Social Sciences*. 2000;55(2):S69–S75.

[96] Wilson R, Bienias J, Berry-Kravis E, Evans D, Bennett D. The apolipoprotein E ε2 allele and decline in episodic memory. *Journal of Neurology, Neurosurgery & Psychiatry*. 2002;73(6):672–677.

[97] Bagyinszky E, Youn YC, An SSA, Kim S. The genetics of Alzheimer's disease. *Clinical Interventions in Aging*. 2014;9:535.

[98] Van Cauwenberghe C, Van Broeckhoven C, Sleegers K. The genetic landscape of Alzheimer disease: clinical implications and perspectives. *Genetics in Medicine*. 2016;18(5):421.

[99] Corder E, Saunders AM, Risch N, Strittmatter W, Schmechel D, Gaskell P, *et al.* Protective effect of apolipoprotein E type 2 allele for late onset Alzheimer disease. *Nature Genetics*. 1994;7(2):180–184.

[100] Farrer LA, Cupples LA, Haines JL, Hyman B, Kukull WA, Mayeux R, *et al.* Effects of age, sex, and ethnicity on the association between apolipoprotein E genotype and Alzheimer disease: a meta-analysis. *JAMA*. 1997;278(16):1349–1356.

[101] Mahley RW, Weisgraber KH, Huang Y. Apolipoprotein E4: a causative factor and therapeutic target in neuropathology, including Alzheimer's disease. *Proceedings of the National Academy of Sciences*. 2006;103(15):5644–5651.

[102] Mahley RW, *et al.* Apolipoprotein E: cholesterol transport protein with expanding role in cell biology. *Science*. 1988;240(4852):622–630.

[103] Kim J, Basak JM, Holtzman DM. The role of apolipoprotein E in Alzheimer's disease. *Neuron*. 2009;63(3):287–303.

[104] Castellano JM, Kim J, Stewart FR, Jiang H, DeMattos RB, Patterson BW, *et al.* Human apoE isoforms differentially regulate brain amyloid-β peptide clearance. *Science Translational Medicine*. 2011;3(89):89ra57.

[105] Verghese PB, Castellano JM, Garai K, Wang Y, Jiang H, Shah A, *et al.* ApoE influences amyloid-β (Aβ) clearance despite minimal apoE/Aβ association in physiological conditions. *Proceedings of the National Academy of Sciences*. 2013;110(19):E1807–E1816.

[106] Atagi Y, Liu CC, Painter MM, Chen XF, Verbeeck C, Zheng H, *et al.* Apolipoprotein E is a ligand for triggering receptor expressed on myeloid cells 2 (TREM2). *Journal of Biological Chemistry*. 2015;290(43):26043–26050.

[107] Bailey CC, DeVaux LB, Farzan M. The triggering receptor expressed on myeloid cells 2 binds apolipoprotein E. *Journal of Biological Chemistry*. 2015;290(43):26033–26042.

[108] Yeh FL, Wang Y, Tom I, Gonzalez LC, Sheng M. TREM2 binds to apolipoproteins, including APOE and CLU/APOJ, and thereby facilitates uptake of amyloid-beta by microglia. *Neuron*. 2016;91(2):328–340.

[109] Guerreiro R, Wojtas A, Bras J, Carrasquillo M, Rogaeva E, Majounie E, *et al.* TREM2 variants in Alzheimer's disease. *New England Journal of Medicine*. 2013;368(2):117–127.

[110] Jonsson T, Stefansson H, Steinberg S, Jonsdottir I, Jonsson PV, Snaedal J, *et al.* Variant of TREM2 associated with the risk of Alzheimer's disease. *New England Journal of Medicine*. 2013;368(2):107–116.

[111] Consortium UBE, *et al.* Rare coding variants in the phospholipase D3 gene confer risk for Alzheimer's disease. *Nature*. 2014;505:550–554.

[112] Sims R, Van Der Lee SJ, Naj AC, Bellenguez C, Badarinarayan N, Jakobsdottir J, *et al.* Rare coding variants in *PLCG2*, *ABI3*, and *TREM2* implicate microglial-mediated innate immunity in Alzheimer's disease. *Nature Genetics*. 2017;49(9):1373–1384.

[113] Harold D, Abraham R, Hollingworth P, Sims R, Gerrish A, Hamshere ML, *et al.* Genome-wide association study identifies variants at CLU and PICALM associated with Alzheimer's disease. *Nature Genetics*. 2009;41(10):1088–1093.

[114] Lambert J, Heath S, Even G, Campion D, Sleegers K, Hiltunen M, *et al.* Genome-wide association study identifies variants at CLU and CR1 associated with Alzheimer's disease. *Nature Genetics*. 2009;41(10):1094–1099.

[115] Naj AC, Jun G, Beecham GW, Wang LS, Vardarajan BN, Buros J, *et al.* Common variants at MS4A4/MS4A6E, CD2AP, CD33 and EPHA1 are associated with late-onset Alzheimer's disease. *Nature Genetics*. 2011;43(5):436–441.

[116] Hollingworth P, Harold D, Sims R, Gerrish A, Lambert JC, Carrasquillo MM, *et al.* Common variants at ABCA7, MS4A6A/MS4A4E, EPHA1, CD33 and CD2AP are associated with Alzheimer's disease. *Nature Genetics*. 2011;43(5):429–435.

[117] Lambert JC, Ibrahim-Verbaas CA, Harold D, Naj AC, Sims R, Bellenguez C, *et al.* Meta-analysis of 74,046 individuals identifies 11 new susceptibility loci for Alzheimer's disease. *Nature Genetics*. 2013;45(12):1452–1458.

[118] Berger SL, Kouzarides T, Shiekhattar R, Shilatifard A. An operational definition of epigenetics. *Genes & Development*. 2009;23(7):781–783.

[119] Jaenisch R, Bird A. Epigenetic regulation of gene expression: how the genome integrates intrinsic and environmental signals. *Nature Genetics*. 2003;33(3s):245.

[120] Chouliaras L, van den Hove DL, Kenis G, Keitel S, Hof PR, van Os J, *et al.* Prevention of age-related changes in hippocampal levels of 5-methylcytidine by caloric restriction. *Neurobiology of Aging*. 2012;33(8):1672–1681.

[121] Chouliaras L, LA van den Hove D, Kenis G, van Draanen M, R Hof P, van Os J, *et al.* Histone deacetylase 2 in the mouse hippocampus: attenuation of age-related increase by caloric restriction. *Current Alzheimer Research.* 2013;10(8):868–876.

[122] Cacabelos R, Torrellas C. Epigenetic drug discovery for Alzheimer's disease. *Expert Opinion on Drug Discovery.* 2014;9(9):1059–1086.

[123] Coppedè F. The potential of epigenetic therapies in neurodegenerative diseases. *Frontiers in Genetics.* 2014;5.

[124] Bennett DA, Yu L, Yang J, Srivastava GP, Aubin C, De Jager PL. Epigenomics of Alzheimer's disease. *Translational Research.* 2015;165(1):200–220.

[125] Marques SC, Oliveira CR, Pereira CM, Outeiro TF. Epigenetics in neurodegeneration: a new layer of complexity. *Progress in Neuro-Psychopharmacology and Biological Psychiatry.* 2011;35(2):348–355.

[126] Wang J, Yu JT, Tan MS, Jiang T, Tan L. Epigenetic mechanisms in Alzheimer's disease: implications for pathogenesis and therapy. *Ageing Research Reviews.* 2013;12(4):1024–1041.

[127] Millan MJ. The epigenetic dimension of Alzheimer's disease: causal, consequence, or curiosity? *Dialogues in Clinical Neuroscience.* 2014;16(3):373.

[128] Jeong S, Liang G, Sharma S, Lin JC, Choi SH, Han H, *et al.* Selective anchoring of DNA methyltransferases 3A and 3B to nucleosomes containing methylated DNA. *Molecular and Cellular Biology.* 2009;29(19):5366–5376.

[129] Urdinguio RG, Sanchez-Mut JV, Esteller M. Epigenetic mechanisms in neurological diseases: genes, syndromes, and therapies. *Lancet Neurology.* 2009;8(11):1056–1072.

[130] Lee JH, Ryu H. Epigenetic modification is linked to Alzheimer's disease: is it a maker or a marker? *BMB Reports.* 2010;43(10):649–655.

[131] Sanchez-Mut JV, Gräff J. Epigenetic alterations in Alzheimer's disease. *Frontiers in Behavioral Neuroscience.* 2015;9.

[132] Mastroeni D, Grover A, Delvaux E, Whiteside C, Coleman PD, Rogers J. Epigenetic mechanisms in Alzheimer's disease. *Neurobiology of Aging.* 2011;32(7):1161–1180.

[133] Chouliaras L, Mastroeni D, Delvaux E, Grover A, Kenis G, Hof PR, *et al.* Consistent decrease in global DNA methylation and hydroxymethylation in the hippocampus of Alzheimer's disease patients. *Neurobiology of Aging.* 2013;34(9):2091–2099.

[134] Smith AR, Smith RG, Condliffe D, Hannon E, Schalkwyk L, Mill J, *et al.* Increased DNA methylation near TREM2 is consistently seen in the superior temporal gyrus in Alzheimer's disease brain. *Neurobiology of Aging.* 2016;47:35–40.

[135] Lunnon K, Smith R, Hannon E, De Jager PL, Srivastava G, Volta M, *et al.* Methylomic profiling implicates cortical deregulation of ANK1 in Alzheimer's disease. *Nature Neuroscience.* 2014;17(9):1164–1170.

[136] De Jager PL, Srivastava G, Lunnon K, Burgess J, Schalkwyk LC, Yu L, *et al.* Alzheimer's disease: early alterations in brain DNA methylation at ANK1, BIN1, RHBDF2 and other loci. *Nature Neuroscience.* 2014;17(9):1156–1163.

[137] Narayan PJ, Lill C, Faull R, Curtis MA, Dragunow M. Increased acetyl and total histone levels in post-mortem Alzheimer's disease brain. *Neurobiology of Disease.* 2015;74:281–294.

[138] Zhang K, Schrag M, Crofton A, Trivedi R, Vinters H, Kirsch W. Targeted proteomics for quantification of histone acetylation in Alzheimer's disease. *Proteomics.* 2012;12(8):1261–1268.

[139] Aisen PS, Schneider LS, Sano M, Diaz-Arrastia R, van Dyck CH, Weiner MF, *et al.* High-dose B vitamin supplementation and cognitive decline in Alzheimer disease: a randomized controlled trial. *JAMA.* 2008;300(15):1774–1783.

[140] Herrmann N, Lanctôt KL, Rothenburg LS, Eryavec G. A placebo-controlled trial of valproate for agitation and aggression in Alzheimer's disease. *Dementia and Geriatric Cognitive Disorders.* 2007;23(2):116.

[141] Hamer M, Chida Y. Physical activity and risk of neurodegenerative disease: a systematic review of prospective evidence. *Psychological Medicine.* 2009;39(1):3–11.

[142] Karp A, Paillard-Borg S, Wang HX, Silverstein M, Winblad B, Fratiglioni L. Mental, physical and social components in leisure activities equally contribute to decrease dementia risk. *Dementia and Geriatric Cognitive Disorders.* 2006;21(2):65–73.

[143] Abbott RD, White LR, Ross GW, Masaki KH, Curb JD, Petrovitch H. Walking and dementia in physically capable elderly men. *JAMA*. 2004;292(12):1447–1453.

[144] Beydoun MA, Beydoun H, Wang Y. Obesity and central obesity as risk factors for incident dementia and its subtypes: a systematic review and meta-analysis. *Obesity Reviews*. 2008;9(3):204–218.

[145] Anstey KJ, Mack HA, Cherbuin N. Alcohol consumption as a risk factor for dementia and cognitive decline: meta-analysis of prospective studies. *The American Journal of Geriatric Psychiatry*. 2009;17(7):542–555.

[146] Barberger-Gateau P, Raffaitin C, Letenneur L, Berr C, Tzourio C, Dartigues JF, *et al.* Dietary patterns and risk of dementia The Three-City cohort study. *Neurology*. 2007;69(20):1921–1930.

[147] Ngandu T, von Strauss E, Helkala EL, Winblad B, Nissinen A, Tuomilehto J, *et al.* Education and dementia What lies behind the association? *Neurology*. 2007;69(14):1442–1450.

[148] Lee Y, Back JH, Kim J, Kim SH, Na DL, Cheong HK, *et al.* Systematic review of health behavioral risks and cognitive health in older adults. *International Psychogeriatrics*. 2010;22(2):174–187.

[149] Anstey KJ, von Sanden C, Salim A, O'kearney R. Smoking as a risk factor for dementia and cognitive decline: a meta-analysis of prospective studies. *American Journal of Epidemiology*. 2007;166(4):367–378.

[150] Nokia MS, Lensu S, Ahtiainen JP, Johansson PP, Koch LG, Britton SL, *et al.* Physical exercise increases adult hippocampal neurogenesis in male rats provided it is aerobic and sustained. *The Journal of Physiology*. 2016;594(7):1855–1873.

[151] Speisman RB, Kumar A, Rani A, Foster TC, Ormerod BK. Daily exercise improves memory, stimulates hippocampal neurogenesis and modulates immune and neuroimmune cytokines in aging rats. *Brain, Behavior, and Immunity*. 2013;28:25–43.

[152] Rovio S, Kåreholt I, Helkala EL, Viitanen M, Winblad B, Tuomilehto J, *et al.* Leisure-time physical activity at midlife and the risk of dementia and Alzheimer's disease. *Lancet Neurology*. 2005;4(11):705–711.

[153] Kivipelto M, Ngandu T, Fratiglioni L, Viitanen M, Kåreholt I, Winblad B, *et al.* Obesity and vascular risk factors at midlife and the risk of dementia and Alzheimer disease. *Archives of Neurology.* 2005;62(10):1556–1560.

[154] Lu Y, Day FR, Gustafsson S, Buchkovich ML, Na J, Bataille V, *et al.* New loci for body fat percentage reveal link between adiposity and cardiometabolic disease risk. *Nature Communications.* 2016;7:10495.

[155] Pedditizi E, Peters R, Beckett N. The risk of overweight/obesity in mid-life and late life for the development of dementia: a systematic review and meta-analysis of longitudinal studies. *Age and Ageing.* 2016;45(1):14–21.

[156] Anttila T, Helkala EL, Viitanen M, Kåreholt I, Fratiglioni L, Winblad B, *et al.* Alcohol drinking in middle age and subsequent risk of mild cognitive impairment and dementia in old age: a prospective population based study. *Bmj.* 2004;329(7465):539.

[157] Huang W, Qiu C, Winblad B, Fratiglioni L. Alcohol consumption and incidence of dementia in a community sample aged 75 years and older. *Journal of Clinical Epidemiology.* 2002;55(10):959–964.

[158] Ruitenberg A, van Swieten JC, Witteman JC, Mehta KM, van Duijn CM, Hofman A, *et al.* Alcohol consumption and risk of dementia: the Rotterdam Study. *Lancet.* 2002;359(9303):281–286.

[159] Paul CA, Au R, Fredman L, Massaro JM, Seshadri S, DeCarli C, *et al.* Association of alcohol consumption with brain volume in the Framingham study. *Archives of Neurology.* 2008;65(10):1363–1367.

[160] Valenzuela MJ, Sachdev P. Brain reserve and dementia: a systematic review. *Psychological Medicine.* 2006;36(4):441–454.

[161] Papp KV, Walsh SJ, Snyder PJ. Immediate and delayed effects of cognitive interventions in healthy elderly: a review of current literature and future directions. *Alzheimer's & Dementia.* 2009;5(1):50–60.

[162] Savva GM, Stephan BC, *et al.* Epidemiological Studies of the Effect of Stroke on Incident Dementia. *Stroke.* 2010;41(1):e41–e46.

[163] Vermeer SE, Hollander M, van Dijk EJ, Hofman A, Koudstaal PJ, Breteler MM. Silent brain infarcts and white matter lesions increase stroke risk in the general population. *Stroke*. 2003;34(5):1126–1129.

[164] Newman AB, Fitzpatrick AL, Lopez O, Jackson S, Lyketsos C, Jagust W, *et al.* Dementia and Alzheimer's disease incidence in relationship to cardiovascular disease in the Cardiovascular Health Study cohort. *Journal of the American Geriatrics Society*. 2005;53(7):1101–1107.

[165] Gottesman RF, Schneider AL, Albert M, Alonso A, Bandeen-Roche K, Coker L, *et al.* Midlife hypertension and 20-year cognitive change: the atherosclerosis risk in communities neurocognitive study. *JAMA Neurology*. 2014;71(10):1218–1227.

[166] Lu FP, Lin KP, Kuo HK. Diabetes and the risk of multi-system aging phenotypes: a systematic review and meta-analysis. *PloS ONE*. 2009;4(1):e4144.

[167] Akomolafe A, Beiser A, Meigs JB, Au R, Green RC, Farrer LA, *et al.* Diabetes mellitus and risk of developing Alzheimer disease: results from the Framingham Study. *Archives of Neurology*. 2006;63(11):1551–1555.

[168] Butterfield DA, Di Domenico F, Barone E. Elevated risk of type 2 diabetes for development of Alzheimer disease: a key role for oxidative stress in brain. *Biochimica et Biophysica Acta (BBA)-Molecular Basis of Disease*. 2014;1842(9):1693–1706.

[169] Rawlings AM, Sharrett AR, Schneider AL, Coresh J, Albert M, Couper D, *et al.* Diabetes in Midlife and Cognitive Change Over 20 Years: A Cohort Study. *Annals of Internal Medicine*. 2014;161(11):785–793.

[170] Exalto LG, Biessels GJ, Karter AJ, Huang ES, Katon WJ, Minkoff JR, *et al.* Risk score for prediction of 10 year dementia risk in individuals with type 2 diabetes: a cohort study. *Lancet Diabetes & Endocrinology*. 2013;1(3):183–190.

[171] Qiu C, Winblad B, Fratiglioni L. The age-dependent relation of blood pressure to cognitive function and dementia. *Lancet Neurology*. 2005;4(8):487–499.

[172] de Bruijn RF, Bos MJ, Portegies ML, Hofman A, Franco OH, Koudstaal PJ, *et al.* The potential for prevention of dementia across two decades: the prospective, population-based Rotterdam Study. *BMC Medicine*. 2015;13(1):132.

[173] Anstey KJ, Lipnicki DM, Low LF. Cholesterol as a risk factor for dementia and cognitive decline: a systematic review of prospective studies with meta-analysis. *The American Journal of Geriatric Psychiatry*. 2008;16(5):343–354.

[174] McGuinness B, Craig D, Bullock R, Passmore P. Statins for the prevention of dementia. *Cochrane Database Syst Rev*. 2009;2(2).

[175] Xue-shan Z, Qi W, Zhong R, Li-hong P, Zhi-han T, Zhi-sheng J, *et al*. Imbalanced cholesterol metabolism in Alzheimer's disease. *Clinica Chimica Acta*. 2016;456:107–114.

[176] Gamba P, Testa G, Sottero B, Gargiulo S, Poli G, Leonarduzzi G. The link between altered cholesterol metabolism and Alzheimer's disease. *Annals of the New York Academy of Sciences*. 2012;1259(1):54–64.

[177] L Ferreira I, Resende R, Ferreiro E, C Rego A, F Pereira C. Multiple defects in energy metabolism in Alzheimer's disease. *Current Drug Targets*. 2010;11(10):1193–1206.

[178] Wiesmann M, Capone C, Zerbi V, Mellendijk L, Heerschap A, AHR Claassen J, *et al*. Hypertension impairs cerebral blood flow in a mouse model for Alzheimer's disease. *Current Alzheimer Research*. 2015;12(10):914–922.

[179] McGuinness B, Todd S, Passmore A, Bullock R. Systematic review: blood pressure lowering in patients without prior cerebrovascular disease for prevention of cognitive impairment and dementia. *Journal of Neurology, Neurosurgery & Psychiatry*. 2008;79(1):4–5.

[180] Scarmeas N, Stern Y, Tang MX, Mayeux R, Luchsinger JA. Mediterranean diet and risk for Alzheimer's disease. *Annals of Neurology*. 2006;59(6):912–921.

[181] Ravaglia G, Forti P, Lucicesare A, Pisacane N, Rietti E, Mangialasche F, *et al*. Plasma tocopherols and risk of cognitive impairment in an elderly Italian cohort. *The American Journal of Clinical Nutrition*. 2008;87(5):1306–1313.

[182] Laurin D, Masaki KH, Foley DJ, White LR, Launer LJ. Midlife dietary intake of antioxidants and risk of late-life incident dementia: the Honolulu-Asia Aging Study. *American Journal of Epidemiology*. 2004;159(10):959–967.

[183] Gray SL, Anderson ML, Crane PK, Breitner J, McCormick W, Bowen JD, *et al.* Antioxidant vitamin supplement use and risk of dementia or Alzheimer's disease in older adults. *Journal of the American Geriatrics Society.* 2008;56(2):291–295.

[184] Malouf M, Grimley EJ, Areosa SA. Folic acid with or without vitamin B12 for cognition and dementia. *Cochrane Database Syst Rev.* 2003;4(4).

[185] Zhang B, Gaiteri C, Bodea LG, Wang Z, McElwee J, Podtelezhnikov AA, *et al.* Integrated systems approach identifies genetic nodes and networks in late-onset Alzheimer's disease. *Cell.* 2013;153(3):707–720.

[186] Bradshaw EM, Chibnik LB, Keenan BT, Ottoboni L, Raj T, Tang A, *et al.* CD33 Alzheimer's disease locus: altered monocyte function and amyloid biology. *Nature Neuroscience.* 2013;16(7):848–850.

[187] Griciuc A, Serrano-Pozo A, Parrado AR, Lesinski AN, Asselin CN, Mullin K, *et al.* Alzheimer's disease risk gene CD33 inhibits microglial uptake of amyloid beta. *Neuron.* 2013;78(4):631–643.

[188] Ginhoux F, Greter M, Leboeuf M, Nandi S, See P, Gokhan S, *et al.* Fate mapping analysis reveals that adult microglia derive from primitive macrophages. *Science.* 2010;330(6005):841–845.

[189] Kierdorf K, Erny D, Goldmann T, Sander V, Schulz C, Perdiguero EG, *et al.* Microglia emerge from erythromyeloid precursors via Pu. 1-and Irf8-dependent pathways. *Nature Neuroscience.* 2013;16(3):273.

[190] Perdiguero EG, Klapproth K, Schulz C, Busch K, Azzoni E, Crozet L, *et al.* Tissue-resident macrophages originate from yolk-sac-derived erythro-myeloid progenitors. *Nature.* 2015;518(7540):547.

[191] Füger P, Hefendehl JK, Veeraraghavalu K, Wendeln AC, Schlosser C, Obermüller U, *et al.* Microglia turnover with aging and in an Alzheimer's model via long-term in vivo single-cell imaging. *Nature Neuroscience.* 2017;.

[192] Kettenmann H, Hanisch UK, Noda M, Verkhratsky A. Physiology of microglia. *Physiological Reviews.* 2011;91(2):461–553.

[193] Ji K, Akgul G, Wollmuth LP, Tsirka SE. Microglia actively regulate the number of functional synapses. *PloS ONE*. 2013;8(2):e56293.

[194] Parkhurst CN, Yang G, Ninan I, Savas JN, Yates JR, Lafaille JJ, *et al.* Microglia promote learning-dependent synapse formation through brain-derived neurotrophic factor. *Cell*. 2013;155(7):1596–1609.

[195] Heneka MT, Carson MJ, El Khoury J, Landreth GE, Brosseron F, Feinstein DL, *et al.* Neuroinflammation in Alzheimer's disease. *Lancet Neurology*. 2015;14(4):388–405.

[196] Jonas RA, Yuan TF, Liang YX, Jonas JB, Tay DK, Ellis-Behnke RG. The spider effect: morphological and orienting classification of microglia in response to stimuli in vivo. *PLoS ONE*. 2012;7(2):e30763.

[197] Ransohoff RM, Perry VH. Microglial physiology: unique stimuli, specialized responses. *Annual Review of Immunology*. 2009;27:119–145.

[198] Gomez-Nicola D, Perry VH. Microglial dynamics and role in the healthy and diseased brain: a paradigm of functional plasticity. *The Neuroscientist*. 2015;21(2):169–184.

[199] Bamberger ME, Harris ME, McDonald DR, Husemann J, Landreth GE. A cell surface receptor complex for fibrillar β-amyloid mediates microglial activation. *Journal of Neuroscience*. 2003;23(7):2665–2674.

[200] Paresce DM, Ghosh RN, Maxfield FR. Microglial cells internalize aggregates of the Alzheimer's disease amyloid β-protein via a scavenger receptor. *Neuron*. 1996;17(3):553–565.

[201] Stewart CR, Stuart LM, Wilkinson K, Van Gils JM, Deng J, Halle A, *et al.* CD36 ligands promote sterile inflammation through assembly of a Toll-like receptor 4 and 6 heterodimer. *Nature Immunology*. 2010;11(2):155–161.

[202] Liu Y, Walter S, Stagi M, Cherny D, Letiembre M, Schulz-Schaeffer W, *et al.* LPS receptor (CD14): a receptor for phagocytosis of Alzheimer's amyloid peptide. *Brain*. 2005;128(8):1778–1789.

[203] Querfurth HW, LaFerla FM. Alzheimer's Disease. *New England Journal of Medicine*. 2010;362(4):329–344.

[204] Kummer MP, Heneka MT. Truncated and modified amyloid-beta species. *Alzheimer's Research & Therapy*. 2014;6(3):28.

[205] El Khoury JB, Moore KJ, Means TK, Leung J, Terada K, Toft M, *et al.* CD36 mediates the innate host response to β-amyloid. *Journal of Experimental Medicine*. 2003;197(12):1657–1666.

[206] Sheedy FJ, Grebe A, Rayner KJ, Kalantari P, Ramkhelawon B, Carpenter SB, *et al.* CD36 coordinates NLRP3 inflammasome activation by facilitating intracellular nucleation of soluble ligands into particulate ligands in sterile inflammation. *Nature Immunology*. 2013;14(8):812–820.

[207] Lee CD, Landreth GE. The role of microglia in amyloid clearance from the AD brain. *Journal of Neural Transmission*. 2010;117(8):949–960.

[208] Mawuenyega KG, Sigurdson W, Ovod V, Munsell L, Kasten T, Morris JC, *et al.* Decreased clearance of CNS β-amyloid in Alzheimer's disease. *Science*. 2010;330(6012):1774–1774.

[209] Hickman SE, Allison EK, El Khoury J. Microglial dysfunction and defective β-amyloid clearance pathways in aging Alzheimer's disease mice. *Journal of Neuroscience*. 2008;28(33):8354–8360.

[210] Prokop S, Miller KR, Drost N, Handrick S, Mathur V, Luo J, *et al.* Impact of peripheral myeloid cells on amyloid-β pathology in Alzheimer's disease–like mice. *Journal of Experimental Medicine*. 2015;p. jem–20150479.

[211] Spangenberg EE, Lee RJ, Najafi AR, Rice RA, Elmore MR, Blurton-Jones M, *et al.* Eliminating microglia in Alzheimer's mice prevents neuronal loss without modulating amyloid-β pathology. *Brain*. 2016;139(4):1265–1281.

[212] Varvel NH, Grathwohl SA, Degenhardt K, Resch C, Bosch A, Jucker M, *et al.* Replacement of brain-resident myeloid cells does not alter cerebral amyloid-β deposition in mouse models of Alzheimer's disease. *Journal of Experimental Medicine*. 2015;212(11):1803–1809.

[213] Sierra-Filardi E, Puig-Kröger A, Blanco FJ, Nieto C, Bragado R, Palomero MI, *et al.* Activin A skews macrophage polarization by promoting a proinflammatory

phenotype and inhibiting the acquisition of anti-inflammatory macrophage markers. *Blood*. 2011;117(19):5092–5101.

[214] Colton CA, Mott RT, Sharpe H, Xu Q, Van Nostrand WE, Vitek MP. Expression profiles for macrophage alternative activation genes in AD and in mouse models of AD. *Journal of Neuroinflammation*. 2006;3(1):27.

[215] Mantovani A, Sica A, Sozzani S, Allavena P, Vecchi A, Locati M. The chemokine system in diverse forms of macrophage activation and polarization. *Trends in Immunology*. 2004;25(12):677–686.

[216] Mantovani A, Sozzani S, Locati M, Allavena P, Sica A. Macrophage polarization: tumor-associated macrophages as a paradigm for polarized M2 mononuclear phagocytes. *Trends in Immunology*. 2002;23(11):549–555.

[217] Koenigsknecht-Talboo J, Landreth GE. Microglial phagocytosis induced by fibrillar β-amyloid and IgGs are differentially regulated by proinflammatory cytokines. *Journal of Neuroscience*. 2005;25(36):8240–8249.

[218] Goerdt S, Orfanos CE. Other functions, other genes: alternative activation of antigen-presenting cells. *Immunity*. 1999;10(2):137–142.

[219] Zelcer N, Khanlou N, Clare R, Jiang Q, Reed-Geaghan EG, Landreth GE, *et al*. Attenuation of neuroinflammation and Alzheimer's disease pathology by liver x receptors. *Proceedings of the National Academy of Sciences*. 2007;104(25):10601–10606.

[220] Martinez FO, Gordon S. The M1 and M2 paradigm of macrophage activation: time for reassessment. *F1000Prime Reports*. 2014;6.

[221] Griffin W, Stanley L, Ling C, White L, MacLeod V, Perrot L, *et al*. Brain interleukin 1 and S-100 immunoreactivity are elevated in Down syndrome and Alzheimer disease. *Proceedings of the National Academy of Sciences*. 1989;86(19):7611–7615.

[222] Patel NS, Paris D, Mathura V, Quadros AN, Crawford FC, Mullan MJ. Inflammatory cytokine levels correlate with amyloid load in transgenic mouse models of Alzheimer's disease. *Journal of Neuroinflammation*. 2005;2(1):9.

[223] Vom Berg J, Prokop S, Miller KR, Obst J, Kälin RE, Lopategui-Cabezas I, *et al.* Inhibition of IL-12/IL-23 signaling reduces Alzheimer's disease-like pathology and cognitive decline. *Nature Medicine.* 2012;18(12):1812–1819.

[224] Fillit H, Ding W, Buee L, Kalman J, Altstiel L, Lawlor B, *et al.* Elevated circulating tumor necrosis factor levels in Alzheimer's disease. *Neuroscience Letters.* 1991;129(2):318–320.

[225] Jekabsone A, Mander PK, Tickler A, Sharpe M, Brown GC. Fibrillar beta-amyloid peptide $A\beta_{1–40}$ activates microglial proliferation via stimulating TNF-α release and H_2O_2 derived from NADPH oxidase: a cell culture study. *Journal of Neuroinflammation.* 2006;3(1):24.

[226] Choi SH, Aid S, Kim HW, Jackson SH, Bosetti F. Inhibition of NADPH oxidase promotes alternative and anti-inflammatory microglial activation during neuroinflammation. *Journal of Neurochemistry.* 2012;120(2):292–301.

[227] Streit WJ, Braak H, Xue QS, Bechmann I. Dystrophic (senescent) rather than activated microglial cells are associated with tau pathology and likely precede neurodegeneration in Alzheimer's disease. *Acta Neuropathologica.* 2009;118(4):475–485.

[228] Krabbe G, Halle A, Matyash V, Rinnenthal JL, Eom GD, Bernhardt U, *et al.* Functional impairment of microglia coincides with Beta-amyloid deposition in mice with Alzheimer-like pathology. *PloS ONE.* 2013;8(4):e60921.

[229] Guillot-Sestier MV, Doty KR, Gate D, Rodriguez J, Leung BP, Rezai-Zadeh K, *et al.* Il10 deficiency rebalances innate immunity to mitigate Alzheimer-like pathology. *Neuron.* 2015;85(3):534–548.

[230] Chakrabarty P, Li A, Ceballos-Diaz C, Eddy JA, Funk CC, Moore B, *et al.* IL-10 alters immunoproteostasis in APP mice, increasing plaque burden and worsening cognitive behavior. *Neuron.* 2015;85(3):519–533.

[231] Lucin KM, O'Brien CE, Bieri G, Czirr E, Mosher KI, Abbey RJ, *et al.* Microglial beclin 1 regulates retromer trafficking and phagocytosis and is impaired in Alzheimer's disease. *Neuron.* 2013;79(5):873–886.

[232] Joutel A, Corpechot C, Ducros A, Vahedi K, Chabriat H, Mouton P, *et al.* Notch3 mutations in CADASIL, a hereditary adult-onset condition causing stroke and dementia. *Nature.* 1996;383(6602):707.

[233] Ruchoux MM, Maurage CA. CADASIL: cerebral autosomal dominant arteriopathy with subcortical infarcts and leukoencephalopathy. *Journal of Neuropathology & Experimental Neurology.* 1997;56(9):947–964.

[234] Kinoshita M, Yoshida K, Oyanagi K, Hashimoto T, Ikeda Si. Hereditary diffuse leukoencephalopathy with axonal spheroids caused by R782H mutation in CSF1R: case report. *Journal of the Neurological Sciences.* 2012;318(1):115–118.

[235] Dos Santos MM, Grond-Ginsbach C, Aksay SS, Chen B, Tchatchou S, Wolf NI, *et al.* Adult-onset autosomal dominant leukodystrophy due to LMNB1 gene duplication. *Journal of Neurology.* 2012;259(3):579–581.

[236] Foulds N, Pengelly RJ, Hammans SR, Nicoll JA, Ellison DW, Ditchfield A, *et al.* Adult-onset leukoencephalopathy with axonal spheroids and pigmented glia caused by a novel R782G mutation in CSF1R. *Scientific Reports.* 2015;5:10042.

[237] Gómez-Nicola D, Fransen NL, Suzzi S, Perry VH. Regulation of microglial proliferation during chronic neurodegeneration. *Journal of Neuroscience.* 2013;33(6):2481–2493.

[238] Olmos-Alonso A, Schetters ST, Sri S, Askew K, Mancuso R, Vargas-Caballero M, *et al.* Pharmacological targeting of CSF1R inhibits microglial proliferation and prevents the progression of Alzheimer's-like pathology. *Brain.* 2016;139(3):891–907.

[239] Jay TR, Miller CM, Cheng PJ, Graham LC, Bemiller S, Broihier ML, *et al.* TREM2 deficiency eliminates TREM2+ inflammatory macrophages and ameliorates pathology in Alzheimer's disease mouse models. *Journal of Experimental Medicine.* 2015;p. jem–20142322.

[240] Butovsky O, Jedrychowski MP, Cialic R, Krasemann S, Murugaiyan G, Fanek Z, *et al.* Targeting miR-155 restores abnormal microglia and attenuates disease in SOD1 mice. *Annals of Neurology.* 2015;77(1):75–99.

[241] Wang Y, Ulland TK, Ulrich JD, Song W, Tzaferis JA, Hole JT, *et al.* TREM2-mediated early microglial response limits diffusion and toxicity of amyloid plaques. *Journal of Experimental Medicine.* 2016;p. jem–20151948.

[242] Sofroniew MV. Molecular dissection of reactive astrogliosis and glial scar formation. *Trends in Neurosciences.* 2009;32(12):638–647.

[243] Sofroniew MV, Vinters HV. Astrocytes: biology and pathology. *Acta Neuropathologica.* 2010;119(1):7–35.

[244] Olabarria M, Noristani HN, Verkhratsky A, Rodríguez JJ. Concomitant astroglial atrophy and astrogliosis in a triple transgenic animal model of Alzheimer's disease. *Glia.* 2010;58(7):831–838.

[245] Olabarria M, Noristani HN, Verkhratsky A, Rodríguez JJ. Age-dependent decrease in glutamine synthetase expression in the hippocampal astroglia of the triple transgenic Alzheimer's disease mouse model: mechanism for deficient glutamatergic transmission? *Molecular Neurodegeneration.* 2011;6(1):55.

[246] Yeh CY, Vadhwana B, Verkhratsky A, Rodríguez JJ. Early astrocytic atrophy in the entorhinal cortex of a triple transgenic animal model of Alzheimer's disease. *ASN Neuro.* 2011;3(5):AN20110025.

[247] Kulijewicz-Nawrot M, Verkhratsky A, Chvatal A, Sykova E, Rodríguez JJ. Astrocytic cytoskeletal atrophy in the medial prefrontal cortex of a triple transgenic mouse model of Alzheimer's disease. *Journal of Anatomy.* 2012;221(3):252–262.

[248] Beauquis J, Pavía P, Pomilio C, Vinuesa A, Podlutskaya N, Galvan V, *et al.* Environmental enrichment prevents astroglial pathological changes in the hippocampus of APP transgenic mice, model of Alzheimer's disease. *Experimental Neurology.* 2013;239:28–37.

[249] Medeiros R, LaFerla FM. Astrocytes: conductors of the Alzheimer disease neuroinflammatory symphony. *Experimental Neurology.* 2013;239:133–138.

[250] Kummer MP, Hammerschmidt T, Martinez A, Terwel D, Eichele G, Witten A, *et al.* Ear2 deletion causes early memory and learning deficits in APP/PS1 mice. *Journal of Neuroscience.* 2014;34(26):8845–8854.

[251] Furman JL, Sama DM, Gant JC, Beckett TL, Murphy MP, Bachstetter AD, *et al.* Targeting astrocytes ameliorates neurologic changes in a mouse model of Alzheimer's disease. *Journal of Neuroscience*. 2012;32(46):16129–16140.

[252] Wyss-Coray T, Loike JD, Brionne TC, Lu E, Anankov R, Yan F, *et al.* Adult mouse astrocytes degrade amyloid-β in vitro and in situ. *Nature Medicine*. 2003;9(4):453–457.

[253] Koistinaho M, Lin S, Wu X, Esterman M, Koger D, Hanson J, *et al.* Apolipoprotein E promotes astrocyte colocalization and degradation of deposited amyloid-β peptides. *Nature Medicine*. 2004;10(7):719–726.

[254] Jiang Q, Lee CD, Mandrekar S, Wilkinson B, Cramer P, Zelcer N, *et al.* ApoE promotes the proteolytic degradation of Aβ. *Neuron*. 2008;58(5):681–693.

[255] Terwel D, Steffensen KR, Verghese PB, Kummer MP, Gustafsson JÅ, Holtzman DM, *et al.* Critical role of astroglial apolipoprotein E and liver X receptor-α expression for microglial Aβ phagocytosis. *Journal of Neuroscience*. 2011;31(19):7049–7059.

[256] Pihlaja R, Koistinaho J, Kauppinen R, Sandholm J, Tanila H, Koistinaho M. Multiple cellular and molecular mechanisms are involved in human Aβ clearance by transplanted adult astrocytes. *Glia*. 2011;59(11):1643–1657.

[257] Iliff JJ, Wang M, Liao Y, Plogg BA, Peng W, Gundersen GA, *et al.* A paravascular pathway facilitates CSF flow through the brain parenchyma and the clearance of interstitial solutes, including amyloid β. *Science Translational Medicine*. 2012;4(147):147ra111–147ra111.

[258] Liddelow SA, Guttenplan KA, Clarke LE, Bennett FC, Bohlen CJ, Schirmer L, *et al.* Neurotoxic reactive astrocytes are induced by activated microglia. *Nature*. 2017;541(7638):481.

[259] Lue LF, Rydel R, Brigham EF, Yang LB, Hampel H, Murphy GM, *et al.* Inflammatory repertoire of Alzheimer's disease and nondemented elderly microglia in vitro. *Glia*. 2001;35(1):72–79.

[260] Heneka MT, Kummer MP, Stutz A, Delekate A, Schwartz S, Saecker A, *et al.* NLRP3 is activated in Alzheimer's disease and contributes to pathology in APP/PS1 mice. *Nature*. 2013;493(7434):674.

[261] Mrak RE, Sheng JG, Griffin WST. Glial cytokines in Alzheimer's disease: review and pathogenic implications. *Human Pathology*. 1995;26(8):816–823.

[262] Tarkowski E, Andreasen N, Tarkowski A, Blennow K. Intrathecal inflammation precedes development of Alzheimer's disease. *Journal of Neurology, Neurosurgery & Psychiatry*. 2003;74(9):1200–1205.

[263] Chou RC, Kane M, Ghimire S, Gautam S, Gui J. Treatment for rheumatoid arthritis and risk of Alzheimer's disease: a nested case-control analysis. *CNS Drugs*. 2016;30(11):1111–1120.

[264] Meda L, Cassatella MA, Szendrei GI, Otvos L, Baron P, Villalba M, *et al*. Activation of microglial cells by β-amyloid protein and interferon-γ. *Nature*. 1995;374(6523):647–650.

[265] Tan J, Town T, Paris D, Mori T, Suo Z, Crawford F, *et al*. Microglial activation resulting from CD40-CD40L interaction after β-amyloid stimulation. *Science*. 1999;286(5448):2352–2355.

[266] Tan J, Town T, Crawford F, Mori T, DelleDonne A, Crescentini R, *et al*. Role of CD40 ligand in amyloidosis in transgenic Alzheimer's mice. *Nature Neuroscience*. 2002;5(12):1288–1294.

[267] Jin JJ, Kim HD, Maxwell JA, Li L, Fukuchi Ki. Toll-like receptor 4-dependent upregulation of cytokines in a transgenic mouse model of Alzheimer's disease. *Journal of Neuroinflammation*. 2008;5(1):23.

[268] Paouri E, Tzara O, Kartalou GI, Zenelak S, Georgopoulos S. Peripheral Tumor Necrosis Factor-alpha (TNF-α) modulates amyloid pathology by regulating blood-derived immune cells and glial response in the brain of AD/TNF transgenic mice. *Journal of Neuroscience*. 2017;37(20):5155–5171.

[269] Chakrabarty P, Ceballos-Diaz C, Beccard A, Janus C, Dickson D, Golde TE, *et al*. IFN-γ promotes complement expression and attenuates amyloid plaque deposition in amyloid β precursor protein transgenic mice. *The Journal of Immunology*. 2010;184(9):5333–5343.

[270] Chakrabarty P, Jansen-West K, Beccard A, Ceballos-Diaz C, Levites Y, Verbeeck C, *et al.* Massive gliosis induced by interleukin-6 suppresses Aβ deposition in vivo: evidence against inflammation as a driving force for amyloid deposition. *The FASEB Journal.* 2010;24(2):548–559.

[271] Chakrabarty P, Herring A, Ceballos-Diaz C, Das P, Golde TE. Hippocampal expression of murine TNFα results in attenuation of amyloid deposition in vivo. *Molecular Neurodegeneration.* 2011;6(1):16.

[272] Shaftel SS, Carlson TJ, Olschowka JA, Kyrkanides S, Matousek SB, O'Banion MK. Chronic interleukin-1β expression in mouse brain leads to leukocyte infiltration and neutrophil-independent blood–brain barrier permeability without overt neurodegeneration. *Journal of Neuroscience.* 2007;27(35):9301–9309.

[273] Ghosh S, Wu MD, Shaftel SS, Kyrkanides S, LaFerla FM, Olschowka JA, *et al.* Sustained interleukin-1β overexpression exacerbates tau pathology despite reduced amyloid burden in an Alzheimer's mouse model. *Journal of Neuroscience.* 2013;33(11):5053–5064.

[274] Savarin-Vuaillat C, Ransohoff RM. Chemokines and chemokine receptors in neurological disease: raise, retain, or reduce? *Neurotherapeutics.* 2007;4(4):590–601.

[275] Xia M, Qin S, Wu L, Mackay CR, Hyman BT. Immunohistochemical study of the β-chemokine receptors CCR3 and CCR5 and their ligands in normal and Alzheimer's disease brains. *The American Journal of Pathology.* 1998;153(1):31–37.

[276] ISHIZUKA K, KIMURA T, IGATA-YI R, KATSURAGI S, TAKAMATSU J, MIYAKAWA T. Identification of monocyte chemoattractant protein-1 in senile plaques and reactive microglia of Alzheimer's disease. *Psychiatry and Clinical Neurosciences.* 1997;51(3):135–138.

[277] El Khoury J, Toft M, Hickman SE, Means TK, Terada K, Geula C, *et al.* Ccr2 deficiency impairs microglial accumulation and accelerates progression of Alzheimer-like disease. *Nature Medicine.* 2007;13(4).

[278] Lee YK, Kwak DH, Oh KW, Nam SY, Lee BJ, Yun YW, *et al.* CCR5 deficiency induces astrocyte activation, Aβ deposit and impaired memory function. *Neurobiology of Learning and Memory.* 2009;92(3):356–363.

[279] Kiyota T, Yamamoto M, Xiong H, Lambert MP, Klein WL, Gendelman HE, *et al.* CCL2 accelerates microglia-mediated Aβ oligomer formation and progression of neurocognitive dysfunction. *PloS ONE.* 2009;4(7):e6197.

[280] Semple BD, Frugier T, Morganti-Kossmann MC. CCL2 modulates cytokine production in cultured mouse astrocytes. *Journal of Neuroinflammation.* 2010;7(1):67.

[281] Smits HA, Rijsmus A, van Loon JH, Wat JW, Verhoef J, Boven LA, *et al.* Amyloid-β-induced chemokine production in primary human macrophages and astrocytes. *Journal of Neuroimmunology.* 2002;127(1):160–168.

[282] Lue LF, Walker DG, Rogers J. Modeling microglial activation in Alzheimer's disease with human postmortem microglial cultures. *Neurobiology of Aging.* 2001;22(6):945–956.

[283] Fuhrmann M, Bittner T, Jung CK, Burgold S, Page RM, Mitteregger G, *et al.* Microglial Cx3cr1 knockout prevents neuron loss in a mouse model of Alzheimer's disease. *Nature Neuroscience.* 2010;13(4):411–413.

[284] Cho SH, Sun B, Zhou Y, Kauppinen TM, Halabisky B, Wes P, *et al.* CX3CR1 protein signaling modulates microglial activation and protects against plaque-independent cognitive deficits in a mouse model of Alzheimer disease. *Journal of Biological Chemistry.* 2011;286(37):32713–32722.

[285] Lee S, Varvel NH, Konerth ME, Xu G, Cardona AE, Ransohoff RM, *et al.* CX3CR1 deficiency alters microglial activation and reduces beta-amyloid deposition in two Alzheimer's disease mouse models. *The American Journal of Pathology.* 2010;177(5):2549–2562.

[286] Sokolowski JD, Chabanon-Hicks CN, Han CZ, Heffron DS, Mandell JW. Fractalkine is a "find-me" signal released by neurons undergoing ethanol-induced apoptosis. *Frontiers in Cellular Neuroscience.* 2014;8.

[287] Vodovotz Y, Lucia MS, Flanders KC, Chesler L, Xie QW, Smith TW, *et al.* Inducible nitric oxide synthase in tangle-bearing neurons of patients with Alzheimer's disease. *Journal of Experimental Medicine.* 1996;184(4):1425–1433.

[288] Nathan C, Calingasan N, Nezezon J, Ding A, Lucia MS, La Perle K, *et al.* Protection from Alzheimer's-like disease in the mouse by genetic ablation of inducible nitric oxide synthase. *Journal of Experimental Medicine.* 2005;202(9):1163–1169.

[289] Murray HW, Teitelbaum RF. L-arginine-dependent reactive nitrogen intermediates and the antimicrobial effect of activated human mononuclear phagocytes. *Journal of Infectious Diseases.* 1992;165(3):513–517.

[290] Schneemann M, Schoedon G, Hofer S, Blau N, Guerrero L, Schaffner A. Nitric oxide synthase is not a constituent of the antimicrobial armature of human mononuclear phagocytes. *Journal of Infectious Diseases.* 1993;167(6):1358–1363.

[291] Weinberg J, Misukonis M, Shami P, Mason S, Sauls D, Dittman W, *et al.* Human mononuclear phagocyte inducible nitric oxide synthase (iNOS): analysis of iNOS mRNA, iNOS protein, biopterin, and nitric oxide production by blood monocytes and peritoneal macrophages. *Blood.* 1995;86(3):1184–1195.

[292] Denis M. Human monocytes/macrophages: NO or no NO? *Journal of Leukocyte Biology.* 1994;55(5):682–684.

[293] Albina JE. On the expression of nitric oxide synthase by human macrophages. Why no NO? *Journal of Leukocyte Biology.* 1995;58(6):643–649.

[294] Schoedon G, Schneemann M, Hofer S, Guerrero L, Blau N, Schaffner A. Regulation of the L-arginine-dependent and tetrahydrobiopterin-dependent biosynthesis of nitric oxide in murine macrophages. *The FEBS Journal.* 1993;213(2):833–839.

[295] Vodovotz Y, Kwon NS, Pospischil M, Manning J, Paik J, Nathan C. Inactivation of nitric oxide synthase after prolonged incubation of mouse macrophages with IFN-gamma and bacterial lipopolysaccharide. *The Journal of Immunology.* 1994;152(8):4110–4118.

[296] Geller DA, Lowenstein CJ, Shapiro RA, Nussler AK, Di Silvio M, Wang SC, *et al.* Molecular cloning and expression of inducible nitric oxide synthase from human hepatocytes. *Proceedings of the National Academy of Sciences.* 1993;90(8):3491–3495.

[297] Linscheid P, Schaffner A, Blau N, Schoedon G. Regulation of 6-pyruvoyltetrahydropterin synthase activity and messenger RNA abundance in human vascular endothelial cells. *Circulation.* 1998;98(17):1703–1706.

[298] Mander P, Brown GC. Activation of microglial NADPH oxidase is synergistic with glial iNOS expression in inducing neuronal death: a dual-key mechanism of inflammatory neurodegeneration. *Journal of Neuroinflammation.* 2005;2(1):20.

[299] Thiabaud G, Pizzocaro S, Garcia-Serres R, Latour JM, Monzani E, Casella L. Heme Binding Induces Dimerization and Nitration of Truncated β-Amyloid Peptide Aβ16 Under Oxidative Stress. *Angewandte Chemie International Edition.* 2013;52(31):8041–8044.

[300] Kummer MP, Hermes M, Delekarte A, Hammerschmidt T, Kumar S, Terwel D, *et al.* Nitration of tyrosine 10 critically enhances amyloid β aggregation and plaque formation. *Neuron.* 2011;71(5):833–844.

[301] Schroder K, Tschopp J. The inflammasomes. *Cell.* 2010;140(6):821–832.

[302] Van de Veerdonk FL, Netea MG, Dinarello CA, Joosten LA. Inflammasome activation and IL-1β and IL-18 processing during infection. *Trends in Immunology.* 2011;32(3):110–116.

[303] Kingham P, Cuzner M, Pocock J. Apoptotic pathways mobilized in microglia and neurones as a consequence of chromogranin A-induced microglial activation. *Journal of Neurochemistry.* 1999;73(2):538–547.

[304] Kingham PJ, Pocock JM. Microglial apoptosis induced by chromogranin A is mediated by mitochondrial depolarisation and the permeability transition but not by cytochrome c release. *Journal of Neurochemistry.* 2000;74(4):1452–1462.

[305] Halle A, Hornung V, Petzold GC, Stewart CR, Monks BG, Reinheckel T, *et al.* The NALP3 inflammasome is involved in the innate immune response to amyloid-β. *Nature Immunology.* 2008;9(8):857–865.

[306] Burguillos MA, Deierborg T, Kavanagh E, Persson A, Hajji N, Garcia-Quintanilla A, *et al.* Caspase signalling controls microglia activation and neurotoxicity. *Nature.* 2011;472(7343):319–324.

[307] Fricker M, Vilalta A, Tolkovsky AM, Brown GC. Caspase inhibitors protect neurons by enabling selective necroptosis of inflamed microglia. *Journal of Biological Chemistry.* 2013;288(13):9145–9152.

[308] Rohn TT, Kokoulina P, Eaton CR, Poon WW. Caspase activation in transgenic mice with Alzheimer-like pathology: results from a pilot study utilizing the caspase inhibitor, Q-VD-OPh. *International Journal of Clinical and Experimental Medicine.* 2009;2(4):300.

[309] Biscaro B, Lindvall O, Tesco G, Ekdahl CT, Nitsch RM. Inhibition of microglial activation protects hippocampal neurogenesis and improves cognitive deficits in a transgenic mouse model for Alzheimer's disease. *Neurodegenerative Diseases.* 2012;9(4):187–198.

[310] Nesargikar P, Spiller B, Chavez R. The complement system: history, pathways, cascade and inhibitors. *European Journal of Microbiology and Immunology.* 2012;2(2):103–111.

[311] Woodruff TM, Ager RR, Tenner AJ, Noakes PG, Taylor SM. The role of the complement system and the activation fragment C5a in the central nervous system. *Neuromolecular Medicine.* 2010;12(2):179–192.

[312] Veerhuis R, Nielsen HM, Tenner AJ. Complement in the brain. *Molecular Immunology.* 2011;48(14):1592–1603.

[313] McGeer P, Akiyama H, Itagaki S, McGeer E. Immune system response in Alzheimer's disease. *Canadian Journal of Neurological Sciences.* 1989;16(S4):516–527.

[314] Strohmeyer R, Ramirez M, Cole GJ, Mueller K, Rogers J. Association of factor H of the alternative pathway of complement with agrin and complement receptor 3 in the Alzheimer's disease brain. *Journal of Neuroimmunology.* 2002;131(1):135–146.

[315] Schafer DP, Lehrman EK, Kautzman AG, Koyama R, Mardinly AR, Yamasaki R, *et al.* Microglia sculpt postnatal neural circuits in an activity and complement-dependent manner. *Neuron.* 2012;74(4):691–705.

[316] Hong S, Dissing-Olesen L, Stevens B. New insights on the role of microglia in synaptic pruning in health and disease. *Current Opinion in Neurobiology.* 2016;36:128–134.

[317] Hong S, Beja-Glasser VF, Nfonoyim BM, Frouin A, Li S, Ramakrishnan S, *et al.* Complement and microglia mediate early synapse loss in Alzheimer mouse models. *Science.* 2016;352(6286):712–716.

[318] Tschopp J, Chonn A, Hertig S, French L. Clusterin, the human apolipoprotein and complement inhibitor, binds to complement C7, C8 beta, and the b domain of C9. *The Journal of Immunology.* 1993;151(4):2159–2165.

[319] Iida K, Nussenzweig V. Complement receptor is an inhibitor of the complement cascade. *Journal of Experimental Medicine.* 1981;153(5):1138–1150.

[320] Buljevac D, Flach H, Hop W, Hijdra D, Laman J, Savelkoul H, *et al.* Prospective study on the relationship between infections and multiple sclerosis exacerbations. *Brain.* 2002;125(5):952–960.

[321] Sibley W, Bamford C, Clark K. Clinical viral infections and multiple sclerosis. *The Lancet.* 1985;325(8441):1313–1315.

[322] Jackson JC, Gordon SM, Hart RP, Hopkins RO, Ely EW. The association between delirium and cognitive decline: a review of the empirical literature. *Neuropsychology Review.* 2004;14(2):87–98.

[323] Fick DM, Agostini JV, Inouye SK. Delirium superimposed on dementia: a systematic review. *Journal of the American Geriatrics Society.* 2002;50(10):1723–1732.

[324] Fong T, Jones R, Shi P, Marcantonio E, Yap L, Rudolph J, *et al.* Delirium accelerates cognitive decline in Alzheimer disease. *Neurology.* 2009;72(18):1570–1575.

[325] Holmes C, Cunningham C, Zotova E, Woolford J, Dean C, Kerr Su, *et al.* Systemic inflammation and disease progression in Alzheimer disease. *Neurology.* 2009;73(10):768–774.

[326] Lee JW, Lee YK, Yuk DY, Choi DY, Ban SB, Oh KW, *et al.* Neuro-inflammation induced by lipopolysaccharide causes cognitive impairment through enhancement of beta-amyloid generation. *Journal of Neuroinflammation.* 2008;5(1):37.

[327] Perry VH, Holmes C. Microglial priming in neurodegenerative disease. *Nature Reviews Neurology.* 2014;10(4):217–224.

[328] Combrinck M, Perry V, Cunningham C. Peripheral infection evokes exaggerated sickness behaviour in pre-clinical murine prion disease. *Neuroscience.* 2002;112(1):7–11.

[329] Cunningham C, Wilcockson DC, Campion S, Lunnon K, Perry VH. Central and systemic endotoxin challenges exacerbate the local inflammatory response and increase neuronal death during chronic neurodegeneration. *Journal of Neuroscience.* 2005;25(40):9275–9284.

[330] Cunningham C, Campion S, Lunnon K, Murray CL, Woods JF, Deacon RM, *et al.* Systemic inflammation induces acute behavioral and cognitive changes and accelerates neurodegenerative disease. *Biological Psychiatry.* 2009;65(4):304–312.

[331] Paloneva J, Manninen T, Christman G, Hovanes K, Mandelin J, Adolfsson R, *et al.* Mutations in two genes encoding different subunits of a receptor signaling complex result in an identical disease phenotype. *The American Journal of Human Genetics.* 2002;71(3):656–662.

[332] Bianchin MM, Capella HM, Chaves DL, Steindel M, Grisard EC, Ganev GG, *et al.* Nasu–Hakola Disease (Polycystic Lipomembranous Osteodysplasia with Sclerosing Leukoencephalopathy—PLOSL): A Dementia Associated with Bone Cystic Lesions. From Clinical to Genetic and Molecular Aspects. *Cellular and Molecular Neurobiology.* 2004;24(1):1–24.

[333] Guerreiro RJ, Lohmann E, Brás JM, Gibbs JR, Rohrer JD, Gurunlian N, *et al.* Using exome sequencing to reveal mutations in TREM2 presenting as a frontotemporal dementia–like syndrome without bone involvement. *JAMA Neurology.* 2013;70(1):78–84.

[334] Giraldo M, Lopera F, Siniard AL, Corneveaux JJ, Schrauwen I, Carvajal J, *et al.* Variants in triggering receptor expressed on myeloid cells 2 are associated with both behavioral variant frontotemporal lobar degeneration and Alzheimer's disease. *Neurobiology of Aging.* 2013;34(8):2077–e11.

[335] Benitez BA, Cruchaga C. TREM2 and neurodegenerative disease. *The New England Journal of Medicine.* 2013;369(16):1567–1568.

[336] Pottier C, Wallon D, Rousseau S, Rovelet-Lecrux A, Richard AC, Rollin-Sillaire A, *et al.* TREM2 R47H variant as a risk factor for early-onset Alzheimer's disease. *Journal of Alzheimer's Disease.* 2013;35(1):45–49.

[337] Guerreiro R, Hardy J. TREM2 and neurodegenerative disease. *New England Journal of Medicine.* 2013;369(16):1569–1570.

[338] Lu Y, Liu W, Wang X. TREM2 variants and risk of Alzheimer's disease: A meta-analysis. *Neurological Sciences.* 2015;36(10):1881–1888.

[339] Borroni B, Ferrari F, Galimberti D, Nacmias B, Barone C, Bagnoli S, *et al.* Heterozygous TREM2 mutations in frontotemporal dementia. *Neurobiology of Aging.* 2014;35(4):934–e7.

[340] Feng Sj, Nie K, Gan R, Huang J, Zhang Yw, Wang Lm, *et al.* Triggering receptor expressed on myeloid cells 2 variants are rare in Parkinson's disease in a Han Chinese cohort. *Neurobiology of Aging.* 2014;35(7):1780–e11.

[341] Soragna D, Tupler R, Ratti M, Montalbetti L, Papi L, Sestini R. An Italian family affected by Nasu-Hakola disease with a novel genetic mutation in the TREM2 gene. *Journal of Neurology, Neurosurgery & Psychiatry.* 2003;74(6):825–826.

[342] Klünemann H, Ridha B, Magy L, Wherrett J, Hemelsoet D, Keen R, *et al.* The genetic causes of basal ganglia calcification, dementia, and bone cysts DAP12 and TREM2. *Neurology.* 2005;64(9):1502–1507.

[343] Bock V, Botturi A, Gaviani P, Lamperti E, Maccagnano C, Piccio L, *et al.* Polycystic lipomembranous osteodysplasia with sclerosing leukoencephalopathy (PLOSL): a new report of an Italian woman and review of the literature. *Journal of the Neurological Sciences.* 2013;326(1):115–119.

[344] Guerreiro R, Bilgic B, Guven G, Brás J, Rohrer J, Lohmann E, *et al.* A novel compound heterozygous mutation in TREM2 found in a Turkish frontotemporal dementia-like family. *Neurobiology of Aging.* 2013;34(12):2890–e1.

[345] Jin SC, Carrasquillo MM, Benitez BA, Skorupa T, Carrell D, Patel D, *et al.* TREM2 is associated with increased risk for Alzheimer's disease in African Americans. *Molecular Neurodegeneration.* 2015;10(1):19.

[346] Yu JT, Jiang T, Wang YL, Wang HF, Zhang W, Hu N, *et al.* Triggering receptor expressed on myeloid cells 2 variant is rare in late-onset Alzheimer's disease in Han Chinese individuals. *Neurobiology of Aging.* 2014;35(4):937–e1.

[347] Chen Y, Chen X, Guo X, Song W, Cao B, Wei Q, *et al.* Assessment of TREM2 rs75932628 association with Parkinson's disease and multiple system atrophy in a Chinese population. *Neurological Sciences.* 2015;36(10):1903–1906.

[348] Tan T, Song Z, Yuan L, Xiong W, Deng X, Ni B, *et al.* Genetic analysis of TREM2 variants in Chinese Han patients with sporadic Parkinson's disease. *Neuroscience Letters.* 2016;612:189–192.

[349] Li Z, Zhong L, Gu L, Huang W, Shi X, Zhang X, *et al.* Association study of TREM2 polymorphism rs75932628 with leucoaraiosis or Parkinson's disease in the Han Chinese population. *BMJ Open.* 2016;6(1):e009499.

[350] Chen X, Chen Y, Wei Q, Guo X, Cao B, Ou R, *et al.* Assessment of TREM2 rs75932628 association with amyotrophic lateral sclerosis in a Chinese population. *Journal of the neurological sciences.* 2015;355(1):193–195.

[351] Ma J, Zhou Y, Xu J, Liu X, Wang Y, Deng Y, *et al.* Association study of TREM2 polymorphism rs75932628 with late-onset Alzheimer's disease in Chinese Han population. *Neurological Research.* 2014;36(10):894–896.

[352] Jiao B, Liu X, Tang B, Hou L, Zhou L, Zhang F, *et al.* Investigation of TREM2, PLD3, and UNC5C variants in patients with Alzheimer's disease from mainland China. *Neurobiology of Aging.* 2014;35(10):2422–e9.

[353] Miyashita A, Wen Y, Kitamura N, Matsubara E, Kawarabayashi T, Shoji M, *et al.* Lack of genetic association between TREM2 and late-onset Alzheimer's disease in a Japanese population. *Journal of Alzheimer's disease.* 2014;41(4):1031–1038.

[354] Huang M, Wang D, Xu Z, Xu Y, Xu X, Ma Y, *et al.* Lack of genetic association between TREM2 and Alzheimer's disease in East Asian population: a systematic review and meta-analysis. *American Journal of Alzheimer's Disease & Other Dementias.* 2015;30(6):541–546.

[355] Cady J, Koval ED, Benitez BA, Zaidman C, Jockel-Balsarotti J, Allred P, *et al.* TREM2 variant p. R47H as a risk factor for sporadic amyotrophic lateral sclerosis. *JAMA Neurology.* 2014;71(4):449–453.

[356] Rayaprolu S, Mullen B, Baker M, Lynch T, Finger E, Seeley WW, *et al.* TREM2 in neurodegeneration: evidence for association of the p. R47H variant with frontotemporal dementia and Parkinson's disease. *Molecular Neurodegeneration.* 2013;8(1):19.

[357] Jin SC, Benitez BA, Karch CM, Cooper B, Skorupa T, Carrell D, *et al.* Coding variants in TREM2 increase risk for Alzheimer's disease. *Human Molecular Genetics.* 2014;23(21):5838–5846.

[358] Le Ber I, De Septenville A, Guerreiro R, Bras J, Camuzat A, Caroppo P, *et al.* Homozygous TREM2 mutation in a family with atypical frontotemporal dementia. *Neurobiology of Aging.* 2014;35(10):2419–e23.

[359] Ghani M, Sato C, Kakhki EG, Gibbs JR, Traynor B, St George-Hyslop P, *et al.* Mutation analysis of the MS4A and TREM gene clusters in a case-control Alzheimer's disease data set. *Neurobiology of Aging.* 2016;42:217–e7.

[360] Thelen M, Razquin C, Hernández I, Gorostidi A, Sánchez-Valle R, Ortega-Cubero S, *et al.* Investigation of the role of rare TREM2 variants in frontotemporal dementia subtypes. *Neurobiology of Aging.* 2014;35(11):2657–e13.

[361] Jiang T, Tan L, Chen Q, Tan MS, Zhou JS, Zhu XC, *et al.* A rare coding variant in TREM2 increases risk for Alzheimer's disease in Han Chinese. *Neurobiology of Aging.* 2016;42:217–e1.

[362] Ulrich JD, Ulland TK, Colonna M, Holtzman DM. Elucidating the Role of TREM2 in Alzheimer's Disease. *Neuron*. 2017;94(2):237–248.

[363] Celarain N, de Gordoa JSR, Zelaya MV, Roldán M, Larumbe R, Pulido L, *et al*. TREM2 upregulation correlates with 5-hydroxymethycytosine enrichment in Alzheimer's disease hippocampus. *Clinical Epigenetics*. 2016;8(1):37.

[364] Ma L, Allen M, Sakae N, Ertekin-Taner N, Graff-Radford NR, Dickson DW, *et al*. Expression and processing analyses of wild type and p. R47H TREM2 variant in Alzheimer's disease brains. *Molecular Neurodegeneration*. 2016;11(1):72.

[365] Satoh Ji, Asahina N, Kitano S, Kino Y. A comprehensive profile of ChIP-Seq-Based PU. 1/Spi1 target genes in microglia. *Gene Regulation and Systems Biology*. 2014;8:127.

[366] Daniel B, Nagy G, Hah N, Horvath A, Czimmerer Z, Poliska S, *et al*. The active enhancer network operated by liganded RXR supports angiogenic activity in macrophages. *Genes & Development*. 2014;28(14):1562–1577.

[367] Lefterov I, Schug J, Mounier A, Nam KN, Fitz NF, Koldamova R. RNA-sequencing reveals transcriptional up-regulation of Trem2 in response to bexarotene treatment. *Neurobiology of Disease*. 2015;82:132–140.

[368] Alexandrov PN, Zhao Y, Jones BM, Bhattacharjee S, Lukiw WJ. Expression of the phagocytosis-essential protein TREM2 is down-regulated by an aluminum-induced miRNA-34a in a murine microglial cell line. *Journal of Inorganic Biochemistry*. 2013;128:267–269.

[369] Bhattacharjee S, Zhao Y, Dua P, Rogaev EI, Lukiw WJ. microRNA-34a-mediated down-regulation of the microglial-enriched triggering receptor and phagocytosis-sensor TREM2 in age-related macular degeneration. *PLoS ONE*. 2016;11(3):e0150211.

[370] Bhattacharjee S, Zhao Y, Lukiw WJ. Deficits in the miRNA-34a-regulated endogenous TREM2 phagocytosis sensor-receptor in Alzheimer's disease (AD); an update. *Frontiers in Aging Neuroscience*. 2014;6.

[371] Zhao Y, Bhattacharjee S, Jones BM, Dua P, Alexandrov PN, Hill JM, *et al.* Regulation of TREM2 expression by an NF-ϰB-sensitive miRNA-34a. *Neuroreport.* 2013;24(6):318.

[372] Zhao Y, Hill JM, Bhattacharjee S, Percy ME, Pogue AI, Lukiw WJ. Aluminum-induced amyloidogenesis and impairment in the clearance of amyloid peptides from the central nervous system in Alzheimer's disease. *Frontiers in Neurology.* 2014;5.

[373] Zhao Y, Jaber V, Lukiw WJ. Over-expressed pathogenic miRNAs in Alzheimer's disease (AD) and prion disease (PrD) drive deficits in TREM2-mediated Aβ42 peptide clearance. *Frontiers in Aging Neuroscience.* 2016;8.

[374] Ozaki Y, Yoshino Y, Yamazaki K, Sao T, Mori Y, Ochi S, *et al.* DNA methylation changes at TREM2 intron 1 and TREM2 mRNA expression in patients with Alzheimer's disease. *Journal of Psychiatric Research.* 2017;92:74–80.

[375] Tserel L, Kolde R, Rebane A, Kisand K, Org T, Peterson H, *et al.* Genome-wide promoter analysis of histone modifications in human monocyte-derived antigen presenting cells. *BMC Genomics.* 2010;11(1):642.

[376] Fujimoto S, Goda T, Mochizuki K. In vivo evidence of enhanced di-methylation of histone H3 K4 on upregulated genes in adipose tissue of diabetic db/db mice. *Biochemical and Biophysical Research Communications.* 2011;404(1):223–227.

[377] Ji JD, Park-Min KH, Shen Z, Fajardo RJ, Goldring SR, McHugh KP, *et al.* Inhibition of RANK expression and osteoclastogenesis by TLRs and IFN-γ in human osteoclast precursors. *The Journal of Immunology.* 2009;183(11):7223–7233.

[378] Kober DL, Alexander-Brett JM, Karch CM, Cruchaga C, Colonna M, Holtzman MJ, *et al.* Neurodegenerative disease mutations in TREM2 reveal a functional surface and distinct loss-of-function mechanisms. *eLife.* 2016;5:e20391.

[379] Park JS, Ji IJ, An HJ, Kang MJ, Kang SW, Kim DH, *et al.* Disease-associated mutations of TREM2 alter the processing of N-linked oligosaccharides in the golgi apparatus. *Traffic.* 2015;16(5):510–518.

[380] Bouchon A, Hernández-Munain C, Cella M, Colonna M. A DAP12-mediated pathway regulates expression of CC chemokine receptor 7 and maturation of human dendritic cells. *Journal of Experimental Medicine*. 2001;194(8):1111–1122.

[381] Gawish R, Martins R, Böhm B, Wimberger T, Sharif O, Lakovits K, *et al.* Triggering receptor expressed on myeloid cells-2 fine-tunes inflammatory responses in murine Gram-negative sepsis. *The FASEB Journal*. 2015;29(4):1247–1257.

[382] Park JS, Ji IJ, Kim DH, An HJ, Yoon SY. The Alzheimer's disease-associated R47H variant of TREM2 has an altered glycosylation pattern and protein stability. *Frontiers in Neuroscience*. 2017;10:618.

[383] Jay TR, von Saucken VE, Landreth GE. TREM2 in neurodegenerative diseases. *Molecular Neurodegeneration*. 2017;12(1):56.

[384] Takahashi K, Rochford CD, Neumann H. Clearance of apoptotic neurons without inflammation by microglial triggering receptor expressed on myeloid cells-2. *Journal of Experimental Medicine*. 2005;201(4):647–657.

[385] Humphrey MB, Daws MR, Spusta SC, Niemi EC, Torchia JA, Lanier LL, *et al.* TREM2, a DAP12-associated receptor, regulates osteoclast differentiation and function. *Journal of Bone and Mineral Research*. 2006;21(2):237–245.

[386] Daws MR, Lanier LL, Seaman WE, Ryan JC. Cloning and characterization of a novel mouse myeloid DAP12-associated receptor family. *European Journal of iImmunology*. 2001;31(3):783–791.

[387] Bouchon A, Dietrich J, Colonna M. Cutting edge: inflammatory responses can be triggered by TREM-1, a novel receptor expressed on neutrophils and monocytes. *The Journal of Immunology*. 2000;164(10):4991–4995.

[388] Lanier LL. DAP10-and DAP12-associated receptors in innate immunity. *Immunological Reviews*. 2009;227(1):150–160.

[389] Call ME, Wucherpfennig KW, Chou JJ. The structural basis for intramembrane assembly of an activating immunoreceptor complex. *Nature Immunology*. 2010;11(11):1023–1029.

[390] Lanier LL, Corliss BC, Wu J, Leong C, Phillips JH. Immunoreceptor DAP12 bearing a tyrosine-based activation motif is involved in activating NK cells. *Nature*. 1998;391(6668):703–707.

[391] Ingley E. Src family kinases: regulation of their activities, levels and identification of new pathways. *Biochimica et Biophysica Acta (BBA)-Proteins and Proteomics*. 2008;1784(1):56–65.

[392] Parsons SJ, Parsons JT. Src family kinases, key regulators of signal transduction. *Oncogene*. 2004;23(48):7906–7909.

[393] Park M, Yi JW, Kim EM, Yoon IJ, Lee EH, Lee HY, *et al.* Triggering receptor expressed on myeloid cells 2 (TREM2) promotes adipogenesis and diet-induced obesity. *Diabetes*. 2015;64(1):117–127.

[394] Takahashi K, Prinz M, Stagi M, Chechneva O, Neumann H. TREM2-transduced myeloid precursors mediate nervous tissue debris clearance and facilitate recovery in an animal model of multiple sclerosis. *PLoS Medicine*. 2007;4(4):e124.

[395] Sun M, Zhu M, Chen K, Nie X, Deng Q, Hazlett LD, *et al.* TREM-2 promotes host resistance against Pseudomonas aeruginosa infection by suppressing corneal inflammation via a PI3K/Akt signaling pathway. *Investigative Ophthalmology & Visual Science*. 2013;54(5):3451–3462.

[396] Peng Q, Malhotra S, Torchia JA, Kerr WG, Coggeshall KM, Humphrey MB. TREM2- and DAP12-dependent activation of PI3K requires DAP10 and is inhibited by SHIP1. *Science Signaling*. 2010;3(122):ra38.

[397] Otero K, Shinohara M, Zhao H, Cella M, Gilfillan S, Colucci A, *et al.* TREM2 and β-catenin regulate bone homeostasis by controlling the rate of osteoclastogenesis. *The Journal of Immunology*. 2012;188(6):2612–2621.

[398] Whittaker GC, Orr SJ, Quigley L, Hughes L, Francischetti IM, Zhang W, *et al.* The linker for activation of B cells (LAB)/non-T cell activation linker (NTAL) regulates triggering receptor expressed on myeloid cells (TREM)-2 signaling and macrophage inflammatory responses independently of the linker for activation of T cells. *Journal of Biological Chemistry*. 2010;285(5):2976–2985.

[399] Zhu M, Li D, Wu Y, Huang X, Wu M. TREM-2 promotes macrophage-mediated eradication of Pseudomonas aeruginosa via a PI3K/Akt pathway. *Scandinavian Journal of Immunology*. 2014;79(3):187–196.

[400] Colonna M, Wang Y. TREM2 variants: new keys to decipher Alzheimer disease pathogenesis. *Nature Reviews Neuroscience*. 2016;17(4):201–207.

[401] Cameron B, Landreth GE. Inflammation, microglia, and Alzheimer's disease. *Neurobiology of Disease*. 2010;37(3):503–509.

[402] Forabosco P, Ramasamy A, Trabzuni D, Walker R, Smith C, Bras J, *et al*. Insights into TREM2 biology by network analysis of human brain gene expression data. *Neurobiology of Aging*. 2013;34(12):2699–2714.

[403] Cella M, Buonsanti C, Strader C, Kondo T, Salmaggi A, Colonna M. Impaired differentiation of osteoclasts in TREM-2–deficient individuals. *Journal of Experimental Medicine*. 2003;198(4):645–651.

[404] Yang AX, Chong N, Jiang Y, Catalano J, Puri RK, Khleif SN. Molecular characterization of antigen-peptide pulsed dendritic cells: immature dendritic cells develop a distinct molecular profile when pulsed with antigen peptide. *PloS ONE*. 2014;9(1):e86306.

[405] Kiialainen A, Veckman V, Saharinen J, Paloneva J, Gentile M, Hakola P, *et al*. Transcript profiles of dendritic cells of PLOSL patients link demyelinating CNS disorders with abnormalities in pathways of actin bundling and immune response. *Journal of Molecular Medicine*. 2007;85(9):971–983.

[406] Hu N, Tan MS, Yu JT, Sun L, Tan L, Wang YL, *et al*. Increased expression of TREM2 in peripheral blood of Alzheimer's disease patients. *Journal of Alzheimer's Disease*. 2014;38(3):497–501.

[407] Rae F, Woods K, Sasmono T, Campanale N, Taylor D, Ovchinnikov DA, *et al*. Characterisation and trophic functions of murine embryonic macrophages based upon the use of a Csf1r–EGFP transgene reporter. *Developmental Biology*. 2007;308(1):232–246.

[408] König S, Regen T, Dittmann K, Engelke M, Wienands J, Schwendener R, *et al.* Empty liposomes induce antitumoral effects associated with macrophage responses distinct from those of the TLR1/2 agonist Pam3CSK4 (BLP). *Cancer Immunology, Immunotherapy.* 2013;62(10):1587–1597.

[409] Li X, Montine KS, Keene CD, Montine TJ. Different mechanisms of apolipoprotein E isoform–dependent modulation of prostaglandin E2 production and triggering receptor expressed on myeloid cells 2 (TREM2) expression after innate immune activation of microglia. *The FASEB Journal.* 2015;29(5):1754–1762.

[410] Elliott R, Li F, Dragomir I, Chua MMW, Gregory BD, Weiss SR. Analysis of the host transcriptome from demyelinating spinal cord of murine coronavirus-infected mice. *PLoS ONE.* 2013;8(9):e75346.

[411] Kiialainen A, Hovanes K, Paloneva J, Kopra O, Peltonen L. Dap12 and Trem2, molecules involved in innate immunity and neurodegeneration, are co-expressed in the CNS. *Neurobiology of Disease.* 2005;18(2):314–322.

[412] Hsieh CL, Koike M, Spusta SC, Niemi EC, Yenari M, Nakamura MC, *et al.* A role for TREM2 ligands in the phagocytosis of apoptotic neuronal cells by microglia. *Journal of Neurochemistry.* 2009;109(4):1144–1156.

[413] Hickman SE, El Khoury J. TREM2 and the neuroimmunology of Alzheimer's disease. *Biochemical Pharmacology.* 2014;88(4):495–498.

[414] Thrash JC, Torbett BE, Carson MJ. Developmental regulation of TREM2 and DAP12 expression in the murine CNS: implications for Nasu-Hakola disease. *Neurochemical Research.* 2009;34(1):38–45.

[415] Zhu C, Herrmann US, Li B, Abakumova I, Moos R, Schwarz P, *et al.* Triggering receptor expressed on myeloid cells-2 is involved in prion-induced microglial activation but does not contribute to prion pathogenesis in mouse brains. *Neurobiology of Aging.* 2015;36(5):1994–2003.

[416] Sessa G, Podini P, Mariani M, Meroni A, Spreafico R, Sinigaglia F, *et al.* Distribution and signaling of TREM2/DAP12, the receptor system mutated in human polycys-

tic lipomembraneous osteodysplasia with sclerosing leukoencephalopathy dementia. *European Journal of Neuroscience*. 2004;20(10):2617–2628.

[417] Jiang T, Tan L, Zhu XC, Zhang QQ, Cao L, Tan MS, *et al*. Upregulation of TREM2 ameliorates neuropathology and rescues spatial cognitive impairment in a transgenic mouse model of Alzheimer's disease. *Neuropsychopharmacology*. 2014;39(13):2949.

[418] Paloneva J, Mandelin J, Kiialainen A, Böhling T, Prudlo J, Hakola P, *et al*. DAP12/TREM2 deficiency results in impaired osteoclast differentiation and osteoporotic features. *Journal of Experimental Medicine*. 2003;198(4):669–675.

[419] Zawawi M, Dharmapatni A, Cantley M, McHugh K, Haynes D, Crotti T. Regulation of ITAM adaptor molecules and their receptors by inhibition of calcineurin-NFAT signalling during late stage osteoclast differentiation. *Biochemical and Biophysical Research Communications*. 2012;427(2):404–409.

[420] Gonçalves LA, Rodrigues-Duarte L, Rodo J, de Moraes LV, Marques I, Penha-Gonçalves C. TREM2 governs Kupffer cell activation and explains belr1 genetic resistance to malaria liver stage infection. *Proceedings of the National Academy of Sciences*. 2013;110(48):19531–19536.

[421] Koth LL, Cambier C, Ellwanger A, Solon M, Hou L, Lanier LL, *et al*. DAP12 is required for macrophage recruitment to the lung in response to cigarette smoke and chemotaxis toward CCL2. *The Journal of Immunology*. 2010;184(11):6522–6528.

[422] Oh JH, Yang MJ, Heo JD, Yang YS, Park HJ, Park SM, *et al*. Inflammatory response in rat lungs with recurrent exposure to welding fumes: a transcriptomic approach. *Toxicology and Industrial Health*. 2012;28(3):203–215.

[423] Song W, Hooli B, Mullin K, Jin SC, Cella M, Ulland TK, *et al*. Alzheimer's disease-associated TREM2 variants exhibit either decreased or increased ligand-dependent activation. *Alzheimer's & Dementia*. 2017;13(4):381–387.

[424] Mori Y, Yoshino Y, Ochi S, Yamazaki K, Kawabe K, Abe M, *et al*. TREM2 mRNA expression in leukocytes is increased in Alzheimer's disease and schizophrenia. *PloS ONE*. 2015;10(9):e0136835.

[425] Satoh Ji, Shimamura Y, Tabunoki H. Gene expression profile of THP-1 monocytes following knockdown of DAP12, a causative gene for Nasu-Hakola disease. *Cellular and Molecular Neurobiology*. 2012;32(3):337–343.

[426] Tan YJ, Ng ASL, Lim JK, Chander RJ, Fang J, Qiu Y, *et al.* Higher peripheral TREM2 mRNA expression levels are related to cognitive deficits and hippocampal atrophy in Alzheimer's Disease and amnestic MCI. *Alzheimer's & Dementia*. 2016;12(7):P241.

[427] Owens R, Grabert K, Davies CL, Alfieri A, Antel JP, Healy LM, *et al.* Divergent Neuroinflammatory Regulation of Microglial TREM Expression and Involvement of NF-κB. *Frontiers in Cellular Neuroscience*. 2017;11.

[428] Melchior B, Garcia AE, Hsiung BK, Lo KM, Doose JM, Thrash JC, *et al.* Dual induction of TREM2 and tolerance-related transcript, Tmem176b, in amyloid transgenic mice: implications for vaccine-based therapies for Alzheimer's disease. *ASN NEURO*. 2010;2(3):AN20100010.

[429] Kawabori M, Kacimi R, Kauppinen T, Calosing C, Kim JY, Hsieh CL, *et al.* Triggering receptor expressed on myeloid cells 2 (TREM2) deficiency attenuates phagocytic activities of microglia and exacerbates ischemic damage in experimental stroke. *Journal of Neuroscience*. 2015;35(8):3384–3396.

[430] Schmid CD, Sautkulis LN, Danielson PE, Cooper J, Hasel KW, Hilbush BS, *et al.* Heterogeneous expression of the triggering receptor expressed on myeloid cells-2 on adult murine microglia. *Journal of Neurochemistry*. 2002;83(6):1309–1320.

[431] Chertoff M, Shrivastava K, Gonzalez B, Acarin L, Giménez-Llort L. Differential modulation of TREM2 protein during postnatal brain development in mice. *PloS ONE*. 2013;8(8):e72083.

[432] Varnum MM, Clayton KA, Yoshii-Kitahara A, Yonemoto G, Koro L, Ikezu S, *et al.* A split-luciferase complementation, real-time reporting assay enables monitoring of the disease-associated transmembrane protein TREM2 in live cells. *Journal of Biological Chemistry*. 2017;p. jbc–M116.

[433] Raha AA, Henderson JW, Stott SR, Vuono R, Foscarin S, Friedland RP, *et al.* Neuroprotective effect of TREM-2 in aging and Alzheimer's disease model. *Journal of Alzheimer's Disease.* 2017;55(1):199–217.

[434] Prada I, Ongania GN, Buonsanti C, Panina-Bordignon P, Meldolesi J. Triggering receptor expressed in myeloid cells 2 (TREM2) trafficking in microglial cells: continuous shuttling to and from the plasma membrane regulated by cell stimulation. *Neuroscience.* 2006;140(4):1139–1148.

[435] Yin J, Liu X, He Q, Zhou L, Yuan Z, Zhao S. Vps35-dependent recycling of Trem2 regulates microglial function. *Traffic.* 2016;17(12):1286–1296.

[436] Cannon JP, O'Driscoll M, Litman GW. Specific lipid recognition is a general feature of CD300 and TREM molecules. *Immunogenetics.* 2012;64(1):39–47.

[437] Poliani PL, Wang Y, Fontana E, Robinette ML, Yamanishi Y, Gilfillan S, *et al.* TREM2 sustains microglial expansion during aging and response to demyelination. *The Journal of Clinical Investigation.* 2015;125(5):2161.

[438] Wang Y, Cella M, Mallinson K, Ulrich JD, Young KL, Robinette ML, *et al.* TREM2 lipid sensing sustains the microglial response in an Alzheimer's disease model. *Cell.* 2015;160(6):1061–1071.

[439] Daws MR, Sullam PM, Niemi EC, Chen TT, Tchao NK, Seaman WE. Pattern recognition by TREM-2: binding of anionic ligands. *The Journal of Immunology.* 2003;171(2):594–599.

[440] Jendresen C, Årskog V, Daws MR, Nilsson LN. The Alzheimer's disease risk factors apolipoprotein E and TREM2 are linked in a receptor signaling pathway. *Journal of Neuroinflammation.* 2017;14(1):59.

[441] Carter DB. The interaction of amyloid-β with ApoE. *Alzheimer's Disease.* 2005;p. 255–272.

[442] Stefano L, Racchetti G, Bianco F, Passini N, Gupta RS, Bordignon PP, *et al.* The surface-exposed chaperone, Hsp60, is an agonist of the microglial TREM2 receptor. *Journal of Neurochemistry.* 2009;110(1):284–294.

[443] Klesney-Tait J, Turnbull IR, Colonna M. The TREM receptor family and signal integration. *Nature Immunology*. 2006;7(12):1266–1273.

[444] Phongsisay V. Campylobacter jejuni targets immunoglobulin-like receptor LMIR5. *Molecular Immunology*. 2015;63(2):574–578.

[445] Phongsisay V, Iizasa E, Hara H, Yamasaki S. 3-O-sulfo-β-D-galactose moiety of endogenous sulfoglycolipids is a potential ligand for immunoglobulin-like receptor LMIR5. *Molecular Immunology*. 2015;63(2):595–599.

[446] N'Diaye EN, Branda CS, Branda SS, Nevarez L, Colonna M, Lowell C, *et al.* TREM-2 (triggering receptor expressed on myeloid cells 2) is a phagocytic receptor for bacteria. *J Cell Biol*. 2009;184(2):215–223.

[447] Charles JF, Humphrey MB, Zhao X, Quarles E, Nakamura MC, Aderem A, *et al.* The innate immune response to Salmonella enterica serovar Typhimurium by macrophages is dependent on TREM2-DAP12. *Infection and Immunity*. 2008;76(6):2439–2447.

[448] Phongsisay V, Iizasa E, Hara H, Yoshida H. Pertussis toxin targets the innate immunity through DAP12, FcRγ, and MyD88 adaptor proteins. *Immunobiology*. 2017;222(4):664–671.

[449] Phongsisay V, Iizasa E, Hara H, Yoshida H. Evidence for TLR4 and FcRγ-CARD9 activation by cholera toxin B subunit and its direct bindings to TREM2 and LMIR5 receptors. *Molecular Immunology*. 2015;66(2):463–471.

[450] Hamerman JA, Jarjoura JR, Humphrey MB, Nakamura MC, Seaman WE, Lanier LL. Cutting edge: Inhibition of TLR and FcR responses in macrophages by triggering receptor expressed on myeloid cells (TREM)-2 and DAP12. *The Journal of Immunology*. 2006;177(4):2051–2055.

[451] Ito H, Hamerman JA. TREM-2, triggering receptor expressed on myeloid cell-2, negatively regulates TLR responses in dendritic cells. *European Journal of Immunology*. 2012;42(1):176–185.

[452] Kleinberger G, Yamanishi Y, Suárez-Calvet M, Czirr E, Lohmann E, Cuyvers E, *et al.* TREM2 mutations implicated in neurodegeneration impair cell surface transport and phagocytosis. *Science Translational Medicine*. 2014;6(243):243ra86–243ra86.

[453] Sirkis DW, Bonham LW, Aparicio RE, Geier EG, Ramos EM, Wang Q, *et al.* Rare TREM2 variants associated with Alzheimer's disease display reduced cell surface expression. *Acta Neuropathologica Communications.* 2016;4(1):98.

[454] Sasaki A, Kakita A, Yoshida K, Konno T, Ikeuchi T, Hayashi S, *et al.* Variable expression of microglial DAP12 and TREM2 genes in Nasu-Hakola disease. *Neurogenetics.* 2015;16(4):265–276.

[455] Roussos P, Katsel P, Fam P, Tan W, Purohit DP, Haroutunian V. The triggering receptor expressed on myeloid cells 2 (TREM2) is associated with enhanced inflammation, neuropathological lesions and increased risk for Alzheimer's dementia. *Alzheimer's & Dementia.* 2015;11(10):1163–1170.

[456] Feuerbach D, Schindler P, Barske C, Joller S, Beng-Louka E, Worringer KA, *et al.* ADAM17 is the main sheddase for the generation of human triggering receptor expressed in myeloid cells (hTREM2) ectodomain and cleaves TREM2 after Histidine 157. *Neuroscience Letters.* 2017;660:109–114.

[457] Matarin M, Salih DA, Yasvoina M, Cummings DM, Guelfi S, Liu W, *et al.* A genome-wide gene-expression analysis and database in transgenic mice during development of amyloid or tau pathology. *Cell Reports.* 2015;10(4):633–644.

[458] Lue LF, Schmitz CT, Serrano G, Sue LI, Beach TG, Walker DG. TREM2 protein expression changes correlate with Alzheimer's disease neurodegenerative pathologies in post-mortem temporal cortices. *Brain Pathology.* 2015;25(4):469–480.

[459] Strobel S, Grünblatt E, Riederer P, Heinsen H, Arzberger T, Al-Sarraj S, *et al.* Changes in the expression of genes related to neuroinflammation over the course of sporadic Alzheimer's disease progression: CX3CL1, TREM2, and PPARγ. *Journal of Neural Transmission.* 2015;122(7):1069–1076.

[460] Martiskainen H, Viswanathan J, Nykänen NP, Kurki M, Helisalmi S, Natunen T, *et al.* Transcriptomics and mechanistic elucidation of Alzheimer's disease risk genes in the brain and in vitro models. *Neurobiology of Aging.* 2015;36(2):1221–e15.

[461] Perez SE, Nadeem M, He B, Miguel JC, Malek-Ahmadi MH, Chen K, *et al.* Neocortical and hippocampal TREM2 protein levels during the progression of Alzheimer's disease. *Neurobiology of Aging.* 2017;54:133–143.

[462] Yeh FL, Hansen DV, Sheng M. TREM2, Microglia, and Neurodegenerative Diseases. *Trends in Molecular Medicine.* 2017;.

[463] Fol R, Braudeau J, Ludewig S, Abel T, Weyer SW, Roederer JP, *et al.* Viral gene transfer of APPsα rescues synaptic failure in an Alzheimer's disease mouse model. *Acta Neuropathologica.* 2016;131(2):247–266.

[464] Frank S, Burbach GJ, Bonin M, Walter M, Streit W, Bechmann I, *et al.* TREM2 is upregulated in amyloid plaque-associated microglia in aged APP23 transgenic mice. *Glia.* 2008;56(13):1438–1447.

[465] Savage JC, Jay T, Goduni E, Quigley C, Mariani MM, Malm T, *et al.* Nuclear receptors license phagocytosis by Trem2+ myeloid cells in mouse models of Alzheimer's disease. *Journal of Neuroscience.* 2015;35(16):6532–6543.

[466] Chan G, White CC, Winn PA, Cimpean M, Replogle JM, Glick LR, *et al.* CD33 modulates TREM2: convergence of Alzheimer loci. *Nature Neuroscience.* 2015;18(11):1556–1558.

[467] Bisht K, Sharma KP, Lecours C, Gabriela Sánchez M, El Hajj H, Milior G, *et al.* Dark microglia: A new phenotype predominantly associated with pathological states. *Glia.* 2016;64(5):826–839.

[468] Jay TR, Hirsch AM, Broihier ML, Miller CM, Neilson LE, Ransohoff RM, *et al.* Disease progression-dependent effects of TREM2 deficiency in a mouse model of Alzheimer's disease. *Journal of Neuroscience.* 2017;37(3):637–647.

[469] Srinivasan K, Friedman BA, Larson JL, Lauffer BE, Goldstein LD, Appling LL, *et al.* Untangling the brain's neuroinflammatory and neurodegenerative transcriptional responses. *Nature Communications.* 2016;7.

[470] Yuan P, Condello C, Keene CD, Wang Y, Bird TD, Paul SM, *et al.* TREM2 haplodeficiency in mice and humans impairs the microglia barrier function leading to

decreased amyloid compaction and severe axonal dystrophy. *Neuron*. 2016;90(4):724–739.

[471] Jiang T, Tan L, Zhu XC, Zhou JS, Cao L, Tan MS, *et al.* Silencing of TREM2 exacerbates tau pathology, neurodegenerative changes, and spatial learning deficits in P301S tau transgenic mice. *Neurobiology of Aging*. 2015;36(12):3176–3186.

[472] Ulrich JD, Finn MB, Wang Y, Shen A, Mahan TE, Jiang H, *et al.* Altered microglial response to Aβ plaques in APPPS1-21 mice heterozygous for TREM2. *Molecular Neurodegeneration*. 2014;9(1):20.

[473] Korvatska O, Leverenz JB, Jayadev S, McMillan P, Kurtz I, Guo X, *et al.* R47H variant of TREM2 associated with Alzheimer disease in a large late-onset family: clinical, genetic, and neuropathological study. *JAMA Neurology*. 2015;72(8):920–927.

[474] Condello C, Yuan P, Schain A, Grutzendler J. Microglia constitute a barrier that prevents neurotoxic protofibrillar Aβ42 hotspots around plaques. *Nature Communications*. 2015;6:6176.

[475] Fahrenhold M, Rakic S, Classey J, Brayne C, Ince PG, Nicoll JA, *et al.* TREM2 expression in the human brain: a marker of monocyte recruitment? *Brain Pathology*. 2017;.

[476] Rosenthal SL, Bamne MN, Wang X, Berman S, Snitz BE, Klunk WE, *et al.* More evidence for association of a rare TREM2 mutation (R47H) with Alzheimer's disease risk. *Neurobiology of Aging*. 2015;36(8):2443–e21.

[477] Camargo LM, Zhang XD, Loerch P, Caceres RM, Marine SD, Uva P, *et al.* Pathway-based analysis of genome-wide siRNA screens reveals the regulatory landscape of APP processing. *PloS ONE*. 2015;10(2):e0115369.

[478] Jiang T, Wan Y, Zhang YD, Zhou JS, Gao Q, Zhu XC, *et al.* TREM2 overexpression has no improvement on neuropathology and cognitive impairment in aging APPswe/PS1dE9 mice. *Molecular Neurobiology*. 2017;54(2):855–865.

[479] Walsh DM, Klyubin I, Fadeeva JV, Cullen WK, Anwyl R, Wolfe MS, *et al.* Naturally secreted oligomers of amyloid β protein potently inhibit hippocampal long-term potentiation in vivo. *Nature*. 2002;416(6880):535–539.

[480] Kayed R, Lasagna-Reeves CA. Molecular mechanisms of amyloid oligomers toxicity. *Journal of Alzheimer's Disease*. 2013;33(s1):S67–S78.

[481] Hu X, Li X, Zhao M, Gottesdiener A, Luo W, Paul S. Tau pathogenesis is promoted by Aβ1-42 but not Aβ1-40. *Molecular Neurodegeneration*. 2014;9(1):52.

[482] Leyns CE, Ulrich JD, Finn MB, Stewart FR, Koscal LJ, Serrano JR, *et al.* TREM2 deficiency attenuates neuroinflammation and protects against neurodegeneration in a mouse model of tauopathy. *Proceedings of the National Academy of Sciences*. 2017;114(43):11524–11529.

[483] Jiang T, Zhang YD, Chen Q, Gao Q, Zhu XC, Zhou JS, *et al.* TREM2 modifies microglial phenotype and provides neuroprotection in P301S tau transgenic mice. *Neuropharmacology*. 2016;105:196–206.

[484] Suárez-Calvet M, Kleinberger G, Caballero MÁA, Brendel M, Rominger A, Alcolea D, *et al.* sTREM2 cerebrospinal fluid levels are a potential biomarker for microglia activity in early-stage Alzheimer9s disease and associate with neuronal injury markers. *EMBO Molecular Medicine*. 2016;p. e201506123.

[485] Benitez BA, Jin SC, Guerreiro R, Graham R, Lord J, Harold D, *et al.* Missense variant in TREML2 protects against Alzheimer's disease. *Neurobiology of Aging*. 2014;35(6):1510–e19.

[486] Rajagopalan P, Hibar DP, Thompson PM. TREM2 and neurodegenerative disease. *The New England Journal of Medicine*. 2013;369(16):1565–1567.

[487] Luis EO, Ortega-Cubero S, Lamet I, Razquin C, Cruchaga C, Benitez BA, *et al.* Frontobasal gray matter loss is associated with the TREM2 p. R47H variant. *Neurobiology of Aging*. 2014;35(12):2681–2690.

[488] Humphrey MB, Ogasawara K, Yao W, Spusta SC, Daws MR, Lane NE, *et al.* The signaling adapter protein DAP12 regulates multinucleation during osteoclast development. *Journal of Bone and Mineral Research*. 2004;19(2):224–234.

[489] Xiang X, Werner G, Bohrmann B, Liesz A, Mazaheri F, Capell A, *et al.* TREM2 deficiency reduces the efficacy of immunotherapeutic amyloid clearance. *EMBO Molecular Medicine*. 2016;8(9):992–1004.

[490] Butovsky O, Jedrychowski MP, Moore CS, Cialic R, Lanser AJ, Gabriely G, *et al.* Identification of a unique TGF-β-dependent molecular and functional signature in microglia. *Nature Neuroscience*. 2014;17(1):131–143.

[491] Sharif O, Gawish R, Warszawska JM, Martins R, Lakovits K, Hladik A, *et al.* The triggering receptor expressed on myeloid cells 2 inhibits complement component 1q effector mechanisms and exerts detrimental effects during pneumococcal pneumonia. *PLoS Pathogens*. 2014;10(6):e1004167.

[492] Chen Q, Zhang K, Jin Y, Zhu T, Cheng B, Shu Q, *et al.* Triggering receptor expressed on myeloid cells-2 protects against polymicrobial sepsis by enhancing bacterial clearance. *American Journal of Respiratory and Critical Care Medicine*. 2013;188(2):201–212.

[493] Cantoni C, Bollman B, Licastro D, Xie M, Mikesell R, Schmidt R, *et al.* TREM2 regulates microglial cell activation in response to demyelination in vivo. *Acta Neuropathologica*. 2015;129(3):429–447.

[494] Trudler D, Weinreb O, Mandel SA, Youdim MB, Frenkel D. DJ-1 deficiency triggers microglia sensitivity to dopamine toward a pro-inflammatory phenotype that is attenuated by rasagiline. *Journal of Neurochemistry*. 2014;129(3):434–447.

[495] Turnbull IR, Gilfillan S, Cella M, Aoshi T, Miller M, Piccio L, *et al.* Cutting edge: TREM-2 attenuates macrophage activation. *The Journal of Immunology*. 2006;177(6):3520–3524.

[496] Zheng H, Liu CC, Atagi Y, Chen XF, Jia L, Yang L, *et al.* Opposing roles of the triggering receptor expressed on myeloid cells 2 and triggering receptor expressed on myeloid cells-like transcript 2 in microglia activation. *Neurobiology of Aging*. 2016;42:132–141.

[497] Gao X, Dong Y, Liu Z, Niu B. Silencing of triggering receptor expressed on myeloid cells-2 enhances the inflammatory responses of alveolar macrophages to lipopolysaccharide. *Molecular Medicine Reports*. 2013;7(3):921–926.

[498] Chang JH, Chang EJ, Kim HH, Kim SK. Enhanced inhibitory effects of a novel CpG motif on osteoclast differentiation via TREM-2 down-regulation. *Biochemical and Biophysical Research Communications*. 2009;389(1):28–33.

[499] Wilkins HM, Carl SM, Weber SG, Ramanujan SA, Festoff BW, Linseman DA, *et al.* Mitochondrial lysates induce inflammation and Alzheimer's disease-relevant changes in microglial and neuronal cells. *Journal of Alzheimer's Disease*. 2015;45(1):305–318.

[500] Sun GY, Guan CX, Zhou Y, Liu YP, Li SF, Zhou HF, *et al.* Vasoactive intestinal peptide re-balances TREM-1/TREM-2 ratio in acute lung injury. *Regulatory Peptides*. 2011;167(1):56–64.

[501] Zhong L, Chen XF, Zhang ZL, Wang Z, Shi XZ, Xu K, *et al.* DAP12 stabilizes the C-terminal fragment of the triggering receptor expressed on myeloid cells-2 (TREM2) and protects against LPS-induced pro-inflammatory response. *Journal of Biological Chemistry*. 2015;290(25):15866–15877.

[502] Wu K, Byers DE, Jin X, Agapov E, Alexander-Brett J, Patel AC, *et al.* TREM-2 promotes macrophage survival and lung disease after respiratory viral infection. *Journal of Experimental Medicine*. 2015;212(5):681–697.

[503] Fujita K, Fukuda M, Fukui H, Horie M, Endoh S, Uchida K, *et al.* Intratracheal instillation of single-wall carbon nanotubes in the rat lung induces time-dependent changes in gene expression. *Nanotoxicology*. 2015;9(3):290–301.

[504] Oh JH, Yang Mj, Yang YS, Park HJ, Heo SH, Lee EH, *et al.* Microarray-based analysis of the lung recovery process after stainless-steel welding fume exposure in Sprague–Dawley rats. *Inhalation Toxicology*. 2009;21(4):347–373.

[505] Morissette MC, Lamontagne M, Berube JC, Gaschler G, Williams A, Yauk C, *et al.* Impact of cigarette smoke on the human and mouse lungs: a gene-expression comparison study. *PLoS ONE*. 2014;9(3):e92498.

[506] Aoki N, Zganiacz A, Margetts P, Xing Z. Differential regulation of DAP12 and molecules associated with DAP12 during host responses to mycobacterial infection. *Infection and Immunity*. 2004;72(5):2477–2483.

[507] Graham LC, Harder JM, Soto I, De Vries WN, John SW, Howell GR. Chronic consumption of a western diet induces robust glial activation in aging mice and in a mouse model of Alzheimer's disease. *Scientific Reports*. 2016;6:21568.

[508] Grant RW, Boler BMV, Ridge TK, Graves TK, Swanson KS. Adipose tissue transcriptome changes during obesity development in female dogs. *Physiological Genomics*. 2011;43(6):295–307.

[509] Crotti TN, Dharmapatni AA, Alias E, Zannettino AC, Smith MD, Haynes DR. The immunoreceptor tyrosine-based activation motif (ITAM)-related factors are increased in synovial tissue and vasculature of rheumatoid arthritic joints. *Arthritis Research & Therapy*. 2012;14(6):R245.

[510] Wang XQ, Tao BB, Li B, Wang XH, Zhang WC, Wan L, *et al*. Overexpression of TREM2 enhances glioma cell proliferation and invasion: a therapeutic target in human glioma. *Oncotarget*. 2016;7(3):2354.

[511] Chakrabarti S, Multani S, Dabholkar J, Saranath D. Whole genome expression profiling in chewing-tobacco-associated oral cancers: a pilot study. *Medical Oncology*. 2015;32(3):60.

[512] Warnecke-Eberz U, Metzger R, Hölscher AH, Drebber U, Bollschweiler E. Diagnostic marker signature for esophageal cancer from transcriptome analysis. *Tumor Biology*. 2016;37(5):6349–6358.

[513] Zhang SL, Chen TS, Xiao L, Ye Y, Xia W, Zhang H. TREM2 siRNA inhibits cell proliferation of human liver cancer cell lines. *International Journal of Clinical and Experimental Pathology*. 2016;9(4):4318–4328.

[514] Alias E, Dharmapatni A, Holding A, Atkins G, Findlay D, Howie D, *et al*. Polyethylene particles stimulate expression of ITAM-related molecules in peri-implant tissues and when stimulating osteoclastogenesis in vitro. *Acta Biomaterialia*. 2012;8(8):3104–3112.

[515] Hopwood B, Tsykin A, Findlay D, Fazzalari N. Gene expression profile of the bone microenvironment in human fragility fracture bone. *Bone*. 2009;44(1):87–101.

[516] Seno H, Miyoshi H, Brown SL, Geske MJ, Colonna M, Stappenbeck TS. Efficient colonic mucosal wound repair requires Trem2 signaling. *Proceedings of the National Academy of Sciences*. 2009;106(1):256–261.

[517] Correale C, Genua M, Vetrano S, Mazzini E, Martinoli C, Spinelli A, *et al.* Bacterial sensor triggering receptor expressed on myeloid cells-2 regulates the mucosal inflammatory response. *Gastroenterology*. 2013;144(2):346–356.

[518] Marcussen M, Bødker JS, Christensen HS, Johansen P, Nielsen S, Christiansen I, *et al.* Molecular Characteristics of High-Dose Melphalan Associated Oral Mucositis in Patients with Multiple Myeloma: A Gene Expression Study on Human Mucosa. *PloS ONE*. 2017;12(1):e0169286.

[519] Preusse C, Goebel HH, Pehl D, Rinnenthal JL, Kley RA, Allenbach Y, *et al.* Th2-M2 immunity in lesions of muscular sarcoidosis and macrophagic myofasciitis. *Neuropathology and Applied Neurobiology*. 2015;41(7):952–963.

[520] Saber M, Kokiko-Cochran O, Puntambekar SS, Lathia JD, Lamb BT. Triggering receptor expressed on myeloid cells 2 deficiency alters acute macrophage distribution and improves recovery after traumatic brain injury. *Journal of Neurotrauma*. 2017;34(2):423–435.

[521] Hernandez A, Donovan V, Grinberg YY, Obenaus A, Carson MJ. Differential detection of impact site versus rotational site injury by magnetic resonance imaging and microglial morphology in an unrestrained mild closed head injury model. *Journal of Neurochemistry*. 2016;136(S1):18–28.

[522] Sieber MW, Jaenisch N, Brehm M, Guenther M, Linnartz-Gerlach B, Neumann H, *et al.* Attenuated inflammatory response in triggering receptor expressed on myeloid cells 2 (TREM2) knock-out mice following stroke. *PloS ONE*. 2013;8(1):e52982.

[523] Kobayashi M, Konishi H, Sayo A, Takai T, Kiyama H. TREM2/DAP12 signal elicits proinflammatory response in microglia and exacerbates neuropathic pain. *Journal of Neuroscience*. 2016;36(43):11138–11150.

[524] Liu G, Liu Y, Jiang Q, Jiang Y, Feng R, Zhang L, *et al.* Convergent genetic and expression datasets highlight TREM2 in Parkinson's disease susceptibility. *Molecular Neurobiology.* 2016;53(7):4931–4938.

[525] Lunnon K, Teeling JL, Tutt AL, Cragg MS, Glennie MJ, Perry VH. Systemic inflammation modulates Fc receptor expression on microglia during chronic neurodegeneration. *The Journal of Immunology.* 2011;186(12):7215–7224.

[526] Petković F, Campbell IL, Gonzalez B, Castellano B. Astrocyte-targeted production of interleukin-6 reduces astroglial and microglial activation in the cuprizone demyelination model: Implications for myelin clearance and oligodendrocyte maturation. *Glia.* 2016;64(12):2104–2119.

[527] Piccio L, Buonsanti C, Cella M, Tassi I, Schmidt RE, Fenoglio C, *et al.* Identification of soluble TREM-2 in the cerebrospinal fluid and its association with multiple sclerosis and CNS inflammation. *Brain.* 2008;131(11):3081–3091.

[528] Fisher Y, Nemirovsky A, Baron R, Monsonego A. T cells specifically targeted to amyloid plaques enhance plaque clearance in a mouse model of Alzheimer's disease. *PloS ONE.* 2010;5(5):e10830.

[529] Jiang T, Yu JT, Zhu XC, Tan MS, Gu LZ, Zhang YD, *et al.* Triggering receptor expressed on myeloid cells 2 knockdown exacerbates aging-related neuroinflammation and cognitive deficiency in senescence-accelerated mouse prone 8 mice. *Neurobiology of Aging.* 2014;35(6):1243–1251.

[530] Sarkar D, Fisher PB. Molecular mechanisms of aging-associated inflammation. *Cancer Letters.* 2006;236(1):13–23.

[531] Takahashi K, Prinz M, Neumann H. Clearance of tissue debris by TREM2-transduced myeloid cells promotes recovery of experimental autoimmune encephalomyelitis. *Journal of Neuroimmunology.* 2006;178:27–28.

[532] Mazaheri F, Snaidero N, Kleinberger G, Madore C, Daria A, Werner G, *et al.* TREM2 deficiency impairs chemotaxis and microglial responses to neuronal injury. *EMBO Reports.* 2017;p. e201743922.

[533] Zheng H, Jia L, Liu CC, Rong Z, Zhong L, Yang L, *et al.* TREM2 promotes microglial survival by activating Wnt/β-catenin pathway. *Journal of Neuroscience.* 2017;37(7):1772–1784.

[534] Wunderlich P, Glebov K, Kemmerling N, Tien NT, Neumann H, Walter J. Sequential proteolytic processing of the triggering receptor expressed on myeloid cells-2 (TREM2) protein by ectodomain shedding and γ-secretase-dependent intramembranous cleavage. *Journal of Biological Chemistry.* 2013;288(46):33027–33036.

[535] Piccio L, Deming Y, Del-Águila JL, Ghezzi L, Holtzman DM, Fagan AM, *et al.* Cerebrospinal fluid soluble TREM2 is higher in Alzheimer disease and associated with mutation status. *Acta Neuropathologica.* 2016;131(6):925–933.

[536] Kim Y, Sato K, Asagiri M, Morita I, Soma K, Takayanagi H. Contribution of nuclear factor of activated T cells c1 to the transcriptional control of immunoreceptor osteoclast-associated receptor but not triggering receptor expressed by myeloid cells-2 during osteoclastogenesis. *Journal of Biological Chemistry.* 2005;280(38):32905–32913.

[537] Zhong L, Chen XF, Wang T, Wang Z, Liao C, Wang Z, *et al.* Soluble TREM2 induces inflammatory responses and enhances microglial survival. *Journal of Experimental Medicine.* 2017;214(3):597–607.

[538] Glebov K, Wunderlich P, Karaca I, Walter J. Functional involvement of γ-secretase in signaling of the triggering receptor expressed on myeloid cells-2 (TREM2). *Journal of Neuroinflammation.* 2016;13(1):17.

[539] Fagan AM, Xiong C, Jasielec MS, Bateman RJ, Goate AM, Benzinger TL, *et al.* Longitudinal change in CSF biomarkers in autosomal-dominant Alzheimer's disease. *Science Translational Medicine.* 2014;6(226):226ra30.

[540] Blennow K, Zetterberg H, Fagan AM. Fluid biomarkers in Alzheimer disease. *Cold Spring Harbor Perspectives in Medicine.* 2012;2(9):a006221.

[541] Brier MR, Gordon B, Friedrichsen K, McCarthy J, Stern A, Christensen J, *et al.* Tau and Aβ imaging, CSF measures, and cognition in Alzheimer's disease. *Science Translational Medicine.* 2016;8(338):338ra66–338ra66.

[542] Heslegrave A, Heywood W, Paterson R, Magdalinou N, Svensson J, Johansson P, *et al.* Increased cerebrospinal fluid soluble TREM2 concentration in Alzheimer's disease. *Molecular Neurodegeneration*. 2016;11(1):3.

[543] Suárez-Calvet M, Caballero MÁA, Kleinberger G, Bateman RJ, Fagan AM, Morris JC, *et al.* Early changes in CSF sTREM2 in dominantly inherited Alzheimer's disease occur after amyloid deposition and neuronal injury. *Science Translational Medicine*. 2016;8(369):369ra178–369ra178.

[544] Öhrfelt A, Axelsson M, Malmeström C, Novakova L, Heslegrave A, Blennow K, *et al.* Soluble TREM-2 in cerebrospinal fluid from patients with multiple sclerosis treated with natalizumab or mitoxantrone. *Multiple Sclerosis Journal*. 2016;22(12):1587–1595.

[545] Henjum K, Almdahl IS, Årskog V, Minthon L, Hansson O, Fladby T, *et al.* Cerebrospinal fluid soluble TREM2 in aging and Alzheimer's disease. *Alzheimer's Research & Therapy*. 2016;8(1):17.

[546] Ran FA, Hsu PD, Wright J, Agarwala V, Scott DA, Zhang F. Genome engineering using the CRISPR-Cas9 system. *Nature Protocols*. 2013;8(11):2281–2308.

[547] Paquet D, Kwart D, Chen A, Sproul A, Jacob S, Teo S, *et al.* Efficient introduction of specific homozygous and heterozygous mutations using CRISPR/Cas9. *Nature*. 2016;533(7601):125–129.

[548] Lin S, Staahl B, Alla RK, Doudna JA. Enhanced homology-directed human genome engineering by controlled timing of CRISPR/Cas9 delivery. *eLife*. 2014;3:e04766.

[549] Kan Y, Ruis B, Takasugi T, Hendrickson EA. Mechanisms of precise genome editing using oligonucleotide donors. *Genome Research*. 2017;.

[550] Hsu PD. RE:Some questions about performing HR-directed genome editing; 2013. Available from: `https://groups.google.com/d/msg/crispr/lKIklFbXjGE/DaPY7aQOXQ0J`.

[551] Hsu PD. RE:Clarification on design of ssDNA oligo template for HR; 2015. Available from: `https://groups.google.com/d/msg/crispr/rCJOlJ91WPY/aL1DpETICEIJ`.

[552] Blasi E, Barluzzi R, Bocchini V, Mazzolla R, Bistoni F. Immortalization of murine microglial cells by a v-raf/v-myc carrying retrovirus. *Journal of Neuroimmunology*. 1990;27(2):229–237.

[553] Graham F, Smiley J, Russell W, Nairn R. Characteristics of a human cell line transformed by DNA from human adenovirus type 5. *Journal of General Virology*. 1977;36(1):59–72.

[554] Ramlee MK, Yan T, Cheung AM, Chuah CT, Li S. High-throughput genotyping of CRISPR/Cas9-mediated mutants using fluorescent PCR-capillary gel electrophoresis. *Scientific Reports*. 2015;5.

[555] Karperien A, Roy TR. Hull And Circle; 2005. Available from: `https://imagej.nih.gov/ij/plugins/hull-circle.html`.

[556] Karperien A, Ahammer H, Jelinek HF. Quantitating the subtleties of microglial morphology with fractal analysis. *Frontiers in Cellular Neuroscience*. 2013;7.

[557] Colonna M. TREMs in the immune system and beyond. *Nature Reviews Immunology*. 2003;3(6):445–453.

[558] Bondolfi L, Calhoun M, Ermini F, Kuhn HG, Wiederhold KH, Walker L, *et al*. Amyloid-associated neuron loss and gliogenesis in the neocortex of amyloid precursor protein transgenic mice. *Journal of Neuroscience*. 2002;22(2):515–522.

[559] Sierra A, Abiega O, Shahraz A, Neumann H. Janus-faced microglia: beneficial and detrimental consequences of microglial phagocytosis. *Frontiers in Cellular Neuroscience*. 2013;7.

[560] Henn A, Lund S, Hedtjärn M, Schrattenholz A, Pörzgen P, Leist M. The suitability of BV2 cells as alternative model system for primary microglia cultures or for animal experiments examining brain inflammation. *ALTEX: Alternatives to Animal Experimentation*. 2009;26(2):83–94.

[561] Stansley B, Post J, Hensley K. A comparative review of cell culture systems for the study of microglial biology in Alzheimer's disease. *Journal of Neuroinflammation*. 2012;9(1):115.

[562] Durafourt BA, Moore CS, Blain M, Antel JP. Isolating, culturing, and polarizing primary human adult and fetal microglia. *Microglia: Methods and Protocols*. 2013;p. 199–211.

[563] De Groot C, Montagne L, Janssen I, Ravid R, Van Der Valk P, Veerhuis R. Isolation and characterization of adult microglial cells and oligodendrocytes derived from postmortem human brain tissue. *Brain Research Protocols*. 2000;5(1):85–94.

[564] Rustenhoven J, Park TI, Schweder P, Scotter J, Correia J, Smith AM, *et al*. Isolation of highly enriched primary human microglia for functional studies. *Scientific Reports*. 2016;6.

[565] Mizee MR, Miedema SS, van der Poel M, Schuurman KG, van Strien ME, Melief J, *et al*. Isolation of primary microglia from the human post-mortem brain: effects of ante- and post-mortem variables. *Acta Neuropathologica Communications*. 2017;5(1):16.

[566] Giulian D, Baker TJ. Characterization of ameboid microglia isolated from developing mammalian brain. *Journal of Neuroscience*. 1986;6(8):2163–2178.

[567] Zhang Y, Su J, Wu S, Teng Y, Yin Z, Guo Y, *et al*. DDR2 (discoidin domain receptor 2) suppresses osteoclastogenesis and is a potential therapeutic target in osteoporosis. *Science Signaling*. 2015;8(369):ra31–ra31.

[568] Muffat J, Li Y, Yuan B, Mitalipova M, Omer A, Corcoran S, *et al*. Efficient derivation of microglia-like cells from human pluripotent stem cells. *Nature Medicine*. 2016;22(11):1358–1367.

[569] Abud EM, Ramirez RN, Martinez ES, Healy LM, Nguyen CH, Newman SA, *et al*. iPSC-derived human microglia-like cells to study neurological diseases. *Neuron*. 2017;94(2):278–293.

[570] Haenseler W, Sansom SN, Buchrieser J, Newey SE, Moore CS, Nicholls FJ, *et al*. A Highly Efficient Human Pluripotent Stem Cell Microglia Model Displays a Neuronal-Co-culture-Specific Expression Profile and Inflammatory Response. *Stem Cell Reports*. 2017;8(6):1727–1742.

[571] Janabi N, Peudenier S, Héron B, Ng KH, Tardieu M. Establishment of human microglial cell lines after transfection of primary cultures of embryonic microglial cells with the SV40 large T antigen. *Neuroscience Letters*. 1995;195(2):105–108.

[572] Nagai A, Nakagawa E, Hatori K, Choi H, McLarnon J, Lee M, *et al*. Generation and characterization of immortalized human microglial cell lines: expression of cytokines and chemokines. *Neurobiology of Disease*. 2001;8(6):1057–1068.

[573] Righi M, Mori L, Libero GD, Sironi M, Biondi A, Mantovani A, *et al*. Monokine production by microglial cell clones. *European Journal of Immunology*. 1989;19(8):1443–1448.

[574] Walker WS, Gatewood J, Olivas E, Askew D, Havenith CE. Mouse microglial cell lines differing in constitutive and interferon-γ-inducible antigen-presenting activities for naive and memory CD4+ and CD8+ T cells. *Journal of Neuroimmunology*. 1995;63(2):163–174.

[575] Alliot F, Marty MC, Cambier D, Pessac B. A spontaneously immortalized mouse microglial cell line expressing CD4. *Developmental Brain Research*. 1996;95(1):140–143.

[576] Ohsawa K, Imai Y, Nakajima K, Kohsaka S. Generation and characterization of a microglial cell line, MG5, derived from a p53-deficient mouse. *Glia*. 1997;21(3):285–298.

[577] Cheepsunthorn P, Radov L, Menzies S, Reid J, Connor JR. Characterization of a novel brain-derived microglial cell line isolated from neonatal rat brain. *Glia*. 2001;35(1):53–62.

[578] Takenouchi T, Ogihara K, Sato M, Kitani H. Inhibitory effects of U73122 and U73343 on Ca^{2+} influx and pore formation induced by the activation of P2X7 nucleotide receptors in mouse microglial cell line. *Biochimica et Biophysica Acta (BBA)-General Subjects*. 2005;1726(2):177–186.

[579] Nagamoto-Combs K, Kulas J, Combs CK. A novel cell line from spontaneously immortalized murine microglia. *Journal of Neuroscience Methods*. 2014;233:187–198.

[580] Das A, Kim SH, Arifuzzaman S, Yoon T, Chai JC, Lee YS, *et al.* Transcriptome sequencing reveals that LPS-triggered transcriptional responses in established microglia BV2 cell lines are poorly representative of primary microglia. *Journal of Neuroinflammation.* 2016;13(1):182.

[581] Horvath RJ, Nutile-McMenemy N, Alkaitis MS, DeLeo JA. Differential migration, LPS-induced cytokine, chemokine, and NO expression in immortalized BV-2 and HAPI cell lines and primary microglial cultures. *Journal of Neurochemistry.* 2008;107(2):557–569.

[582] Dang Y, Xu Y, Wu W, Li W, Sun Y, Yang J, *et al.* Tetrandrine suppresses lipopolysaccharide-induced microglial activation by inhibiting NF-κB and ERK signaling pathways in BV2 cells. *PloS One.* 2014;9(8):e102522.

[583] Floden AM, Li S, Combs CK. β-Amyloid-stimulated microglia induce neuron death via synergistic stimulation of tumor necrosis factor α and NMDA receptors. *Journal of Neuroscience.* 2005;25(10):2566–2575.

[584] Floden AM, Combs CK. β-Amyloid stimulates murine postnatal and adult microglia cultures in a unique manner. *Journal of Neuroscience.* 2006;26(17):4644–4648.

[585] Pan Xd, Zhu Yg, Lin N, Zhang J, Ye Qy, Huang Hp, *et al.* Microglial phagocytosis induced by fibrillar β-amyloid is attenuated by oligomeric β-amyloid: implications for Alzheimer's disease. *Molecular Neurodegeneration.* 2011;6(1):45.

[586] Cizkova D, Le Marrec-Croq F, Franck J, Slovinska L, Grulova I, Devaux S, *et al.* Alterations of protein composition along the rostro-caudal axis after spinal cord injury: proteomic, in vitro and in vivo analyses. *Frontiers in Cellular Neuroscience.* 2014;8.

[587] Wyman C, Kanaar R. DNA double-strand break repair: all's well that ends well. *Annual Review of Genetics.* 2006;40:363–383.

[588] Jacquier A, Dujon B. An intron-encoded protein is active in a gene conversion process that spreads an intron into a mitochondrial gene. *Cell.* 1985;41(2):383–394.

[589] Plessis A, Perrin A, Haber J, Dujon B. Site-specific recombination determined by I-SceI, a mitochondrial group I intron-encoded endonuclease expressed in the yeast nucleus. *Genetics*. 1992;130(3):451–460.

[590] Kouranova E, Forbes K, Zhao G, Warren J, Bartels A, Wu Y, *et al.* CRISPRs for optimal targeting: Delivery of CRISPR components as DNA, RNA, and protein into cultured cells and single-cell embryos. *Human Gene Therapy*. 2016;27(6):464–475.

[591] Kim YG, Cha J, Chandrasegaran S. Hybrid restriction enzymes: zinc finger fusions to Fok I cleavage domain. *Proceedings of the National Academy of Sciences*. 1996;93(3):1156–1160.

[592] Beerli RR, Barbas CF. Engineering polydactyl zinc-finger transcription factors. *Nature Biotechnology*. 2002;20(2):135–141.

[593] Liu Q, Segal DJ, Ghiara JB, Barbas CF. Design of polydactyl zinc-finger proteins for unique addressing within complex genomes. *Proceedings of the National Academy of Sciences*. 1997;94(11):5525–5530.

[594] Durai S, Mani M, Kandavelou K, Wu J, Porteus MH, Chandrasegaran S. Zinc finger nucleases: custom-designed molecular scissors for genome engineering of plant and mammalian cells. *Nucleic Acids Research*. 2005;33(18):5978–5990.

[595] Gonzalez B, Schwimmer LJ, Fuller RP, Ye Y, Asawapornmongkol L, Barbas III CF. Modular system for the construction of zinc-finger libraries and proteins. *Nature Protocols*. 2010;5(4):791.

[596] Moscou MJ, Bogdanove AJ. A simple cipher governs DNA recognition by TAL effectors. *Science*. 2009;326(5959):1501–1501.

[597] Boch J, Scholze H, Schornack S, Landgraf A, Hahn S, Kay S, *et al.* Breaking the code of DNA binding specificity of TAL-type III effectors. *Science*. 2009;326(5959):1509–1512.

[598] Gaj T, Gersbach CA, Barbas CF. ZFN, TALEN, and CRISPR/Cas-based methods for genome engineering. *Trends in Biotechnology*. 2013;31(7):397–405.

[599] Wiedenheft B, Sternberg SH, Doudna JA. RNA-guided genetic silencing systems in bacteria and archaea. *Nature*. 2012;482(7385):331.

[600] Jinek M, Chylinski K, Fonfara I, Hauer M, Doudna JA, Charpentier E. A programmable dual-RNA–guided DNA endonuclease in adaptive bacterial immunity. *Science*. 2012;337(6096):816–821.

[601] Mojica F, Diez-Villasenor C, Garcia-Martinez J, Almendros C. Short motif sequences determine the targets of the prokaryotic CRISPR defence system. *Microbiology*. 2009;155(3):733–740.

[602] Cong L, Ran FA, Cox D, Lin S, Barretto R, Habib N, *et al*. Multiplex genome engineering using CRISPR/Cas systems. *Science*. 2013;339(6121):819–823.

[603] Liang X, Potter J, Kumar S, Zou Y, Quintanilla R, Sridharan M, *et al*. Rapid and highly efficient mammalian cell engineering via Cas9 protein transfection. *Journal of Biotechnology*. 2015;208:44–53.

[604] Ran FA. Puromycin selection problems with PX459 and PX462; 2015. Available from: `https://groups.google.com/d/msg/crispr/CQN9SbqReVg/KK7T1h8VdN4J`.

[605] Ann Ran F, Hsu PD, Lin CY, Gootenberg JS, Konermann S, Trevino AE, *et al*. Double nicking by RNA-guided CRISPR Cas9 for enhanced genome editing specificity. *Cell*. 2013;154(6):1380–1389.

[606] Hornik TC, Neniskyte U, Brown GC. Inflammation induces multinucleation of Microglia via PKC inhibition of cytokinesis, generating highly phagocytic multinucleated giant cells. *Journal of Neurochemistry*. 2014;128(5):650–661.

[607] Hsu PD, Lander ES, Zhang F. Development and applications of CRISPR-Cas9 for genome engineering. *Cell*. 2014;157(6):1262–1278.

[608] Lee TT, Martin FC, Merrill JE. Lymphokine induction of rat microglia multinucleated giant cell formation. *Glia*. 1993;8(1):51–61.

[609] Suzumura A, Tamaru T, Yoshikawa M, Takayanagi T. Multinucleated giant cell formation by microglia: induction by interleukin (IL)-4 and IL-13. *Brain Research*. 1999;849(1):239–243.

[610] Beyer M, Gimsa U, Eyüpoglu I, Hailer N, Nitsch R. Phagocytosis of neuronal or glial debris by microglial cells: upregulation of MHC class II expression and multinuclear giant cell formation in vitro. *Glia*. 2000;31(3):262–266.

[611] Kusyk C, Hsu T. Induction of high frequencies of endoreduplication in mammalian cell cultures with 33258 Hoechst and rubidazone. *Cytogenetic and Genome Research*. 1979;23(1-2):39–43.

[612] Durand RE, Olive PL. Cytotoxicity, Mutagenicity and DNA damage by Hoechst 33342. *Journal of Histochemistry & Cytochemistry*. 1982;30(2):111–116.

[613] Parrilla I, Vazquez J, Cuello C, Gil M, Roca J, Di Berardino D, *et al*. Hoechst 33342 stain and uv laser exposure do not induce genotoxic effects in flow-sorted boar spermatozoa. *Reproduction*. 2004;128(5):615–621.

[614] Todaro GJ, Green H. Quantitative studies of the growth of mouse embryo cells in culture and their development into established lines. *The Journal of Cell Biology*. 1963;17(2):299–313.

[615] Orchard RC, Wilen CB, Doench JG, Baldridge MT, McCune BT, Lee YCJ, *et al*. Discovery of a proteinaceous cellular receptor for a norovirus. *Science*. 2016;353(6302):933–936.

[616] Yang L, Yang JL, Byrne S, Pan J, Church GM. CRISPR/Cas9-Directed Genome Editing of Cultured Cells. *Current Protocols in Molecular Biology*. 2014;p. 31.1.

[617] Mali P, Aach J, Stranges PB, Esvelt KM, Moosburner M, Kosuri S, *et al*. CAS9 transcriptional activators for target specificity screening and paired nickases for cooperative genome engineering. *Nature Biotechnology*. 2013;31(9):833–838.

[618] Chang N, Sun C, Gao L, Zhu D, Xu X, Zhu X, *et al*. Genome editing with RNA-guided Cas9 nuclease in zebrafish embryos. *Cell Research*. 2013;23(4):465.

[619] Agudelo D, Bozoyan L, Duringer A, Huard CC, Carter S, Loehr J, *et al*. A marker-free co-selection strategy for high efficiency human genome engineering. *bioRxiv*. 2017;p. 116251.

[620] Heyer WD, Ehmsen KT, Liu J. Regulation of homologous recombination in eukaryotes. *Annual Review of Genetics*. 2010;44:113–139.

[621] Orthwein A, Fradet-Turcotte A, Noordermeer SM, Canny MD, Brun CM, Strecker J, *et al*. Mitosis inhibits DNA double-strand break repair to guard against telomere fusions. *Science*. 2014;344(6180):189–193.

[622] Takata M, Sasaki MS, Sonoda E, Morrison C, Hashimoto M, Utsumi H, *et al.* Homologous recombination and non-homologous end-joining pathways of DNA double-strand break repair have overlapping roles in the maintenance of chromosomal integrity in vertebrate cells. *The EMBO Journal.* 1998;17(18):5497–5508.

[623] Shrivastav M, De Haro LP, Nickoloff JA. Regulation of DNA double-strand break repair pathway choice. *Cell Research.* 2008;18(1):134.

[624] Woodard LE, Wilson MH. piggyBac-ing models and new therapeutic strategies. *Trends in Biotechnology.* 2015;33(9):525–533.

[625] Parwaresch M, Radzun H, Kreipe H, Hansmann M, Barth J. Monocyte/macrophage-reactive monoclonal antibody Ki-M6 recognizes an intracytoplasmic antigen. *The American Journal of Pathology.* 1986;125(1):141.

[626] Pulford KA, Sipos A, Cordell JL, Stross WP, Mason DY. Distribution of the CD68 macrophage/myeloid associated antigen. *International Immunology.* 1990;2(10):973–980.

[627] Yu CY, Yang Z, Blanchong CA, Miller W. The human and mouse MHC class III region: a parade of 21 genes at the centromeric segment. *Immunology Today.* 2000;21(7):320–328.

[628] Roche PA, Furuta K. The ins and outs of MHC class II-mediated antigen processing and presentation. *Nature Reviews: Immunology.* 2015;15(4):203.

[629] McGeer P, Itagaki S, Tago H, McGeer E. Occurrence of HLA-DR Reactive Microglia in Alzheimer's Disease. *Annals of the New York Academy of Sciences.* 1988;540(1):319–323.

[630] McGeer P, Itagaki S, McGeer E. Expression of the histocompatibility glycoprotein HLA-DR in neurological disease. *Acta Neuropathologica.* 1988;76(6):550–557.

[631] Mattiace LA, Davies P, Dickson DW. Detection of HLA-DR on microglia in the human brain is a function of both clinical and technical factors. *The American Journal of Pathology.* 1990;136(5):1101.

[632] Gehrmann J, Banati RB, Kreutzberg GW. Microglia in the immune surveillance of the brain: human microglia constitutively express HLA-DR molecules. *Journal of Neuroimmunology*. 1993;48(2):189–198.

[633] Köhler C. Allograft inflammatory factor-1/Ionized calcium-binding adapter molecule 1 is specifically expressed by most subpopulations of macrophages and spermatids in testis. *Cell and Tissue Research*. 2007;330(2):291–302.

[634] Ahmed Z, Shaw G, Sharma VP, Yang C, McGowan E, Dickson DW. Actin-binding proteins coronin-1a and IBA-1 are effective microglial markers for immunohistochemistry. *Journal of Histochemistry & Cytochemistry*. 2007;55(7):687–700.

[635] Ito D, Imai Y, Ohsawa K, Nakajima K, Fukuuchi Y, Kohsaka S. Microglia-specific localisation of a novel calcium binding protein, Iba1. *Molecular Brain Research*. 1998;57(1):1–9.

[636] Ohsawa K, Imai Y, Kanazawa H, Sasaki Y, Kohsaka S. Involvement of Iba1 in membrane ruffling and phagocytosis of macrophages/microglia. *Journal of Cell Science*. 2000;113(17):3073–3084.

[637] Ajami B, Bennett JL, Krieger C, Tetzlaff W, Rossi FM. Local self-renewal can sustain CNS microglia maintenance and function throughout adult life. *Nature Neuroscience*. 2007;10(12):1538.

[638] Ransohoff RM. Microgliosis: the questions shape the answers. *Nature Neuroscience*. 2007;10(12):1507–1509.

[639] Torres-Platas SG, Comeau S, Rachalski A, Dal Bo G, Cruceanu C, Turecki G, *et al*. Morphometric characterization of microglial phenotypes in human cerebral cortex. *Journal of Neuroinflammation*. 2014;11(1):12.

[640] Zanier ER, Fumagalli S, Perego C, Pischiutta F, De Simoni MG. Shape descriptors of the "never resting" microglia in three different acute brain injury models in mice. *Intensive Care Medicine Experimental*. 2015;3(1):7.

[641] Braak H, Braak E, Ohm T, Bohl J. Alzheimer's disease: mismatch between amyloid plaques and neuritic plaques. *Neuroscience Letters*. 1989;103(1):24–28.

[642] Ravichandran KS. "Recruitment signals" from apoptotic cells: invitation to a quiet meal. *Cell*. 2003;113(7):817–820.

[643] Russell DG. Mycobacterium tuberculosis and the intimate discourse of a chronic infection. *Immunological Reviews*. 2011;240(1):252–268.

[644] Kurushima H, Ramprasad M, Kondratenko N, Foster D, Quehenberger O, Steinberg D. Surface expression and rapid internalization of macrosialin (mouse CD68) on elicited mouse peritoneal macrophages. *Journal of Leukocyte Biology*. 2000;67(1):104–108.

[645] Beranek J. CD68 is not a macrophage-specific antigen. *Annals of the Rheumatic Diseases*. 2005;64(2):342–344.

[646] McGeer PL, Itagaki S, Tago H, McGeer EG. Reactive microglia in patients with senile dementia of the Alzheimer type are positive for the histocompatibility glycoprotein HLA-DR. *Neuroscience Letters*. 1987;79(1):195–200.

[647] Styren SD, Civin WH, Rogers J. Molecular, cellular, and pathologic characterization of HLA-DR immunoreactivity in normal elderly and Alzheimer's disease brain. *Experimental Neurology*. 1990;110(1):93–104.

[648] Perlmutter L, Scott S, Barron E, Chui H. MHC class II-positive microglia in human brain: Association with Alzheimer lesions. *Journal of Neuroscience Research*. 1992;33(4):549–558.

[649] McGeer P, Itagaki S, Boyes B, McGeer E. Reactive microglia are positive for HLA-DR in the substantia nigra of Parkinson's and Alzheimer's disease brains. *Neurology*. 1988;38(8):1285–1285.

[650] Sapp E, Kegel K, Aronin N, Hashikawa T, Uchiyama Y, Tohyama K, *et al*. Early and progressive accumulation of reactive microglia in the Huntington disease brain. *Journal of Neuropathology & Experimental Neurology*. 2001;60(2):161–172.

[651] Neumann H, Boucraut J, Hahnel C, Misgeld T, Wekerle H. Neuronal control of MHC class II inducibility in rat astrocytes and microglia. *European Journal of Neuroscience*. 1996;8(12):2582–2590.

[652] Beach T, Woodhurst W, MacDonald D, Jones M. Reactive microglia in hippocampal sclerosis associated with human temporal lobe epilepsy. *Neuroscience Letters*. 1995;191(1):27–30.

[653] Xiang Z, Haroutunian V, Ho L, Purohit D, Pasinetti GM. Microglia activation in the brain as inflammatory biomarker of Alzheimer's disease neuropathology and clinical dementia. *Disease markers*. 2006;22(1-2):95–102.

[654] Rogers J, Lue LF. Microglial chemotaxis, activation, and phagocytosis of amyloid β-peptide as linked phenomena in Alzheimer's disease. *Neurochemistry International*. 2001;39(5):333–340.

[655] Rogers J, Luber-Narod J, Styren SD, Civin WH. Expression of immune system-associated antigens by cells of the human central nervous system: relationship to the pathology of Alzheimer's disease. *Neurobiology of Aging*. 1988;9:339–349.

[656] Streit W, Sparks DL. Activation of microglia in the brains of humans with heart disease and hypercholesterolemic rabbits. *Journal of Molecular Medicine*. 1997;75(2):130–138.

[657] DiPatre PL, Gelman BB. Microglial cell activation in aging and Alzheimer disease: partial linkage with neurofibrillary tangle burden in the hippocampus. *Journal of Neuropathology & Experimental Neurology*. 1997;56(2):143–149.

[658] Sheffield L, Berman N. Microglial expression of MHC class II increases in normal aging of nonhuman primates. *Neurobiology of Aging*. 1998;19(1):47–55.

[659] Frank MG, Barrientos RM, Biedenkapp JC, Rudy JW, Watkins LR, Maier SF. mRNA up-regulation of MHC II and pivotal pro-inflammatory genes in normal brain aging. *Neurobiology of aAging*. 2006;27(5):717–722.

[660] Melchior B, Puntambekar SS, Carson MJ. Microglia and the control of autoreactive T cell responses. *Neurochemistry International*. 2006;49(2):145–153.

[661] Becher B, Prat A, Antel JP. Brain-immune connection: Immuno-regulatory properties of CNS-resident cells. *Glia*. 2000;29(4):293–304.

[662] Aloisi F. Immune function of microglia. *Glia*. 2001;36(2):165–179.

[663] Barker CF, Billingham R. Immunologically privileged sites. *Advances in Immunology*. 1978;25:1–54.

[664] Williams KA, Hart DN, Fabre JW, Morris PJ. Distribution and quantitation of HLA-ABC and DR (Ia) antigens on human kidney and other tissues. *Transplantation*. 1980;29(4):274–279.

[665] Hauser SL, Bhan AK, Gilles FH, Hoban CJ, Reinherz EL, Schlossman SF, *et al*. Immunohistochemical staining of human brain with monoclonal antibodies that identify lymphocytes, monocytes, and the Ia antigen. *Journal of Neuroimmunology*. 1983;5(2):197–205.

[666] Cuzner M, Hayes G, Newcombe J, Woodroofe M. The nature of inflammatory components during demyelination in multiple sclerosis. *Journal of Neuroimmunology*. 1988;20(2):203–209.

[667] Hickey WF, Cohen JA, Burns JB. A quantitative immunohistochemical comparison of actively versus adoptively induced experimental allergic encephalomyelitis in the Lewis rat. *Cellular Immunology*. 1987;109(2):272–281.

[668] Hickey WF, Osborn JP, Kirby WM. Expression of Ia molecules by astrocytes during acute experimental allergic encephalomyelitis in the Lewis rat. *Cellular Immunology*. 1985;91(2):528–535.

[669] Paterson PY, Day ED, Whitacre CC. Neuroimmunologic diseases: effector cell responses and immunoregulatory mechanisms. *Immunological Reviews*. 1981;55(1):89–120.

[670] Paterson P, Day E. Current perspectives of neuroimmunologic disease: multiple sclerosis and experimental allergic encephalomyelitis (1, 2). *Clinical Immunology Reviews*. 1980;1(4):581–697.

[671] Traugott U. Characterization and distribution of lymphocyte subpopulations in multiple sclerosis plaques versus autoimmune demyelinating lesions. In: Springer Seminars in Immunopathology. vol. 8. Springer; 1985. p. 71–95.

[672] Hayes G, Woodroofe M, Cuzner M. Microglia are the major cell type expressing MHC class II in human white matter. *Journal of the Neurological Sciences*. 1987;80(1):25–37.

[673] Lassman H, Vass K, Brunner C, Seitelberger F. Characterization of inflammatory infiltrates in experimental allergic encephalomyelitis. *Progress in Neuropathology*. 1986;6:33–62.

[674] Lo D, Feng L, Li L, Carson MJ, Crowley M, Pauza M, *et al.* Integrating innate and adaptive immunity in the whole animal. *Immunological Reviews*. 1999;169(1):225–239.

[675] Carson MJ, Reilly CR, Sutcliffe JG, Lo D. Disproportionate recruitment of CD8+ T cells into the central nervous system by professional antigen-presenting cells. *The American Journal of Pathology*. 1999;154(2):481–494.

[676] Krakowski ML, Owens T. Naive T lymphocytes traffic to inflamed central nervous system, but require antigen recognition for activation. *European Journal of Immunology*. 2000;30(4):1002–1009.

[677] Byram SC, Carson MJ, DeBoy CA, Serpe CJ, Sanders VM, Jones KJ. CD4-positive T cell-mediated neuroprotection requires dual compartment antigen presentation. *Journal of Neuroscience*. 2004;24(18):4333–4339.

[678] Carson MJ, Doose JM, Melchior B, Schmid CD, Ploix CC. CNS immune privilege: hiding in plain sight. *Immunological Reviews*. 2006;213(1):48–65.

[679] Juedes AE, Ruddle NH. Resident and infiltrating central nervous system APCs regulate the emergence and resolution of experimental autoimmune encephalomyelitis. *The Journal of Immunology*. 2001;166(8):5168–5175.

[680] Carson MJ, Sutcliffe JG, Campbell IL. Microglia stimulate naive T-cell differentiation without stimulating T-cell proliferation. *Journal of Neuroscience Research*. 1999;55(1):127–134.

[681] Magnus T, Schreiner B, Korn T, Jack C, Guo H, Antel J, *et al.* Microglial expression of the B7 family member B7 homolog 1 confers strong immune inhibition: implications for immune responses and autoimmunity in the CNS. *Journal of Neuroscience*. 2005;25(10):2537–2546.

[682] Monsonego A, Zota V, Karni A, Krieger JI, Bar-Or A, Bitan G, *et al.* Increased T cell reactivity to amyloid β protein in older humans and patients with Alzheimer disease. *Journal of Clinical Investigation.* 2003;112(3):415.

[683] Zota V, Nemirovsky A, Baron R, Fisher Y, Selkoe DJ, Altmann DM, *et al.* HLA-DR alleles in amyloid β-peptide autoimmunity: a highly immunogenic role for the DRB1* 1501 allele. *The Journal of Immunology.* 2009;183(5):3522–3530.

[684] Monsonego A, Imitola J, Petrovic S, Zota V, Nemirovsky A, Baron R, *et al.* Aβ-induced meningoencephalitis is IFN-γ-dependent and is associated with T cell-dependent clearance of Aβ in a mouse model of Alzheimer's disease. *Proceedings of the National Academy of Sciences.* 2006;103(13):5048–5053.

[685] Belkhelfa M, Rafa H, Medjeber O, Arroul-Lammali A, Behairi N, Abada-Bendib M, *et al.* IFN-γ and TNF-α are involved during Alzheimer disease progression and correlate with nitric oxide production: a study in Algerian patients. *Journal of Interferon & Cytokine Research.* 2014;34(11):839–847.

[686] Butovsky O, Koronyo-Hamaoui M, Kunis G, Ophir E, Landa G, Cohen H, *et al.* Glatiramer acetate fights against Alzheimer's disease by inducing dendritic-like microglia expressing insulin-like growth factor 1. *Proceedings of the National Academy of Sciences.* 2006;103(31):11784–11789.

[687] Town T, Laouar Y, Pittenger C, Mori T, Szekely CA, Tan J, *et al.* Blocking TGF-β–Smad2/3 innate immune signaling mitigates Alzheimer-like pathology. *Nature Medicine.* 2008;14(6):681.

[688] Manczak M, Mao P, Nakamura K, Bebbington C, Park B, Reddy PH. Neutralization of granulocyte macrophage colony-stimulating factor decreases amyloid beta 1-42 and suppresses microglial activity in a transgenic mouse model of Alzheimer's disease. *Human Molecular Genetics.* 2009;18(20):3876–3893.

[689] Landel V, Baranger K, Virard I, Loriod B, Khrestchatisky M, Rivera S, *et al.* Temporal gene profiling of the 5XFAD transgenic mouse model highlights the importance of microglial activation in Alzheimer's disease. *Molecular Neurodegeneration.* 2014;9(1):33.

[690] Akiyama H, McGeer P. Brain microglia constitutively express β-2 integrins. *Journal of Neuroimmunology.* 1990;30(1):81–93.

[691] Kamphuis W, Kooijman L, Schetters S, Orre M, Hol EM. Transcriptional profiling of CD11c-positive microglia accumulating around amyloid plaques in a mouse model for Alzheimer's disease. *Biochimica et Biophysica Acta.* 2016;1862(10):1847–1860.

[692] Hendrickx DA, van Eden CG, Schuurman KG, Hamann J, Huitinga I. Staining of HLA-DR, Iba1 and CD68 in human microglia reveals partially overlapping expression depending on cellular morphology and pathology. *Journal of Neuroimmunology.* 2017;309:12–22.

[693] Turnbull IR, Colonna M. Activating and inhibitory functions of DAP12. *Nature Reviews Immunology.* 2007;7(2):155–161.

[694] Gaikwad S, Larionov S, Wang Y, Dannenberg H, Matozaki T, Monsonego A, *et al.* Signal regulatory protein-β1: a microglial modulator of phagocytosis in Alzheimer's disease. *The American Journal of Pathology.* 2009;175(6):2528–2539.

[695] Lu J, Wu X, Teh BK. The regulatory roles of C1q. *Immunobiology.* 2007;212(4):245–252.

[696] Gao D, Ashraf MZ, Kar NS, Lin D, Sayre LM, Podrez EA. Structural basis for the recognition of oxidized phospholipids in oxidized low density lipoproteins by class B scavenger receptors CD36 and SR-BI. *Journal of Biological Chemistry.* 2010;285(7):4447–4454.

[697] Kodama T, Reddy P, Kishimoto C, Krieger M. Purification and characterization of a bovine acetyl low density lipoprotein receptor. *Proceedings of the National Academy of Sciences.* 1988;85(23):9238–9242.

[698] Doi Y, Mizuno T, Maki Y, Jin S, Mizoguchi H, Ikeyama M, *et al.* Microglia activated with the toll-like receptor 9 ligand CpG attenuate oligomeric amyloid β neurotoxicity in in vitro and in vivo models of Alzheimer's disease. *The American Journal of Pathology.* 2009;175(5):2121–2132.

[699] Lowell CA. Src-family and Syk kinases in activating and inhibitory pathways in innate immune cells: signaling cross talk. *Cold Spring Harbor Perspectives in Biology*. 2011;3(3):a002352.

[700] Deckert M, Tartare-Deckert S, Couture C, Mustelin T, Altman A. Functional and physical interactions of Syk family kinases with the Vav proto-oncogene product. *Immunity*. 1996;5(6):591–604.

[701] Law CL, Chandran KA, Sidorenko SP, Clark EA. Phospholipase C-gamma1 interacts with conserved phosphotyrosyl residues in the linker region of Syk and is a substrate for Syk. *Molecular and Cellular Biology*. 1996;16(4):1305–1315.

[702] Moon KD, Post CB, Durden DL, Zhou Q, De P, Harrison ML, *et al*. Molecular basis for a direct interaction between the Syk protein-tyrosine kinase and phosphoinositide 3-kinase. *Journal of Biological Chemistry*. 2005;280(2):1543–1551.

[703] Mócsai A, Ruland J, Tybulewicz VL. The SYK tyrosine kinase: a crucial player in diverse biological functions. *Nature Reviews Immunology*. 2010;10(6):387.

[704] Crowley MT, Costello PS, Fitzer-Attas CJ, Turner M, Meng F, Lowell C, *et al*. A critical role for Syk in signal transduction and phagocytosis mediated by Fcγ receptors on macrophages. *Journal of Experimental Medicine*. 1997;186(7):1027–1039.

[705] Hara H, Saito T. CARD9 versus CARMA1 in innate and adaptive immunity. *Trends in Immunology*. 2009;30(5):234–242.

[706] Hauck CR, Klingbeil CK, Schlaepfer DD. Focal adhesion kinase functions as a receptor-proximal signaling component required for directed cell migration. *Immunologic Research*. 2000;21(2-3):293–303.

[707] Ostergaard HL, Lysechko TL. Focal adhesion kinase-related protein tyrosine kinase Pyk2 in T-cell activation and function. *Immunologic Research*. 2005;31(3):267–281.

[708] Otero K, Turnbull IR, Poliani PL, Vermi W, Cerutti E, Aoshi T, *et al*. Macrophage colony-stimulating factor induces the proliferation and survival of macrophages via a pathway involving DAP12 and β-catenin. *Nature Immunology*. 2009;10(7):734–743.

[709] Stanley ER, Chitu V. CSF-1 receptor signaling in myeloid cells. *Cold Spring Harbor Perspectives in Biology*. 2014;6(6):a021857.

[710] Lev S, Moreno H, Martinez R, Canoll P, Peles E, Musacchio J, *et al.* Protein tyrosine kinase PYK2 involved in Ca2+-induced regulation of ion channel and MAP kinase functions. *Nature.* 1995;376(6543):737–745.

[711] Bartos JA, Ulrich JD, Li H, Beazely MA, Chen Y, MacDonald JF, *et al.* Postsynaptic clustering and activation of Pyk2 by PSD-95. *Journal of Neuroscience.* 2010;30(2):449–463.

[712] Kohno T, Matsuda E, Sasaki H, Sasaki T. Protein-tyrosine kinase CAKβ/PYK2 is activated by binding Ca2+/calmodulin to FERM F2 α2 helix and thus forming its dimer. *Biochemical Journal.* 2008;410(3):513–523.

[713] Park SY, Avraham HK, Avraham S. RAFTK/Pyk2 activation is mediated by trans-acting autophosphorylation in a Src-independent manner. *Journal of Biological Chemistry.* 2004;279(32):33315–33322.

[714] Avraham H, Park SY, Schinkmann K, Avraham S. RAFTK/Pyk2-mediated cellular signalling. *Cellular Signalling.* 2000;12(3):123–133.

[715] Kedzierska K, Vardaxis NJ, Jaworowski A, Crowe SM. FcγR-mediated phagocytosis by human macrophages involves Hck, Syk, and Pyk2 and is augmented by GM-CSF. *Journal of Leukocyte Biology.* 2001;70(2):322–328.

[716] Paone C, Rodrigues N, Ittner E, Santos C, Buntru A, Hauck CR. The tyrosine kinase Pyk2 contributes to complement-mediated phagocytosis in murine macrophages. *Journal of Innate Immunity.* 2016;8(5):437–451.

[717] Okigaki M, Davis C, Falasca M, Harroch S, Felsenfeld D, Sheetz M, *et al.* Pyk2 regulates multiple signaling events crucial for macrophage morphology and migration. *Proceedings of the National Academy of Sciences.* 2003;100(19):10740–10745.

[718] Lloyd AC. Distinct functions for ERKs? *Journal of Biology.* 2006;5(5):13.

[719] Ramos JW. The regulation of extracellular signal-regulated kinase (ERK) in mammalian cells. *The International Journal of Biochemistry & Cell Biology.* 2008;40(12):2707–2719.

[720] Subramanian M, Shaha C. Up-regulation of Bcl-2 through ERK phosphorylation is associated with human macrophage survival in an estrogen microenvironment. *The Journal of Immunology*. 2007;179(4):2330–2338.

[721] Scheid MP, Schubert KM, Duronio V. Regulation of Bad phosphorylation and association with Bcl-xL by the MAPK/Erk kinase. *Journal of Biological Chemistry*. 1999;274(43):31108–31113.

[722] Biswas SC, Greene LA. Nerve growth factor (NGF) down-regulates the Bcl-2 homology 3 (BH3) domain-only protein Bim and suppresses its proapoptotic activity by phosphorylation. *Journal of Biological Chemistry*. 2002;277(51):49511–49516.

[723] Allan LA, Morrice N, Brady S, Magee G, Pathak S, Clarke PR. Inhibition of caspase-9 through phosphorylation at Thr 125 by ERK MAPK. *Nature Cell Biology*. 2003;5(7):647–654.

[724] Park RK, Izadi KD, Deo YM, Durden DL. Role of Src in the modulation of multiple adaptor proteins in FcαRI oxidant signaling. *Blood*. 1999;94(6):2112–2120.

[725] Suzuki T, Kono H, Hirose N, Okada M, Yamamoto T, Yamamoto K, *et al.* Differential involvement of Src family kinases in Fcγ receptor-mediated phagocytosis. *The Journal of Immunology*. 2000;165(1):473–482.

[726] Mina-Osorio P, Ortega E. Signal regulators in FcR-mediated activation of leukocytes? *Trends in Immunology*. 2004;25(10):529–535.

[727] Vauquelin G, Charlton SJ. Exploring avidity: understanding the potential gains in functional affinity and target residence time of bivalent and heterobivalent ligands. *British Journal of Pharmacology*. 2013;168(8):1771–1785.

[728] O'Neill SK, Getahun A, Gauld SB, Merrell KT, Tamir I, Smith MJ, *et al.* Monophosphorylation of CD79a and CD79b ITAM motifs initiates a SHIP-1 phosphatase-mediated inhibitory signaling cascade required for B cell anergy. *Immunity*. 2011;35(5):746–756.

[729] Kanamaru Y, Pfirsch S, Aloulou M, Vrtovsnik F, Essig M, Loirat C, *et al.* Inhibitory ITAM signaling by FcαRI-FcRγ chain controls multiple activating responses and prevents renal inflammation. *The Journal of Immunology*. 2008;180(4):2669–2678.

[730] Hamerman JA, Ni M, Killebrew JR, Chu CL, Lowell CA. The expanding roles of ITAM adapters FcRγ and DAP12 in myeloid cells. *Immunological Reviews*. 2009;232(1):42–58.

[731] Peng Q, Long CL, Malhotra S, Humphrey MB. A physical interaction between the adaptor proteins DOK3 and DAP12 is required to inhibit lipopolysaccharide signaling in macrophages. *Science Signaling*. 2013;6(289):ra72.

[732] Underhill DM, Goodridge HS. The many faces of ITAMs. *Trends in Immunology*. 2007;28(2):66–73.

[733] Zhang J, Somani AK, Siminovitch KA. Roles of the SHP-1 tyrosine phosphatase in the negative regulation of cell signalling. In: Seminars in Immunology. vol. 12. Elsevier; 2000. p. 361–378.

[734] Veillette A, Latour S, Davidson D. Negative regulation of immunoreceptor signaling. *Annual Review of Immunology*. 2002;20(1):669–707.

[735] Luo Y, Lu Z, Raso SW, Entrican C, Tangarone B. Dimers and multimers of monoclonal IgG1 exhibit higher in vitro binding affinities to Fcγ receptors. In: MAbs. vol. 1. Taylor & Francis; 2009. p. 491–504.

[736] Den Dunnen J, Vogelpoel LT, Wypych T, Muller FJ, de Boer L, Kuijpers TW, *et al*. IgG opsonization of bacteria promotes Th17 responses via synergy between TLRs and FcγRIIa in human dendritic cells. *Blood*. 2012;120(1):112–121.

[737] Wang M, Kaufman RJ. Protein misfolding in the endoplasmic reticulum as a conduit to human disease. *Nature*. 2016;529(7586):326–335.

[738] Schröder M, Kaufman RJ. ER stress and the unfolded protein response. *Mutation Research/Fundamental and Molecular Mechanisms of Mutagenesis*. 2005;569(1):29–63.

[739] Hetz C, Saxena S. ER stress and the unfolded protein response in neurodegeneration. *Nature Reviews Neurology*. 2017;13(8):477.

[740] Hamerman JA, Lanier LL. Inhibition of immune responses by ITAM-bearing receptors. *Science's STKE*. 2006;2006(320):re1–re1.

[741] Zou W, Reeve JL, Liu Y, Teitelbaum SL, Ross FP. DAP12 couples c-Fms activation to the osteoclast cytoskeleton by recruitment of Syk. *Molecular Cell*. 2008;31(3):422–431.

[742] Guilliams M, Bruhns P, Saeys Y, Hammad H, Lambrecht BN. The function of Fcγ receptors in dendritic cells and macrophages. *Nature Reviews Immunology*. 2014;14(2):94.

[743] Bergtold A, Desai DD, Gavhane A, Clynes R. Cell surface recycling of internalized antigen permits dendritic cell priming of B cells. *Immunity*. 2005;23(5):503–514.

[744] Dai X, Jayapal M, Tay HK, Reghunathan R, Lin G, Too CT, *et al*. Differential signal transduction, membrane trafficking, and immune effector functions mediated by FcγRI versus FcγRIIa. *Blood*. 2009;114(2):318–327.